CATALYTIC BORYLATION OF C-H BONDS: A ROUTE TO PHOTOPHYSICALLY INTERESTING PYRENE DERIVATIVES

ANDREW CRAWFORD

CATALYTIC BORYLATION OF C-H BONDS: A ROUTE TO PHOTOPHYSICALLY INTERESTING PYRENE DERIVATIVES

Andrew George Crawford

A thesis presented to Durham University in fulfilment of the thesis requirement for the degree of Doctor of Philosophy in Chemistry

Department of Chemistry
Durham
2011

CATALYTIC BORYLATION OF C-H BONDS: A ROUTE TO PHOTOPHYSICALLY INTERESTING PYRENE DERIVATIVES

Andrew G. Crawford

Pyrene derivatives have found use in a wide range of applications that make use of the unique structural, optical and charge-transfer properties of pyrene. Nearly all pyrene derivatives are substituted at the 1-, 3-, 6- and 8-positions, i.e. the sites of electrophilic aromatic substitution. In contrast, derivatives substituted at the 2- and 2,7-postions of pyrene are rare, as their syntheses involve laborious multistep processes. Such derivatives are of interest because they retain the long axis of symmetry and display unusual photophysical properties.

Using the regiospecific direct C-H borylation of pyrene with an Ir-based catalyst, prepared *in situ* via reaction of $[Ir(OMe)COD]_2$ with 4,4'-di-*tert*-butyl-2,2'-bipyridine, 2,7-bis(Bpin)pyrene **1** and 2-(Bpin)pyrene **2** (pin = $OCMe_2CMe_2O$) were synthesized. Straightforward derivatization strategies, converted **1** and **2** into nominally nucleophilic and electrophilic pyrene derivatives, which were further utilized in Suzuki-Miyaura, Sonogashira, Buchwald-Hartwig and Negishi cross-coupling reactions. Using this methodology, a library of 2- and 2,7-substituted pyrenes bearing donor and acceptor groups, including aryl, ethynyl, arylethynyl, alkyl, hydroxy, alkoxy, diarylamino, carboxylic acid and diarylboryl derivatives, was prepared.

The solid-state structures of several derivatives obtained by single-crystal X-ray diffraction revealed a diverse range of structures and packing modes.

The influence of the substitution position and the nature of the substituent upon pyrene was investigated in a detailed photophysical study. The existence of nodal planes passing through the 2- and 7-positions, perpendicular to the molecular plane, in both the HOMO and LUMO of pyrene accounts for the differing photophysical behaviour of derivatives substituted at 2- and 2,7-positions from those substituted at the 1-position.

Finally, the applicability of iridium-catalysed C-H borylation and metal-catalyzed cross-coupling is further demonstrated on a range of interesting substrates.

Table of Contents

List of Tables

List of Figures

Abbreviations

Ar: Aryl

ASAP: Atmospheric Solids Analysis Probe

B3LYP: Becke, three-parameter, Lee-Yang-Parr

Bpy: 2,2'-Bipyridine

CAM: Coulomb-attenuating method

CD: Circular Dichromism

CNT: Carbon nanotube

COD: Cyclooctadiene

COE: Cyclooctene

COF: Covalent-Organic Framework

C-T: Charge-transfer

dA: Deoxyadenine

dC: Deoxycytidine

dG: Deoxyguanosine

DMF: Dimethylformamide

DMSO: Dimethyl sulfoxide

DNA: Deoxyribonucleic acid

dppf: 1,1'-Bis(diphenylphosphino)ferrocene

dU: deoxyuridine

EA: Elemental Analysis

EI: Electron Ionisation

ESI: Electrospray Ionisation

Et: Ethyl

Fc: Ferrocene

FRET: Fluorescence Resonance Energy Transfer

GC-MS: Gas Cromatography-Mass Spectrometry

HOMO: Highest Occupied Molecular Orbital

IR: Infra-Red

LUMO: Lowest Unoccupied Molecular Orbital

MALDI: Matrix-Assisted Laser Desorption/Ionization

Me: Methyl

MS: Mass spectrometry

MW: Molecular Weight

NDI: Naphthalene diimide

NMR: Nuclear Magnetic Resonance

MOF: Metal-Organic Framework

OLED: Organic Light Emitting Diodes

PES: Potential Energy Surface

Phen: 1,10-Phenanthroline

Ph: Phenyl

RNA: Ribonucleic acid

RT: Room Temperature

S_0: Singlet ground state

S_1: Lowest singlet excited state

S_2: Second lowest singlet excited state

^{t}Bu: tertiary butyl

TD-DFT: Time Dependent-Densisty Functional Theory

THF: Tetrahydrofuran

TOF: Time of Flight

TON: Turnover number

TPA: Two-photon absorption

TMS: Trimethylsilyl

UV: Ultra-Violet

Vis.: Visible

λ : Wavelength

ϕ : Florescence Quantum Yield

τ : Florescence Lifetime

τ_o : Radiative Lifetime ($= \tau/\phi$)

Declaration

The work described in this thesis was carried out in the Department of Chemistry at Durham University between October 2007 and December 2010, under the supervision of Professor Todd B. Marder. All the work is my own, unless otherwise stated, and has not been submitted previously for a degree at this or any other university.

Andrew G. Crawford

Statement of Copyright

Acknowledgements

Thank you to Professor Todd Marder, for his supervision over the last three years. I have learnt so much throughout my PhD and I am very grateful for having received the opportunity to experience a wide variety of chemistry, meet many exciting people from around the world as well as to develop myself as a scientist.

Thanks also to Dr. Andrei Batsanov for measuring the crystal structures reported herein and for helpful discussions. Thanks to the group of Dr. Andrew Beeby for assistance with fluorescence quantum yield and lifetime measurements. Thanks to Austin Dwyer and Professor David Tozer for carrying out the TD-DFT calculations. Thank you to all of the above for the long discussions and hard work towards our publications.

My acknowledgements go out to Dr. Jon Collings, for his patient and careful proof reading of my thesis. Furthermore, thanks for all the advice and support given to me in the lab.

Much of this work would not have been possible without the assistance of the Durham University staff, who were always on hand to help out. Thanks to all the cleaning staff, glassblowers, technicians and stores staff. In particular, thanks to Judith Magee, Dr. Alan Kenwright, Ian McKeag, Catherine Heffernan, Dr. Mike Jones, Dr. Jackie Mosely, Dave Parker and Lara Turner for running excellent analytical services.

Over the last three years, I have been very fortunate to work with many people, who I have learnt a lot from and shared many good times. So thanks to: Brian Hall, Dr. Kittya Wongkhan, Dr. Jonathan Barnard, Meng-Guan Tay, Dr. Andreas Steffen, Dr. Manuel Romero, Dr. Zhiqiang Liu, Duangduan Chaiyaveij, Josef Gluyas, Tom Turner, Li Qiang, Peter Harrisson, Veronkia Angerer, Dr. Christian Kleeberg, Dr. Bianca Bitterlich, Laura Sewell, Laura Mackay, Dr. Marie-Hélène Thibault, Chao Liu, Martin Drafz, Hazmi Tajuddin, Christina Pubill, Garr-Layy Zhou, Wu Na, Ji Lei, Neil Sim, Will Trenholme and Keigo Sasaki.

Thanks to all my friends: old and new, some gone and some just arrived. There have been many memorable times over the last few years, which have helped keep things in perspective and have kept me motivated right to the end. So thank you to all.

Finally, thank you to Mum, Dad and Joanna for your continued love and support, for continuing to believe in and support me; without whose advice this would be a lesser PhD and without whom I'd be a lesser person.

"Would you tell me, please, which way I ought to walk from here?"
"That depends a good deal on where you want to get to," said the Cat.
"I don't much care where-" said Alice.
"Then it doesn't matter which way you walk," said the Cat.
"-so long as I get *somewhere*," Alice added as an explanation.
"Oh, you're sure to do that," said the Cat, "if you only walk long enough."

Alice's Adventures in Wonderland by Lewis Carroll

To Mum, Dad and Joanna

Chapter 1: Chemistry and Applications of Pyrene and its Derivatives

1.0 Introduction

Pyrene is a rigid aromatic molecule that, due to its unique structural and optical properties, has found use in a wide variety of applications.

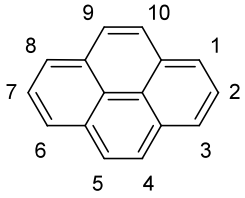

Figure 1 Pyrene with the C-H bonds numbered

This work investigates the synthesis, crystal packing and photophysics of a range of previously unknown pyrene derivatives that are substituted at the 2- and 2,7-positions. Despite derivatives substituted at these positions retaining the long axis of symmetry and displaying unique photophysical properties, very few studies have been carried out due to difficult and laborious synthetic routes. Herein, a straightforward and high-yielding synthetic route to 2- and 2,7-substituted pyrene derivatives, along with an examination of the optical properties of these new derivatives, is reported.

This introductory chapter is divided into two parts. Firstly, the justification for studying pyrene and in particular derivatives substituted at the 2- and 2,7-positions is presented. Secondly, the numerous applications of pyrene that make use of its structural, optical and charge-transfer properties, are reviewed.

1.1 Pyrene

Pyrene displays unique properties, in particular:

i. it undergoes π-π stacking interactions;
ii. it displays long lived fluorescence;
iii. it can participate in charge-transfer complexes;

i) Due to its planar aromatic nature, pyrene readily undergoes π-π stacking interactions both in solution and in the solid state. π-π Stacking interactions have played an

important role in supramolecular chemistry,[1] in particular, in the construction of complex supramolecules,[2] novel types of co-crystal[3] and nano-devices (e.g. switches, machines, transistors on the nanoscale).[4] In solution, at high concentrations, π-π stacking interactions are formed between pyrene molecules and are responsible for the formation of excimers (*vide infra*). Solid, unsubstituted pyrene is found to pack in a sandwich-herringbone fashion, where two parallel molecules form a sandwich via π-π interactions and the sandwiches are arranged into a herringbone motif.[5] The stacking properties of pyrene and its derivatives are discussed in more detail in Chapter 2.

ii) Pyrene displays unique and interesting photophysical properties.[6] As a monomer in solution, pyrene displays a long fluorescence lifetime of 354 ns (in toluene).[6c] As a result of this long lived fluorescence, the emission from pyrene is very sensitive to changes in local environment, such as addition of external substrates or changes in solvent polarity. As mentioned above, due to π-π stacking interactions, pyrene can form excimers, where an excited and ground-state molecule form a complex that displays a range of photophysical properties that differ from those of the monomer.[6b] In solution, at concentrations above *ca*. 10^{-5} mol dm^{-3}, a broad, structureless emission band centred at 480 nm is observed, while the intensity of emission due to the monomer decreases with increasing concentration. The photophysical properties of pyrene and its derivatives are discussed in more detail in Chapter 3.

iii) Pyrene derivatives are known to display charge-transfer behaviour, with pyrene acting as either an electron-donor or an electron-acceptor depending on the nature of the attached substituent.

1.2 The Chemistry of Pyrene

Derivatives of pyrene that take advantage of the aforementioned properties are generally synthesized via electrophilic aromatic substitution of the pyrene moiety. Maximum contributions of the HOMO (and also the LUMO) can be found at the 1-, 3-, 6- and 8-positions (Figure 2); therefore, nearly all pyrene derivatives synthesized by electrophilic aromatic substitution are substituted at these positions. Substituting pyrene at the 2- and 2,7-positions is synthetically challenging because of the presence of nodal planes in the HOMO and LUMO, which lie perpendicular to the molecular plane and pass through the 2- and 7-positions. Substitution at the 2- and 7-positions is only known to take place using $AlCl_3$ and ^tBuCl, as a result of unfavourable steric interactions, which preclude reaction at the normal 1-, 3-, 6- and 8-positions.[7]

Figure 2 The HOMO (left) and LUMO (right) of pyrene

1.3 2- and 2,7-Substituted Pyrene Derivatives

Pyrene derivatives substituted at the 2- and 7-position are of particular interest as the few examples known exhibit useful properties. The long axis of 2,7-pyrene derivatives makes them attractive for the synthesis of metal-organic frameworks (MOFs) and covalent-organic frameworks (COFs), which require rigid linear linkers in order to maintain a cubic structure. A MOF consisting of zinc ions linked by 2,7-bis(carboxylato)pyrene was found to adsorb molecular hydrogen with high uptake, increased by the high interaction energy of the polyaromatic system with the H_2 gas.[8] Several pyrene-based COFs have been synthesized. A COF consisting of pyrene-2,7-bis(boronic acid) and triphenylene units displayed intense blue luminescence at 474 nm upon excitation with visible light, as well as semiconductor behavior when a voltage was applied.[9a] More recently, a COF solely based on pyrene-2,7-bis(boronic acid) was synthesized and found to be photoconductive.[9b] Incorporation of the COF into a thin film device and irradiation with visible light led to current generation. Furthermore the

device was shown to be very stable, with no deterioration in conductivity after extensive on-off switching. Molecular rotors are also required to be linear in nature with high symmetry. Pyrene with two ethynyl triptycyl groups attached at the 2,7-positions has been used in such applications, the molecule undergoing frictional rotation at temperatures as low as 25 K.[10] Symmetrical star-shaped molecules, designed to investigate energy-transfer and storage in chromophore aggregates, have also been synthesized from 2,7-substituted pyrenes.[11]

The cross-coupling between 2-(Bpin)pyrene (pin = $OCMe_2CMe_2O$) and a uridine base under harsh conditions and with long reaction times gave a pyrene-modified nucleotide (Figure 3).[12] Calculations and photophysical studies showed that this derivative retained the optical properties of pyrene (weak electronic interaction between pyrene and the nucleotide). In contrast, the isomeric 1-pyrenyl uridine was found to exhibit a strong electronic interaction between the pyrene moiety and the uridine π-system. In the study of electron-transfer in DNA, the absence of spectral signals due to π-orbital conjugation with the uridine in the 2-substituted system leads to more straightforward spectra, from which it is easier to assign the electron-transfer dynamics.[12]

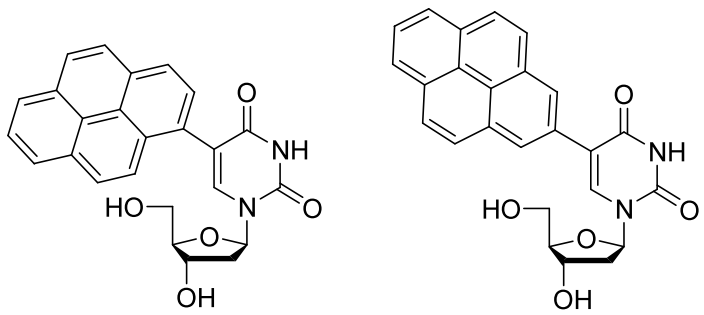

Figure 3 The structure of 5-(1-Pyrenyl)-2'-deoxyuridine (1PydU) and 5-(2-Pyrenyl)-2'-deoxyuridine (2PydU).[12]

A comparison of the effects of substitution of 1-, 2- and 4-ethynylpyrenes onto uridine,[13a] or DNA modified by 2- or 4-iodophenylmethylglycerol,[13b] has shown that the position of substitution has an effect on the photophysical properties of the compounds. For example, an absorption maximum of 357 nm for the 1-substituted compound is observed, and compares to 336 nm for the 2-substituted compound.[13]

An electrochemical study of oligomers consisting of two (Pyr_2) and three (Pyr_3) pyrene molecules (Figure 4) connected at the 2- and 7-positions[14] showed that the first reduction potentials are independant of the number of pyrene units (Pyr_2: -2.24 eV, Pyr_3: -2.27 eV). Furthermore, the Coulomb repulsions upon dianion (E_1-E_2 = 0.16 eV) and trianion (E_2-E_3 = 0.07 eV) formation were small. The dianion was found to exist as a diradical with the zero-field splitting almost equal to that in Pyr_3^{2-}, suggesting that, in the latter, two adjacent pyrene units are charged instead of the two terminal ones.

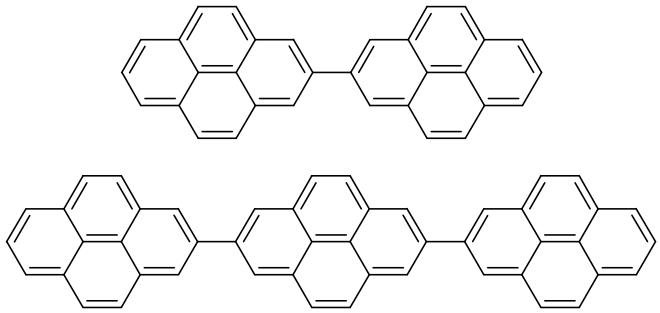

Figure 4 Pyrene oligomers, Py_2 (top) and Py_3 (bottom).[14]

A similar study investigated a 2-substituted pyrene-dihydrophenazine dyad.[15] It was found that, upon oxidation, a bis(radical cation) species was formed. In the UV-vis spectrum, separate transitions relating to the different radical cations were observed, reflecting the weak interaction at the 2-position. If the orbitals of the two radical cations had directly overlapped, a completely different absorption band would have been observed. In both of these studies, the electronic interaction between pyrene units connected at the 2- and 7-positions was shown to be very weak.

Despite these interesting observations, only a few examples of pyrene derivatives substituted at the 2- and 2,7-positions exist and the influence of substitution at these positions is under-studied. This is due to the difficulties associated with synthesizing 2- and 2,7-derivatives by traditional aromatic substitution routes (*vide supra*). As a result, alternative synthetic strategies must be employed to obtain 2,7-derivatives (Figure 5), such as the laborious oxidation of substituted [2.2]metacyclophanes,[16] photochemical ring-closure of 2,2'-divinylbiphenyls[14] and, more commonly, the electrophilic aromatic substitution of the tetra-hydrogenated pyrene derivative, 4,5,9,10-tetrahydropyrene, followed by subsequent dehydrogenation.[17]

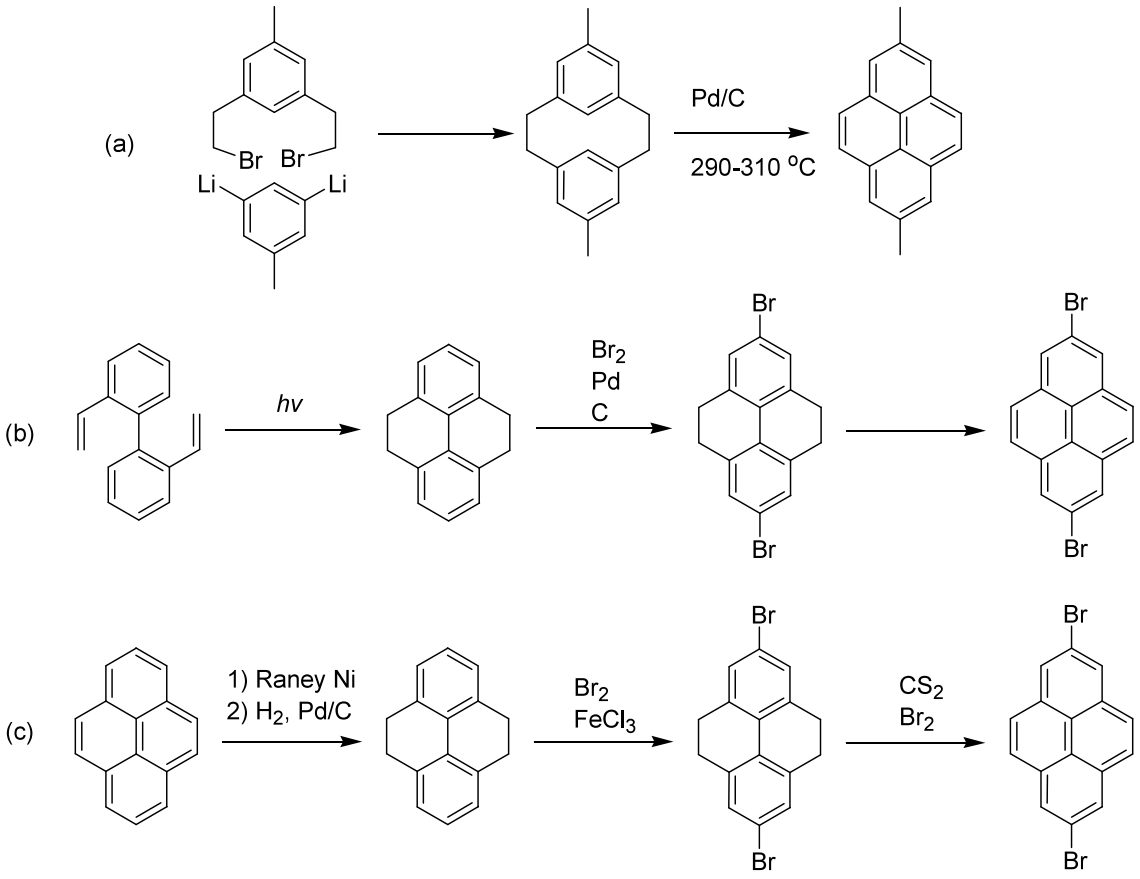

Figure 5 Synthetic routes to 2,7-pyrene derivatives: a) oxidation of substituted [2.2]metacyclophanes;[16] b) photochemical ring-closure of 2,2'-divinylbiphenyls;[14] c) electrophilic aromatic substitution of 4,5,9,10-tetrahydropyrene, followed by subsequent dehydrogenation.[17]

The latter route is the current method of choice to access 2,7-bis-substituted pyrene derivatives, although preparation of 4,5,9,10-tetrahydropyrene requires prior hydrogenation of commercial pyrene over Raney nickel[17f] and lengthy separation from various hydrogenated by-products.[17a,c] The absence of a straightforward and high-yielding route to 2- and 2,7-substituted pyrene derivatives has hindered their development and investigation.

More recently, direct iridium-catalyzed borylation of the C–H bonds at the 2- and 7-positions of pyrene has been reported, giving 2,7-bis(Bpin)pyrene and 2-(Bpin)pyrene (pin = $OCMe_2CMe_2O$).[18] The catalyst,[19] prepared *in situ* via the reaction of

$[Ir(OMe)COD]_2$ with 4,4'-di-*tert*-butyl-2,2'-bipyridine (dtbpy), is known to borylate arenes selectively at unhindered positions, i.e. not *ortho* to a substituent or ring-junction.[20] The sterically driven selectivity is presumably due to the crowded nature of the five-coordinate trisboryl species $[Ir(dtbpy)(Bpin)_3]$, which is the key intermediate in the catalytic cycle responsible for the C–H activation step (see Chapter 4 for a more detailed discussion). In the synthesis of 2,7-bis(Bpin)pyrene and 2-(Bpin)pyrene, no prior purification of commercial pyrene was required, and 2,7-bis(Bpin)pyrene was obtained in 94 % yield after removal of catalyst and Kugelrohr distillation, whereas purification by column chromatography gave 2-(Bpin)pyrene in 65 % yield.[18]

In this work, I have been able to improve the above borylation procedure and subsequently convert the boronic esters, 2,7-bis(Bpin)pyrene and 2-(Bpin)pyrene into a library of previously unknown pyrene derivatives which can serve as nucleophilic or electrophilic partners in cross-coupling reactions, as demonstrated by their employment in Suzuki-Miyaura, Sonogashira, Buchwald-Hartwig and Negishi cross-couplings (Chapter 2). Thus, a straightforward and high-yielding route to pyrene derivatives that are substituted at the 2- and 2,7-positions is reported. Furthermore, for the first time, a detailed investigation into the effect of position of substituents upon the photophysical properties of pyrene has been undertaken by comparing the library of 2- and 2,7-derivatives with previously known 1-substituted derivatives (Chapter 3). Finally, the applicability of iridium-catalyzed C-H borylation, along with metal-catalyzed cross-coupling reactions, is further demonstrated in the preparation of a range of interesting derivatives (Chapter 4).

2.0 Application of Pyrene Derivatives

In the second part of this chapter, the applications of pyrene and its derivatives are discussed. Examples are shown that make use of the structural, optical and charge-transfer properties of pyrene.

2.1 Structural Applications

Firstly, applications that make use of the rigid, planar nature of pyrene and its ability to undergo π-π stacking interactions are considered.

2.1.1 Binding to Carbon Nanotubes (CNTs)

Due to their unique mechanical and electronic properties, carbon nanotubes (CNTs) show great potential for a number of applications. However, their use has been limited by their polydispersity and poor solubility in organic solvents.[21] To overcome these problems, functionalization of CNTs with various substrates is required. One method is to tether a pyrene-containing substrate to a CNT. In these cases, pyrene is thought of as a small piece of graphite that binds to the CNT by π-π stacking interactions.

In one study, poly(methyl methacrylate) (PMMA) chains of varying length were end-capped with a pyrene molecule (Figure 6a).[22] When added to a mixture of multi-walled CNTs, it was found that the pyrene moiety grafted onto the CNT surface, causing the mixture to solubilize and disentangle, leading to separate nanotubes. At high concentrations of the PMMA-pyrene derivative, it was found that the nanotubes self-organized to form a liquid crystal phase. An alternative approach makes use of the long range order found in liquid crystals to provide macroscopic-scale control of the orientation of a mixture of dispersed nanotubes, which are solubilized by the addition of a pyrene substituted by a cyanobiphenyl motif with a tetra(ethylene oxide) spacer (Figure 6b).[23] In another study, a pyrene-capped poly(poly(ethylene glycol) acrylate) (polyPEGA) polymer was spin-coated onto a silicon surface, which was then patterned by electron-beam lithography (Figure 6c). When a solution of CNTs was added, assembly onto the silicon pattern was observed. The π-π stacking interactions between pyrene and the CNTs allow location-control of CNTs to give nanoscale patterns.[24]

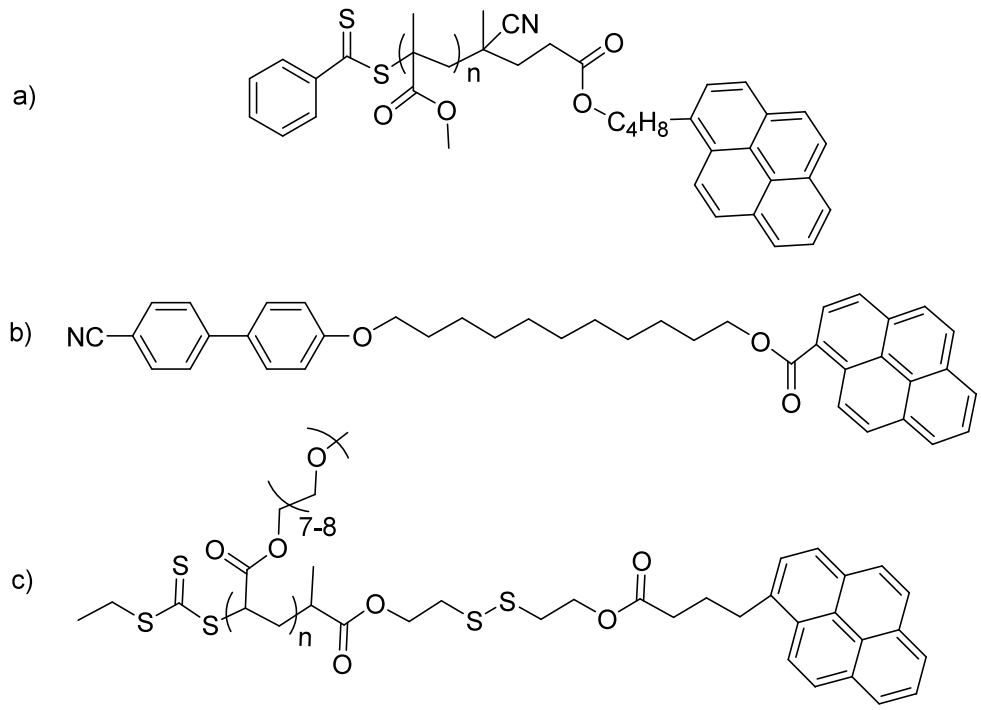

Figure 6 Pyrene derivatives used for the solubilization and dispersion of CNTs: a) pyrene-functionalized PMMA;[22] b) pyrene-1-carboxylic acid 11-(4'-cyano-biphenyl-4-yloxy)-undecyl ester;[23] c) pyrene-functionalized poly(PEGA).[24]

For medicinal applications, solubilization and dispersion of CNTs in water has been investigated. Traditional ways of dissolving organic substrates in water involve the use of surfactants. Generally, these molecules contain both a hydrophilic moiety and a hydrophobic (lipophilic) moiety. Replacement of the hydrophobic part of a surfactant with a pyrene moiety allows the surfactant to bind to CNTs through π-π stacking interactions, while favourable interactions with water can occur through the remaining hydrophilic moiety. Using this approach, it has been shown that CNTs can be dissolved in water;[25] however, further work is required to improve the selective dispersion of different-sized nanotubes. Similarly, solubilization in water has been affected by the addition of pyrene-substituted poly(ethylene glycol) (PEG), poly(γ-glutamic acid) (γ-PGA) and poly(maleic anhydride-*alt*-1-octadecene) ($PMHC_{18}$)-branched polymers.[26] In this study, other nano-structures such as gold nanoparticles and gold nano-rods were also dissolved at a range of temperatures and pH values. The authors used these findings to demonstrate the solubility of nano-materials in blood. It was found that the PEG-modified pyrene successfully solubilized a single-walled CNT for 22.1 h in the

bloodstream of mice (previous studies had shown the maximum to be 5.4 h). This long blood-circulation time is useful for *in vivo* applications, such as imaging and drug delivery.[26]

One advantage of using π-π stacking interactions between pyrene and CNTs is that it ensures the electronic properties of the CNT are not impacted by chemical modification of the carbon skeleton. Using this approach, several nano-materials based upon CNTs have been developed. Zinc porphyrins containing four pendant pyrene groups were attached to various CNTs through π-π stacking interactions (Figure 7).[27] These new nano-hybrids were isolated, characterized and investigated for their charge-transfer properties. It was shown by free-energy calculations and fluorescence studies that photo-induced electron-transfer occurred from the zinc porphyrin to the CNT. These zinc porphyrin-CNT species were incorporated into solar cells and their efficiency in such an application investigated.[27] In a separate study, another set of mono-substituted pyrene zinc porphyrin complexes was attached to CNTs by π-π interactions. The photo-induced electron-transfer in these systems was shown to have a photo-conversion efficiency of up to 23 %.[28] A further example of incorporation of a CNT material into solar cells was reported, this time using pyrene-functionalized CdTe quantum dots.[29] After grafting the quantum-dot substrate onto CNTs, their electronic interactions in solution-processed solar cells were investigated. Detailed studies revealed the electronic processes involved in the charge-transfer/recombination steps, leading to a greater understanding of the role of these systems in devices that undergo a change when activated by light.

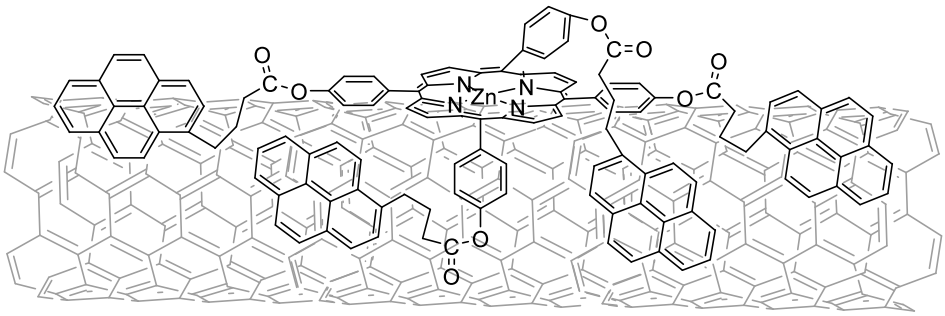

Figure 7 Structure of a pyrene-appended zinc porphyrin, $ZnP(pyr)_4$ bound to a single-walled CNT.[27]

The attachment of metal complexes through pyrene-CNT interactions has been useful for the development of electrochemical methodologies. The complex $[Co(tpy{\sim}py)_2]^{2+}$,

(tpy~py = 4-pyren-1-yl-*N*-[5-([2,2',6',2"]terpyridin-4'-yloxy)-pentyl]-butyramide) with pendant pyrene groups, was used for the *in situ* examination of the adsorption processes of pyrene to CNTs.[30] In another study, a single-molecule magnet, bis(phthalocyaninato)-terbium(III) with a pendant pyrene group, was tethered to a CNT.[31] It was found that attachment to the CNT avoided intermolecular interactions between separate Tb(III) complexes; therefore, analysis of the magnetic properties was more straightforward. As a result, the authors were able to examine the complex as a single-molecule magnet.[31]

Biological moieties have also been tethered to CNTs via pyrene derivatives. The compound pyren-1-yl butyric acid succinimidyl ester has been tethered to a CNT by π-π interactions, then covalent amide bonds were formed between the succinimidyl ester and the protein part of a multi-copper oxidase, thus attaching the enzyme to the CNT surface.[32] These biological nano-materials facilitate the direct electron-transfer between enzyme and CNT, thus improving the catalytic oxygen-reduction activity of the multi-copper oxidase system. DNA has also been attached to CNTs for investigations into DNA-recognition probes and gene-delivery applications. Tethering of a positively charged pyrene derivative to a CNT, then making use of the electrostatic interactions between the negatively charged phosphate backbone on DNA, and the positively charged pyrene derivative has allowed formation of DNA nano-structures for these applications.[33]

2.1.2 Host-Guest Complexes

The π stacking ability of pyrene has also been used to form host-guest systems. One potential application of this area is drug delivery. A host can be used to transport a guest to a specific site in the body, where the guest is released to carry out its drug action. This approach minimizes any unwanted side effects arising from the interaction between the drug and healthy parts of the body. A set of host-guest systems based upon ruthenium metalla-cages as the host, and pyrene derivatives as the guest, have been developed.[34] The π-π interactions between the pyrene and the cage act to hold the guest within the host, while the substituent on the pyrene derivatives is designed to be cytotoxic towards various cancer cells. It is hoped that the Ru-cage containing the cytotoxic pyrene derivative (Figure 8) will accumulate in cancer cells and subsequent slow release of the pyrene derivative will occur. *In vitro* studies have highlighted the high cytotoxicity of the pyrene derivatives used,[34c] and also show that, after cell-uptake,

the pyrene derivative is released from the metalla-cage by a diffusion pathway.[34d] Further *in vivo* studies are planned.

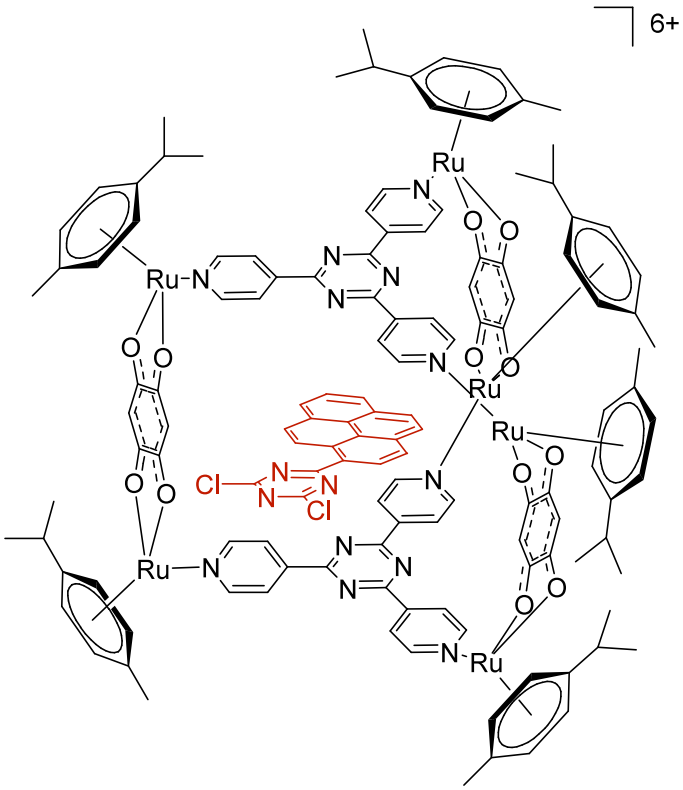

Figure 8 $[Ru_6(p\text{-}i\text{PrC}_6H_4Me)_6(tpt)_2\text{-}(C_6H_2O_4)_3]^{6+}$, (tpt = 2,4,6-tris(pyridine-4-yl)-1,3,5-triazine) host containing a cyctotoxic 1-(4,6-dichloro-1,3,5-triazin-2-yl)pyrene guest.[34d]

In host-guest chemistry, the selective inclusion of a guest into a host is a major objective. The tetra-substituted 2,6-dimethyl-4-methoxyphenyl pyrene has been shown to have three distinct domains (trough, concave and basin) for guest inclusion (Figure 9).[35] Co-crystallization with a variety of polycyclic aromatic and aliphatic guests has shown that binding occurs in different domains, dependant on the nature of the substrate. This has allowed formation of ternary co-crystals in a predictable manner, and hence demonstrates selective inclusion for host-guest systems.

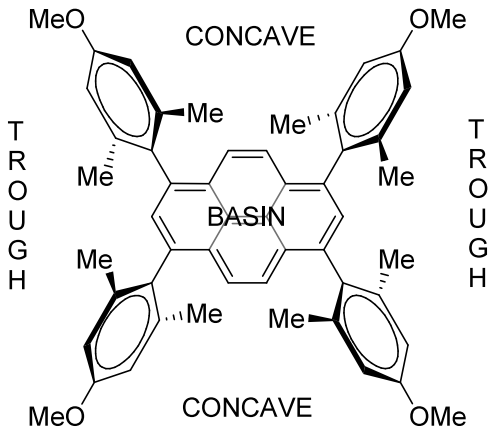

Figure 9 Molecular structure of a tetra-substituted 2,6-dimethyl-4-methoxyphenyl pyrene host showing the three domains for guest-binding.[35]

As well as selective inclusion, host-guest chemistry involving pyrene has also been used to investigate the nature of π-π stacking interactions in supramolecular systems. The formation of 1:1 complexes between various pyrene derivatives and macrocyclic aromatic ether imide sulfones was investigated,[36] with binding studies carried out by ^{1}H NMR and UV/Vis. Spectroscopy, as well as X-ray crystallography in the solid state, showed that strong attractive forces exist between electronically complementary aromatic systems, such as pyrene and the naphthalene diimide (NDI) moiety.[36] A separate study suggested the reason for this strong interaction between the electron-donating pyrene and the electron-accepting NDI was the result of the similar nature of the pyrene HOMO and NDI LUMO.[37] Maximum overlap occurs when the long axes of pyrene and NDI are aligned (Figure 10).

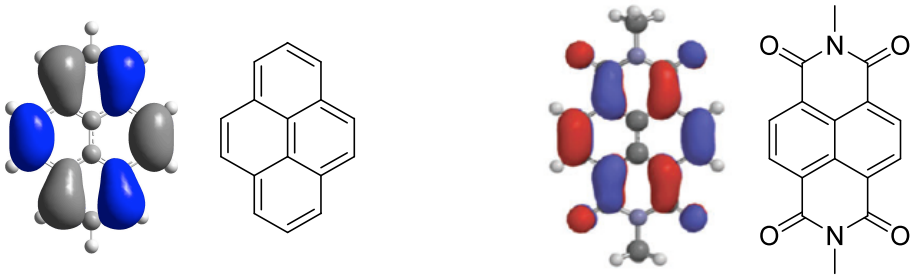

Figure 10 The HOMO of pyrene (left) and LUMO of *N*,*N*'-dimethyl naphthalenediimide (right) are nearly identical, leading to efficient overlap to form a pyrene-NDI π-stacked pair.[37] LUMO of NDI reproduced by permission of The Royal Society of Chemistry.

These findings have been used to construct supramolecular polymers by self-assembly.[38] A blend comprising a chain-folding polyimide and a telechelic polyurethane with pyrenyl end-groups is formed by π-π stacking interactions between the pyrene and NDI moieties. The resulting polymer was found to have a high modulus of toughness, and is elastomeric in nature.[38] In another study, rotaxanes containing an electron-rich wheel with a pendant pyrene, and an axle, containing an NDI unit, were synthesized and the strong interaction between pyrene and NDI exploited (Figure 11).[39] Addition of a base leads to strong intermolecular charge-transfer (ICT) and the π-π stacking between pyrene and NDI prevents rotation, whereas addition of acid leads to weak ICT and dissociation of the pyrene-NDI complex, giving rotation of the wheel around the axle.

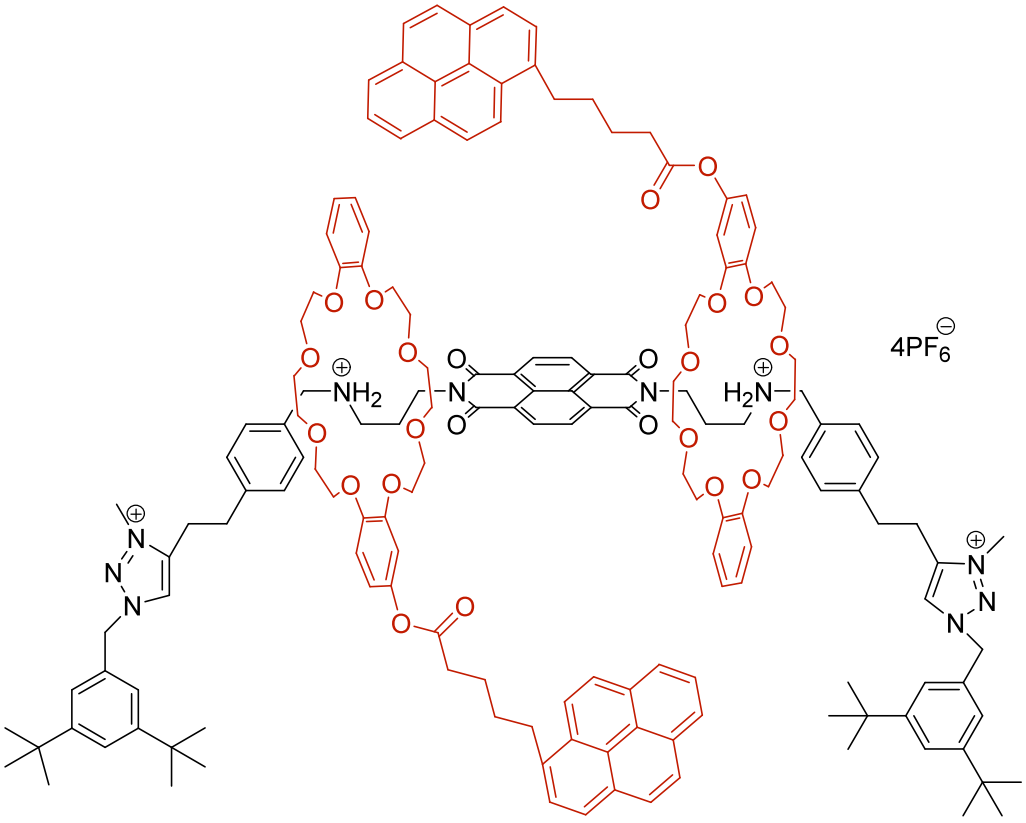

Figure 11 A [3]rotaxane, consisting of a wheel with a pendant pyrene and an NDI axle.[39]

2.1.3 Aggregates and Crystalline Complexes

As well as the formation of supramolecular macrostructures, the π-π interactions of pyrene have applications in optical and electrochemically active materials. In particular, these interactions have been used to form nano-fibres and supramolecular hydrogels.[40] Pentapeptides were functionalized with pyrene and other aromatic moieties, such as fluorene or naphthalene.[40b] In aqueous solution, these pentapeptide derivatives formed hydrogels by π-π stacking and hydrogen bonding. Elsewhere, poly(ethylene glycol)s end-capped with a pyrene molecule were incorporated into aqueous solutions with octafluoronapthalene (OFN).[40a] Due to the strong pyrene-OFN (arene-perfluoroarene) interactions, aggregation occurred to form a highly viscous liquid/gel. Other pyrene-based gels were formed when pyrene was functionalized with two *N*-(4-ethynylpheny)-3,4,5-tris(hexadecyloxy)benzamide fragments.[41] Formation of highly fluorescent gels was observed in DMF, toluene and cyclohexane. The formation of pyrene based gels is another example of the π stacking ability of pyrene.

When the pyrene was tetra-substituted with the aforementioned ethynyl moiety (Figure 12a), a discotic liquid-crystalline material was formed that was stable between room temperature and 200 °C.[41] Other tetra-substituted pyrene derivatives have also been shown to display liquid-crystal behaviour. Most systems are based upon discotics, which consist of flat, disc-like aromatic cores substituted with hydrocarbon chains. These flat molecules self-organise into columns. Several 1,3,6,8-tetraphenylpyrene derivatives bearing long ester, thioester, alkoxy- and tri(alkoxy)benzoate groups in the *para*-position were synthesized.[42] It was hoped that the steric bulk of the phenyl substituents would cause the derivatives to pack in a non-parallel fashion, and hence form a columnar mesophase. However, it was found that none of the derivatives showed liquid-crystal properties. On going from solution to the solid state, there was only a slight shift in the absorption and emission maxima, suggesting weak intermolecular interactions between separate pyrenes. Furthermore, a crystal structure showed that the pyrene derivatives stack one-dimensionally, and have a large separation distance between adjacent pyrene units of 4.8 Å. The authors conclude that to achieve columnar mesophases, substitutents with less steric hindrance are required.[42] Therefore, in another study, a substituent with even less steric bulk was used. Four oligo-ether side chains were attached to pyrene. However, the newly formed derivatives displayed pure liquid

behaviour and no liquid-crystalline behaviour.[43] The balance between too much and too little steric interaction is important when designing pyrene-based liquid crystal systems. This balance was achieved by using 3,4,5-trisdodecyloxyphenylacetylene, which was cross-coupled onto the pyrene unit to give the compound 1,3,6,8-tetrakis(3,4,5-trisdodecyloxyphenylethynyl)pyrene (Figure 12b). The compound was found to form hexagonal and rectangular columnar mesophases.[44]At 40 ºC, the rectangular columnar mesophases form, with the disc-like pyrene derivatives stacking on top of each other. Upon heating to 60 ºC, the hexagonal columnar mesophases are formed. In this case, the addition of an ethynyl spacer has reduced the steric interactions and allowed the pyrene units to form columnar mesophases. Cooling to 20 ºC led to a solid crystalline phase. The photophysical properties of the pyrene derivative in solution (as a free molecule) and in the solid crystalline phase were measured. It was found that the fluorescence quantum yield in the crystalline phase was 0.62, one of the highest recorded for solid-state discotic materials. The emitting species is believed to be a solid-state excimer.[44]

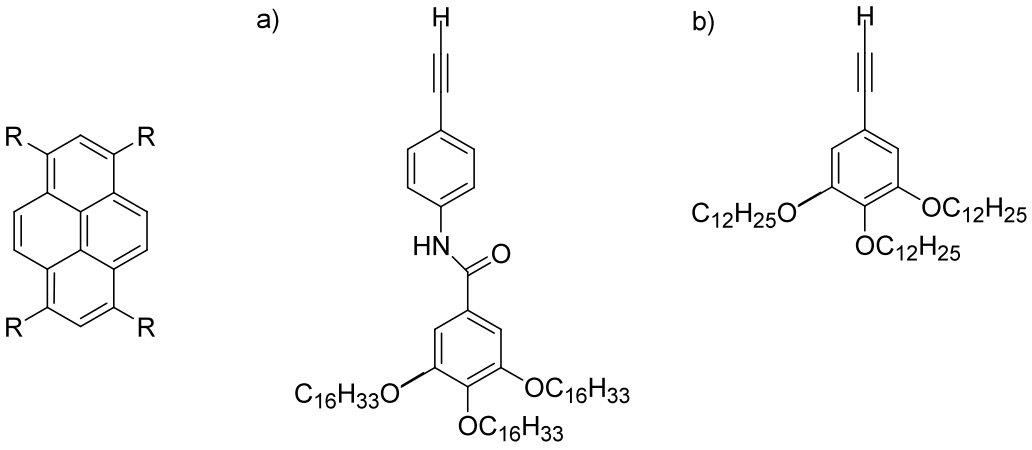

Figure 12 Pyrene derivatives for liquid crystal applications: a) 1,3,6,8-tetrakis(*N*-{4-ethynylpheny}-3,4,5-tris{hexadecyloxy}benzamide)pyrene;[41] b) 1,3,6,8-tetrakis(3,4,5-trisdodecyloxyphenylethynyl)pyrene.[44]

The ability of pyrene derivatives to form solid crystalline phases is also used to investigate the process of crystallization. Pyrene-2,7-dicarboxylic acid and 4,5,9,10-tetrahydropyrene-2,7-dicarboxylic acid were crystallized from a saturated solution in DMSO.[45] Scanning tunnelling microscopy and X-ray crystallography were used to determine the crystallisation process. It was found that the hydrogen bonding between

carboxylic acid groups leads to molecular chains, which then align in a parallel fashion to form 2D sheets. These sheets form a 3D structure via π-π stacking interactions between the pyrene cores of adjacent sheets, thus giving a highly ordered crystalline material.[45] This study gives insight into the formation and structure of crystalline materials.

Finally, as described in Section 1.3, the structural properties of pyrene, including its long axis of symmetry and polyaromatic nature, have allowed its use in MOFs,[8] COFs[9] and molecular rotors.[10]

2.2 Optical Applications

2.2.1 Optical Materials

The unique photophysical properties of pyrene have allowed it to be used in a wide variety of optical applications. Pyrene, as an excited monomer in solution, is known to emit in the UV region at ~370 nm. For optical applications, emission in the visible region is often required. Therefore, conjugating groups, which extend π-conjugation and lead to a bathochromic shift in the emission to the visible region, are often substituted onto pyrene. Substitution with various donor and acceptor arylethynyl groups at the 1-position has been shown to alter the emission properties of pyrene.[46] Strong (NMe_2) and moderate (^{i}PrO) donors were compared to strong (anthronitrile) and moderate (2-quinolinyl) acceptors. Comparisons with the neutral 1-phenylethynylpyrene were also carried out. Bathochromic shifts were observed in the absorption and emission spectra, for both strong donor and acceptor moieties. These results suggest that the emitting state possesses charge-transfer character. Both the electron-acceptors and electron-donors are able to affect charge-transfer in the excited state, with the pyrene behaving as an electron-donor with the former and an electron-acceptor with the latter.[46] This charge-transfer nature of aryl-ethynyl pyrenes was further probed in a study which investigated 1,8- and 1,6-bis(aryl ethynyl)pyrene dyes using fluorescence spectroscopy and DFT calculations.[47] Again, the largest influence on the emission of pyrene was observed when a strong donor (NMe_2) was attached to the *para* position on the phenyl ring. The large bathochromic shift and loss of fine structure that were observed were shown to be the result of intramolecular charge-transfer between the strong donor and pyrene.

Oligomers and polymers synthesized from 1,8- and 1,6-ethynyl pyrene derivatives have also been reported.[48] These highly conjugated systems involve the linking of aromatic

units to acetylene linkers by Sonogashira cross-coupling reactions. In one study, a comparison of the photophysical properties of *para*- and *meta*-linked alkynylpyrene oligomers was carried out (Figure 13).[48b] It was found that the *para*-linked oligomers displayed a greater bathochromic shift in their absorption and emission maxima, suggesting that *para*-linkages are better for extended π-conjugation.

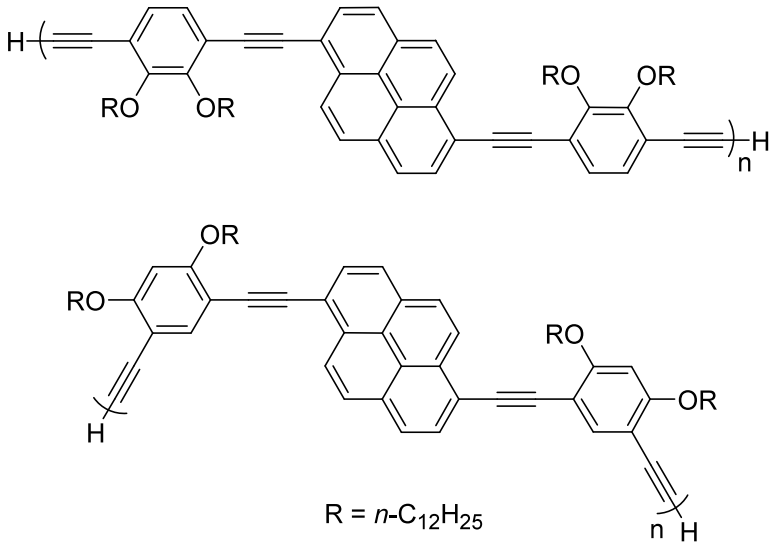

Figure 13 *para*- (top) and *meta*- (bottom) linked alkynylpyrene oligomers.[48b]

The bathochromic shift in the emission maximum is believed to be somewhat reduced in these systems due to the rotation of the benzene ring, which facilitates non-radiative decay processes. Furthermore, the fluorescence quantum yields were shown to decrease upon increasing oligomer length; this is due to the added flexibility of the longer oligomers, which leads to increased quenching. It is hoped that these oligomers will find application as optical materials.[48b]

Tetra-substitution of pyrene with ethynyl groups has also been used to extend π-conjugation and synthesize optical materials. The tetra-bromination of pyrene followed by Sonogashira cross-coupling with C≡C-R moieties (R = TMS, $C(Me)_2OH$, CH_2OH, $CH(OEt)_2$, Ph and 4-$CF_3C_6H_4$) produced a range of tetraethynylpyrenes.[49] Comparison of the absorption and emission data showed that the addition of ethynyl groups induced bathochromic shifts in the absorption and emission bands. However, when the fluorescence quantum yields were compared, the phenylethynyl derivatives were shown to have much lower values than the non-phenyl containing ones. Like the oligomers,

this is believed to be due to the rotation of the phenyl substituent which facilitates non-radiative decay processes. Broadening in the absorption and emission spectra is also attributed to this phenomenon.[49]

In another study, the two-photon absorption (TPA) properties of a set of ethynyl-pyrenes were investigated (TPA: simultaneous absorption of two photons, with the energy difference between the lower and upper states equal to the sum of the energies of the two photons).[50a] The magnitude of the TPA cross section (a measure of molecular absorbance in a TPA process, similar to a molar extinction coefficient in a one-photon absorption process) is known to be influenced by donor and acceptor strengths, conjugation length, and planarity of the π-centre.[50a] The authors synthesized a series of pyrene derivatives with varying numbers of 4-(*N*,*N*-dimethylamino)phenylethynyl (DMA-phenylethynyl) substituents (Figure 14). These pyrene derivatives have a large planer π-centre, an increased conjugation length and a strong electron-donation from the DMA moieties to the pyrene. Upon increasing the number of DMA-phenylethynyl substitutents, the one-photon absorption spectra show gradual bathochromic shifts in λ_{max} values, but the extinction coefficients remain fairly constant at *ca.* $\varepsilon = 67000$ $mol^{-1}cm^{-1}L$ after the addition of two substituents. When excited at 780-830 nm, the maximum two-photon cross sections (δ_{max}) of the various compounds differ significantly. Upon bis-substitution to give the 1,6-isomer, the δ_{max} value increases by a factor of nine, a result of the increased conjugation length. In contrast, the non-linear 1,8-isomer displays a much smaller δ_{max}, thus highlighting the importance of increased conjugation length on the TPA cross section. The δ_{max} value increases slightly upon addition of a third DMA-ethynyl substituent, whilst upon addition of a fourth substituent, the TPA cross section doubles. Furthermore, the two-photon action cross section (the product of the fluorescence quantum yield and TPA cross section) is 1150 GM, which is comparable to the most efficient TPA materials. This study has shown pyrene to be a very efficient core which has great potential in the design and synthesis of TPA materials.[50a]

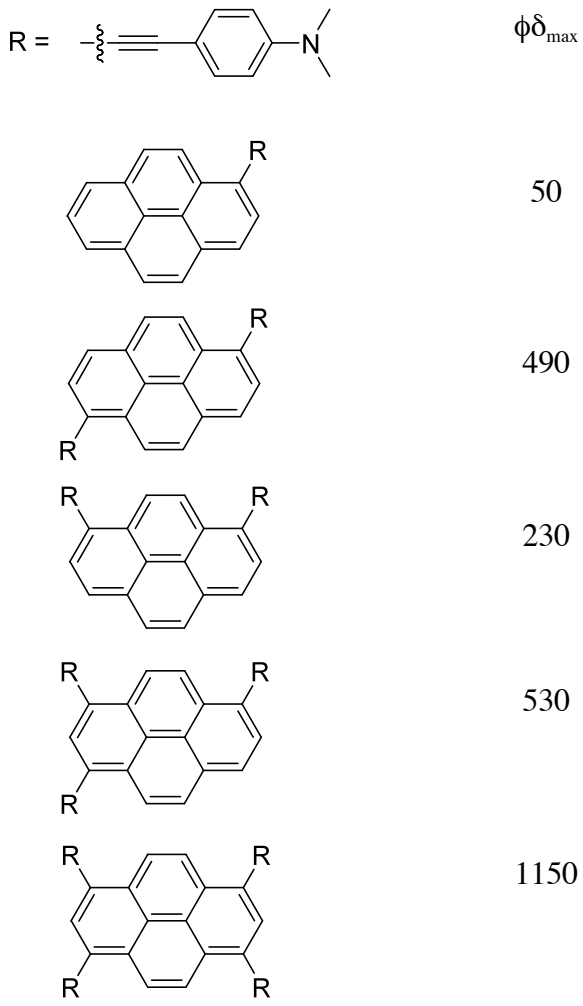

Figure 14 TPA action cross-sections of a series of DMA-phenylethynyl-pyrene derivatives.[50a]

These compounds were also studied for their electro-generated chemiluminescence (ECL) properties (ECL is defined as the emission of light from the electron-transfer reaction, between electrochemically generated ion radicals in the vicinity of an electrode).[50b] Previously, pyrene has been shown to display poor ECL properties due to the instability of its cation radical. However, in the case of tetra-substitution of pyrene with DMA-phenylethynyl moieties, ECL was measured with high intensities (no intensity values were reported). The authors used photophysical, electrochemical and theoretical studies to attribute this enhanced ECL to the highly conjugated nature of the system, which gives stability to the electro-chemically generated ion radicals.[50b]

Pyrene has also been tetra-substituted with ethynyl groups at the 4-, 5-, 9- and 10-positions.[51] To synthesize these derivatives, pyrene was first substituted at the 2- and 7-positions with *tert*-butyl groups (*vide supra*), which are sterically demanding enough to preclude electrophilic aromatic bromination at the neighbouring 1-, 3-, 6- and 8-positons. Hence, bromination now occurs at the 4-, 5-, 9- and 10-positions, and subsequent Sonogashira cross-couplings are used to obtain the desired derivatives. Photophysical studies show that the emission maximum is bathochromically shifted into the blue region. Interestingly, a comparison of 2,7-di-*tert*-butyl-4,5,9,10-tetrakis[(4-methoxyphenyl)ethynyl]pyrene with 1,3,6,8-tetrakis[(4-methoxyphenyl)ethynyl]pyrene (Figure 15) shows that the emission maximum in the latter is bathochromically shifted by 126 nm from that of unsubstitued pyrene, compared to 83 nm in the former.[51] Hence substitution at the 4-, 5-, 9- and 10-positions appears to have less influence on the photophysical properties of pyrene than substitution at the 1-, 3-, 6- and 8-positons, consistent with the fact that, both the HOMO and LUMO of pyrene have their maximum contributions at these positions.

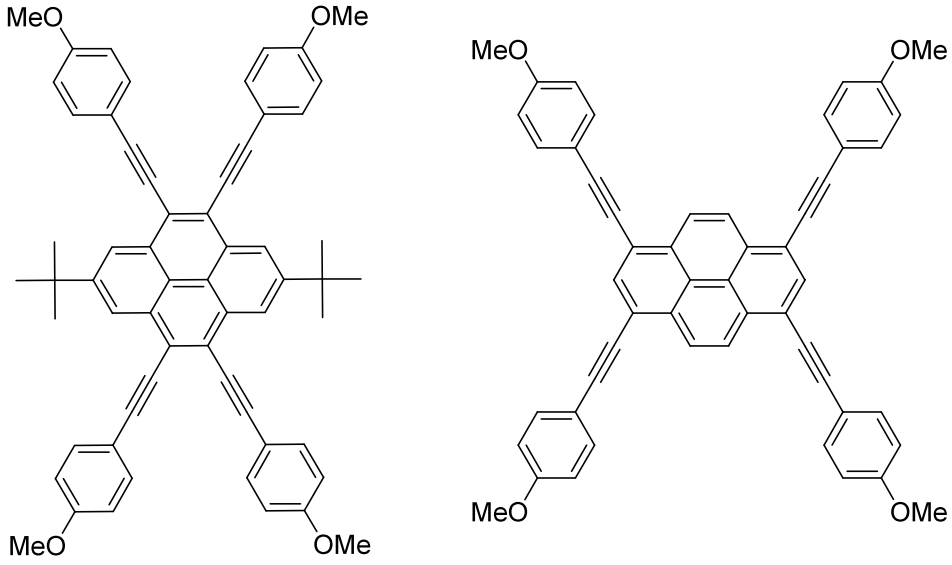

λ_{em} / nm 453 496

Figure 15 2,7-Di-*tert*-butyl-4,5,9,10-tetrakis[(4-methoxyphenyl)ethynyl]pyrene (left) and 1,3,6,8-tetrakis[(4-methoxyphenyl)ethynyl]pyrene (right) and their emission maxima (λ_{em}).[51] The λ_{em} of unsubstitued pyrene is at 370 nm.

Having demonstrated that substitution of pyrene with conjugating groups can induce a bathochromic shift into the visible region, the applications of these observations are now considered. Due to their strongly emissive nature, boron-based dyes are of interest for fluorescent labels and optical devices. A dye based upon a boron-containing diisoindolodithienylpyrromethane, (Figure 16a) which was substituted at the boron centre by two 1-ethynylpyrene chromophores was shown to display an emission at 750 nm, thus shifting the emission maximum to the near-IR region.[52] Another boron-based dye, bis((*E*)-2-pyren-1-yl-vinyl)-2,4,6-triisopropylphenylborane, (Figure 16b) was synthesized by the hydroboration reaction, and contained pyrene units connected to the boron by a vinyl group.[53] Emission occurred at 490 nm in solution, whilst in the solid state, it occurred at 530 nm. This large bathochromic shift in the solid state is believed to be due to the efficient π-stacking of the pyrene molecules. In a different study, solid-state emission from a binuclear boron complex containing two pyrene ligands (Figure 16c) was found to occur at 602 nm; furthermore, the complex was shown to have potential as an electron-transporting material in OLED devices.[54]

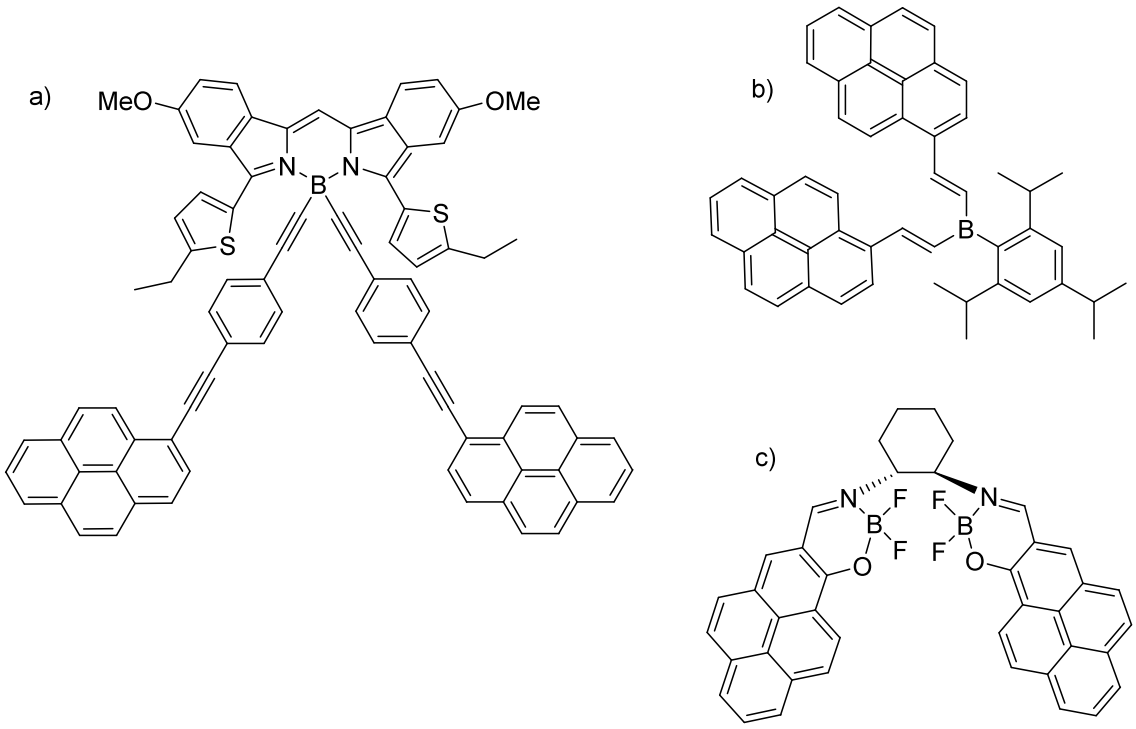

Figure 16 Boron-based dyes containing pyrene: a) diisoindolodithienylpyrromethane-dialkynyl borane dye;[52] b) bis((*E*)-2-pyren-1-yl-vinyl)-2,4,6-triisopropylphenylborane;[53] c) (bis-[(1-hydroxy-2-pyrenylidene)-(1'R,2'R)-cyclohexane-1',2'-diamine]-difluorbor-chelat).[54]

It might be expected that the emissive nature of pyrene would make it suitable candidate for OLED devices. However, due to the fact that pyrene undergoes π-π stacking interactions and excimer emission in both solution and the solid state, its use in OLED applications is limited. In order to reduce the effects of stacking and excimer formation, bulky substituents are required. The compound 1,3,6,8-tetraisopropylpyrene was synthesised by bromination of pyrene, followed by a Suzuki-Miyaura cross-coupling reaction with isopropenylboronic acid and then catalytic hydrogenation.[55] The absorption spectrum of this derivative was similar to that of the parent pyrene; however, there was no broad excimer emission band, and only monomer emission is observed. The isopropyl groups cause enough steric inhibition to prevent π-stacking and excimer formation.[55] The steric hindrance around pyrene was further increased by tetra-substitution with tetraphenylethene moieties at the 1-, 3-, 6- and 8-positions to yield 1,3,6,8-tetrakis[4-(1,2,3-triphenylvinyl)phenyl]pyrene.[56] This system displayed aggregation-induced emission (AIE). When fully dissolved, no emission is observed; however, upon the formation of aggregates (due to poor solubility), bright luminescence is observed. The AIE effect in this pyrene derivative occurs as a result of restricted intermolecular rotations. In solution, the rotations cause non-radiative decay; but in the aggregate state, the rotations are hindered, making the molecule emissive.[56] Even greater steric hindrance, and hence subsequent prevention of unwanted π-π stacking interactions, was achieved by synthesizing polypyrene dendrimers using Suzuki-Miyaura cross-coupling reactions to attach several pyrene molecules around a central pyrene core.[57] Two examples have been synthesized, consisting of five (Py5) and seventeen (Py17) pyrene units (Figure 17). These derivatives have a large amount of steric hindrance, which gives rise to a high degree of twisting. Calculations show a dihedral angle between the core and the first branch of 65-66° in Py5 and 71-73° in Py17, with the second branch in Py17 having a dihedral angle of 84-89°. The system incorporates a defined number of pyrene units in a confined volume, and displays a rigid and strongly twisted 3D structure. Furthermore, the dendrimers were found to have large extinction coefficients (ε = 93000 (Py5) and 323000 (Py17) $mol^{-1}cm^{-1}L$) and fluorescence quantum yields (ϕ_f = 0.70 (Py5) and 0.70 (Py17)).[57]

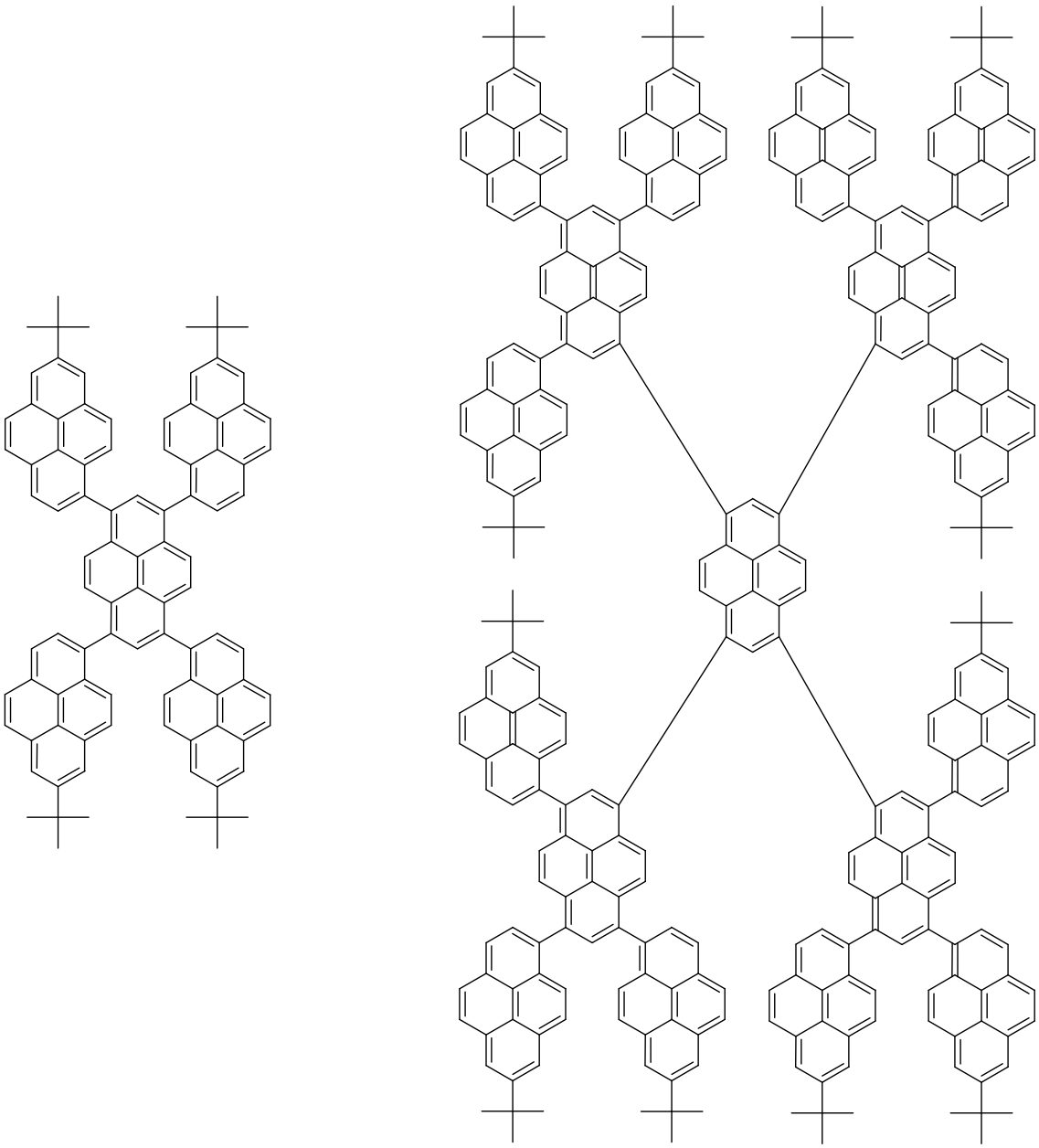

Figure 17 Polypyrene dendrimers, Py5 (left), Py17 (right).[57]

Examples of tetra-substituted pyrene OLED devices, include the sterically hindered pyrene, 1,3,6,8-tetraphenylpyrene, which was incorporated into a film doped with 1 wt% rubrene.[58a] The device displayed bright electroluminescence. It was found that electron-accumulation and injection limited the device performance. The system can also be classed as an organic field-effect transistor (a transistor that relies on an electric field to change the conductivity of one channel), which are of potential interest for optical communication systems, display technologies, solid-state lighting and organic laser applications.[58b] A more recent study involved using Suzuki-Miyaura cross-

coupling reactions to synthesize a range of 1-, 3-, 6- and 8-substituted pyrene derivatives bearing various bithiophene, phenylene, thieno-thiophene and benzothiadiazole-thiophene moieties.[59] These derivatives, were shown to have a large influence on the opto-electronic and thermal properties of pyrene-based organic electronic devices. In particular, an OLED based on 1,3,6,8-tetrakis(4-butoxyphenyl)pyrene shows deep-blue emission (Figure 18a). The search for efficient blue emitters for OLED devices is an ongoing area of research and several other examples of blue-emitting pyrene-containing systems exist. A series of triarylamines containing both a pyrene and a hexaphenylbenzene was synthesized (Figure 18b).[60] The compounds were used to fabricate blue-emitting electroluminescent devices, with the pyrene derivatives used as the hole-transporting layer, and 1,3,5-tris(*N*-phenylbenzimidazol-2-yl)benzene (TPBI) as the electron-transporting layer. The colour of emission could be further tuned by changing the electron-transport layer to tris(8-hydroxyqunioline)aluminium (Alq_3) to give green emission. The addition of a thin hole-blocking layer was required to achieve recombination, and again give blue emission.[60] Blue emission was also observed in a simpler system when 1,1'-dipyrene and 1,4'-dipyrenylbenzene were incorporated into an OLED system, along with a blue material (not specified in the publication).[61] Both systems show strong luminescence, although the device containing the phenyl linker shows better performance in terms of brightness, luminance efficiency and power efficiency. In another study, 1,3,5-tri(1-pyrenyl)-benzene (Figure 18c) has been synthesized, and was shown to be a blue emitter with high luminance and high efficiency.[62] Elsewhere, a series of 1,6-bis(*N*-phenyl-*p*-(R)-phenylamino)pyrenes was synthesised using Buchwald-Hartwig coupling reactions, between 1,6-dibromopyrene and *N*-phenyl-*p*-(R)-phenylamines.[63] Variation in the nature of the R group (R = CN, F, H, Me, ^{t}Bu, OMe, NPh_2, NMePh) allowed the emission from these derivatives to be tuned over the full-visible colour range. In particular, when incorporated into an OLED device, deep-blue emission was observed with the CN derivative (Figure 18d). Another study[64] involved the syntheses of the related 1,6-$(BMes_2)_2$pyrene (Figure 18e) and 1-$(BMes_2)$pyrene. Along with other aromatic boryl compounds, these derivatives were investigated for their photophysical, electrochemical and fluoride-binding properties. The compound, 1-$(BMes_2)$pyrene was assembled in an electroluminescent device and, using an additional electron-transport

layer, displayed bright electroluminescence. Furthermore, the potential of these derivatives as electron-transport materials was highlighted.[64]

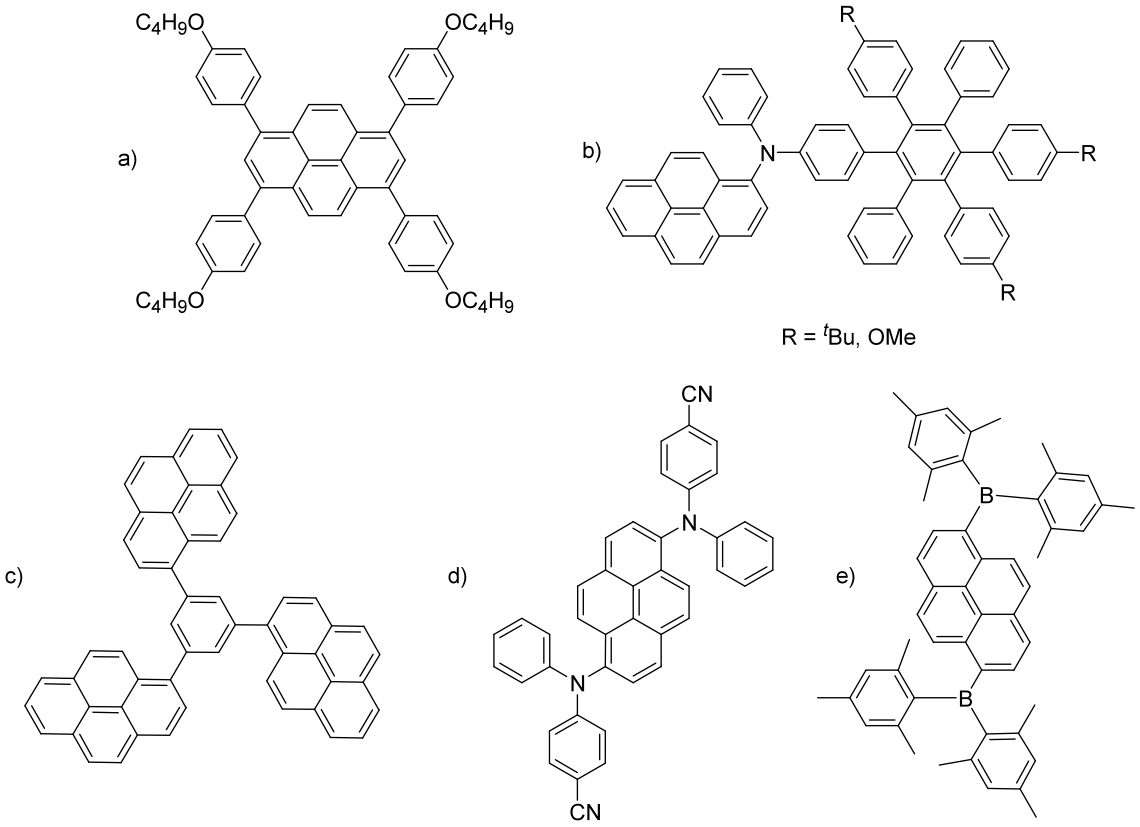

Figure 18 A selection of pyrene-based blue emitters for OLED devices: a) 1,3,6,8-tetrakis(4-butoxyphenyl)pyrene;[59] b) pyrene- hexaphenylbenzene-based triarylamine;[60] c) 1,3,5-tri(1-pyrenyl)benzene;[62] d) 1,6-bis(*N*-phenyl-*p*-cyanophenylamino)pyrene;[63] e) 1,6-$(BMes_2)_2$pyrene.[64]

Further solid-state emitters are now discussed. Highly crystalline oligopyrene nano-wires were synthesized via template-assisted electro-polymerization of pyrene.[65] They exhibited strong fluorescence which could be tuned by altering the excitation wavelength. Blue, green and red emission were observed upon increasing the excitation wavelength. In other work,[66] polypyrene polymers were synthesised by direct chemical oxidative polymerization of pyrene using $FeCl_3$. Characterization of the polypyrene using IR, UV-Vis, ^{1}H NMR, 2D NMR and MALDI-TOF MS found that the polymers were formed mainly through coupling between 2- or 1- or 7- or 8- positions on the pyrene ring. Although the virgin polypyrene polymer has low conductivity (3.4×10^{-8} S

cm^{-1}), doping with iodine was found to increase the conductivity to 2.3×10^{-4} S cm^{-1}. When the virgin polymer was heated to 1300 ºC, its conductivity increased to 81.2 S cm^{-1}. Furthermore, a strong turquoise fluorescence was observed due to the large conjugated π-system. It is hoped that the polymer will find use in photoluminescent devices, including sensors and highly conducting carbon based materials.[66] $FeCl_3$-mediated reactions have also been used to form polypyrene porphyrins.[67] Two pyrene units were incorporated into a diporphyrin tape and were shown to absorb in the near-IR region. Such materials have been used in communications technologies and organic electronics. The inclusion of pyrene moieties also makes the system display intermolecular interactions in both the solid state and supramolecular assemblies.

Another pyrene-containing optical device has been shown to emit circular-polarized luminescence.[68] 1-Pyrenesulfonic acid and (R)-1-phenylethylamine were co-crystallized in EtOH solution to give a 2D layered network, which was characterized by X-ray crystallography. The complex was shown to exhibit circular-polarized luminescence in the solid state and will be useful in the development of solid-state chiral fluorophores.

The discussion so far has focused on materials that are entirely organic based. Several pyrene-containing optical materials that incorporate transition metals are known. One example is a ruthenium(II) bipyridine complex, in which a 1-ethynylpyrene moiety has been attached to the 2,2'-bipyridine ligand (Figure 19a).[69] The complex displayed well-defined absorption and emission spectra. No comparison of its photophysical properties with those of the $[Ru(2,2'\text{-bipyridine})_3]^{2+}$ complex was made; however, it was suggested that the added pyrene acts as a tuning device for the complex, thus modifying it properties for optical applications. In another study,[70] a cyclometallating bridging ligand, 1,3,6,8-tetra(2-pyridyl)pyrene (tppyr) was synthesized (Figure 19b). Reactions of this ligand with $Ru(tpy)Cl_3$ afforded cyclometallated Ru and bis-Ru complexes in moderate yields. Electrochemical studies, suggest that the new ligand could effectively mediate electronic communication between the two cyclometallated centres, which would be of interest in the area of molecular electronics.

Other metal-containing pyrene systems include the complexes from the reactions of 1-(diphenylphosphino)pyrene (1-PyP) and 1,6-bis(diphenylphosphino)pyrene (1,6-PyP) with $M(dppm)(OTf)_2$ (M = Pd, Pt) to give $[M(dppm)(1\text{-PyP})]^+$ and $[M_2(dppm)_2(1,6\text{-PyP})]^{2+}$ (Figure 19c).[71] These complexes with the pyrene unit bound to the metal centres were compared to the dangling complexes $[M(dppm)Cl(1\text{-PyP-H})]^+$ and

$[M_2(dppm)Cl_2(1,6\text{-}PyP\text{-}H_2)]^{2+}$. A comparison of the absorption spectra showed that they were all similar. This is surprising considering that the electronic properties of the two metals are different, and leads to the suggestion that the greatest perturbation of the pyrene is by the PPh_2 group rather than by coordination to the metal. Therefore, there is a weak π-interaction between the metal ions and the pyrene moiety. The difference between the metallated and dangling compounds was observed when the phosphorescence was investigated, as it was found that the metallated complexes displayed phosphorescence quantum yields around three orders of magnitude higher. It is therefore shown that for the enhancement of phosphorescence, in pyrene, direct coordination to a heavy atom is required.[71] However, in another study,[72] the opposite was observed in a series of Pt-based pyrene derivatives. In this case, pyrene-containing cycloplatinated complexes in which the pyrene is directly cycloplatinated (Pt-1), (Figure 19d) attached to a ppy ligand through a C-C single bond (Pt-2) (Figure 19d) or attached to a ppy ligand through a C≡C triple bond (Pt-3) (Figure 19d). All of the complexes exhibited deep-red phosphorescence at room temperature, although the phosphorescence was most intense with Pt-2, in which the pyrene moiety is not directly cycloplatinated.[72]

A different system involves mono- and di-gold(I) pyrenes (Figure 19e), synthesized from arylation of gold(I) substrates by 2,7-bis(Bpin)pyrene and 2-(Bpin)pyrene in the presence of Cs_2CO_3.[73] The gold fragment is added to the pyrene to increase the spin-orbit coupling, and hence increase phosphorescence. The latter was observed both at room temperature and at 77 K. Detailed studies showed that the absorption spectra consisted of characteristics of the aromatic skeleton, and that the emission came from the ππ* states of the aromatic core.

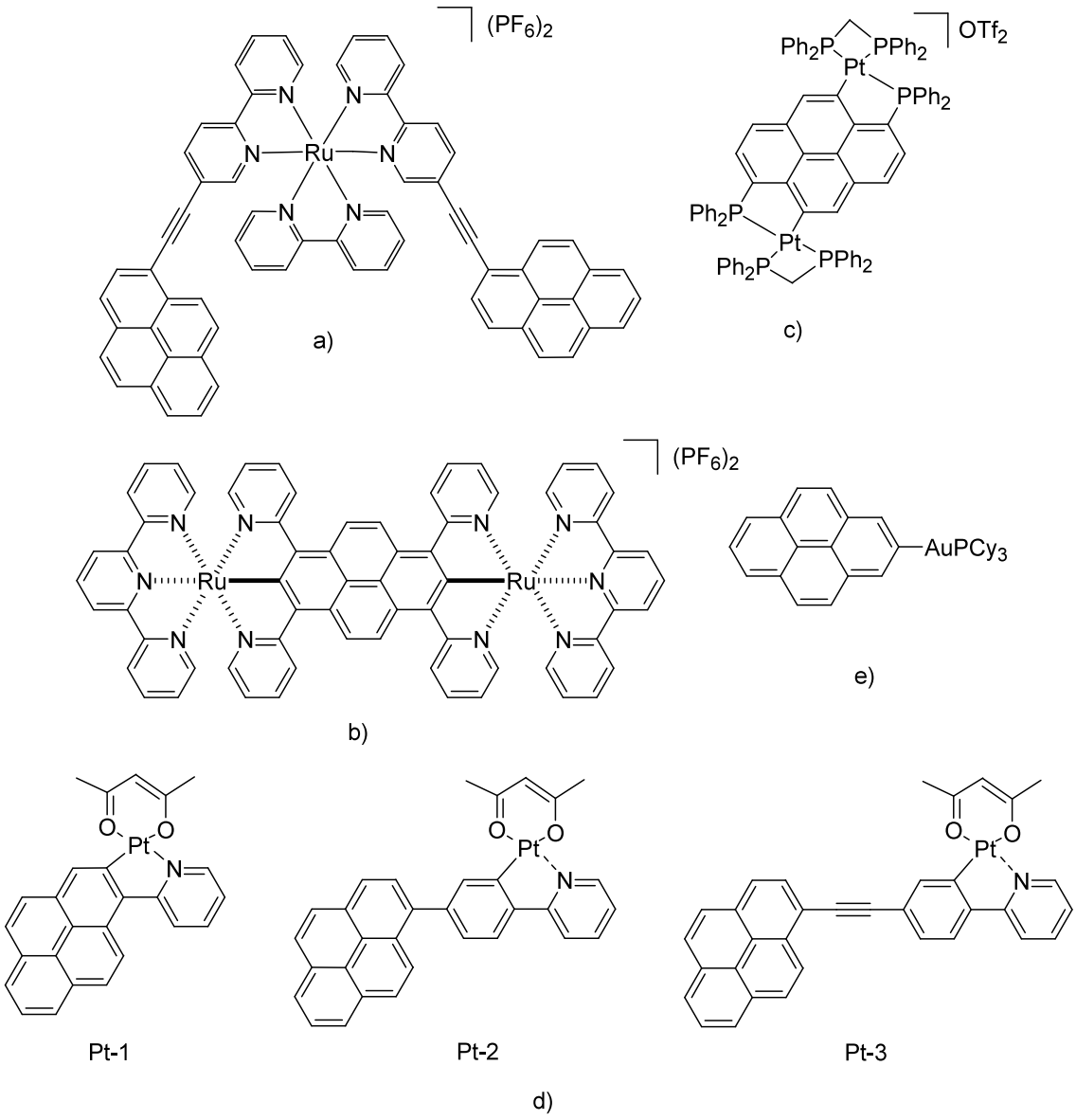

Figure 19 Selected metal-containing pyrene derivatives for optical applications: a) pyrene modified ruthenium(II) bipyridine complex;[69] b) cyclometallated ruthenium with a tppyr bridge;[70] c) $[Pt_2(dppm)_2(1,6\text{-}PyP)](OTf)_2$;[71] d) cycloplatinated complexes Pt1-3;[72] e) Pyrene-2-$AuPCy_3$.[73]

Metal-containing pyrene-based optical devices can also be used to study the photophysical properties of organometallic systems. A series of 2-(R)-5-pyrenylacetylene-thiophenes (R = H, Br, COH, $CHC(CN)_2$) was synthesized, and shown to display strong fluorescence (intense emission spectrum) at room temperature in solution. Upon addition of $Co_2(CO)_6$ and subsequent coordination via the ethynyl bridge, the emission is quenched.[74] It is suggested that this is a result of energy-transfer

from the pyrene moiety to the cobalt metal centres. Upon cooling to 77 K, the energy transfer is not observed and the quenching of the fluorescence is less efficient. This study gives insight into the photophysical processes that occur in organometallic complexes.

2.2.2 Fluorescence Probes

In the above examples, it has been shown that the photophysical properties of pyrene can be modified by derivatization. Changes in the surrounding environment and addition of external substrates can also influence the photophysical properties of pyrene. This influence has been used to develop fluorescent probes and sensors, which are now discussed.

In Section 1.1, it was stated that pyrene had a long fluorescence lifetime (354 ns in toluene). As a result of this long-lived fluorescence, the vibronic bands in the emission spectra of unsubstituted pyrene are very susceptible to changes in local environment (known as the Ham effect).[75] In the presence of polar solvents, there is significant enhancement in the intensity of the (0,0) vibronic band at the expense of other bands in the emission spectrum (Figure 20).[75a] It has been shown that perturbation is dependant upon the dipole moment of the solvent rather than the dielectric constant of the bulk solvent. This suggests that a pyrene-solvent dipole-dipole interaction mechanism is responsible for the changes in the emission spectrum. A later study demonstrated the influence of a non-polar solvent, C_6F_6, on the photophysics of pyrene, and detailed experimental and theoretical studies revealed the formation of weak complexes formed by arene-perfluoroarene interactions, even in very dilute solutions.[76]

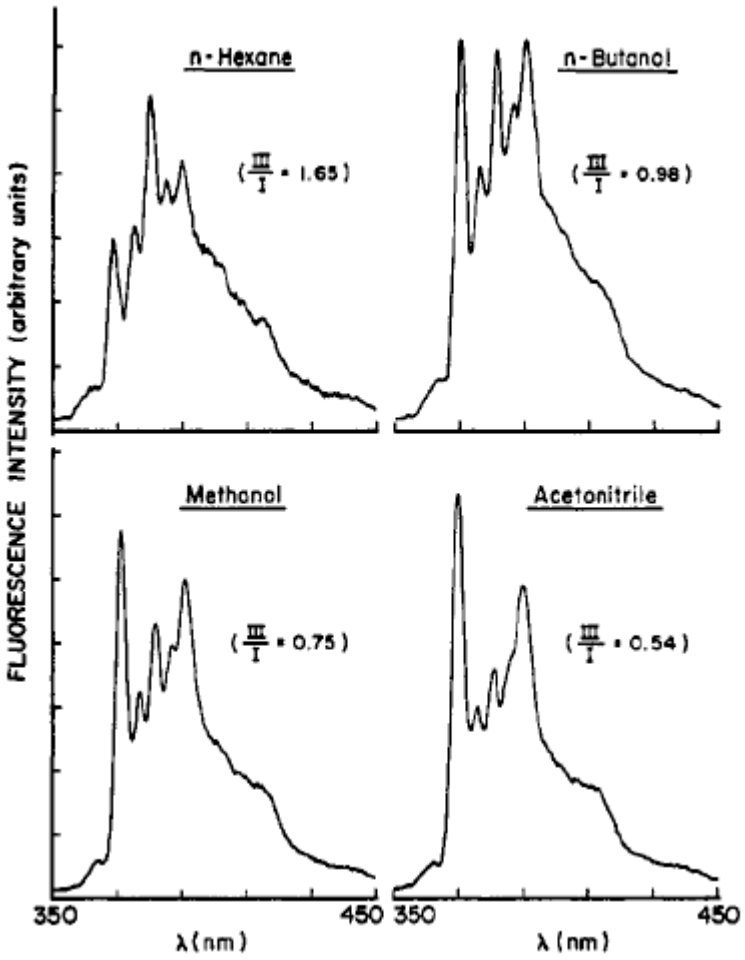

Figure 20 Solvent-dependence of vibronic band intensities in pyrene monomer fluorescence.[75a] Reproduced by permission of The American Chemical Society.

The above observations have also been used to determine critical micelle concentrations (CMC).[75a] Pyrene is insoluble in water; however, the addition of surfactant molecules acts to dissolve pyrene. Upon micelle formation, the pyrene molecules become enclosed in the hydrophobic centre of the micelle, and thus are now in a different environment. The change in environment, from individual molecules in solution to micelles, is reflected in the emission spectrum of pyrene, whereas a change in vibronic fine structure is observed. As more surfactant is added, the change in the emission spectrum is monitored by calculating the ratio of the 0-0 and the 3-0 peaks (0-0 corresponds to the transition between the lowest vibrational level in the excited state to the lowest vibrational level in the ground state; 3-0 originates from the third vibrational level in the excited state). Accurate CMC values have been determined, which are in good agreement with those obtained by other methods.[75a] More recently, the incorporation of

pyrene into the centre of micelle systems has been used for the detection of chloride anions in water.[77] Along with pyrene, a rhodium-based receptor molecule ([Rh(Cp*)H_2O(3-(2-pyridyl)-5,6-diphenyl-1,2,4-triazine-*p*,*p*'-disulfonic acid)] was added that quenched the fluorescence of pyrene when bound to a chloride ion. Hence, by monitoring the changes in the emission spectrum of pyrene, a quantitative measure of chloride ions present in solution can be obtained.

Sensing applications in which pyrene derivatives are used are now considered. Several 1-substituted derivatives with various aryl and heteroaryl groups were used to investigate changes in solvent polarity.[78] In particular, 4-(pyren-1-yl)benzonitrile and ethyl 4-(pyren-1-yl)benzoate probes showed high fluorescence quantum yields and strong solvatochromism. These two species are proposed as probes for the detection of changes in the polarity of surrounding media. In another example, a pyrene-based ligand, 1,3,6,8-tetrakis(*p*-benzoic acid)pyrene was incorporated into an indium-based MOF.[79] It was found that the fluorescence properties of pyrene (and structural properties of the MOF) changed upon the addition of various non-polar (toluene) and polar (DMF, dioxane) solvents.

Pyrene-based probes have also been used to investigate biological systems.[80-83] One of the most common fluorescent probes is the commercially available 4-(pyren-1-yl)-butyric acid **31** (Figure 21). This derivative is used to determine oxygen concentrations in biological systems.[80] In an oxygen-free environment, 4-(pyren-1-yl)-butyric acid has a long fluorescence lifetime (τ_f = 460 ns in MeOH). Thus, substrates that can perturb the nature of the excited state have time to diffuse to the excited state molecules before emission. Oxygen is known to be a strong quencher of electronic excited states. In systems with short fluorescence lifetimes, the effect of oxygen on the excited state is negligible; however, due to the long lifetime value of 4-(pyren-1-yl)-butyric acid, the influence of oxygen can be observed by changes in the fluorescence quantum yield and lifetime.[80a] As several biological processes involve the consumption (mitochondrial electron-transport chain) or expulsion (photosynthesis) of oxygen, methods to detect oxygen and determine its concentration are of use in the investigation of biological systems. Generally, a probe is placed in a macromolecule, such as a protein or even a living cell, and changes in the fluorescence intensity[80e] or fluorescence lifetime[80g] due to quenching by oxygen are monitored. The advantage of the latter method is that fluorescence lifetimes are not dependant on the absolute intensity of the emitted light,

and are therefore independent of the concentration of the probe. To determine oxygen concentrations, control experiments are first needed to calibrate the response of the probe.

The deprotonated form of 4-(pyren-1-yl)-butyric acid has also been used to translocate arginine-rich peptides across cell membranes.[81a] It is believed that the hydrophobic nature of the pyrene moiety aids the translocation through the lipid bilayers of the cell. If modified arginine peptides can be translocated into a cell, then this method can be used to introduce external substrates into a cell, which has potential medicinal and labelling applications. However, a recent study has shown that modified arginine peptides containing a semiconductor quantum dot are not translocated into a cell,[81b] presumably due to their large size; hence, careful modification of the arginine peptide is required.

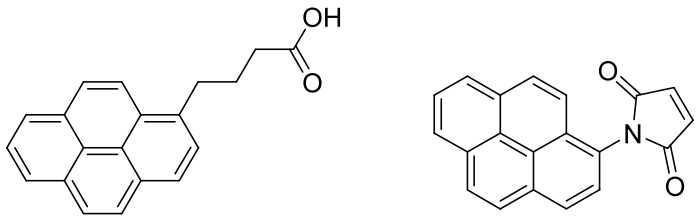

Figure 21 Commerically available pyrene probes: 4-(pyren-1-yl)-butyric acid (left) and *N*-(1-pyrenyl)maleimide (right).

Another commercially available pyrene-based probe is *N*-(1-pyrenyl)maleimide (Figure 21).[82] This probe is used for labelling thiol side-chains on cysteine (Cys) residues in proteins and peptides. Before formation of the thiol adduct, the fluorescence of *N*-(1-pyrenyl)maleimide is quenched, whereas upon binding to the thiol, the fluorescence is restored. Hence an 'on-off' switch for the labelling of Cys residues is presented.[82] Furthermore, the *N*-(1-pyrenyl)maleimide-Cys adduct can be monitored by fluorescence depolarization studies. In these experiments, the pyrene moiety is excited by plane-polarized radiation, then the fluorescence monitored. The extent of depolarization in the emitted fluorescence is dependant upon the motion of the pyrene moiety during the time between absorption and emission. When *N*-(1-pyrenyl)maleimide is bound to a Cys residue in a tightly packed environment, the amount of depolarization will be small because the pyrene moiety is not free rotate or move. In contrast, extensive depolarization will be observed when the pyrene is in an environment where it is free to

rotate and move.[82] When attached to a Cys residue in a protein, *N*-(1-pyrenyl)maleimide allows the conformation and movement of the Cys residue to be monitored. This application makes use of the long fluorescence lifetime of pyrene, which occurs on a timescale that is similar to that of the changes in molecular conformation of the Cys residues in the proteins under study. More recently, pyrene probes which contain a maleimide moiety that is separated from pyrene by an aryl-ethynyl spacer group have been developed.[83] These probes were shown to display an improved fluorescence quantum yield when bound to Cys residues, compared to *N*-(1-pyrenyl)maleimide. Many other examples of pyrene-based biomolecular probes exist for labelling and conformational studies on specific sites in proteins and other biological macromolecules, including a dialkynylpyrene skeleton with an oxyethylene unit.[84] This derivative was synthesized to interact with and probe the nature of hydrophobic cavities in proteins. In another example, the pyrene-functionalized bis(thiosemicarbazonato)-zinc and copper complexes were synthesized and were shown to have potential for use as both *in vitro* fluorescence probes and *in vivo* PET (positron emission tomography) imaging probes.[85] Nearly all these probes make use of the high sensitivity of the emission of pyrene to changes in environment, as well as its long fluorescence lifetime.

2.2.3 Pyrene Based Sensors

As well as probing changes in local environment, pyrene derivatives have been incorporated into sensors to detect external substrates. Often, these systems contain two or more pyrene moieties. Generally, in the absence of an external substrate, monomer emission is observed from the pyrenes, and when the external substrate is detected, it effects some conformational change in the sensor, which brings the two pyrene units together and excimer emission is observed. The amount of substrate can be determined by the monomer/excimer fluorescence-intensity ratio. Several examples are discussed below.

In biological systems, sensors bearing two pendant pyrene moieties bound to a Zn(II)-cyclen complex have been used to detect thymidine-phosphate residues (Figure 22a).[86] Upon binding of the thymidine-phosphate to the zinc atom, as well as several of the nitrogen atoms in the cyclen backbone, the two pyrene units are brought close together and excimer emission is observed. This system was shown to be selective for thymidine residues over other nucleotides and ions. In a related system, two Zn(II) complexes

containing one pyrene moiety each were used as the sensing system (Figure 22b). A macromolecular complex was formed between uridine or thymidine phosphates and two Zn(II) complexes. Upon formation of this macromolecule, the pyrene moieties from two separate Zn(II) complexes formed the excimer.[87] Other zinc-based sensing systems include the [Fc-bis{Zn(II)(1,4,7-triazacyclononane)-(pyrene)}] complex (Figure 22c), which not only detects a range of polyphosphate nucleotides by making use of the excimer fluorescence from the two pyrenes, but also through changes in the electrochemical properties of the ferrocene.[88] A similar system, which contains a pyrene linked to a ferrocene by a 1,2,3-triazole ring (Figure 22d), also displays changes in its electrochemical and fluorescence properties upon binding to the pyrophosphate anion.[89] Such systems are said to display dual-mode recognition, as they can detect substrates by using two different techniques. Biological molecules other than nucleotides can also be detected. Heparin is a clinically used anti-coagulant in cardio-pulmonary surgery; however, if an overdose is taken, potentially lethal effects can occur. A quinine derivative bearing a pyrenyl group as a fluorophore has been designed and synthesized (Figure 22e).[90] It was shown that two of these molecules bind to heparin to form a supramolecular complex that leads to excimer emission. The formation of this complex is believed to be made favourable by intermolecular π-π stacking interactions between the pyrene moieties. Overall, the sensor showed high selectivity and sensitivity for heparin at clinically relevant concentrations. Other supramolecular assemblies have been used to detect glucose, which has potential for the monitoring of blood glucose concentration, and may be useful for patients suffering from diabetes.[91] The detection method involved formation of a polymer containing multiple boronic acid functional groups. These can then interact with the alcohol units on the glucose structure to form polyanions. The next stage is to add a positively charged trimethylpentylammonium substituted pyrene fluorescent probe (Figure 22f). Aggregation of the cationic pyrene compounds around the polyanion occurs and, as a result, excimer emission is observed. It was found that the excimer emission intensity increased with increasing glucose concentration. Studies with other sugars showed similar results.[91]

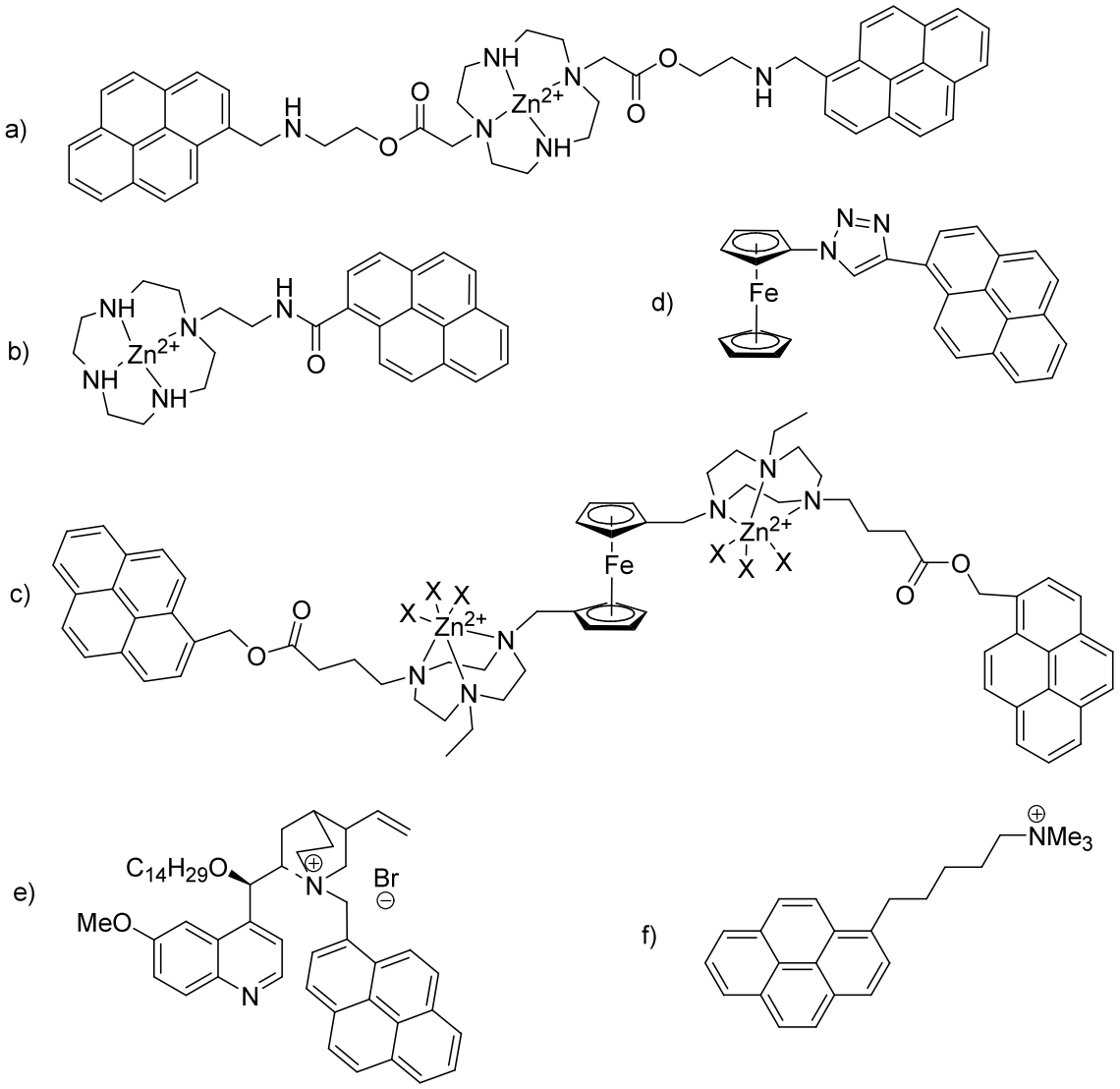

Figure 22 Pyrene-based sensors. For the detection of phosphate residues: a) Zn(II)-cyclen complexes with two pendant pyrenes[86]; b) one pendant pyrene[87]; c) [Fc-bis{Zn(II)(1,4,7-triazacyclononane)-(pyrene)}] complex[88]; d) Ferrocene-pyrene dyad;[89] For heparin detection: e) Pyrene based quinine derivative.[90] For glucose detection: f) trimethylpentylammonium pyrene.[91]

Pyrene excimer emission has also been used to study natural systems. The natural product *myo*-inositol 1,2,3-triphosphate (Ins(1,2,3)P_3) is known to be an iron chelator and an anti-oxidant.[92] In work to determine the structure of the iron bound complex, DFT calculations showed the possibility of two isomers. Studies by NMR failed to give any insight due to peak broadening, so conformational studies were developed. Addition of pyrene units to the analogous Ins(1,2,3,5)P_4 compound allowed excimer emission to be observed when the conformation flipped between the penta-equatorial

and penta-axial conformations (Figure 23). The fluorescence emission spectra were recorded in the absence and presence of Fe^{3+} and it was found that, upon metal-ion addition, the excimer fluorescence increased with simultaneous decrease in the monomer fluorescence. This excimer emission is due to the penta-axial conformation.[92] The study gives evidence for a penta-axial conformation in Ins(1,2,3)P_3 in the presence of iron and also shows how a fluorescent probe can be used to determine conformational changes in chemical systems.

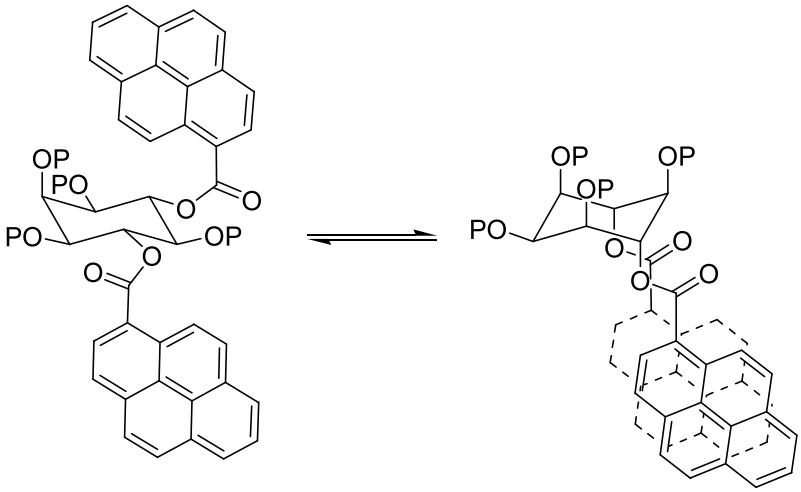

Figure 23 Penta-equatorial (2A) and penta-axial (2B) conformations of Ins(1,2,3,5)P_4.[92]

In the last example, the addition of a metal ion was used to bring about change in a sensing system. The detection of metal ions using pyrene-excimer emission is a well-studied area and is discussed.

A selective system for the detection of Cu^{2+} ions was developed by synthesizing a monopyrenylalkyl derivative bearing a sulphonamide (Figure 24a).[93a] In free solution, the derivatives form dimer species by hydrogen bonding between the amine NH and oxygen. No excimer emission is observed due to the pyrene units being kept apart. Upon addition of Cu^{2+}, the dimer undergoes a conformational change, the pyrene units are brought together and excimer emission is observed, with subsequent decrease in monomer emission. No changes in the fluorescence spectra were observed upon addition of other metal ions.

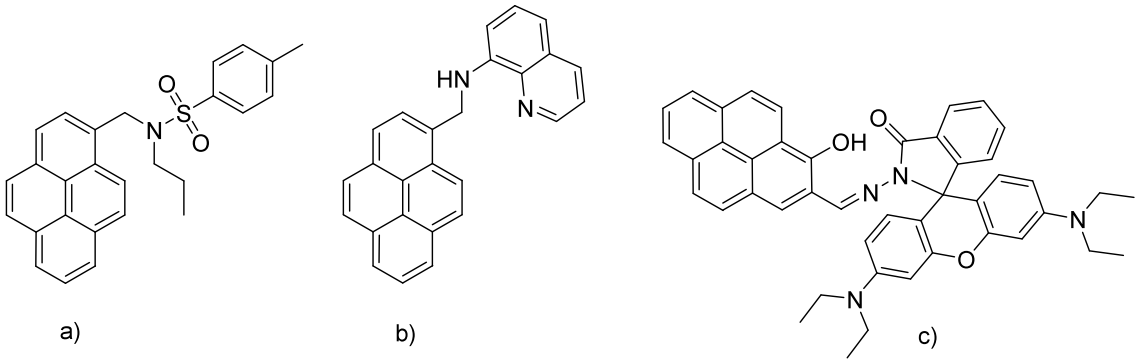

Figure 24 Pyrene based Cu^{2+} sensors: a) monopyrenylalkylsulfonamide derivative;[93a] b) pyrenylquinoline derivative;[93b] c) pyrene-rhodamine derivative.[94]

The system has been further developed by replacement of the sulfonamide with a quinoline (Figure 24b).[93b] Upon addition of Cu^{2+}, individual pyrene derivatives formed dimers and excimer emission was observed. The most intense excimer emission was observed when the spacer length between pyrene and quinoline was kept to a minimum. Later, a pyrene-rhodamine derivative was synthesized for the selective detection of Cu^{2+} (Figure 24c).[94] In this case, a change in fluorescence in the sensor was caused by a ring-opening/closing process facilitated by the addition of Cu^{2+} ions.

Other metal ions, such as Ag^{+}, can be detected by the changes in the structure of the sensor molecule. An adenine-pyrene conjugate was synthesized. In the presence of Ag^{+} ions, individual conjugates join together in a polymer-like structure.[95] These chains of alternating pyrene and silver-coordinated adenine were shown to pack together in a box-like structure, through hydrogen bonding and π-π stacking interactions. The resulting supramolecular assembly displayed excimer emission.

An important class of pyrene-based sensors contain a calix[4]arene framework. These systems generally contain two or more pyrene moieties attached to a calix[4]arene (Figure 25a). When a metal ion is present, a change in the conformation of the system occurs leading to excimer formation, which can be monitored by measuring the monomer/excimer fluorescence-intensity ratio. These systems have been shown to detect toxic metal ions, such as Hg^{2+}, Pb^{2+} and Cd^{2+}, and have the potential to be used as cheap, selective and sensitive sensors for these ions in drinking water supplies.[96]

A range of calix[4]arene systems containing two, three and four pyrene units has been synthesized.[97] As expected, the intensity of excimer emission increased with the number

of pyrene units, along with a decrease in the monomer emission intensity. Various metal ions (Li^+, Na^+, K^+, Zn^{2+} Co^{2+}, Mg^{2+}, Al^{3+}, Cu^{2+} and Pb^{2+}) were added and the fluorescence spectra recorded. In the case of the calix[4]arene containing two pyrene units, the change in fluorescence occurs for nearly all of the metal ions. However, in the case of the tri- and tetra-pyrenyl calix[4]arenes, no changes in the emission are observed, except with Pb^{2+} and Cu^{2+}. It is suspected that for Pb^{2+} the fluorescence is quenched by a heavy metal ion effect, while in the case of Cu^{2+}, charge-transfer from the Cu^{2+} d-orbitals to the pyrene π*-orbitals is thought to lead to quenching. These complexes display a form of selective detection for different metal ions.[97]

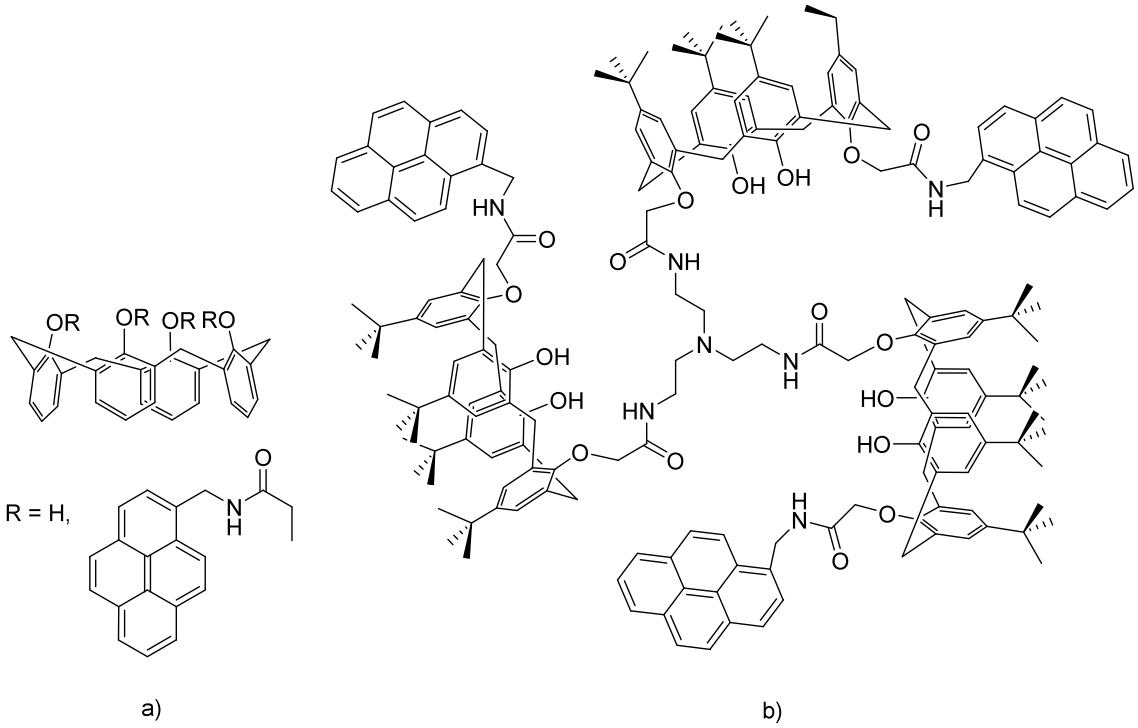

Figure 25 Pyrene based calix[4]arenes for the detection of metal ions. These systems generally involve (a) substitution of the calix[4]arene with 2-4 pyrene units[97] or (b) three calix[4]arene moieties connected to a central nitrogen atom.[98]

In another study, a *tren-N*-tri-calix[4]arene with three pyrenyl groups was synthesized (Figure 25b).[98] This molecule consists of a central nitrogen atom, bound to three seperate calix[4]arenes, each with a pyrenyl group. In the absence of metal ions, excimer emission was observed. However, when Al^{3+} was added, the excimer emission decreased and the monomer emission increased. NMR and MALDI-TOF mass

spectroscopy studies showed evidence for a 1:1 complex in solution, and led to the conclusion that the Al^{3+} was bound symmetrically in the centre of the tri-calix[4]arene. In contrast, a related structure with only two pyrene appended calix[4]arenes showed no change in its properties upon addition of Al^{3+} ions; hence the tripod structure is required for Al^{3+}-binding.[98]

Further *tren-N*-tri-calix[4]arenes were reported. A *N*-tripodal molecule containing two calix[4]arene branches with an amido-pyrenylmethyl moiety attached and a third branch, which is a rhodamine B moiety, was synthesized.[99] Upon addition of Hg^{2+} ions to a solution containing the sensor, enhanced fluorescence emission was displayed. In this case, the fluorescence is the result of fluorescence-resonance energy-transfer (FRET). This is the excited state energy interaction between two fluorophores: an excited donor transfers energy to an acceptor, which undergoes fluorescence. The addition of Hg^{2+} affects energy-transfer from the pyrenyl excimer to the rhodamine moiety, a so-called FRET-ON process. When Al^{3+} cations are added, only an increase in the pyrene excimer emission and no FRET-ON behaviour is observed. It was found that the modified calix[4]arene was selective for the binding of Hg^{2+} over other metal ions, except for Al^{3+} which displaced the Hg^{2+} upon addition. Recently, a different calix[4]arene sensor bearing a rhodamine and two pyrene fluorophores was synthesized, and was shown to display higher selectivity for Hg^{2+} ions (Figure 26). Upon coordination, a FRET-ON process occurs from the newly formed pyrene excimer to the rhodamine moiety, which has undergone a ring-opening transformation.[100]

Another system has two pyrene units bound to a calix[4]arene by 1,2,3-triazole linkers.[101] The compound displayed strong excimer emission in solution; however, upon addition of various metal ions, it was found that the excimer emission decreased and the monomer emission increased. It is believed that the ions are bound between the two triazole linkers and, upon binding, force the pyrene units apart, thereby reducing excimer emission. To examine the selectivity of the chemosensor, competing metal ions were added to the mixture. It was found that the calix[4]arene was selective for Zn^{2+} and Cd^{2+} cations over Group 1 and 2 metal ions, as well as silver and lead. However, the addition of mercury and copper caused fluorescence quenching.[101]

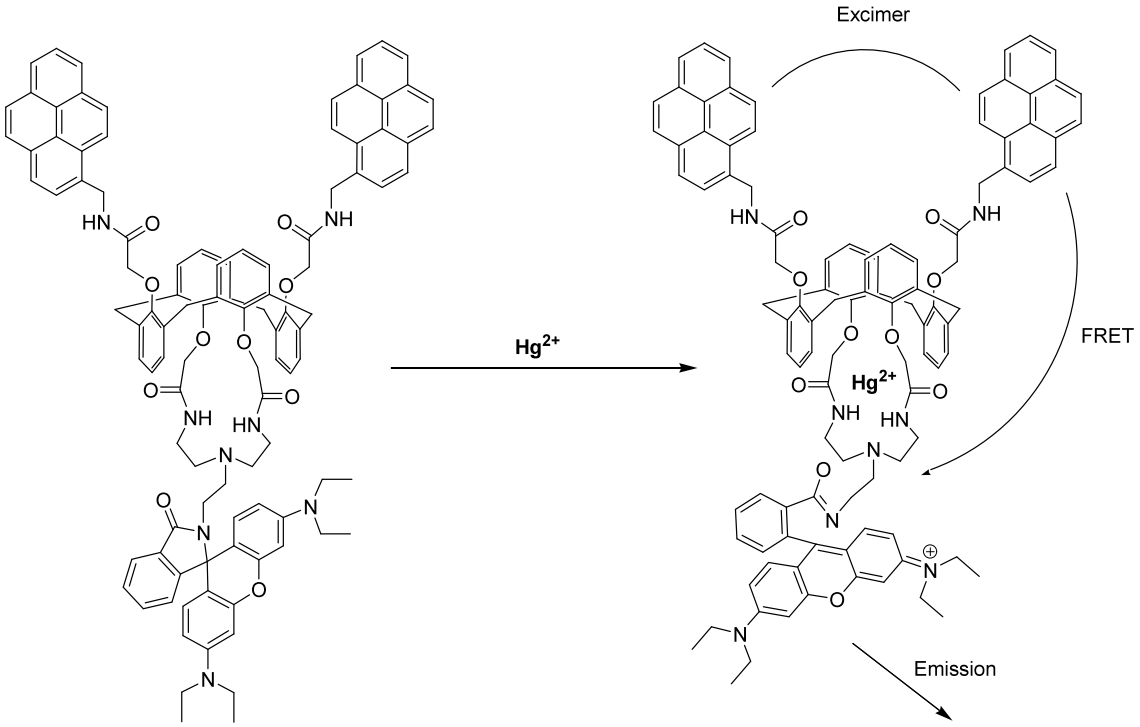

Figure 26 Detection of Hg^{2+} by FRET between a pyrene excimer and rhodamine in a pyrene-based calix[4]arene chemosensor.[100]

Other calixarene-based pyrene sensors have been developed to detect organic substrates. In the presence of fluoride (from tetrabutylammonium fluoride), the chemosensor calix[1]pyreno[3]pyrrole undergoes a conformational change (Figure 27a).[102] This conformational change facilitates the detection of C_{70}. This study was undertaken to demonstrate the ability of calixarene-based pyrene sensors to detect electron-deficient guests. This concept has been developed to detect other electron-deficient guests, such as trinitroaromatic explosives.[103] A dipyrenylcalix[4]arene was found to display excimer emission in the absence of any explosive substrate (Figure 27b). Upon detection of a highly nitrated aromatic species, the excimer emission is quenched. The authors use X-ray crystallography and theoretical studies to show evidence for a charge-transfer mechanism between the pyrene and the trinitroaromatic analyte.

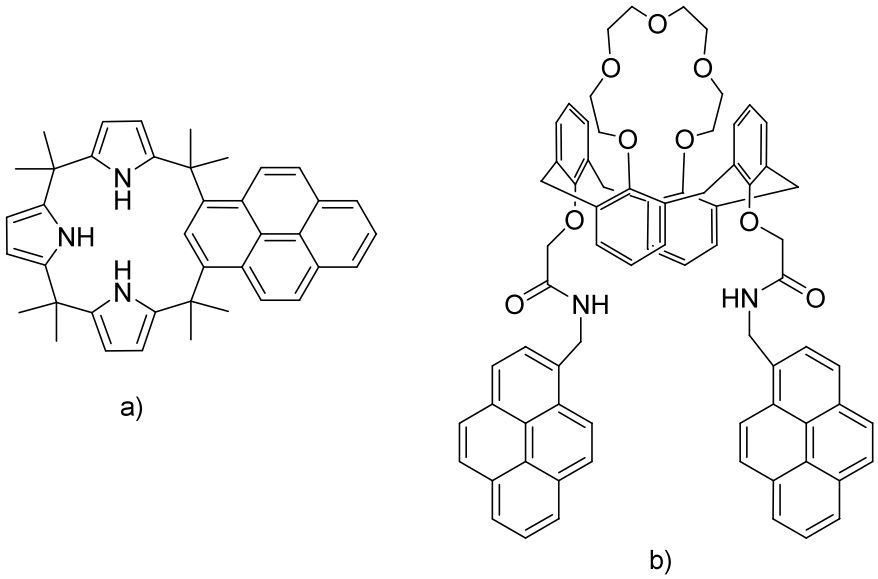

Figure 27 Calixarene-based pyrene sensors for the detection of organic substrates: a) calix[1]pyreno[3]pyrrole for C_{70} sensing;[102] b) the dipyrenyl calix[4]arene can detect trinitrotoluene (TNT).[103]

2.3 Charge-Transfer Applications: DNA and RNA Systems

Applications that make use of the charge-transfer properties of pyrene are now considered. Although charge-transfer applications involving pyrene are numerous, this section will focus on charge-transfer applications in biological systems that contain DNA and RNA. Further applications of pyrene-based DNA/RNA systems that make use of the aforementioned structural and optical properties will also be discussed. These examples are included in this section in order to group all of the pyrene-based DNA/RNA applications together.

2.3.1 Electron-Transfer in DNA and RNA

Numerous pyrene-modified DNA and RNA systems have been synthesized by addition of the pyrene moiety to nucleobases. A Suzuki-Miyaura cross-coupling between the iodinated nucleoside and pyrene-1-boronic acid gave the pyrene-modified nucleosides shown in Figure 28 in good yields.[104]

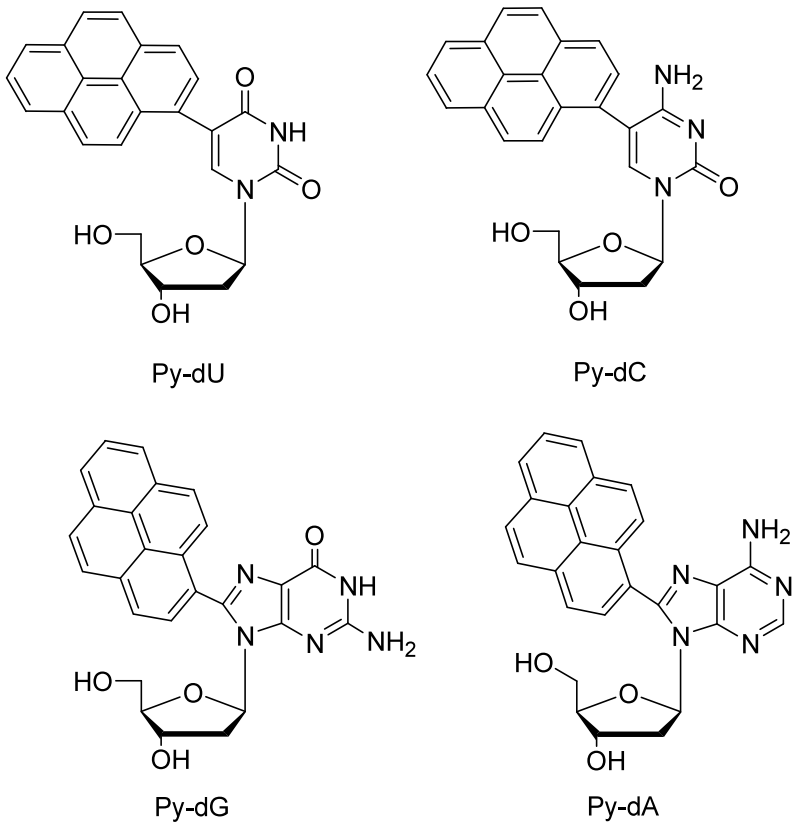

Figure 28 Pyrene-modified nucleosides, 5-(1-pyrenyl)-2'-deoxyuridine (Py-dU), 5-(1-pyrenyl)-2'-deoxycytidine (Py-dC), 8-(1-pyrenyl)-2'-deoxyguanosine (Py-dG), 8-(1-pyrenyl)-2'-deoxyadenosine (Py-dA).[104]

These compounds were synthesized to investigate DNA-mediated charge-transfer, which involves injection of a negative charge into DNA bases by a donor molecule. The charge can then move through DNA over significant distances to an acceptor molecule. As well as gaining insight into biological processes, this charge-transfer process has potential application in nanoscale devices.[105]

Transfer of charge along DNA involves oxidation and reduction of DNA bases, which in turn, affects their acidity and basicity. Altering the pH of the surrounding solution gives insight into the effect of proton addition or removal on the charge-transfer.[104b] Excitation of the pyrene moiety on the above nucleoside gave DNA radical bases via electron-transfer from the pyrene. Two pathways are now possible: either electron transfer back to the excited state and then emission, or quenching by addition or removal of a proton. Emission spectra recorded at different pH values show the effect of addition or removal of a proton on the electron-transfer process. The results showed that

proton-transfer does not interfere with electron transfer between dU-dA base pairs, but has a large influence on the electron-transfer between dC-dG base pairs.[104b] The importance of protons in electron-transfer along DNA was further probed by comparing the dynamics of Py-dU in an aprotic solvent (MeCN) and a protic solvent (MeOH).[106] Observation of the charge-transfer state, Py^{+}-dU^{-} (due to electron-transfer), by various spectroscopic methods showed a greater electron-transfer yield in MeOH. The presence of protons is therefore shown to facilitate electron-transfer in DNA bases.[106] These studies give insight into the mechanism of charge-transport along DNA, which in turn give insight into DNA damage caused by radical nucleobases.

Further investigation into the mechanism of electron-transfer used Py-dU as an electron-donor and Br-dU as an acceptor. Several DNA duplexes were synthesized with the donor and acceptor placed adjacent to each other, or separated by one A-T base pair.[107] Femtosecond pump-probe spectroscopy was used to monitor the electron-transfer dynamics. Excitation gave the pyrene excited state (Py-dU*), which then underwent electron-transfer to form an ion pair (Py^{+}-dU^{-}). The rate of electron-transfer to the nucleotide can be obtained from the decay of the Py-dU* absorption band. The time taken to return to the Py-dU ground state was found to be around 250 ps longer than the lifetime of the ion pair state, suggesting that an additional decay mechanism was occurring, as well as charge recombination. Chemical monitoring of the Br-dU nucleotide showed that this other mechanism was electron-transfer along the DNA to the acceptor. As Br-dU undergoes chemical change after a one electron reduction, this change can be monitored using piperidine-induced strand-cleavage. The rate of cleavage occurred faster when the Py-dU and Br-dU moieties were adjacent to each other than when they were interspaced by one A-T base pair. Hence, the rate of electron-transfer in DNA is related to its structural configuration.[107]

A more recent study investigated the products formed after excitation of pyrene and subsequent electron-transfer along a polynucleotide.[108] It was shown that the variation in distance between pyrene donor and Br acceptor influenced the oxidation product (Figure 29). Upon irradiation, an electron is transported along the oligodeoxynucleotide (ODN) backbone, leading to radical cleavage of the Br acceptor. The remaining radical can transfer to a neighbouring sugar ring by abstraction of a proton from either the C1' or C2' positions. Two different pathways are now possible, and the rate of each pathway was found to be dependant upon the distance between the donor and acceptor

in the DNA backbone. This radical can now recombine with the one on pyrene, through charge-transfer along the DNA backbone, and the remaining positive charge on the sugar ring can form an OH at the C1' or C2' position when H_2O is added. The second pathway involves no recombination of radicals, and instead oxy-pyrene is formed, as well as the OH at the C1' or C2' position. At larger distances between the donor and acceptor, it was found that the latter pathway dominated.[108]

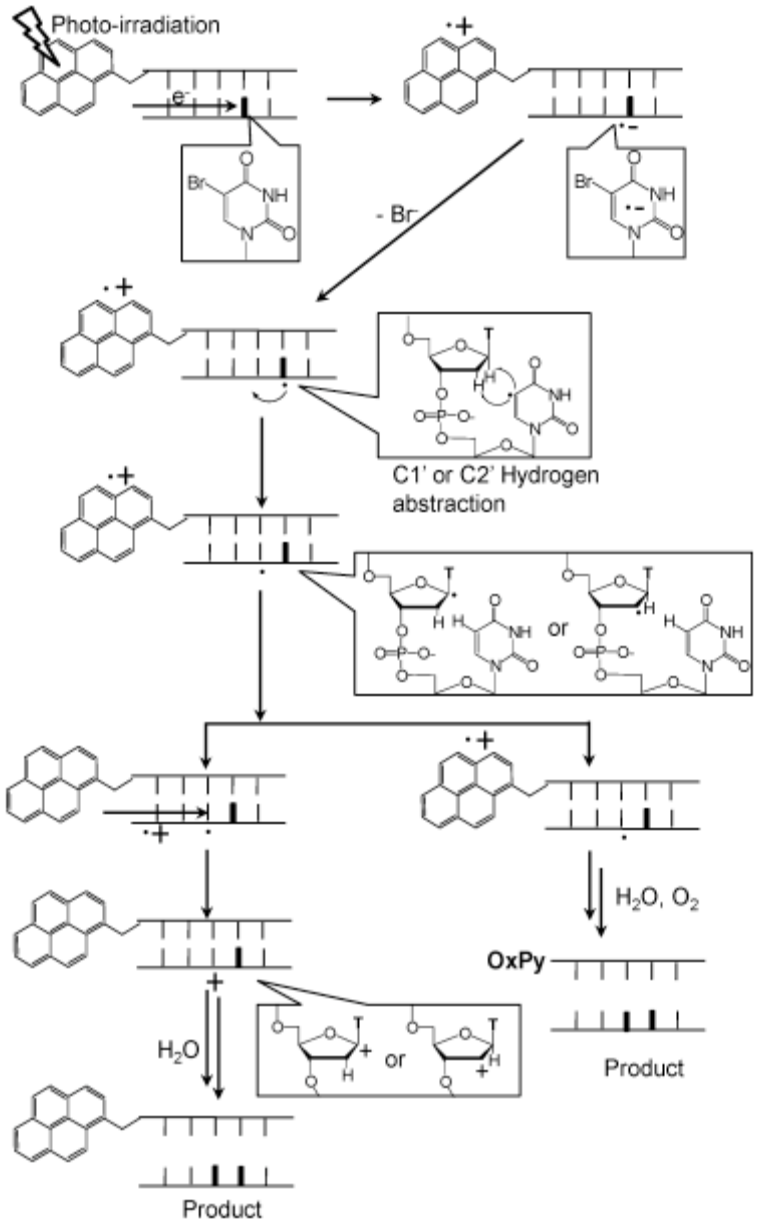

Figure 29 Electron-transfer along the DNA backbone leads to different oxidation products depending on the number of nucleotides between donor and acceptor.[108] Reproduced by permission of The American Chemical Society.

The mediated electron-transfer has also been investigated in RNA.[109] After excitation of pyrene and subsequent electron-injection into RNA, it was shown that the electron can travel large distances along the RNA stacks. Using pyrene as the electron-donor and nitrobenzene as the acceptor, it was shown that, upon excitation, the level of quenching could be monitored by measuring the fluorescence quantum yield. Upon irradiation of pyrene, the electron could return to the ground state and emit (fluoresce), or transfer along the RNA backbone to the nitrobenzene acceptor, leading to a quenching of fluorescence. The quantum yields were found to be much lower for the donor/acceptor-containing nucleotides than the ones containing just pyrene and no acceptor (Table 1). Hence, transfer of electrons along the RNA backbone occurs. The quantum yields were shown to increase with an increase in the number of uridine bases inbetween the donor and acceptor, highlighting the high efficiency of electron-transfer over short distances.[109]

Duplexes with rA_{20}	ϕ
5'-r**U**$_4$U$_{Pyr}$**U**$_{14}$U-3'	0.152
5'-r**U**$_4$U$_{Pyr}$U$_{NB}$**U**$_{13}$U-3'	0.008
5'-r**U**$_4$U$_{Pyr}$**U**U$_{NB}$**U**$_{12}$U-3'	0.022
5'-r**U**$_4$U$_{Pyr}$**UU**U$_{NB}$**U**$_{11}$U-3'	0.075
5'-r**U**$_4$U$_{Pyr}$**UUUU**U$_{NB}$**U**$_9$U-3'	0.104
5'-r**U**$_4$U$_{Pyr}$**UUUUUU**U$_{NB}$**U**$_7$U-3'	0.117
5'-r**U**$_4$U$_{Pyr}$**UUUUUUUUU**U$_{NB}$**U**$_4$U-3'	0.123

Table 1 Fluorescence quantum yields of oligo-RNA duplexes: rA_{20} = A 20 riboadenine nucleotide strand. U_{Pyr} = pyrene-modified nucleotide (electron-donor). **U** = unmodified uridine nucleotide. U_{NB} = nitrobenzene-modified nucleotide (electron-acceptor).[109]

Another study of DNA/RNA-mediated charge-transfer was discussed in Section 1.3, where the properties of 2-pyrenyluridine were compared with those of the 1-pyrenyl-uridine isomer.[12]

Medicinal applications have also made use of the electron-transfer process between nucleotides. A series of pyrene-viologen (donor-acceptor) derivatives was synthesized and shown to display cytotoxicity towards cells upon photo-excitation.[110] These

derivatives can bind to DNA through intercalation of the pyrene moiety and binding of the viologen to DNA grooves. A mechanism for the oxidation of DNA has been proposed (Figure 30). After photo-excitation, an electron is transferred from the excited state of pyrene to the viologen moiety, and this is followed by electron-transfer from the DNA base to the radical cation on pyrene. Hence, DNA oxidation is effected, leading to DNA damage. Irradiation with UV light (360 nm) for 22.5 minutes was shown to reduce significantly the concentration of leukemia cells.[110b] The advantage of these systems is that they can be selectively activated by an external photo-excitation source, which can be applied to a specific piece of surface tissue, thus removing unwanted side-effects and damage to healthy DNA.

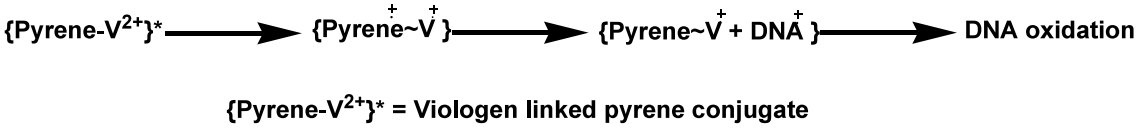

Figure 30 Mechanism for the oxidation of DNA using pyrene-viologen complexes.[110]

2.3.2 DNA/RNA Hybridisation

Pyrene has also been used in many other DNA/RNA applications. The hybridization of oligonucleotide strands to form a duplex can be monitored by a pyrene-modified nucleotide that displays dual-fluorescence.[111] This property arises from two relaxed singlet excited states, an intramolecular charge-transfer state and a locally excited state. Deoxyuridine was cross-coupled with an *N*,*N*-dimethylaminophenyl-substituted pyrene, and then incorporated into oligonucleotides. When in the single strand, only one peak in the emission spectrum was observed. Upon duplex formation, two peaks in the emission spectrum (dual-fluorescence) and a colour change were observed. Hence, a detection method for DNA or RNA hybridization was achieved.

Hybridization can also be monitored by changes in the fluorescence properties of pyrene that occur upon a change in local environment. Modified deoxyguanosine, Py-dG, was incorporated into an oligonucleotide.[112] Upon hybridization, the absorbance and fluorescence properties of pyrene were found to differ from those observed in the single strand.

Another hybridization detection method involves excimer formation. One study involved the attachment of a pyrene moiety onto the sugar residue of a uridine base.[113]

Incorporation of this nucleotide into RNA and DNA showed that in RNA oligonucleotides, weak emission was observed in the single strand, yet when binding to a complimentary strand, strong excimer emission was observed. In contrast, the DNA-modified strands showed weak emission in both the single strand and duplex forms. Therefore, the modified nucleotide provides a useful tool for monitoring RNA-hybridization. Analysis of the structures of the duplexes by molecular dynamics simulations, fluorescence, CD and NMR studies shows that, in DNA, the pyrene units intercalate into the double helix between the base pairs; hence, excimer emission is not possible. However, in RNA, the pyrene units are found to be on the outside of the duplex and are therefore able to display excimer emission.[113]

As well as detecting hybridization of oligonucleotides, pyrene can be used to induce a hybridization process. An oligonucleotide, consisting of deoxyadenosine bases, was modified by covalent attachment with ethynylpyrene moieties.[114] When adjacent pyrene units were separated by at least two adenosine bases, a reddish emission at 580 nm was observed. Spectroscopic studies suggested that this red emission was the result of intermolecular self-duplex formation, where the pyrene moieties were inducing the formation of a duplex, and thus showing a change in fluorescence. It was also shown that if the pyrene units were adjacent, a green emission was observed; however, if they were separated by one adenosine unit, the emission changed to blue, or if by two units, an orange emission was observed.[114] In this example, it was shown that when pyrene is incorporated into a oligonucleotide backbone, it can assist with the self-assembly of single strands through π-π stacking interactions. It has also been reported that interstrand π-π stacking interactions between pyrene moieties substituted onto a DNA backbone lead to high duplex stability.[115]

In RNA, a pyrene zipper array has been used to form RNA duplexes (Figure 31).[116] Upon duplex formation, the π-π stacking interactions between the multi-pyrene-modified RNA strands produce a specific type of double helix structure. Elsewhere, substitution of the sugar residues on RNA with pyrene has led to the formation of a helical pyrene array.[117] In a more detailed study, an investigation of the external structure of the pyrene-modified RNA showed that the pyrene units form a helical array along the minor groove of the RNA duplexes.[118] In such cases, the double helix acts as a structural scaffold for groups such as pyrene to be added and arranged in certain conformations.

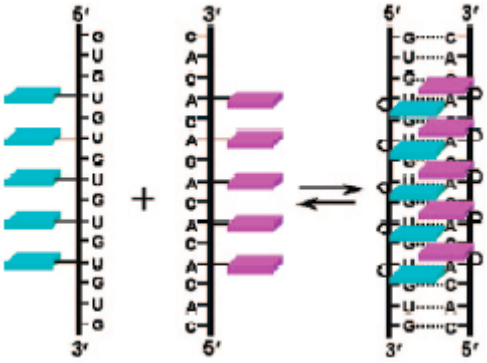

Figure 31 Schematic representation of duplex formation between multipyrene-modified RNA sequences.[116] Reproduced by permission of The American Chemical Society.

Another approach to facilitating self-assembly is to use pyrene as a bridge between two nucleotides in an oligonucleotide backbone. Two isomeric dialkynylpyrene phosphoramidites were synthesized and incorporated into oligonucleotides (Figure 32a).[119] The pyrene-modified DNA was shown to be able to self-organise single strands into duplexes. Strong fluorescence, due to the formation of either intra- or inter-strand excimers, was also observed.[119] The properties of pyrene in these bridging systems can be modified by the addition of other subsitituents to the pyrene ring. It has been shown that placing different substituents at the 3- and 6-positions on 1,8-pyrenedicarboxylate oligonucleotide bridges (Figure 32b) can tune the photophysicial properties of the pyrene moiety.[120] Substitution at the 3- and 6-positions with 3-*N*-methyl-pyridinium moieties was found to have a strong quenching influence and an undeterminable fluorescence quantum yield. In contrast, the triisopropylsilanyl-ethynyl derivative exhibited intense fluorescence with $\phi_f = 0.99$. Further work is underway to incorporate these derivatives into an oligonucleotide backbone.[120] These examples demonstrate the importance of pyrene-modified DNA and RNA duplexes as structural scaffolds for the design and construction of nano-architectures and π-systems.[121]

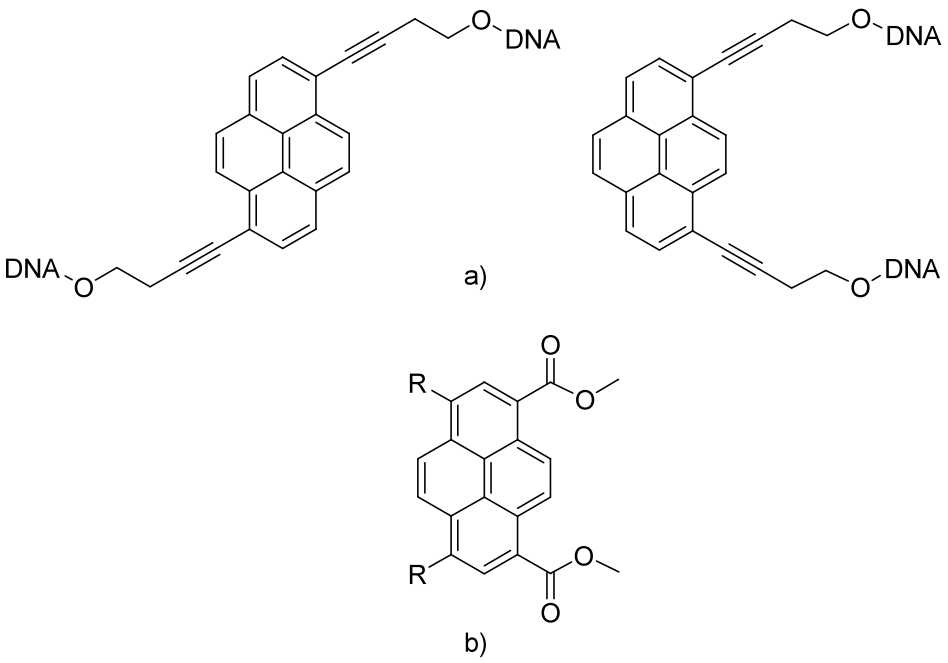

Figure 32 Pyrene derivatives as bridges in the DNA backbone: a) Dialkynylpyrene phosphoramidites;[119] b) 1,8-pyrenedicarboxylates substituted at the 3- and 6-positions (R= 3-C_6H_4-NO_2, 3-pyridyl, C≡C-Si(^{i}Pr)$_3$, C≡CH, 3-*N*-methyl-pyridinium).[120]

Hybridization of pyrene-modified DNA and RNA strands has also been used for medicinal applications. The detection of mismatched base pairs and, in particular, single-nucleotide polymorphisms (SNPs) is an important area, as such defects lead to genetic mutation and are responsible for several diseases. One way of detecting mismatches is using base-discriminating fluorescent (BDF) nucleobases.[122] Two BDF nucleobases, Py-U and Py-C, were synthesized which contain a pyrene-carboxamide chromophore on the natural base (Figure 33). These nucleosides were found to fluoresce when paired with their complimentary base, Py-U with adenine and Py-C with guanine. When a mismatch occurred, this fluorescence was quenched and the emission intensity found to be much weaker; hence, detection of SNPs is achieved (Figure 33).[122] In a more recent study, pyrene-functionalized triazole-linked 2'-deoxyuridines were used to detect SNPs in a similar manner.[123]

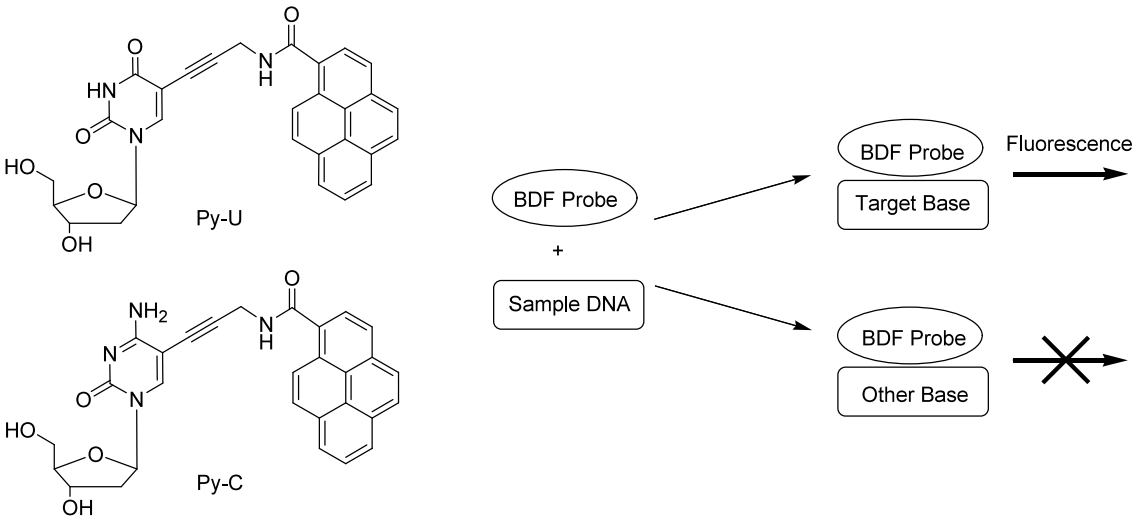

Figure 33 Base-discriminating fluorescent (BDF) probes (left) only give strong fluorescence when the base opposite the BDF base is a target base (right).[122]

Another method of detecting base mismatches is to use an excimer-forming pyrene probe.[124] A oligonucleotide probe which involved the attachment of two pyrene moieties to separate nucleobases was synthesized. In the single-strand form the probe was found to exhibit weak fluorescence, but upon formation of a duplex, strong excimer fluorescence was observed. The authors used a polycation-accelerated strand-exchange reaction to exchange the strands of both healthy and mutant DNA with the pyrene-excimer probe strand, and thus create duplexes. It was found that the mutant strand exchanged much faster than the healthy strand. Therefore, by monitoring time-dependant changes in the excimer emission, mutations could be detected.[124] In another example, a duplex was synthesized that contained five adjacent Py-U moieties.[125] Upon DNA hybridization, the highly ordered structure gave strong emission intensity, due to interactions between the chromophores. Furthermore, it was shown that the five-fold stack exhibits sequence selectivity, as a variation in the emission properties was observed when the strand was hybridized with different sequences, and is able to function as a probe for base mismatches.

Another type of mutation in DNA is a deletion polymorphism, where a nucleotide base is missing from the DNA backbone. Excimer-emission can again be used as a detection method.[126] Two pyrene moieties were attached to an oligonucleotide, on either side of a intervening base. When there is no deletion, only monomer-emission was detected.

However, upon detection of one or two base deletions, excimer-emission was observed (Figure 34).[126]

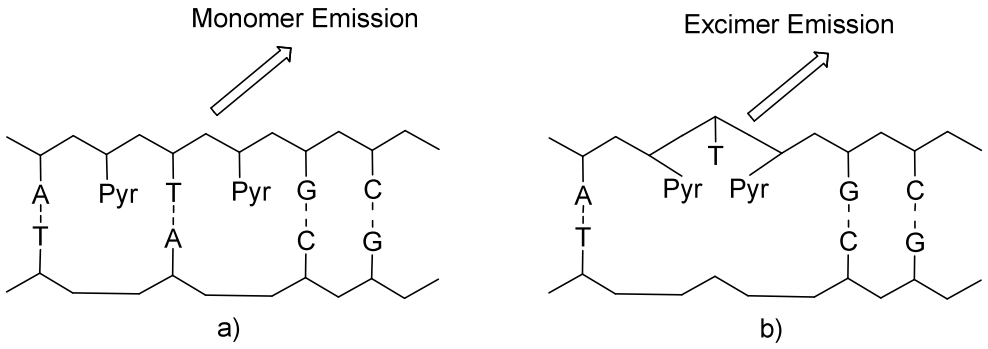

Figure 34 Detection of deletion polymorphisms in DNA by excimer emission: a) with no deletion; b) with deletion. Pyr = pyrene; A = adenine; T = thymine; G = guanine; C = cytosine.[126]

More recently, fluorescence resonance energy-transfer (FRET) between pyrene (donor) and perylene (acceptor) moieties assembled onto a DNA duplex has been used to detect deletion polymorphisms.[127] Using FRET reduces the overlap between the absorption and emission in a system. This is an advantage in DNA systems, which contain a large amount of aromatic and heteroaromatic species that display their own absorption and emission properties. Therefore, using FRET reduces the interference from these species by shifting the emission from the perylene label to longer wavelengths.[127]

2.3.3 Nucleotide Base Replacement

Thus far, all of the pyrene-modified DNA systems have involved attachment of a pyrene moiety to a DNA base via a cross-coupling reaction. It is also possible to replace an entire nucleotide base with a pyrene moiety. The polar natural DNA base in a nucleotide was replaced with a pyrene unit to form a pyrene nucleoside P (Figure 35).[128a] Such modifications are of interest for the design of new base-pairs and can give insight into the non-covalent interactions in DNA as unlike the natural bases, the pyrene unit will undergo no hydrogen bonding. A new base-pair design consisted of P with an abasic nucleoside (one where the base has been replaced with a hydrogen); hence, when paired the large size of the pyrene fills the space left after the removal of the base.[128a] In related work,[128b] P was modified with a polyphosphate chain to give dPTP (Figure 35)

and the abasic nucleoside was incorporated in a DNA strand. In the presence of DNA polymerases (an enzyme that catalyzes the polymerisation of DNA), it was found that dPTP acts as a substrate and is paired with the abasic nucleoside. Surprisingly, this pairing is highly efficient and selective, with the polymerase pairing dPTP and the abasic nucleotide over other natural DNA bases. Thus, it is possible to design new base-pairs that pair in an efficient and selective manner without the need for hydrogen bonding, a finding that will be of interest for the design and synthesis of new supramolecular systems and biomolecules.[128]

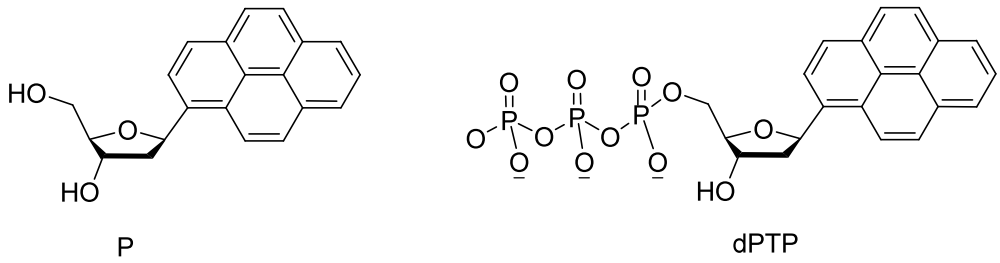

Figure 35 A pyrene nucleoside P (left) and pyrene triphosphate, dPTP (right).[128]

In another study, a natural nucleotide base of DNA was replaced with a pyrene or a perylene moiety.[129] These modifications were joined together in various combinations to form oligodeoxyfluorosides (ODFs). It was found that by varying the sequence and spacing in these ODFs, changes in fluorescence were observed, with emission maxima ranging from 380 to 557 nm. Combination of the two fluorophores can give rise to emission over most of the visible spectrum with just one excitation. It was shown that the different emissions arose from various interactions, including pyrene-pyrene excimers and pyrene-perylene exciplexes.[129] Further adjustment of the emission properties of the pyrene-functionalized oligomers can occur by replacement of the natural bases with a quencher.[130] The quencher 5-(10-methyl-phenothiazin-3-yl)-2'-deoxyuridine quenches the emission of both pyrene-labelled ODFs and the associated excimer complexes. Variation of the sequence of pyrene and quencher units in the ODF was shown to lead to a tuning of the emission (Figure 36). In a different study, these oligomers were incorporated into biological systems.[131] Incorporation into zebrafish embryos showed low toxicity, high tissue penetration and bio-stability. Furthermore, the various ODFs displayed emission colours across the entire visible spectrum after

excitation with just one wavelength. These results suggest that ODFs could be used as labels in biological systems, particularly for the monitoring of dynamic processes and tracking of multiple species by colour.[131]

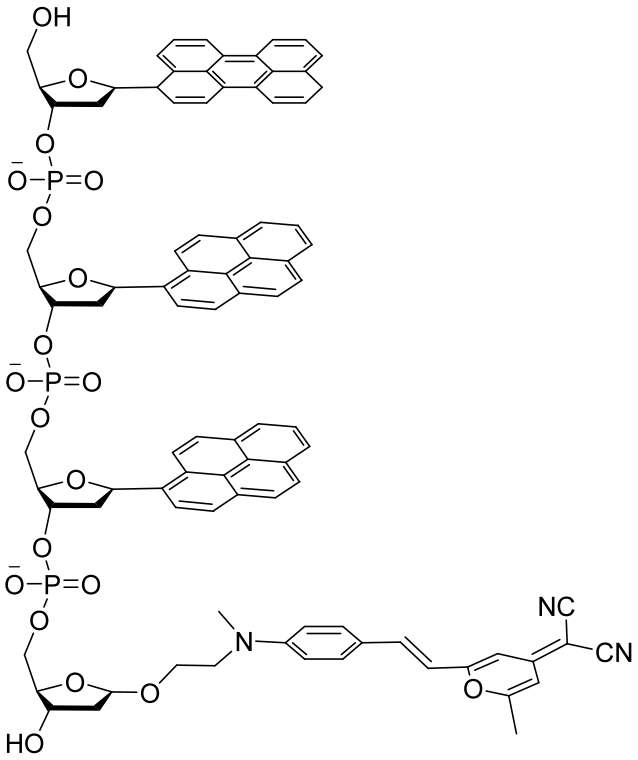

Figure 36 Polyfluorophores on a DNA backbone: the structure of a typical ODF.[131]

More recently, it has also been shown that the same ODFs can behave as vapour sensors.[132] In this case, different emission colours are observed upon interaction of the ODFs with small molecule analytes such as acrolein, mesitylene, propionic acid and nitrobenzene. The range of different sequences of polyaromatic hydrocarbons and quenchers on the DNA backbone, and their ease of synthesis, means these systems have potential to be developed into a wide range of sensors, capable of detecting a wide range of analytes.[132]

3.0 Conclusions

Pyrene, a rigid aromatic molecule, displays a series of useful properties. It can undergo π-π stacking interactions, leading to the formation of excimers. It displays long-lived fluorescence, which is very sensitive to changes in environment. Furthermore, it can participate in charge-transfer complexes, usually acting as an electron-donor.

As a result of these properties, pyrene has been used for a wide range of applications. As discussed, these applications make use of the structural, optical and charge-transfer properties of pyrene in a range of different systems, ranging from nano-engineering to biology.

Generally, pyrene derivatives used in these applications are substituted at the 1-, 3-, 6- and 8-positions, which are the sites of maximum contributions in the HOMO (and also the LUMO), and therefore the site of electrophilic aromatic substitution.
In contrast, derivatives substituted at the 2- and 2,7-positions are relatively rare. As a result of the presence of the nodal planes in the HOMO (and LUMO), which lie perpendicular to the molecule and pass through the 2- and 7-positions, the synthesis of these derivatives is lengthy. However, derivatives substituted at these positions are of interest because they retain the long axis of symmetry, and also display a unique range of photophysical properties that differ from those of the analogous 1-substituted derivatives.

Using iridium-catalyzed C-H borylation, straightforward and high-yielding syntheses of 2,7-bis(Bpin)pyrene and 2-(Bpin)pyrene have been achieved. The present work uses this finding as a starting point to synthesize a range of 2- and 2,7-substituted pyrenes bearing donor and acceptor groups, including aryl, ethynyl, arylethynyl, alkyl, hydroxy, alkoxy, diarylamino, carboxylic acid and diarylboryl substituents. The molecular structures and crystal packing, as well as the photophysical properties of the new derivatives were also investigated.
The synthetic methodology, crystal packing and optical properties reported herein will allow 2- and 2,7-pyrene derivatives to be incorporated into many existing and new pyrene-based applications, and will hopefully make their use become as mainstream as the related 1-substitued derivatives.

4.0 References

[1] (a) Hunter, C. A.; Sanders, J. K. M. *J. Am. Chem. Soc.* **1990**, *112*, 5525–5534. (b) Lehn, J. M. *Supramolecular Chemistry: Concepts and Perspectives,* VCH, Weinheim, 1995. (c) Steed, J. W.; Atwood, J. L. *Supramolecular Chemistry,* Wiley: Chichester,

2000. (d) Hunter, C. A.; Lawson, K. R.; Perkins, J.; Urch, C. J. *J. Chem. Soc., Perkin Trans.* **2001**, *2*, 651–669. (e) Rowan, S. J.; Cantrill, S. J.; Cousins, G. R. L.; Sanders, J. K. M.; Stoddart, J. F. *Angew. Chem., Int. Ed.* **2002**, *41*, 898–952. (f) Waters, M. L. *Biopolymers* **2004**, *76*, 435–445.

[2] (a) Colquhoun, H. M.; Stoddart, J. F.; Williams, D. J. *Angew. Chem. Int. Ed.* **1986**, *25*, 487-507. (b) Amabilino, D. B.; Stoddart, J. F. *Chem. Rev.* **1995**, *95*, 2725–2828. (c) Philp, D.; Stoddart, J. F. *Angew. Chem. Int. Ed.* **1996**, *108*, 1242–1286. (d) Stoddart, J. F. *Acc. Chem. Res.* **2001**, *34*, 410–411. (e) Stoddart, J. F.; Colquhoun, H. M. *Tetrahedron* **2008**, *64*, 8231–8263. (f) Bhosale, S. V.; Jani, C.-H.; Langford, S. J. *Chem. Soc. Rev.* **2008**, *37*, 331–342.

[3] (a) Dai, C.; Nguyen, P.; Marder, T. B.; Scott, A. J.; Clegg, W.; Viney, C. *Chem. Commun.* **1999**, 2493–2494. (b) Collings, J. C.; Roscoe, K. P.; Thomas, R. L.; Batsanov, A. S.; Stimson, L. M.; Howard, J. A. K.; Marder, T. B. *New J. Chem.* **2001**, *25*, 1410–1417. (c) Collings, J. C.; Roscoe, K. P.; Robins, E. G.; Batsanov, A. S.; Stimson, L. M.; Howard, J. A. K.; Clark, S. J.; Marder, T. B. *New J. Chem.* **2002**, *26*, 1740–1746. (d) Watt, S. W.; Dai, C.; Scott, A. J.; Burke, J. M.; Thomas, R. L.; Collings, J. C.; Viney, C.; Clegg, W.; Marder, T. B. *Angew. Chem. Int. Ed.* **2004**, *43*, 3061–3063.

[4] (a) Credi, A.; Balzani, V.; Langford, S. J.; Stoddart, J. F. *J. Am. Chem. Soc.* **1997**, *119*, 2679–2681. (b) Asakawa, M.; Ashton, P. R.; Balzani, V.; Credi, A.; Hamers, C.; Mattersteig, G.; Montalti, M.; Shipway, A. N.; Spencer, N.; Stoddart, J. F.; Tolley, M. S.; Venturi, M.; White, A. J. P.; Williams, D. J. *Angew. Chem. Int. Ed.* **1998**, *37*, 333–337. (c) Ashton, P. R.; Balzani, V.; Kocian, O.; Prodi, L.; Spencer, N.; Stoddart, J. F. *J. Am. Chem. Soc.* **1998**, *120*, 11190–11191. (d) Collier, C. P.; Wong, E. W.; Belohradsky, M.; Raymo, F. M.; Stoddart, J. F.; Kuekes, P. J.; Williams, R. S.; Heath, J. R. *Science* **1999**, *285*, 391–394. (e) Balzani, V.; Credi, A.; Mattersteig, G.; Matthews, O. A.; Raymo, F. M.; Stoddart, J. F.; Venturi, M.; White, A. J. P.; Williams, D. J. *J. Org. Chem.* **2000**, *65*, 1924–1936. (f) Jeppesen, J. O.; Perkins, J.; Becher, J.; Stoddart, J. F. *Angew. Chem. Int. Ed.* **2001**, *40*, 1216–1221. (g) Kang, S.; Vignon, S. A.; Tseng, H.-R.; Stoddart, J. F. *Chem. Eur. J.* **2004**, *10*, 2555–2564. (h) Simpson, C. D.; Wu, J.; Watson, M. D.; Müllen, K. *J. Mater. Chem.* **2004**, *14*, 494-504. (i) Hoeben, F. J. M.; Jonkheijm, P.; Meijer, E. W.; Schenning, A. P. H. J. *Chem. Rev.* **2005**, *105*, 1491-1546. (j) Saha, S.;

Johansson, E.; Flood, A. H.; Tseng, H.-R.; Zink, J. I.; Stoddart, J. F. *Chem. Eur. J.* **2005**, *11*, 6846–6858.

[5] (a) Robertson, J. M.; White, J. G. *J. Chem. Soc.* **1947**, 358-368. (b) Allmann, R. *Z. Kristallogr.* **1970**, *132*, 416-416. (c) Hazell, A. C.; Larsen, F. K.; Lehmann, M. S. *Acta Crystallogr.* **1972**, *B28*, 2977-2984. (d) Kai, Y.; Hama, F.; Yasuoka, N.; Kasai, N. *Acta Crystallogr.* **1978**, *B34*, 1263-1270. (e) Knight, K. S.; Shankland, K.; David, W. I. F.; Shankland, N.; Love, S. W. *Chem. Phys. Lett.* **1996**, *258*, 490-494. (f) Frampton, C. S.; Knight, K. S.; Shankland, K.; Shankland, N. *J. Mol. Struct.* **2000**, *520*, 29-32.

[6] (a) Birks, J. B. *Photophysics of Aromatic Molecules*. Wiley-Interscience: London, 1970. (b) Turro, N. J.; Ramamurthy, V.; Scaiano, J. C. *Principles of Molecular Photochemistry, An Introduction*. University Science Books: Sausalito, 2009. (c) Values measured by the author.

[7] (a) Hazell, A. C.; Lomborg, J. G. *Acta Crystallogr.* **1972**, *B28*, 1059-1064. (b) Miura, Y.; Yamano, R.; Tanaka, A.; Yamauchi, J. *J. Org. Chem.* **1994**, *59*, 3294-3300.

[8] (a) Eddaoudi, M.; Kim, J.; Rosi, N.; Vodak, D.; Wachter, J.; O'Keeffe, M.; Yaghi, O. M. *Science* **2002**, *295*, 469-472. (b) Rowsell, J. L. C.; Yaghi, O. M. *J. Am. Chem. Soc.* **2006**, *128*, 1304-1315.

[9] (a) Wan, S.; Guo, J.; Kim, J.; Ihee, H.; Jiang, D. *Angew. Chem. Int. Ed.* **2008**, *47*, 8826-8830. (b) Wan, S.; Guo, J.; Kim, J.; Ihee, H.; Jiang. D. *Angew. Chem. Int. Ed.* **2009**, *48*, 5439-5442.

[10] Godinez, C. E.; Zepeda, G.; Garcia-Garibay, M. A. *J. Am. Chem. Soc.* **2002**, *124*, 4701-4707.

[11] Rausch, D.; Lambert, C. *Org. Lett.* **2006**, *8*, 5037-5040.

[12] Wanninger-Weiss, C.; Wagenknecht, H.-A. *Eur. J. Org. Chem.* **2008**, 64-71.

[13] (a) Astakhova, I. V.; Korshun, V. A. *Russ. J. Bioinorg. Chem.* **2008**, *34*, 510-512. (b) Filichev, V. V.; Astakhova, I. V.; Malakhov, A. D.; Korshun, V. A.; Pedersen, E. B. *Chem. Eur. J.* **2008**, *14*, 9968-9980. (c) Astakhova, I. V.; Lindegaard, D.; Korshun, V. A.; Wengel, J. *Chem. Commun.* **2010**, *46*, 8362-8364.

[14] Kreyenschmidt, M.; Baumgarten, M.; Tyutyulkov, N.; Müllen, K. *Angew. Chem. Int. Ed.* **1994**, *33*, 1957-1959.

[15] Suzuki, S.; Takeda, T.; Kuratsu, M.; Kozaki, M.; Sato, K.; Shiomi, D.; Takui, T.; Okada, K. *Org. Lett.* **2009**, *11*, 2816-2818.

[16] Irngartinger, H.; Kirrstetter, R. G. H.; Krieger, C.; Rodewald, H.; Staab, H. A. *Tetrahedron Lett.* **1977**, *18*, 1425-1428.

[17] (a) Fu, P.; Lee, H. M.; Harvey, R. G. *J. Org. Chem.* **1980**, *45*, 2797-2803. (b) Harvey, R. G.; Konieczny, M.; Pataki, J. *J. Org. Chem.* **1983**, *48*, 2930-2932. (c) Minabe, M.; Nakada, K. *Bull. Chem. Soc. Jpn.* **1985**, *58*, 1962-1967. (d) Lee, H.; Harvey, R. G. *J. Org. Chem.* **1986**, *51*, 2847-2848. (e) Miller, D. W.; Herreno-Saenz, D.; Huang, K. H.; Heinze, T. M.; Fu, P. P. *J. Org. Chem.* **1992**, *57*, 3746-3748. (f) Connor, D. M.; Allen, S. D.; Collard, D. M.; Liotta, C. L.; Schiraldi, D. A. *J. Org. Chem.* **1999**, *64*, 6888-6890.

[18] (a) Coventry, D. N.; Batsanov, A. S.; Goeta, A. E.; Howard, J. A. K.; Marder, T. B.; Perutz, R. N. *Chem. Commun.* **2005**, 2172-2174. (b) Crawford, A. G.; Liu, Z.; Mkhalid, I. A. I.; Thibault, M.-H.; Schwarz, N.; Alcaraz, G.; Steffen, A.; Batsanov, A. S.; Howard, J. A. K.; Dwyer, A. D.; Beeby, A.; Pålsson, L.-O.; Tozer, D. J.; Marder, T. B. 93rd Canadian Chemistry Conference and Exhibition, Toronto, Canada, May 29 - June 2, 2010, Abstract 0964.

[19] (a) Ishiyama, T.; Takagi, J.; Ishida, K.; Miyaura, N.; Anastasi, N. R.; Hartwig, J. F. *J. Am. Chem. Soc.* **2002**, *124*, 390-391. (b) Ishiyama, T.; Takagi, J.; Hartwig, J. F.; Miyaura, N. *Angew. Chem. Int. Ed.* **2002**, *41*, 3056-3058. (c) Ishiyama, T.; Miyaura, N. *J. Organomet. Chem.* **2003**, *680*, 3-11.

[20] (a) Mkhalid, I. A. I.; Coventry, D. N.; Albesa-Jové, D.; Batsanov, A.S.; Howard, J. A. K.; Perutz, R. N.; Marder, T. B. *Angew. Chem. Int. Ed.* **2006**, *45*, 489-491. (b) Harrisson, P.; Morris, J.; Steel, P. G.; Marder, T. B. *Synlett* **2009**, 147-150. (c) Harrisson, P.; Morris, J.; Marder, T. B; Steel, P. G. *Org. Lett.* **2009**, *11*, 3586-3589. (d) Mkhalid, I. A. I.; Barnard, J. H.; Marder, T. B.; Murphy, J. M.; Hartwig, J. F. *Chem. Rev.* **2010**, *110*, 890-931.

[21] Tasis, D.; Tagmatarchis, N.; Bianco, A.; Prato, M. *Chem. Rev.* **2006**, *106*, 1105-1136.

[22] Meuer, S.; Braun, L.; Zentel, R. *Chem. Commun.* **2008**, 3166-3168.

[23] Kühnast, M.; Tschierske, C.; Lagerwall, J. *Chem. Commun.* **2010**, 6989-6991.

[24] Schopf, E.; Broyer, R.; Tao, L.; Chen, Y.; Maynard, H. D. *Chem. Commun.* **2009**, 4818-4820.

[25] (a) Petrov, P.; Stassin, F.; Pagnoulle, C.; Jérôme, R. *Chem. Commun.* **2003**, 2904-2905. (b) Backes, C.; Mundloch, U.; Ebel, A.; Hauke, F.; Hirsch, A. *Chem. Eur. J.* **2010**, *16*, 3314-3317.

[26] Prencipe, G.; Tabakman, S. M.; Welsher, K.; Liu, Z.; Goodwin, A. P.; Zhang, L.; Henry, J.; Dai, H. *J. Am. Chem. Soc.* **2009**, *131*, 4783-4787.

[27] Maligaspe, E.; Sandanayaka, A. S. D.; Hasobe, T.; Ito, O.; D'Souza, F. *J. Am. Chem. Soc.* **2010**, *132*, 8158-8164.

[28] Bartelmess, J.; Ballesteros, B.; de la Torre, G.; Kiessling, D.; Campidelli, S.; Prato, M.; Torres, T.; Guldi, D. M. *J. Am. Chem. Soc.* **2010**, *132*, 16202-16211.

[29] Schulz-Drost, C.; Sgobba, V.; Gerhards, C.; Leubner, S.; Krick Calderon, R. M.; Ruland, A.; Guldi, D. M. *Angew. Chem. Int. Ed.* **2010**, *49*, 6425-6429.

[30] McQueen, E. W.; Goldsmith, J. I. *J. Am. Chem. Soc.* **2009**, *131*, 17554-17556.

[31] (a) Kyatskaya, S.; Mascarós, J. R. G.; Bogani, L.; Hennrich, F.; Kappes, M.; Wernsdorfer, W.; Ruben, M. *J. Am. Chem. Soc.* **2009**, *131*, 15143-15151. (b) Bogani, L.; Danieli, C.; Biavardi, E.; Bendiab, N.; Barra, A.-L.; Dalcanale, E.; Wernsdorfer, W.; Cornia, A. *Angew. Chem. Int. Ed.* **2009**, *48*, 746-750.

[32] (a) Chen, R. J.; Zhang, Y.; Wang, D.; Dai, H. *J. Am. Chem. Soc.* **2001**, *123*, 3838-3839. (b) Ramasamy, R. P.; Luckarift, H. R.; Ivnitski, D. M.; Atanassov, P. B.; Johnson, G. R. *Chem. Commun.* **2010**, 6045-6047.

[33] Chung, C.-L.; Gautier, C.; Campidelli, S.; Filoramo, A. *Chem. Commun.* **2010**, 6539-6541.

[34] (a) Barry, N. P. E.; Therrien, B. *Eur. J. Inorg. Chem.* **2009**, 4695-4700. (b) Barry, N. P. E.; Furrer, J.; Freudenreich, J.; Süss-Fink, G.; Therrien, B. *Eur. J. Inorg. Chem.* **2010**, 725-728. (c) Mattsson, J.; Zava, O.; Renfew, A. K.; Sei, Y.; Yamaguchi, K.; Dyson, P. J.; Therrien, B. *Dalton Trans.* **2010**, *39*, 8248-8255. (d) Zava, O.; Mattsson, J.; Therrien, B.; Dyson, P. J. *Chem. Eur. J.* **2010**, *16*, 1428-1431.

[35] Moorthy, J. N.; Natarajan, P.; Venugopalan, P. *Chem. Commun.* **2010**, 3574-3576.

[36] Colquhoun, H. M.; Zhu, Z.; Williams, D. J.; Drew, M. G. B.; Cardin, C. J.; Gan, Y.; Crawford, A. G.; Marder, T. B. *Chem. Eur. J.* **2010**, *16*, 907-918.

[37] Kumar, N. S. S.; Gujrati, M. D.; Wilson, J. N. *Chem. Commun.* **2010**, 5464-5466.

[38] Burattini, S.; Greenland, B. W.; Merino, D. H.; Weng, W.; Seppala, J.; Colquhoun, H. M.; Hayes, W.; Mackay, M. E.; Hamley, I. W.; Rowan, S. J. *J. Am. Chem. Soc.* **2010**, *132*, 12051-12058.

[39] Jiang, Q.; Zhang, H.-Y.; Han, M.; Ding, Z.-J.; Liu, Y. *Org. Lett.* **2010**, *12*, 1728-1731.

[40] (a) Kilbinger, A. F. M.; Grubbs, R. H. *Angew. Chem. Int. Ed.* **2002**, *41*, 1563-1566. (b) Ma, M.; Kuang, Y.; Gao, Y.; Zhang, Y.; Gao, P.; Xu, B. *J. Am. Chem. Soc.* **2010**, *132*, 2719-2728.

[41] Diring, S.; Camerel, F.; Donnio, B.; Dintzer, T.; Toffanin, S.; Capelli, R.; Muccini, M.; Ziessel, R. *J. Am. Chem. Soc.* **2009**, *131*, 18177-18185.

[42] de Halleux, V.; Calbert, J.-P.; Brocorens, P.; Cornil, J.; Declercq, J.-P.; Bredas, J.-L.; Geerts, Y. *Adv. Funct. Mater.* **2004**, *14*, 649-659.

[43] de Halleux, V.; Mamdouh, W.; De Feyter, S.; De Schryver, F.; Levin, J.; Geerts, Y. H. *J. Photochem. Photobiol. A: Chem.* **2006**, *178*, 251-257.

[44] Hayer, A.; de Halleux, V.; Koehler, A.; El-Garoughy, A.; Meijer, E. W.; Barbera, J.; Tant, J.; Levin, J.; Lehmann, M.; Gierschner, J.; Cornil, J.; Geerts, Y. H. *J. Phys. Chem. B* **2006**, *110*, 7653-7659.

[45] Dang, H.; Maris, T.; Yi, J.-H.; Rosei, F.; Nanci, A.; Wuest, J. D. *Langmuir* **2007**, *23*, 11980-11985.

[46] Yang, S.-W.; Elangovan, A.; Hwang, K.-C.; Ho, T.-I. *J. Phys. Chem. B* **2005**, *109*, 16628-16635.

[47] Ji, S.; Yang, J.; Yang, Q.; Liu, S.; Chen, M.; Zhao, J. *J. Org. Chem.* **2009**, *74*, 4855-4865.

[48] (a) Leroy-Lhez, S.; Fages, F. *Eur. J. Org. Chem.* **2005**, 2684-2688. (b) Shimizu, H.; Fujimoto, K.; Furusyo, M.; Maeda, H.; Nanai, Y.; Mizuno, K.; Inouye, M. *J. Org. Chem.* **2007**, *72*, 1530-1533.

[49] Venkataramana, G.; Sankararaman, S. *Eur. J. Org. Chem.* **2005**, 4162-4166.

[50] (a) Kim, H. M.; Lee, Y. O.; Lim, C. S.; Kim, J. S.; Cho, B. R. *J. Org. Chem.* **2008**, *73*, 5127-5130. (b) Oh, J.-W.; Lee, Y. O.; Kim, T. H.; Ko, K. C.; Lee, J. Y.; Kim, H.; Kim, J. S. *Angew. Chem. Int. Ed.* **2009**, *48*, 2522-2524.

[51] Hu, J.-Y.; Era, M.; Elsegood, M. R. J.; Yamato, T. *Eur. J. Org. Chem.* **2010**, 72-79.

[52] Goeb, S.; Ziessel, R. *Org. Lett.* **2007**, *9*, 737-740.

[53] Nagata, Y.; Chujo, Y. *J. Organomet. Chem.* **2009**, *694*, 1723-1726.

[54] Zhou, Y.; Kim, J. W.; Kim, M. J.; Son, W.-J.; Han, S. J.; Kim, H. N.; Han, S.; Kim, Y.; Lee, C.; Kim, S.-J.; Kim, D. H.; Kim, J.-J.; Yoon, J. *Org. Lett.* **2010**, *12*, 1272-1275.

[55] Banerjee, M.; Vyas, V. S.; Lindeman, S. V.; Rathore, R. *Chem. Commun.* **2008**, 1889-1891.

[56] Zhao, Z.; Chen, S.; Lam, J. W. Y.; Lu, P.; Zhong, Y.; Wong, K. S.; Kwok, H. S.; Tang, B. Z. *Chem. Commun.* **2010**, 2221-2223.

[57] Figueria-Duarte, T. M.; Simon, S. C.; Wagner, M.; Druzhinin, S. I.; Zachariasse, K. A.; Müllen, K. *Angew. Chem. Int. Ed.* **2008**, *47*, 10175-10178.

[58] (a) Oyamada, T.; Uchiuzou, H.; Akiyama, S.; Oku, Y.; Shimoji, N.; Matsushige, K.; Sasabe, H.; Adachi, C. *J. Appl. Phys.* **2005**, *98*, 074506. (b) Muccini, M. *Nat. Mater.* **2006**, *5*, 605-613.

[59] Sonar, P.; Soh, M. S.; Cheng, Y. H.; Henssler, J. T.; Sellinger, A. *Org. Lett.* **2010**, *12*, 3292-3295.

[60] Justin Thomas, K. R.; Velusamy, M.; Lin, J. T.; Chuen, C. H.; Tao, Y.-T. *J. Mater. Chem.* **2005**, *15*, 4453-4459.

[61] Yang, C.-H.; Guo, T.-F.; Sun, I.-W. *J. Lumin.* **2007**, *124*, 93-98.

[62] Suzuki, K.; Seno, A.; Tanabe, H.; Ueno, K. *Synth. Met.* **2004**, *143*, 89-96.

[63] Wee, K.-R.; Ahn, H.-C.; Son, H.-J.; Han, W.-S.; Kim, J.-E.; Cho, D. W.; Kang, S. O. *J. Org. Chem.* **2009**, *74*, 8472-8475.

[64] Zhao, S.-B.; Wucher, P.; Hudson, Z. M.; McCormick, T. M.; Liu, X.-Y.; Wang, S.; Feng, X.-D.; Lu, Z.-H. *Organometallics* **2008**, *27*, 6446-6456.

[65] Qu, L.; Shi, G. *Chem. Commun.* **2004**, 2800-2801.

[66] Li, X.-G.; Liu, Y.-W.; Huang, M.-R.; Peng, S.; Gong, L.-Z.; Moloney, M. G. *Chem. Eur. J.* **2010**, *16*, 4803-4813.

[67] Diev, V. V.; Hanson, K.; Zimmerman, J. D.; Forrest, S. R.; Thompson, M. E. *Angew. Chem. Int. Ed.* **2010**, *49*, 5523-5526.

[68] Imai, Y.; Murata, K.; Nakano, Y.; Harada, T.; Sato, T.; Tajima, N.; Fujiki, M.; Kuroda, R.; Matsubara, Y. *Eur. J. Org. Chem.* **2009**, 3244-3248.

[69] Goze, C.; Kozlov, D. V.; Castellano, F. N.; Suffert, J.; Ziessel, R. *Tetrahedron Lett.* **2003**, *44*, 8713-8716.

[70] Yao, C.-J.; Sui, L.-Z.; Xie, H.-Y.; Xiao, W.-J.; Zhong, Y.-W.; Yao, J. *Inorg. Chem.* **2010**, *49*, 8347-8350.

[71] Hu, J.; Yip, J. H. K.; Ma, D.-L.; Wong, K.-Y.; Chung, W.-H. *Organometallics*, **2009**, *28*, 51-59.

[72] Wu, W.; Wu, W.; Ji, S.; Guo, H.; Zhao, J. *Eur. J. Org. Chem.* **2010**, 4470-4482.

[73] Gao, L.; Peay, M. A.; Partyka, D. V.; Updegraff, J. B., III; Teets, T. S.; Esswein, A. J.; Zeller, M.; Hunter, A. D.; Gray, T. G. *Organometallics* **2009**, *28*, 5669-5681.

[74] Coleman, A.; Pryce, M. T. *Inorg. Chem.* **2008**, *47*, 10980-10990.

[75] (a) Kalyanasundaram, K.; Thomas, J. K. *J. Am. Chem. Soc.* **1977**, *99*, 2039-2044. (b) Kalyanasundaram, K. *Photochemistry in Microheterogeneous Systems*, Academic Press: Orlando, 1987, 39-41.

[76] Perry, M.; Carra, C.; Chrétien, M. N.; Scaiano, J. C. *J. Phys. Chem. A* **2007**, *111*, 4884-4889.

[77] Riis-Johannessen, T.; Severin, K. *Chem. Eur. J.* **2010**, *16*, 8291-8295.

[78] Beinhoff, M.; Weigel, W.; Jurczok, M.; Rettig, W.; Modrakowski, C.; Brüdgam, I.; Hartl, H.; Schlüter, A. D. *Eur. J. Org. Chem.* **2001**, 3819-3829.

[79] Stylianou, K. C.; Heck, R.; Chong, S. Y.; Bacsa, J.; Jones, J. T. A.; Khimyak, Y. Z.; Bradshaw, D.; Rosseinsky, M. J. *J. Am. Chem. Soc.* **2010**, *132*, 4119-4130.

[80] (a) Vaughan, W. M.; Weber, G. *Biochemistry* **1970**, *3*, 464-473. (b) Flamm, M.; Schachter, D. *Nature* **1982**, *298*, 290-292. (c) Fujimori, E.; Shambaugh, N. *Biochem. Biophys. Acta* **1983**, *742*, 155-161. (d) Lee, J. A.; Fortes, P. A. *Biochemistry* **1985**, *24*, 322-330. (e) Lissi, E. A.; Caceres, T. *J. Bioeng. Biomemb.* **1989**, *21*, 375-385. (f) Ebata, K.; Masuko, M.; Ohtani, H.; Kashiwasake-Jibu, M. *Photochem. Photobiol.* **1995**, *62*, 836-839. (g) Huglin, D.; Seiffert, W.; Zimmermann, H. W. *J. Photochem. Photobiol. B: Biol.* **1995**, *31*, 145-148. (h) Sugahara, D.; Amano, J.; Irimura, T. *Anal. Sci.* **2003**, *19*, 167-169. (i) Ribou, A.-C.; Vigo, J.; Salmon, J.–M. *Photochem. Photobiol.* **2004**, *80*, 274-280. (j) Berezin, M. Y.; Achilefu, S. *Chem. Rev.* **2010**, *110*, 2641-2684.

[81] (a) Takeuchi, T.; Kosuge, M.; Tadokoro, A.; Sugiura, Y.; Nishi, M.; Kawata, M.; Sakai, N.; Matile, S.; Futaki, S. *ACS Chem. Biol.* **2006**, *1*, 299-303. (b) Jablonski, A. E.; Kawakami, T.; Ting, A. Y.; Payne, C. K. *J. Phys. Chem. Lett.* **2010**, *1*, 1312-1315.

[82] (a) Weltman, J. K.; Szaro, R. P.; Frackelton, S. A. R., Jr.; Dowben, R. M.; Bunting, J. R.; Cathou, R. E. *J. Biol. Chem.* **1973**, *248*, 3173-3177. (b) Wu, C.-W.; Yarbrough, L. R.; Wu, F. Y. H. *Biochemistry* **1976**, *15*, 2863-2868. (c) Drewes, G.; Faulstich, H. *J. Biol. Chem.* **1991**, *266*, 5508-5513. (d) Panda, D.; Bhattacharyya, B. *Eur. J. Biochem.* **1992**, *204*, 783-787. (e) Suzuki, T.; Kawakita, M. *J. Biochem.* **1995**, *117*, 881-887. (f)

Gao, J.; Yin, D. H.; Yao, Y.; Sun, H.; Qin, Z.; Schöneich, C.; Williams, T. D.; Squier, T. C. *Biophys. J.* **1998**, *74*, 1115-1134.

[83] Maeda, H.; Maeda, T.; Mizuno, K.; Fujimoto, K.; Shimizu, H.; Inouye, M. *Chem. Eur. J.* **2006**, *12*, 824-831.

[84] Shinmori, H.; Furukawa, H.; Fujimoto, K.; Shimizu, H.; Inouye, M.; Takeuchi, T. *Chem. Lett.* **2009**, *38*, 84-85.

[85] Holland, J. P.; Fisher, V.; Hickin, J. A.; Peach, J. M. *Eur. J. Inorg. Chem.* **2010**, 48-58.

[86] Zeng, Z.; Spiccia, L. *Chem. Eur. J.* **2009**, *15*, 12941-12944.

[87] Schmidt, F.; Stadlbauer, S.; König, B. *Dalton Trans.* **2010**, *39*, 7250-7261.

[88] Zeng, Z.; Torriero, A. A. J.; Bond, A. M.; Spiccia, L. *Chem. Eur. J.* **2010**, *16*, 9154-9163.

[89] Romero, T.; Caballero, A.; Tárraga, A.; Molina, P. *Org. Lett.* **2009**, *11*, 3466-3469.

[90] Zeng, L.; Wang, P.; Zhang, H.; Zhuang, X.; Dai, Q.; Liu, W. *Org. Lett.* **2009**, *11*, 4294-4297.

[91] Yu, C.; Yam, V. W. *Chem. Commun.* **2009**, 1347-1349.

[92] Mansell, D.; Rattray, N.; Etchells, L. L.; Schwalbe, C. H.; Blake, A. J.; Bichenkova, E. V.; Bryce, R. A.; Barker, C. J.; Diaz, A.; Kremer, C.; Freeman. S. *Chem. Commun.* **2008**, 5161-5163.

[93] (a) Kim, H. J.; Hong, J.; Hong, A.; Ham, S.; Lee, J. H.; Kim, J. S. *Org. Lett.* **2008**, *10*, 1963-1966. (b) Jung, H. S.; Park, M.; Han, D. Y.; Kim, E.; Lee, C.; Ham, S.; Kim, J. S. *Org. Lett.* **2009**, *11*, 3378-3381.

[94] Zhou, Y.; Wang, F.; Kim, Y.; Kim, S.-J.; Yoon, J. *Org. Lett.* **2009**, *11*, 4442-4445.

[95] Pandey, M. D.; Mishra, A. K.; Chandrasekhar, V.; Verman, S. *Inorg. Chem.* **2010**, *49*, 2020-2022.

[96] Leray, I.; Valeur, B. *Eur. J. Inorg. Chem.* **2009**, 3525-3535.

[97] Kim, H. J.; Bok, J. H.; Vicens, J.; Suh, I.-H.; Ko, J.; Kim, J. S. *Tetrahedron Lett*. **2005**, *46*, 8765-8768.

[98] Othman, A. B.; Lee, J. W.; Huh, Y.-D.; Abidi, R.; Kim, J. S.; Vicens, J. *Tetrahedron* **2007**, *63*, 10793-10800.

[99] Othman, A. B.; Lee, J. W.; Wu, J. S.; Kim, J. S.; Abidi, R.; Thury, P.; Strub, J. M.; Dorsselaer, A. V.; Vicens. J. *J. Org. Chem*. **2007**, *72*, 7634-7640.

[100] Lee, Y. H.; Lee, M. H.; Zhang, J. F.; Kim, J. S. *J. Org. Chem*. **2010**, *75*, 7159-7165.

[101] Park, S. Y.; Yoon, J. H.; Hong, C. S.; Souane, R.; Kim, J. S.; Matthews, S. E.; Vicens, J. *J. Org. Chem*. **2008**, *73*, 8212-8218.

[102] Yoo, J.; Kim, Y.; Kim, S.-J.; Lee, C.-H. *Chem. Commun*. **2010**, 5449-5451.

[103] Lee, Y. H.; Liu, H.; Lee, J. Y.; Kim, S. H.; Kim, S. K.; Sessler, J. L.; Kim, Y.; Kim, J. S. *Chem. Eur. J*. **2010**, *16*, 5895-5901.

[104] (a) Amann, N.; Pandurski, E.; Fiebig T.; Wagenknecht, H.-A. *Angew. Chem. Int. Ed*. **2002**, *41*, 2978-2980. (b) Huber, R.; Fiebig, T.; Wagenknecht, H.-A. *Chem. Commun*. **2003**, 1878-1879.

[105] (a) Lewis, F. D. In *Electron Transfer in Chemistry*, Balzani, V., Ed.; Wiley-VCH: Weinheim, Germany, 2001; Vol. 3, p 10. (b) O'Neill, M. A. and Barton, J. K. *Charge Transfer in DNA: From Mechanism to Application*s, Wagenknecht, H.-A., Ed.; Wiley: New York, 2005; p 27. (c) Giese, B., Amaudrut, J., Kohler, A.-K., Spormann, M. and Wessely, S. *Nature* **2001**, *412*, 318– 320. (d) Carell, T., Behrens, C. and Gierlich, *J. Org. Biomol. Chem*. **2003**, *1*, 2221– 2228. (e) Schuster, G. B., Ed. *Long-Range Electron Transfer in DNA, I and II*; Springer: New York, 2004; Vol. 236, p 237.

[106] (a) Netzel, T. L.; Nafisi, K.; Headrick, J.; Eaton, B. E. *J. Phys. Chem*. **1995**, *99*, 17936-17947. (b) Trifonov, A.; Buchvarov, I.; Wagenknecht, H.-A.; Fiebig, T. *Chem. Phys. Lett*. **2005**, *409*, 277-280.

[107] Kaden, P.; Mayer-Enthart, E.; Trifonov, A.; Fiebig, T.; Wagenknecht, H.-A. *Angew. Chem. Int. Ed*. **2005**, *44*, 1636-1639.

[108] Maie, K.; Miyagi, K.; Takada, T.; Nakamura, M.; Yamana, K. *J. Am. Chem. Soc.* **2009**, *131*, 13188-13189.

[109] Tashiro, R.; Ohtsuki, A.; Sugiyama, H. *J. Am. Chem. Soc.* **2010**, *132*, 14361-14363.

[110] (a) Hariharan, M.; Joseph, J.; Ramaiah, D. *J. Phys. Chem. B* **2006**, *110*, 24678-24686. (b) Hariharan, M.; Karunakaran, S. C.; Ramaiah, D.; Schulz, I.; Epe, B. *Chem. Commun.* **2010**, *46*, 2064-2066.

[111] Okamoto, A.; Tainaka, K.; Nishiza, K.-I.; Saito, I. *J. Am. Chem. Soc.* **2005**, *127*, 13128-13129.

[112] Valis, L.; Mayer-Enthart, E.; Wagenknecht, H.-A. *Bioorg. Med. Chem. Lett.* **2006**, *16*, 3184-3187.

[113] Nakamura, M.; Fukunaga, Y.; Sasa, K.; Ohtoshi, Y.; Kanaori, K.; Hayashi, H.; Nakano, H.; Yamana, K. *Nucleic Acids Res.* **2005**, *33*, 5887-5895.

[114] Seo, Y. J.; Rhee, H.; Joo, T.; Kim, B. H. *J. Am. Chem. Soc.* **2007**, *129*, 5244-5247.

[115] Malinovskii, V. L.; Samain, F.; Häner, R. *Angew. Chem. Int. Ed.* **2007**, *46*, 4464-4467.

[116] Nakamura, M.; Murakami, Y.; Sasa, K.; Hayashi, H.; Yamana, K. *J. Am. Chem. Soc.* **2008**, *130*, 6904-6905.

[117] Nakamura, M.; Ohtoshi, Y.; Yamana, K. *Chem. Commun.* **2005**, 5163-5165.

[118] Nakamura, M.; Shimomura, Y.; Ohtoshi, Y.; Sasa, K.; Hayashi, H.; Nakano, H.; Yamana, K. *Org. Biomol. Chem.* **2007**, *5*, 1945-1951.

[119] Bittermann, H.; Siegemund, D.; Malinovskii, V. L.; Häner, R. *J. Am. Chem. Soc.* **2008**, *130*, 15285-15287.

[120] Malinovskii, V. L.; Häner, R. *Eur. J. Org. Chem.* **2006**, 3550-3553.

[121] Wagenknecht, H.-A. *Angew. Chem. Int. Ed.* **2009**, *48*, 2838-2841.

[122] Okamoto, A.; Kanatani, K.; Saito, I. *J. Am. Chem. Soc.* **2004**, *126*, 4820-4827.

[123] Østergaard, M. E.; Guenther, D. C.; Kumar, P.; Baral, B.; Deobald, L.; Paszczynski, A. J.; Sharma, P. K.; Hrdlicka, P. J. *Chem. Commun.* **2010**, *46*, 4929-4931.

[124] Yamana, K.; Fukunaga, Y.; Ohtani, Y.; Sato, S.; Nakamura, M.; Kim, W. J.; Akaike, T.; Maruyama, A. *Chem. Commun.* **2005**, 2509-2511.

[125] Mayer-Enthart, E.; Wagenknecht, H.-A. *Angew. Chem. Int. Ed.* **2006**, *45*, 3372-3375.

[126] Kashida, H.; Asanuma, H.; Komiyama, M. *Chem. Commun.* **2006**, 2768-2770.

[127] Kashida, H.; Takatsu, T.; Sekiguchi, K.; Asanuma, H. *Chem. Eur. J.* **2010**, *16*, 2479-2486.

[128] (a) Matray, T. J.; Kool, E. T. *J. Am. Chem. Soc.* **1998**, *120*, 6191-6192. (b) Matray, T. J.; Kool, E. T. *Nature* **1999**, *399*, 704-708. (c) Kool, E. T.; Morales, J. C.; Guckian, K. M. *Angew. Chem. Int. Ed.* **2000**, *39*, 990-1009.

[129] Wilson, J. N.; Gao, J.; Kool, E. T. *Tetrahedron*, **2007**, *63*, 3427-3433.

[130] Mayer-Enthart, E.; Wagner, C.; Barbaric, J.; Wagenknecht, H.-A. *Tetrahedron*, **2007**, *63*, 3434-3439.

[131] Teo, Y. N.; Wilson, J. N.; Kool, E. T. *J. Am. Chem. Soc.* **2009**, *131*, 3923-3933.

[132] Samain, F.; Ghosh, S.; Teo, Y. N.; Kool, E. T. *Angew. Chem. Int. Ed.* **2010**, *49*, 7025-7029.

Chapter 2: Functionalization of Pyrene at the 2- or 2,7-Positions: Synthesis, Crystal Structures and Packing

1.0 Introduction

Despite retaining a long axis of symmetry and displaying unique photophysical properties, 2- and 2,7-substituted pyrene derivatives are understudied (*vide supra*) because they are laborious and difficult to synthesize. Before the full potential of such systems can be investigated, a straightforward and high-yielding synthetic route to these derivatives is required.

This chapter reports the synthesis and characterization of a library of 2-mono and 2,7-bis-functionalized pyrenes starting from the boronic esters 2,7-bis(Bpin)pyrene **1** and 2-(Bpin)pyrene **2** (pin = $OCMe_2CMe_2O$) prepared via the C–H borylation of pyrene.[1] Subsequent reactions convert the boronic esters to pyrene derivatives that are used as nucleophilic or electrophilic partners in cross-coupling reactions, leading to synthetically and photophysically interesting systems. The crystal structures and packing for compounds **1**-**3, 7, 9**-**11, 15**-**17, 22, 24** are reported and discussed. For comparison purposes, a series of 1-(R)-substituted pyrenes was also prepared.

Several of these compounds had initially been synthesized by Drs Zhiqiang Liu, Nicolle Schwarz, Marie-Hélène Thibault, Gilles Alcaraz and Ibraheem A. I. Mkhalid in low to moderate yields and were only partially characterized. I developed optimized syntheses of these compounds which often involved implementing alternative strategies, modified reaction conditions or new work-up procedures. I also synthesized new derivatives, thus expanding the range of synthetic approaches used in this work. High yields of pure materials were achieved in all cases making the chemistry suitable for applications.

2.0 Results and Discussion

2.1 Synthesis and Characterization

In order to provide access to a library of pyrene derivatives, which are mono- or bis-substituted at the 2- and 7-positions, the regio-controlled C–H borylation of pyrene was employed to give **1** and **2** as starting compounds (Figure 1). This reaction has been previously communicated;[1] however, this work shows the applicability of this reaction on a larger scale (3-5 g) and with lower catalyst loadings (1 mol % $[Ir(OMe)COD]_2$). Compound **1** was isolated in a 94% yield, whereas in the case of **2**, competing di-

substitution to give **1** lowers the yield of the mono-substitution product. However, replacing THF by the nonpolar solvent, hexane, aids selectivity, leading to a higher isolated yield (65%) of **2** after column chromotography. Trace amounts (< 1%) of tris-borylated pyrene were observed by GC-MS in the reaction mixture of **1** when using 2.2 molar equivalents of B_2pin_2 and extended reaction times of 2-4 days. During the chromatographic isolation of **2**, a fraction containing a mixture of tris- and bis-borylated pyrene isomers (by GC-MS) was recovered in less than 1% yield. Substitution at the 2-position of pyrene with a *tert*-butyl group[2] blocked this position and allowed subsequent selective borylation at the 7- position to give 2-^{t}Bu-7-Bpin-pyrene **3** in a high yield (85%). This is a more straightforward route to a mono-borylated pyrene, due to the ease of purification of the product (Figure 1).

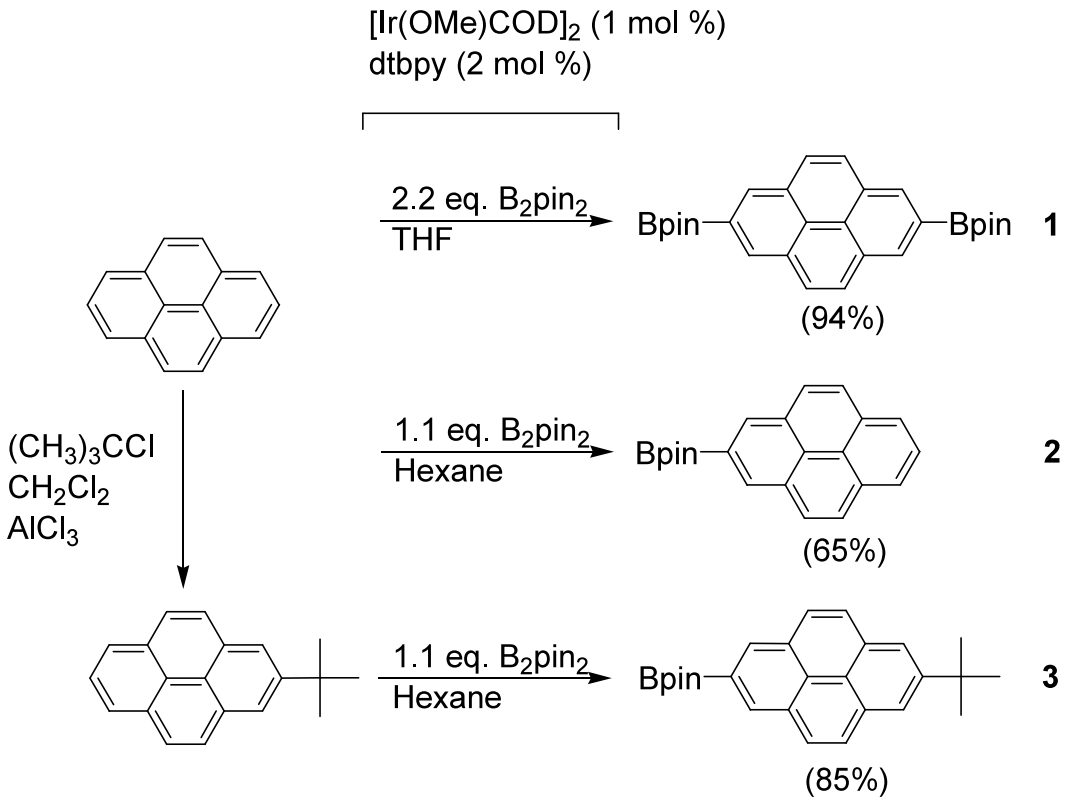

Figure 1 Iridium Catalyzed C-H Borylation of Pyrene

Although aryl boronate esters have been used extensively in Suzuki-Miyaura cross-coupling reactions,[3] attempts to employ compounds **1** and **2** in cross-coupling reactions under mild conditions were unsuccessful. This unusually low reactivity may be due to the fact that neither the HOMO nor LUMO of pyrene have any contributions at the 2,7-

positions. As mentioned in Chapter 1, **2** has been coupled to a uridine base, but long reaction times and harsh conditions were required.[4] Clearly, different methodologies are required to prepare derivatives of synthetic and photophysical interest from **1** and **2**. These methods are now discussed in detail.

All reactions were monitored by GC-MS and ^{1}H NMR spectroscopy, and the isolated compounds were fully characterized by NMR spectroscopy, mass spectrometry, elemental analysis (EA) and by single crystal X-ray diffraction studies for compounds **1-3, 7, 9-11, 15-17, 22, 24**. In the case of the bis-substituted pyrenes, two singlets of equal intensity due to the pyrene protons are observed in the region of 7.8-8.9 ppm in the ^{1}H NMR spectra, whereas in the spectra of mono-substituted pyrenes, a singlet, three doublets and a triplet are observed in the region of 7.7-8.6 ppm. The signals for pyrene itself appear in the region of 8.0-8.2 ppm; thus substituents at the 2- and 7-positions do influence the chemical shift of the pyrene protons, presumably by inductive effects.

In order to increase the reactivity of the borylated compounds **1** and **2** in Suzuki-Miyaura cross-couplings, the esters were converted into their corresponding boronic acids, **4** and **5**, by oxidative cleavage of pinacol with $NaIO_4$ and subsequent acidification, analogous to reported general procedures (Figure 2).[5, 6] Compound **4** is a known compound that has application in COF's (covalent organic frameworks).[6] The boronic acids were indeed much more reactive than the Bpin esters towards Suzuki-Miyaura cross-coupling with octyl 4-bromobenzoate and methyl 4-iodobenzoate, respectively, to give the pyrenyl 4-benzoic acid esters, pyrenyl-2,7-bis[4-(octylbenzoate)] **6** (75% yield) and pyrenyl-2-[4-(methylbenzoate)] **7** (60% yield), with the long chains added to compound **6** to improve solubility for further applications (Figure 2). It was found that addition of H_2O (1 mL) to improve solubility of the K_3PO_4 base used in the synthesis of **6** reduced the yield to 12%, presumably a result of a competing protodeborylation process.

The boronic acids, **4** and **5**, show evidence (MALDI-TOF MS) of condensation to form oligomers, as is usual for arylboronic acids, and to overcome this problem, the respective potassium trifluoroborates,[5] **8a** and **9**, were prepared. Compound **1** was reacted with six equivalents of KHF_2 to form $[K^+]_2[2,7\text{-}(BF_3)_2\text{pyrene}]^{2-}$ **8a** with complete conversion as shown by in situ NMR spectroscopy. Further purification was difficult due to the low solubility of the compound. Addition of six equivalents of 18-crown-6

ether improved the solubility of **8a**, and pure samples were isolated with the composition of **8a**·1.5(18-crown-6) **8b**, as determined by ^{1}H NMR spectroscopy and elemental analysis. Reaction of **2** with three equivalents of KHF_2 gave K^{+}[2-(BF_3)-pyrene]$^{-}$ **9** in good yields. The reactions with KHF_2 proceed under ambient conditions and require minimal workup, as the products, **8a** and **9**, precipitate as colourless solids (Figure 2). Reaction of **8a** and **9** with six and three equivalents of LiOH, respectively, followed by acidification, provided an alternative route to the boronic acids, **4** and **5**, with slightly higher yields (Figure 2). The products isolated using this method tended to require less purification than those prepared via the oxidation of the pinacol boronates. In the MALDI-TOF mass spectrum of **4**, higher mass signals corresponding to three or more units of the parent boronic acid less nH_2O were observed, consistent with the aforementioned condensation. In a further reaction, **9** underwent cross coupling with 1-iodo-4-dimesitylboryl-benzene under Suzuki-Miyaura conditions at 90 ºC, to give 2-(4-(dimesitylboryl)phenyl)pyrene **10** in a 65% yield after recrystallisation (Figure 2). The dimesitylboron moiety was chosen as it serves as an efficient π-acceptor[7] and is part of further work into π-conjugated organic compounds containing three-coordinate boron centres.[8] Such compounds have had a significant impact on the area of materials chemistry[7] as they display linear, nonlinear and electro-optical properties, which are useful for applications in OLEDs, sensors, solar cells and other optical materials.

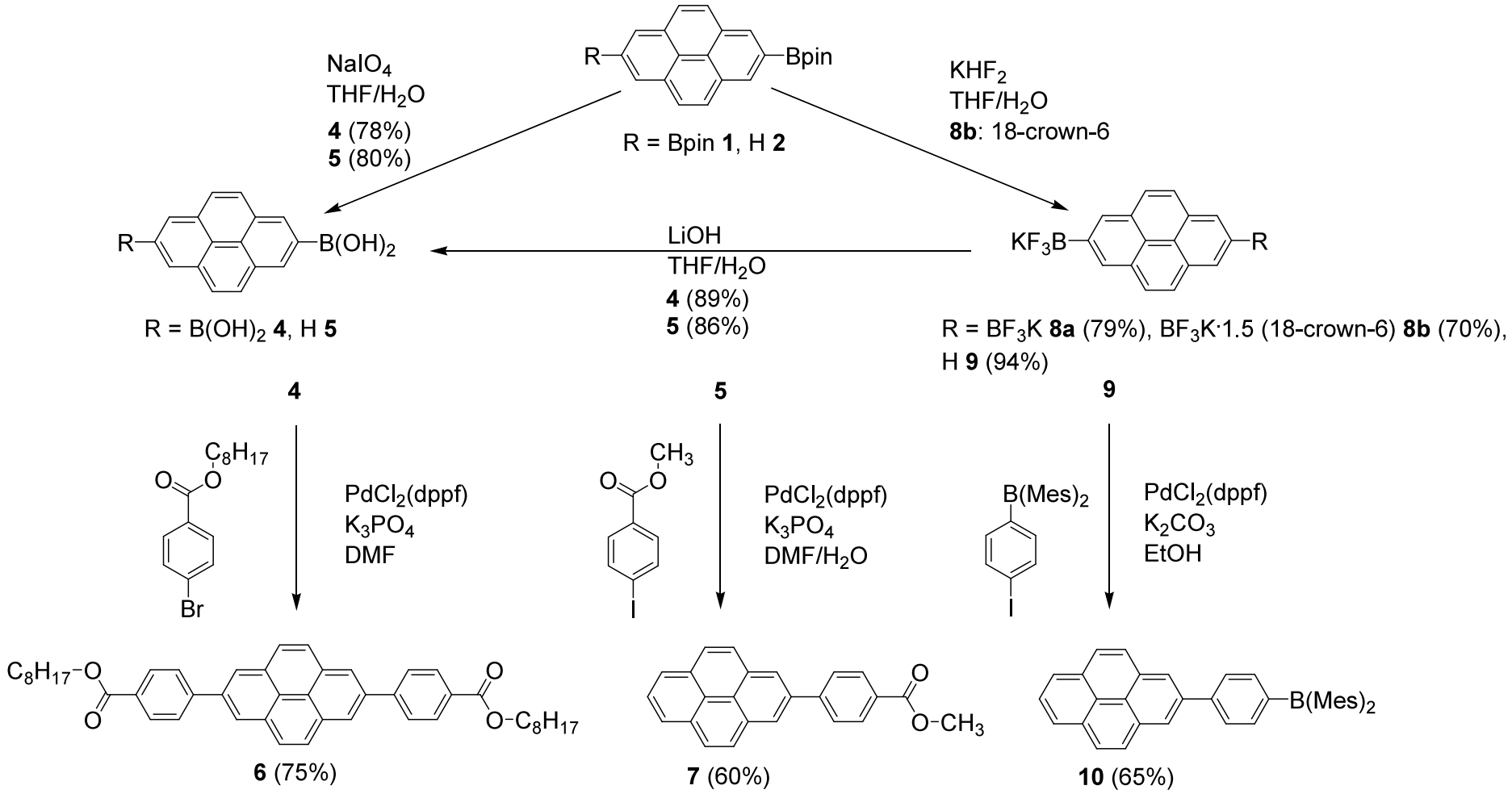

Figure 2 Synthesis and cross coupling of nucleophilic 2- and 2,7-substituted pyrenes

All of the above reactions have employed the pyrenyl boron reagent as a masked carbon nucleophile. A complementary approach to employ 2,7-substituted pyrene systems in cross-coupling reactions would be to convert the pyrene compound into an electrophile. Common electrophilic reagents for cross-couplings are aryl halides, and conversion of aryl boronate esters to the corresponding bromides using $CuBr_2$ has been reported.[9] Reaction of compound **1** with six equivalents of $CuBr_2$ in a mixture of THF, MeOH and H_2O gave 2,7-dibromo-pyrene **11**, and the analogous reaction of **2** with three equivalents of $CuBr_2$ gave 2-bromo-pyrene **12** (Figure 3). Aryl bromides **11** and **12**, were isolated in 70% and 88% yields, respectively, as they precipitated from the reaction mixture as colourless solids, which were easily purified by filtration and washing with water and hexane. Synthesis of **11** from [2.2]metacyclophanes[10] or dehydrogenated pyrene[11] has been reported. However, the current method allows the target compound to be obtained in two simple steps, compared to three steps. Furthermore, it is possible to carry out the C-H borylation/bromination sequence as a one-pot process,[9] isolating **11** in a 71% yield from pyrene. In the analogous one-pot synthesis of **12**, a mixture of unreacted pyrene and **12** was recovered, which proved difficult to separate. However, this mixture could be used for further reactions, such as cross-couplings, where separation of the unreacted pyrene from final products can be easier. The lithiation of 2,7-dibromo-pyrene **11**, followed by reaction with CO_2 is known to yield pyrene-2,7-dicarboxylic acid **13** (Figure 4).[12] The number of reaction steps is cut from four to three using the C-H borylation/bromination sequence and gives straightforward access in high yields to compounds that were previously laborious to synthesize. Lithiation of **12** and subsequent addition of dimesitylboron fluoride gave 2-(dimesitylboryl)pyrene **14** in a moderate yield (Figure 4).

Aryl triflates have also been used as electrophiles in many different coupling reactions, and conversion of boronic esters to alcohols and then triflates is known (Figure 3).[13] Oxidation of compound **1** with six equivalents of H_2O_2 and NaOH gave 2,7-dihydroxypyrene **15**; analogously, **2** was converted to 2-hydroxypyrene **16** (Figure 3). Both reactions gave high yields of the respective products, although if reaction times were longer than 16 hours, sample purity and yields were adversely affected.

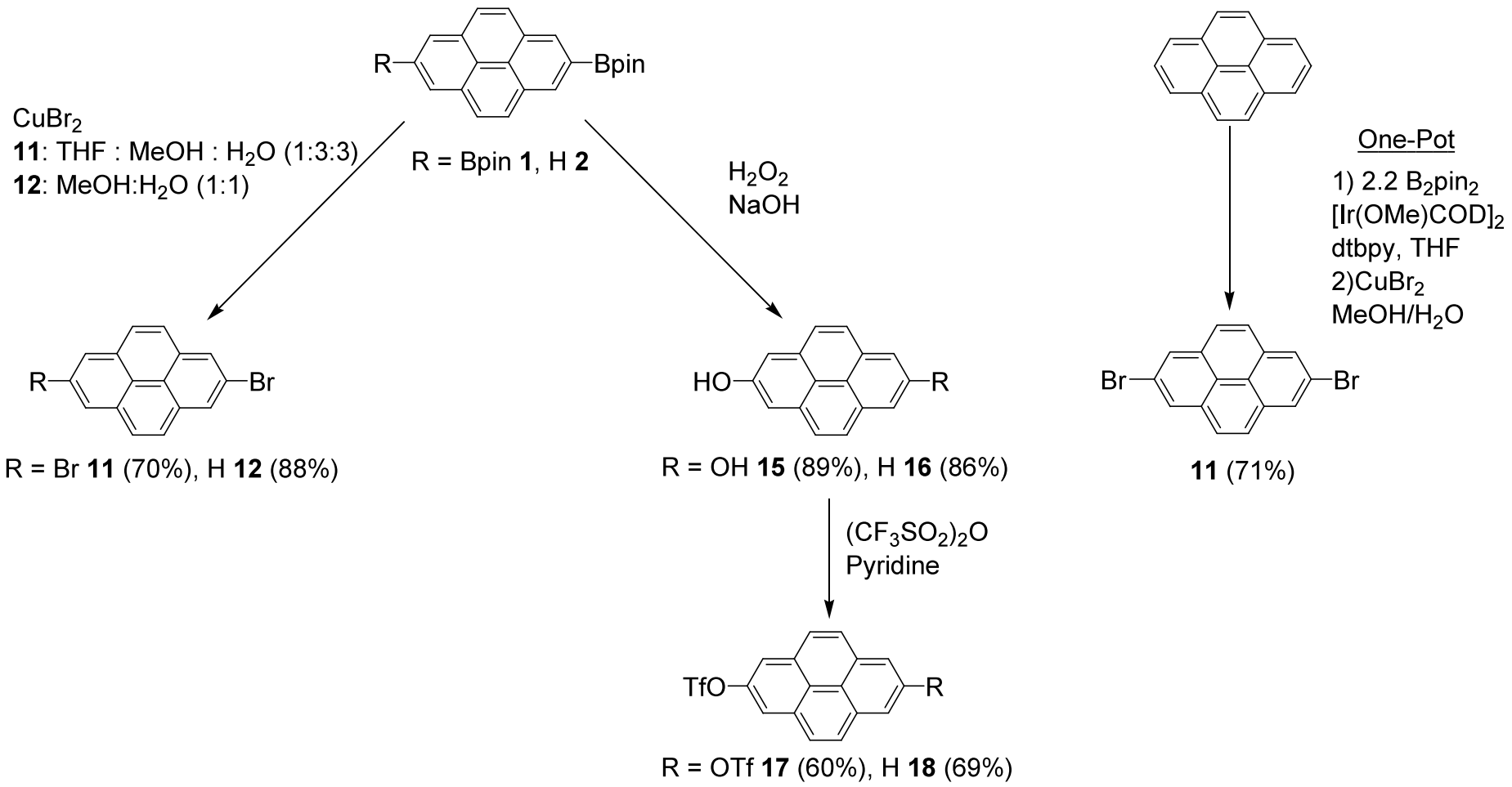

Figure 3 Synthesis of electrophilic 2- and 2,7-substituted pyrenes.

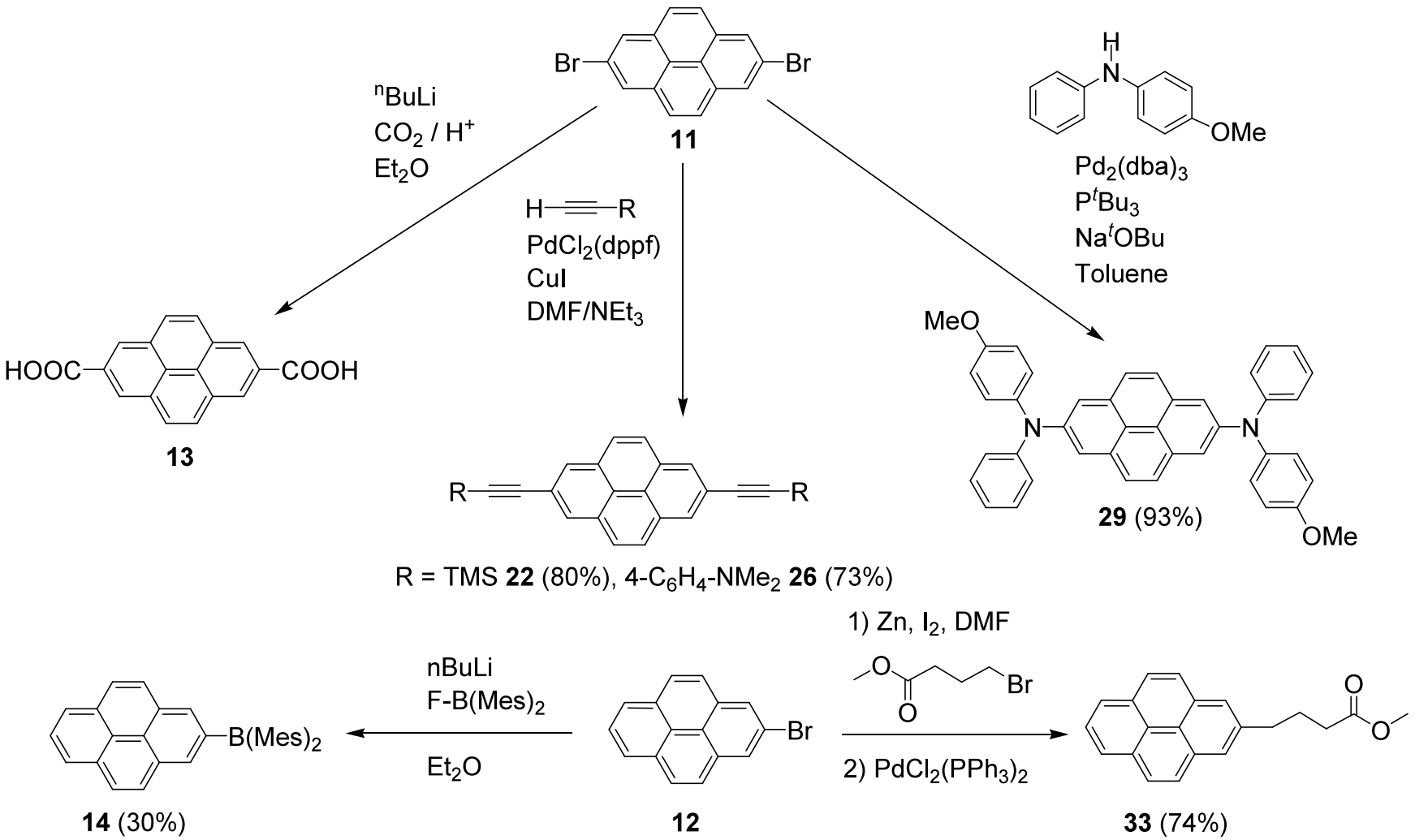

Figure 4 Lithiation and cross-coupling reactions of 2-(Br)-pyrene and 2,7-$(Br)_2$-pyrene.

The π-stacking properties of **15** have recently been investigated via conversion to its more soluble dibenzylether, which allowed complexation with macrocyclic systems.[14] To synthesize the aryl triflates, reaction of **15** and **16** with excess triflic anhydride in dry pyridine gave 2,7-bis(trifluoromethanesulfonyl)pyrene **17** and 2-(trifluoromethanesulfonyl)pyrene **18**, respectively (Figure 3); unlike the parent (Bpin)pyrene compounds, these elute rapidly with hexane:Et_2O on a silica column, making purification facile.

The above demonstrated synthetic routes not only provide pyrenes substituted with weak π-donors (Br, OH, OTf) or strong π-acceptors (CO_2H, $B(Mes)_2$) at the 2- and 2,7-positions, but also allow expansion of the library of pyrene compounds by further reaction; in particular, cross-coupling reactions utilizing compounds **11**, **12**, **17** and **18**. Thus reaction of **17** with two equivalents of phenylboronic acid under Suzuki-Miyaura conditions afforded 2,7-diphenyl-pyrene **19** in a 79% yield (Figure 5), although the product was rather insoluble, and heating to 100 ºC in the NMR spectrometer was required to obtain spectra of the compound. Sonogashira cross-coupling reactions of **17** with phenylethyne, 4-(dimesitylboryl)phenylethyne, and trimethylsilylethyne gave the respective products, 2,7-bis(phenylethynyl)-pyrene **20**, 2,7-bis(4-dimesitylborylphenylethynyl)pyrene **21** and 2,7-bis(trimethylsilylethynyl)pyrene **22**. During the workup of compound **22**, the mono coupled by-product, 2-(trifluoromethanesulfonyl)-7-(trimethylsilylethynyl)pyrene **23**, was isolated in a 22% yield (Figure 5). Further derivatization should be possible via the triflate moiety in **23**, leading to interesting unsymmetrically disubstituted pyrenes. Under similar conditions, coupling of **18** with phenylethyne and trimethylsilylethyne gave 2-(phenylethynyl)pyrene **24** and 2-(trimethylsilylethynyl)pyrene **25** in 78 and 75% yields, respectively (Figure 5). In order to demonstrate the synthetic value of 2,7-dibromopyrene **11** in cross-coupling reactions, it was coupled with 2.1 equivalents of TMSC≡CH under Sonogashira conditions as an alternative route to **22** (Figure 4). Initially, $[PdCl_2(PPh_3)_2]$ was used as the catalyst, but after overnight heating, incomplete conversion was observed by GC-MS. Using the more electron donating 1,1'-bis(diphenylphosphino)ferrocene (dppf) ligand led to complete conversion (by GC-MS) giving **22** in 80% isolated yield after column chromatography. The same method was used to synthesize 2,7-bis(4-*N*,*N*-dimethylaminophenylethynyl)pyrene **26** in a 73%

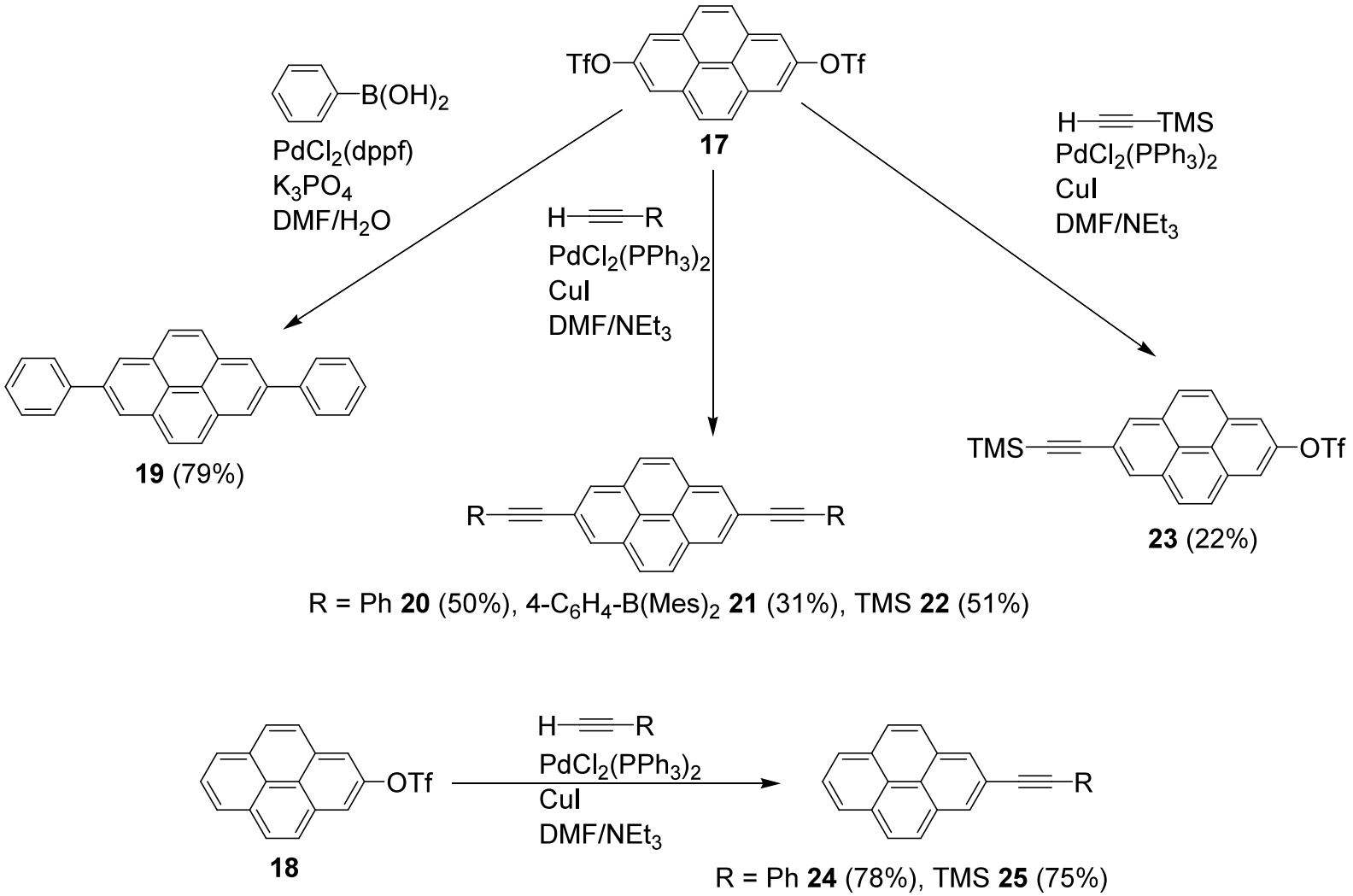

Figure 5 Cross coupling reactions of 2-(OTf)-pyrene and 2,7-$(OTf)_2$-pyrene.

yield providing an extended conjugated system containing the strong π-donor dimethylamino group (Figure 4). Deprotection of **22** and **25** with sodium carbonate in MeOH led to the isolation of the terminal alkynes 2,7-diethynylpyrene **27** and 2-ethynylpyrene **28**, in 86% and 81% yields, respectively (Figure 6). Both compounds are stable under ambient conditions for several days, and would be suitable for further elaboration via Sonogashira cross-coupling.

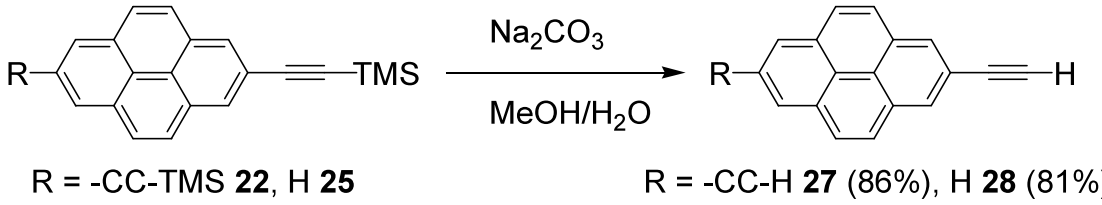

Figure 6 Synthesis of 2- and 2,7-ethynyl-substituted pyrenes

N, *N*, *N'*, *N'*-tetraaryl-1,1'-biphenyl-4,4'diamines (TPDs) are an important class of hole transporters for OLEDs.[15] Thus, to demonstrate the utility of Buchwald-Hartwig amination technology to the synthesis of analogous 2,7-bis(diarylamino)pyrenes, the reaction of **11** and (4-methoxy-phenyl)-phenyl-amine was carried out. The reaction gave 2,7-bis{(4-methoxy-phenyl)-phenyl-amino}-pyrene **29** in 93% yield (Figure 4). In contrast to the recent report[16] of the synthesis of the 1,6-isomer of **29** from 1,6-dibromopyrene, which employed $Pd_2(dba)_3$ as the catalyst, the synthesis of **29** from **11** required a more active catalyst, prepared *in situ* from $Pd_2(dba)_3$ and P^tBu_3. This observation, similar to that of the Sonogashira couplings of **11** (*vide supra*), again demonstrates the lower reactivity of 2,7-dibromopyrene in cross-coupling reactions compared with that of pyrenes substituted at the 1,3,6 and 8 positions. Presumably, this is a result of the fact that neither the HOMO nor LUMO of pyrene have a contribution at C2 or C7 due to the presence of a nodal plane passing through these carbon atoms.

Commercially available 4-(pyren-1-yl)-butyric acid **30** is used to determine oxygen concentrations in biological systems[17] and to investigate intracellular delivery of bioactive molecules.[18] For comparison of their photophysical properties to **30**, the related 4-(pyren-2-yl)-butyric acid **31** and 4-(pyren-2-yloxy)-butyric acid **32** were synthesised. Demonstrating the application of a Negishi coupling, alkylation of pyrene at the 2-position was performed. Zinc powder and a catalytic amount of iodine[19] were used to form the zinc reagent from 4-bromo-butyric acid methyl ester, which was then cross coupled to **12** using $[PdCl_2(PPh_3)_2]$ to give 4-pyren-2-yl-butyric acid methyl ester **33** in a 74% yield (Figure 4). Deprotonation of **16** with Na^{t}OBu followed by the addition of excess 4-bromo-butyric acid methyl ester gave 4-(pyren-2-yloxy)-butyric acid methyl ester **34** (Figure 7). Ester hydrolysis of compounds **33** and **34** using $LiOH{\cdot}H_2O$ gave acids **31** and **32** in 80 and 66% yields respectively (Figure 8). Similar to the synthesis of **34**, reaction of 1,12-dibromo-dodecane and **16** in the presence of Na^{t}OBu gave 2-(12-bromo-dodecyloxy)-pyrene **35** (Figure 7). Compound **35**, has the potential for further derivatization at the bromo end of the carbon chain, for example, the introduction of polar moieties, thus allowing it to be used as a fluorescence probe in biological systems.

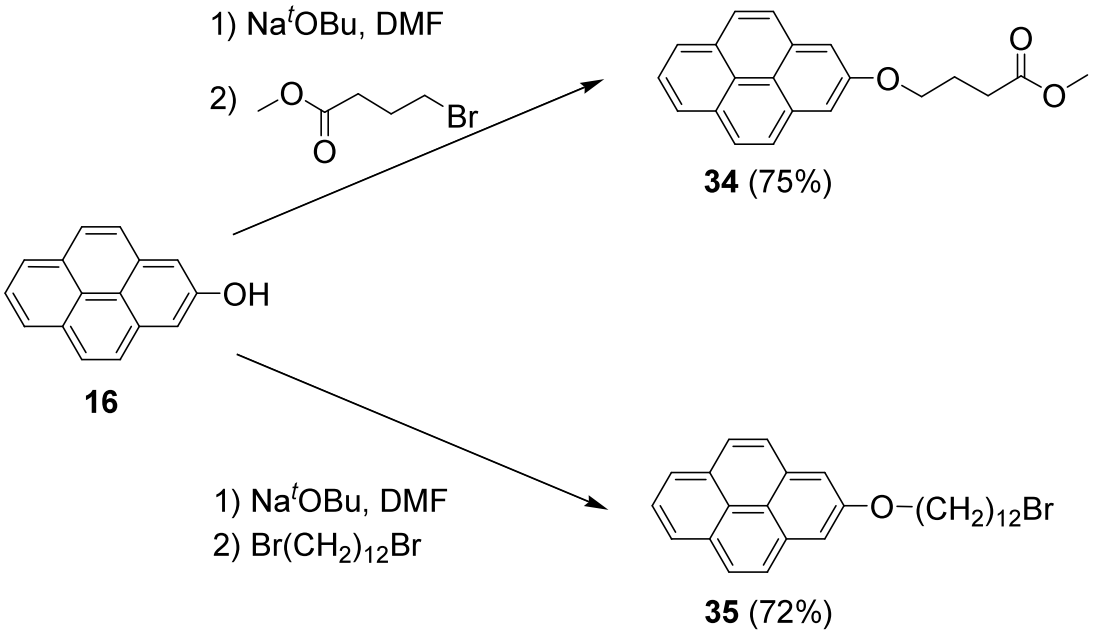

Figure 7 Synthesis of 2-substituted pyrene ethers

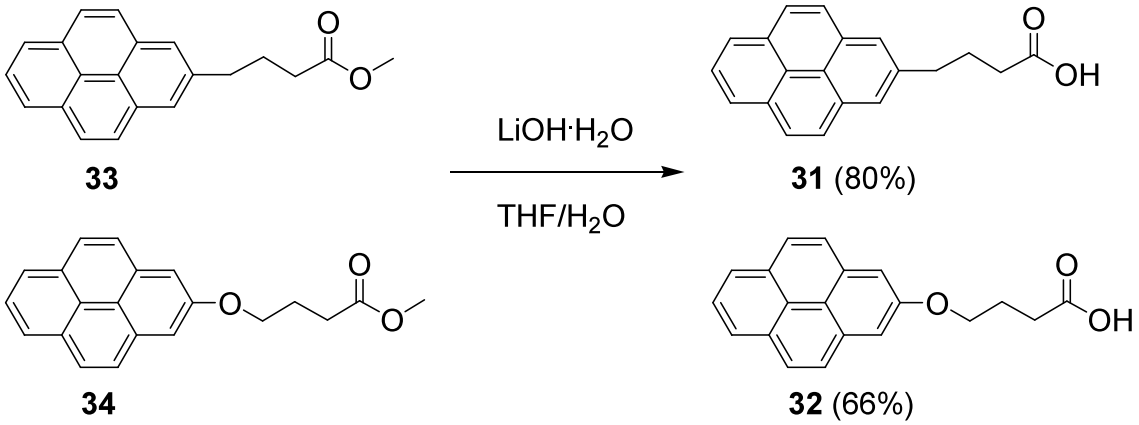

Figure 8 Ester deprotection to yield 2-substituted pyrene acids

For comparison of their photophysical properties with the 2-, and 2,7-substituted pyrenes, several pyrene derivatives substituted at the 1-position were synthesized (Figure 9). Reactions were followed by GC-MS. Bromination of pyrene by electrophilic aromatic substitution using HBr and hydrogen peroxide gave the known 1-bromopyrene **36**.[20] Sonogashira cross-coupling of **36** with phenylethyne gave 1-(phenylethynyl)pyrene **37**. ^{1}H and ^{13}C NMR spectroscopic data for **37** are in good agreement with those reported previously for the compound, which had been synthesized via cross-coupling between 1-ethynylpyrene and bromobenzene.[21] Analogous to the 2-substituted compounds, lithiation of **36** with $^{n}BuLi$ and subsequent reaction with dimesitylboron fluoride gave the recently reported 1-(dimesitylboryl)pyrene **38**.[22] Suzuki-Miyaura cross-coupling of **36** with 1-Bpin-4-(dimesitylboryl)benzene gave the previously unknown 1-(4-dimesitylborylphenyl)pyrene **39** in 61% yield. Reaction of **36** with B_2pin_2 via Pd-catalyzed borylation gave 1-(Bpin)pyrene **40** in 77% yield.[23]

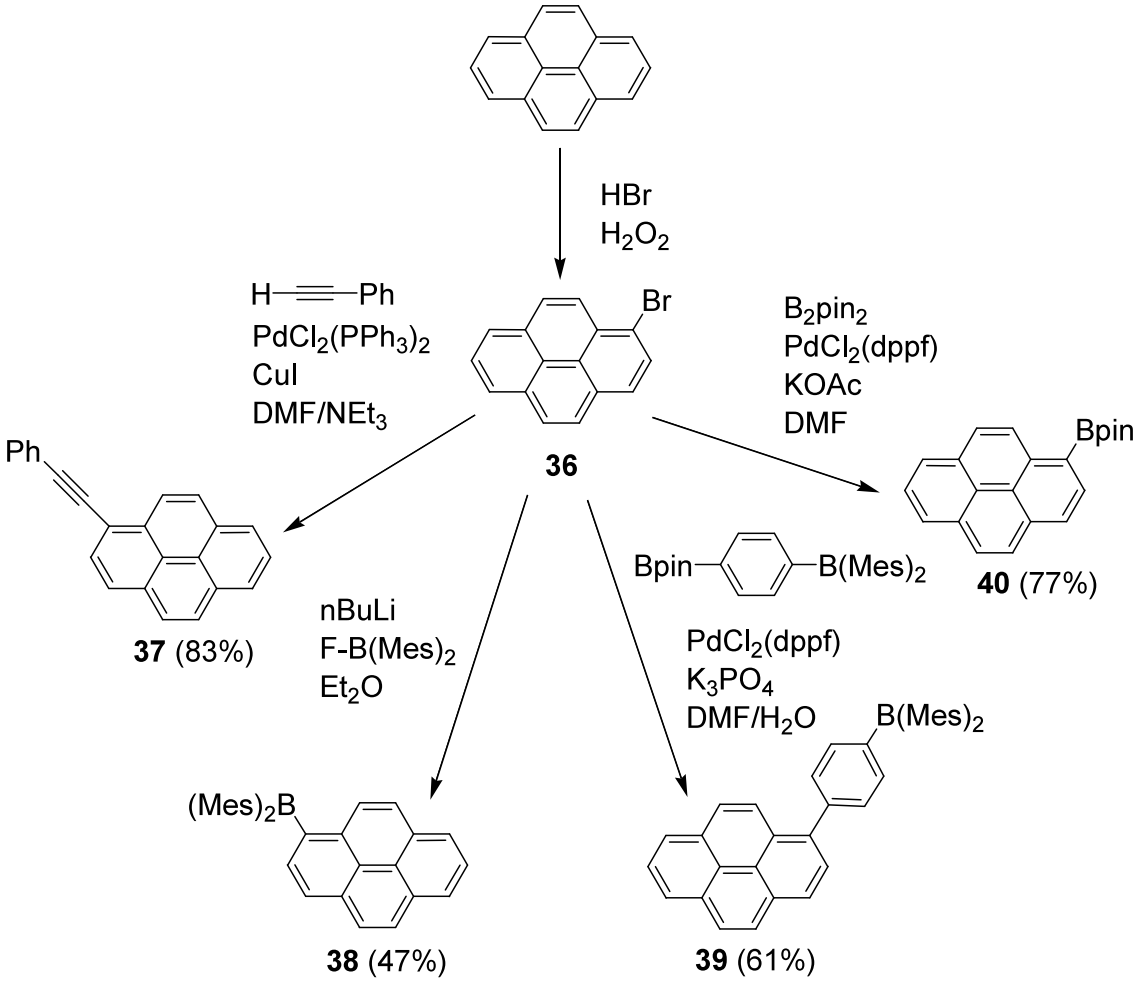

Figure 9 Synthesis of 1-substituted pyrene derivatives

2.2 Crystal Structures

To investigate the effects of substitution at the 2- and 2,7-positions on the crystal packing and hence the stacking properties of pyrene, single-crystal X-ray diffraction studies were carried out on compounds **1**-**3, 7, 9**-**11, 15**-**17, 22, 24**. The data collection and structural solutions were carried out by Dr. Andrei Batsanov.

The crystal packing of polycyclic aromatic hydrocarbons (PAH), such as pyrene have been classified[24] into four types (Figure 10):

a) Herringbone, dominated by edge-to-face (C-H…π) intermolecular interactions.

b) Sandwich-herringbone, wherein two parallel molecules form a sandwich via π-π interactions, and the sandwiches are arranged into a herringbone motif.

c) γ, comprising stacks of parallel (but offset) molecules, with π-π interactions within stacks and herringbone-type interaction between stacks.

d) β, a layered structure with strong π-π and negligible C-H…π interactions, usually without a large offset.

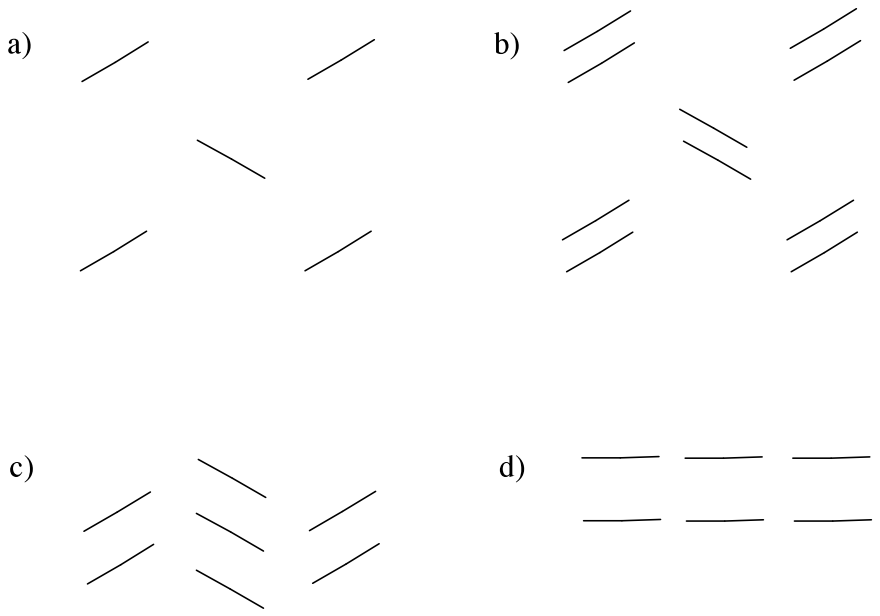

Figure 10 The crystal packing of polycyclic aromatic hydrocarbons (PAHs).[24]

The different packing types can by approximated by considering the shortest cell axis (l) and the dihedral angle (θ) between nearest contacting molecules.[24c] However, care must be taken when assigning crystal packing types using these criteria alone.

Pyrene has been found to have three polymorphs. Pyrene-I obtained under ambient conditions[25] and pyrene-II obtained by cooling or compression of solid pyrene-I.[26] Both belong to the sandwich-herringbone type packing (b), with two inversion-related molecules stacked face-to-face, with a dihedral angle between contacting diads of θ = 82.8° (I) or 76.5° (II). The third polymorph, pyrene-III, crystallized from solution at high pressure,[27] displays a denser β-packing (d), although has an exceptionally large θ value of 60° (usually for this type, θ < 30°).

The 2- and 2,7-pyrene derivatives are now discussed in detail, with reference to the above packing types.

Crystals of **1** (α-**1**, $P2_12_12_1$) grown from a THF/CH_2Cl_2 mixture have already been reported.[1] A second batch of monoclinic crystals of **1** grown by slow evaporation of ether solvent showed a new polymorph β-**1** (Figure 11). The molecule lies on a crystallographic inversion centre in the space group $P2_1/n$. When considering the

density difference between the polymorphs, it was found that β-**1** was 2% less dense than α-**1** (at 120 K, D_x = 1.200 (β-**1**) vs. 1.226 g cm^{-3} (α-**1**)). This observation is of interest because it conflicts Wallach's rule,[28] which states that racemic (centrosymmetric) polymorphs should be denser than chiral (non-centrosymmetric) ones. The rule was shown to be consistent with the discovery of a third polymorph γ-**1** ($P2_1/n$), which lies on a crystallographic inversion centre similar to β-**1**; however, it displays a different packing with a density (1.249 g cm^{-3} at 120 K) 2% higher than α-**1**. These findings need to be considered in discussions on the applicability of Wallach's rule in the literature.[29] Polymorph γ-**1** was obtained as small crystals from a bulk sample of **1**, that was predominantly a fine powder. (*cf*. white solid, experimental section).

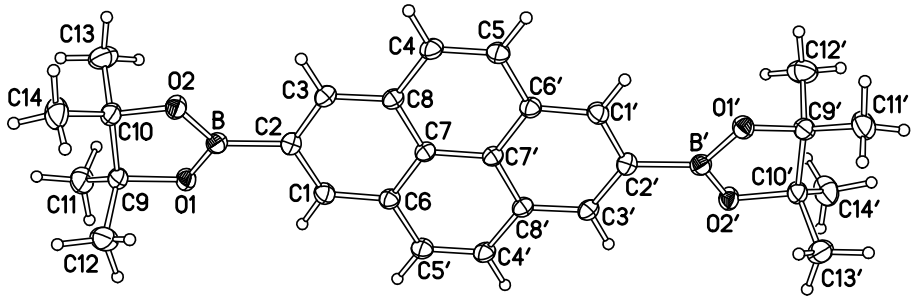

Figure 11 Molecular Structure of β-**1**; primed atoms are generated by the inversion centre.

Solvates of **1** were crystallized from a hexafluorobenzene (HFB) solution to obtain **1**·2HFB (Figure 12), whilst in toluene the following was observed: plate like crystals formed α-**1**·PhMe (Figure 13) which rapidly desolvated in air but, when left in toluene, dissolved and re-crystallized into oblong blocks found to be β-**1**. Upon evaporation, a different polymorph, β-**1**·PhMe (Figure 13), crystallized as prisms (needles) which, unlike α-**1**·PhMe, were stable to desolvation in air.

The structure and packing of the different polymorphs of **1** will now be discussed in detail.

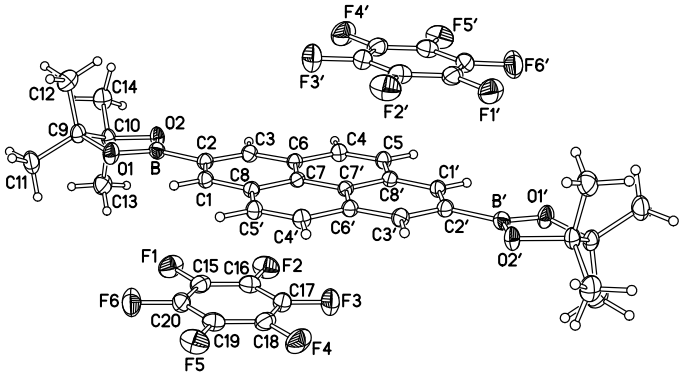

Figure 12 Formula unit of **1**·2HFB; primed atoms are generated by the inversion centre.

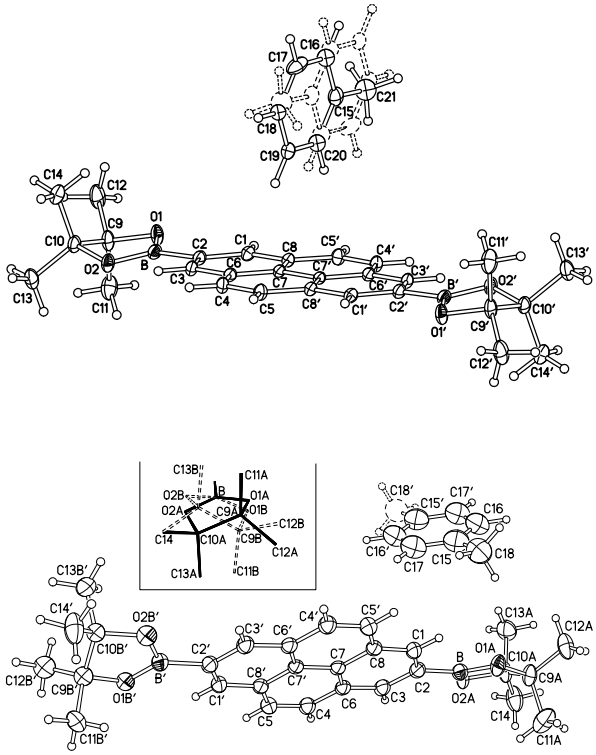

Figure 13 Molecular structure of α-**1**·PhMe (top) and β-**1**·PhMe (bottom, insert: disorder in Bpin group); primed atoms are generated by the inversion centres. Disorder in toluene molecules is shown.

The previously reported α-**1** structure was shown to have no crystallographic symmetry, with a dihedral angle (τ) between pyrene and the C(2)BO_2 planes of τ = 11.5° for one Bpin, while the second Bpin is equally disordered between two conformations, τ = 9.9° and 31.5°.[1] The pyrene moiety has a slight bend with the two substituted 6-membered rings having an interplanar angle of 3.5°. This compares to β-**1** and γ-**1** where the pyrene

moiety is planar and the Bpin rings adopt twisted conformations with $\tau = 17.6^{o}$ (β-**1**) and 3.1^{o} (γ-**1**).

Due to the structural importance of the Bpin groups, the three polymorphs are difficult to fit into the categories of PAH packing (*vide supra*). All three pack in a herringbone fashion; however, they exhibit large differences. The α-**1** form packs with contacts between methyl groups of one molecule and the face of the pyrene moiety of another, as well as pyrene-pyrene contacts. The dihedral angle (θ) between nearest contacting molecules is 52.4^{o}. In both β-**1** and γ-**1**, the methyl group-pyrene contacts dominate, with very little direct pyrene-pyrene interaction. In β-**1**, the long axes of the contacting molecules are more co-planar (angle 53.8^{o}), while in γ-**1**, they are perpendicular with an angle of 92.6^{o} (Figure 14).

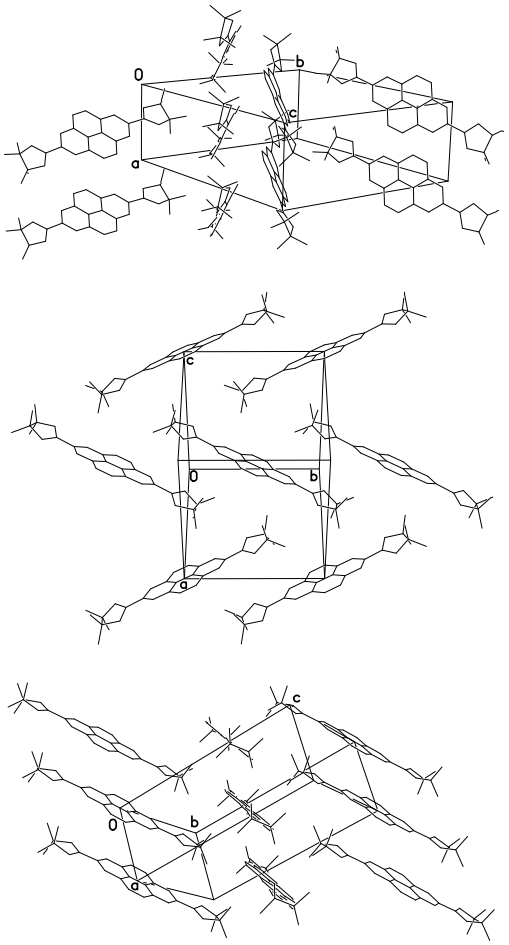

Figure 14 Crystal packing in polymorphs α-**1** (top), β-**1** (middle) and γ-**1** (bottom). Disorder and H atoms are omitted.

In **1**·2HFB, the components are stacked in the –pyrene-HFB-HFB-pyrene-HFB-HFB- sequence. The molecule of **1** lies at a crystallographic inversion centre, while the two adjacent HFB molecules (related by an inversion centre) are parallel and offset so that a fluorine atom of each molecule lies over the ring centre of the other. The interplanar separation between the HFB molecules is d = 3.23 Å and compares to d_{mean} = 3.41 Å for the separation of the HFB and pyrene planes, which are inclined to each other by 4.4° (Figure 15). This structure is unusual because planar arene and perfluoroarene molecules tend to co-crystallize in a 1:1 ratio, in which parallel (or nearly parallel) molecules of the two components alternate, forming mixed stacks.[30] A 1:2 co-crystallization is very rare with only two reported examples: *p*-t-butylcalix(4)arene·2HFB[31] and octadecamethoxyhexabenzocoronene·2HFB[32] clathrates. In both these cases, the host molecule is much larger than **1** and consists of non-coplanar arene rings. In the case of **1**, the out-of-plane orientation of the methyl groups appears to create suitable pockets for the $(HFB)_2$ diads.

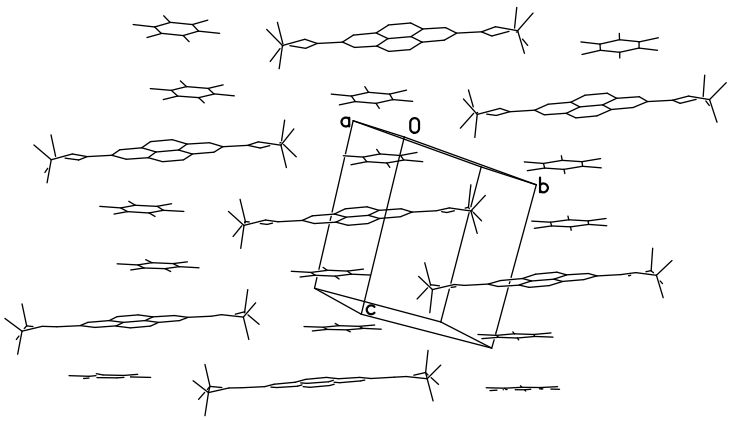

Figure 15 Crystal packing of **1**·2HFB

Molecule **1** lies at a crystallographic inversion centre in both polymorphs of **1**·PhMe, with the toluene molecule disordered between two overlapping positions related via another inversion centre. Further disorder is observed in β-**1**·PhMe, as the pinacol moiety is in a 3:2 ratio between two oppositely twisted conformations, with τ = 18.9° and 6.7°, respectively (α-**1**·PhMe: τ = 10.1°). The packing arrangement shows that in both structures, toluene occupies infinite channels between the host molecules, with the edges of the toluene molecule contacting two pyrene faces in a herringbone style

(Figure 16). Differences arise in the interplanar angles between pyrene and toluene planes, θ being 83.5° (α-**1**·PhMe) and 53.2° (β-**1**·PhMe). In the former, the face of the toluene molecule is in contact with the methyl groups of two host molecules, whereas in β-**1**·PhMe the toluene is enclosed by both the methyls and oxygens of the Bpin groups. These observations are of interest, as recent literature[33] discusses how dumbbell shaped host molecules (e.g., bis-adamantyl- or bis-*tert*-alkyl oligoalkynes) are able to form porous networks with nanometer-sized parallel channels, suitable for physical property design.

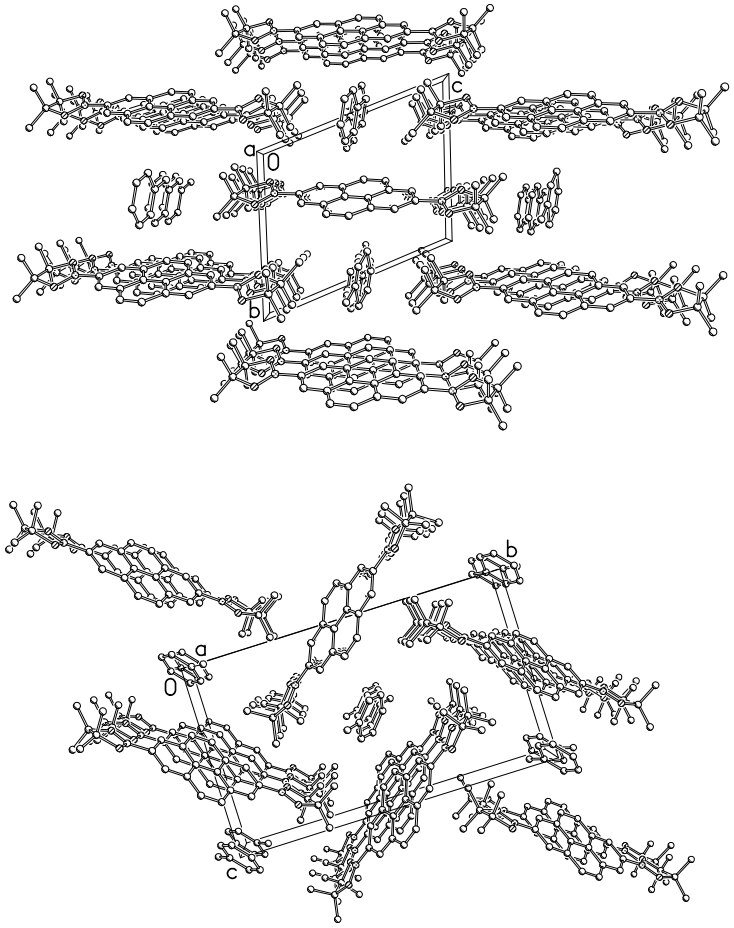

Figure 16 Crystal packing of α-**1**·PhMe (top) and β-**1**·PhMe (bottom) viewed down the toluene filled channels. Disorder and hydrogen atoms not shown.

Mono-borylated pyrene **2**, was crystallized from hexane on two separate occasions to yield monoclinic α-**2** and triclinic β-**2** polymorphs (Figure 17). A co-crystal of **2**·HFB was also obtained from a mixture of HFB and Et_2O.

Both the α-**2** and β-**2** polymorphs have asymmetric units comprised of three molecules *A*, *B* and *C*. In α-**2**, an envelope conformation is seen in the Bpin rings of all three molecules, with one carbon atom tilting out of the mean plane of the remaining four atoms by 0.39 Å (*A*), 0.42 Å (*B*) and 0.46 Å (*C*); whereas a twisted conformation is observed for the Bpin rings in β-**2**, with the two carbon displaced from the BO_2 plane in opposite directions, by 0.22 and –0.21 Å (*A*), 0.24 and –0.19 Å (*B*) and 0.26 and –0.20 Å (*C*). Similar to **1**, there is a dihedral angle between pyrene and the C(2)BO_2 plane with τ = 7.4° (*A*), 12.2° (*B*), 12.6° (*C*, 90%) and 22° (*C*, 10%) in α-**2**, and 6.0° (*A*), 6.3° (*B*) and 2.2° (*C*) in β-**2**.

There is a small resemblance to the sandwich-herringbone motif (PAH packing type (b) *vide supra*) in the packing of α-**2** (Figure 17). A face-to-face diad is formed between the pyrene moieties of molecule *A* and its inversion equivalent with a separation between the parallel aromatic planes of *d* = 3.37 Å. Similarly, B and C form a diad, this time with a staggered overlap and a pyrene/pyrene angle of 7.9°, the shortest separation being C(13*B*)…C(7*C*), *d* = 3.37 Å. The two diads are arranged in a near-perpendicular fashion with θ = 83.2° between molecules *A* and *B* and 89.9° between *A* and *C*. Similar diads are observed in β-**2** with molecule *A* and its inversion equivalent separated by 3.46 Å and offset by 3.34 Å. These *A* diads are arrayed in chains, interspersed with zones of molecules *B* and *C* and their equivalents, packed in a herringbone fashion (Figure 18).

In the structure of **2**·HFB (Figure 19), the BO_2 fragment of **2** is nearly coplanar with pyrene τ = 4.0°, while the C_2Me_4 moiety is disordered with equal probability between two oppositely twisted conformations (Figure 19). Unlike **1**·2HFB (*vide supra*), the co-crystal **2**·HFB has the usual arene-perfluoroarene[30] 1:1 composition, with mixed stacks of alternating (nearly parallel, θ = 2.9°) pyrene moieties and HFB molecules. The angles between aromatic moieties in different stacks show that they are nearly parallel: maximum pyrene/pyrene, pyrene/HFB and HFB/HFB angles are 10.7°, 13.7° and 14.2° respectively. Interestingly, this stacking is very similar to that of the co-crystal pyrene·HFB[30c] with the lengths of the shortest cell axes (also the stacking direction) similar despite the differences in lattices, **2**·HFB (tetragonal, *c* = 6.74 Å) and pyrene·HFB (monoclinic, *a* = 6.95 Å). A slight difference is observed in the pyrene…HFB interplanar separations with **2**·HFB slightly tighter (3.33 Å vs. 3.39 Å).

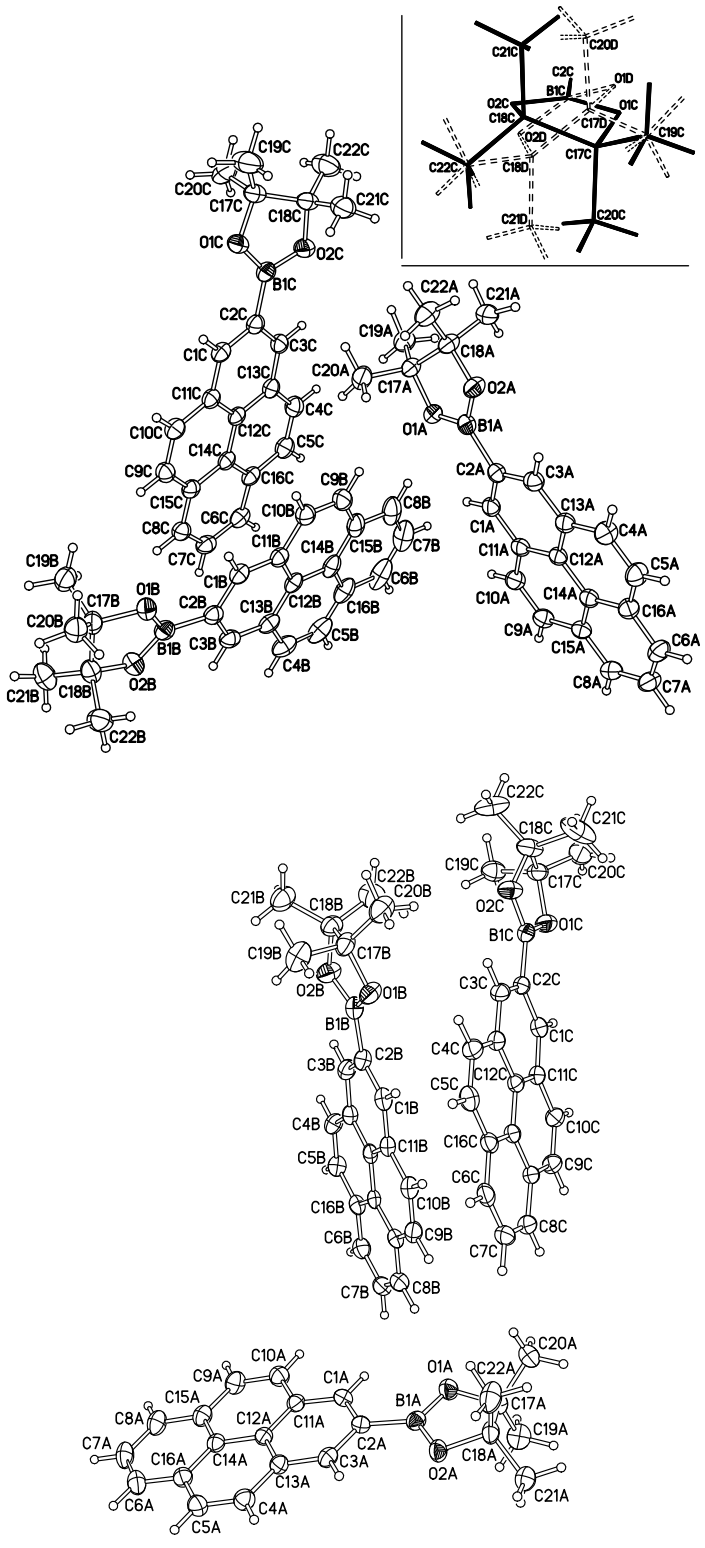

Figure 17 Molecular structure of α-**2** (above, disorder of the Bpin group in molecule *C* is shown) and β-**2** (below). There are three independent molecules in each crystal.

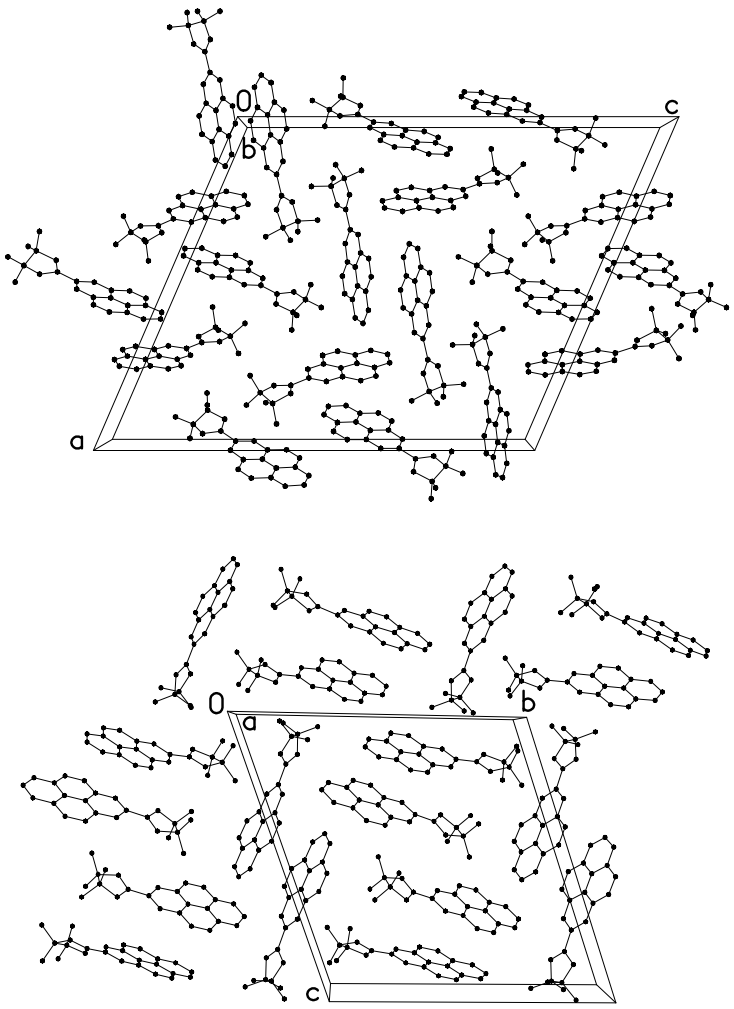

Figure 18 Crystal packing of α-**2** (top) and β-**2** (bottom). H atoms and disorder are omitted.

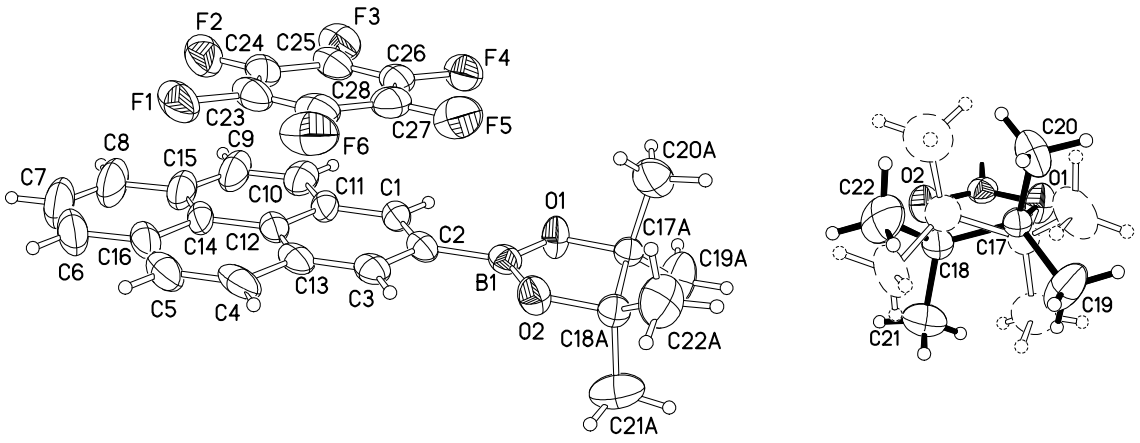

Figure 19 Formula unit of **2**·HFB (left); disorder in the Bpin moiety (right).

In molecule **3**, 2-^{t}Bu-7-Bpin-pyrene, there is no crystallographic symmetry (Figure 20). A dihedral angle between pyrene and the C(2)BO_2 plane of $\tau = 15°$ is observed and the Bpin ring displays a twisted conformation. Packing is in brickwork-type layers with molecules in each layer translationally related and therefore parallel. Between adjacent layers, the molecules are related by a screw axis and have a 17° inclination between the pyrene planes (Figure 20).

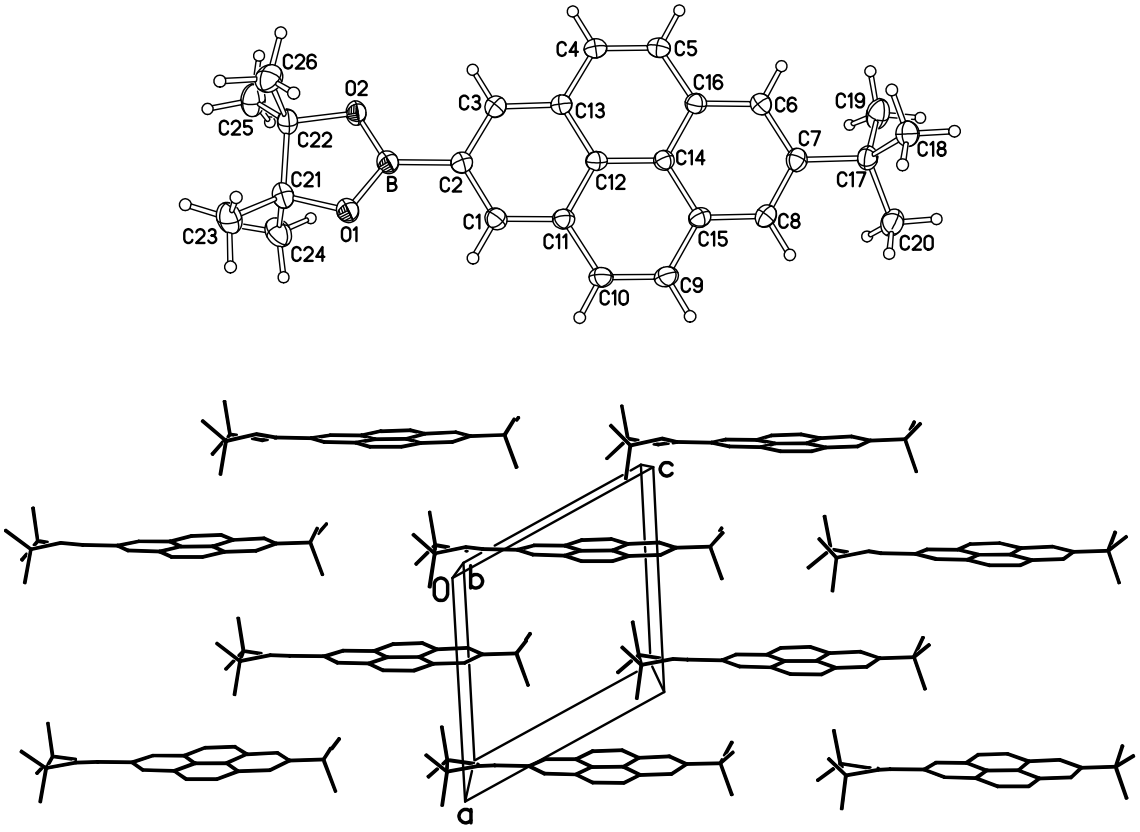

Figure 20 Molecular structure (top) and crystal packing (bottom) of **3**.

The ionic compound **9**, was found to have a polymeric structure. Seven fluorine atoms from five different anions, along with the C(2) atom of one of these anions surround the potassium cation in a non-uniform fashion (Figure 21). The K…F distances (*d*) and corresponding bond valences (calculated as $v = \exp[(1.99-d)/0.37]$[34] are listed (Table 1). In agreement with Pauling's rule,[35] (stable ionic structures are arranged to preserve local electroneutrality) the sum of the bond valences (Σv) is close to 1. Only two other structures have been reported in which potassium coordinates to fluoroborate groups only, although numerous structures are known with coordination to fluoroborate

derivatives along with other ligands, such as crown ethers. In KBF_4[36] the potassium cation is surrounded by twelve fluorine atoms (d = 2.76 to 3.32 Å, Σv at K^+ = 1.026), while $K_2[o\text{-}C_6F_4(BF_3)_2]$[37] contains two independent K+ cations surrounded by ten fluorine atoms each (d = 2.65 to 3.20 Å and d = 2.60 to 3.40 Å and Σv at K^+ = 0.970 and Σv at K^+ = 1.030, respectively).

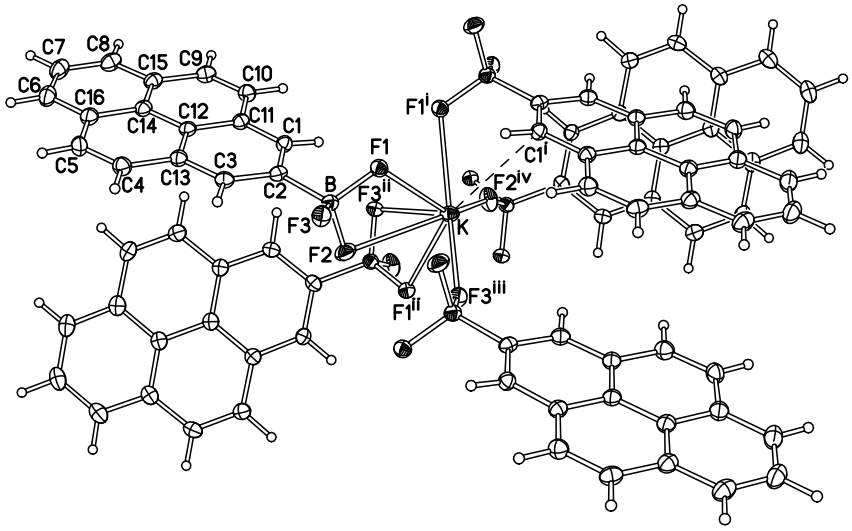

Figure 21 The potassium coordination in solid **9**.

	d (Å)	v
K–F(1)	2.728(1)	0.1362
K–F(1^{i})	2.671(1)	0.1586
K–F(1^{ii})	2.729(1)	0.1356
K–F(2^{iii})	2.634(1)	0.1756
K–F(2)	2.981(1)	0.0687
K–F(3^{ii})	2.784(1)	0.1169
K–F(3^{iv})	2.615(1)	0.1848
total		0.9764

Table 1 Bond distances (d) and orders (v) in **9**.

The crystal packing of **9** (Figure 22) comprises alternating polar (BF_3 and K) and non-polar (pyrene) layers, with the pyrene forming a herringbone pattern with $\theta = 53.6^{o}$ (*cf.* **7** and **17**).

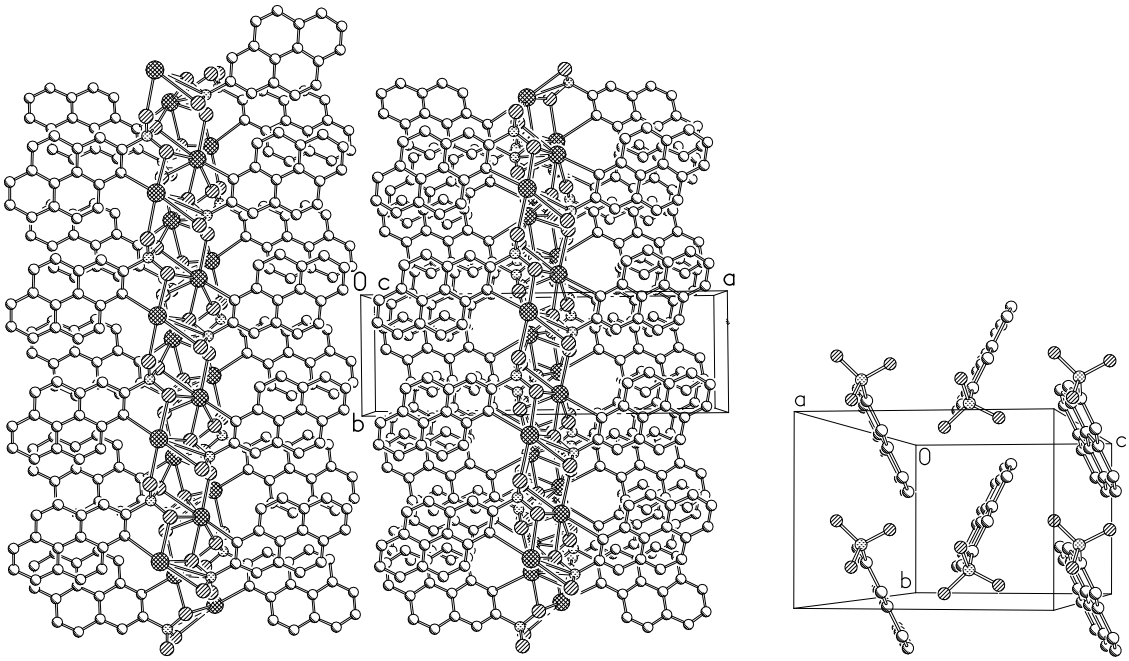

Figure 22 Crystal packing of **9** (left, H atoms omitted) and the herringbone packing of pyrene moieties therein (right, K and H atoms omitted).

Cross-coupling of **9** with 1-iodo-4-dimesitylboryl-benzene gave compound **10**, which was crystallized from $CDCl_3$ to give the solvate **10**·$CDCl_3$, containing one formula unit per asymmetric unit (Figure 23). The $CDCl_3$ molecule shows rotational disorder. The substituted ring (*i*) on the pyrene molecule is puckered while the other three rings (*ii*, *iii*, *iv*) lie in one plane. Atoms C(1), C(2) and C(3) deviate by 0.11, 0.21 and 0.14 Å, respectively, and this is comparable to compound **16** where the C(1), C(2), C(3) and O atoms deviate by 0.05, 0.06, 0.02 and 0.08 Å, respectively, from the *ii*/*iii*/*iv* plane. Otherwise, most of the pyrene derivatives in this study have planar pyrene systems.

In **10**, the C(2) atom has trigonal-planar geometry, with dihedral angles between its plane and the *ii*/*iii*/*iv* plane of 8.1° and the phenylene ring *v* of 37.8°. The three aromatic rings around the trigonal-planar boron atom (phenylene *v*, mesityl *vi* and *vii*) are inclined in a propeller-like fashion by 23.4, 53.6 and 60.2°, respectively, similar to other Aryl-$B(Mes)_2$ structures.[8h] Highly efficient stacking is not observed due to the non-planarity of the $B(Mes)_2$ groups and instead the pyrene moiety form diads via face-to-face contact with its inversion equivalent. These diads have an interplanar separation of 3.54 Å and are interspersed with solvent molecules and $B(Mes)_2$ groups.

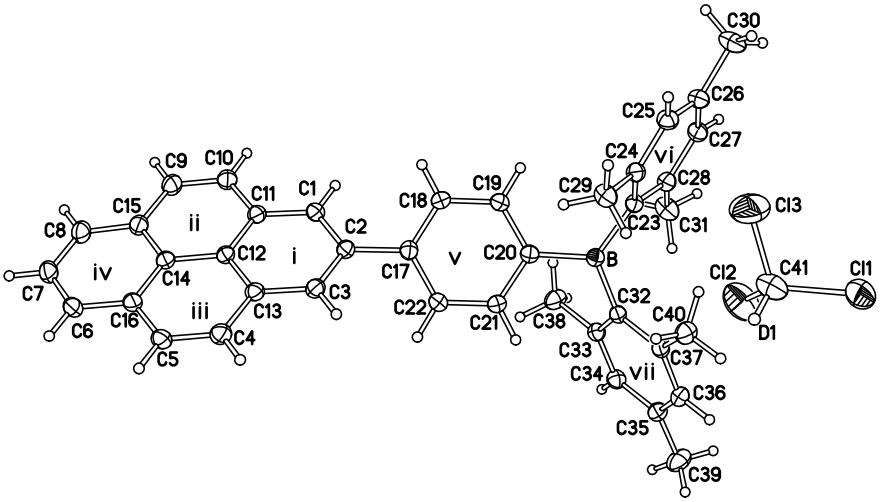

Figure 23 The asymmetric unit of **10**·$CDCl_3$. The solvent molecule is shown in the major orientation of its rotational disorder.

In contrast, **7**, which differs only in the replacement of the $B(Mes)_2$ group with an ester, packs in segregated layers of aromatic moieties and ester groups. The pyrene moieties are in a herringbone arrangement with θ = 54.5° (*cf.* **9** and **17**). In the molecule, the phenylene ring forms dihedral angles of 42.3° with the pyrene plane and 8.5° with the ester group (Figure 24).

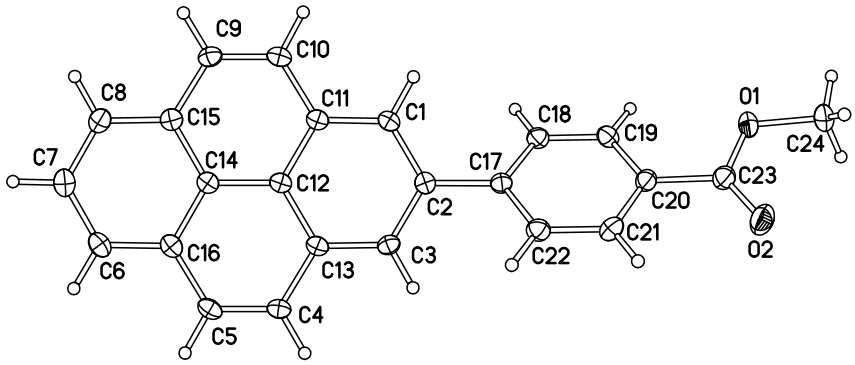

Figure 24 Molecular structure of **7**.

The bis-substituted compounds, 2,7-dibromo- **11** and 2,7-dihydroxy-pyrene **15** display similar packing (Figure 25). Slanted stacks are formed from parallel molecules with the pyrene moieties overlapping with uniform interplanar separations of 3.36 and 3.44 Å respectively (**15** is strengthened by infinite zigzag chains of interstack hydrogen bonds).

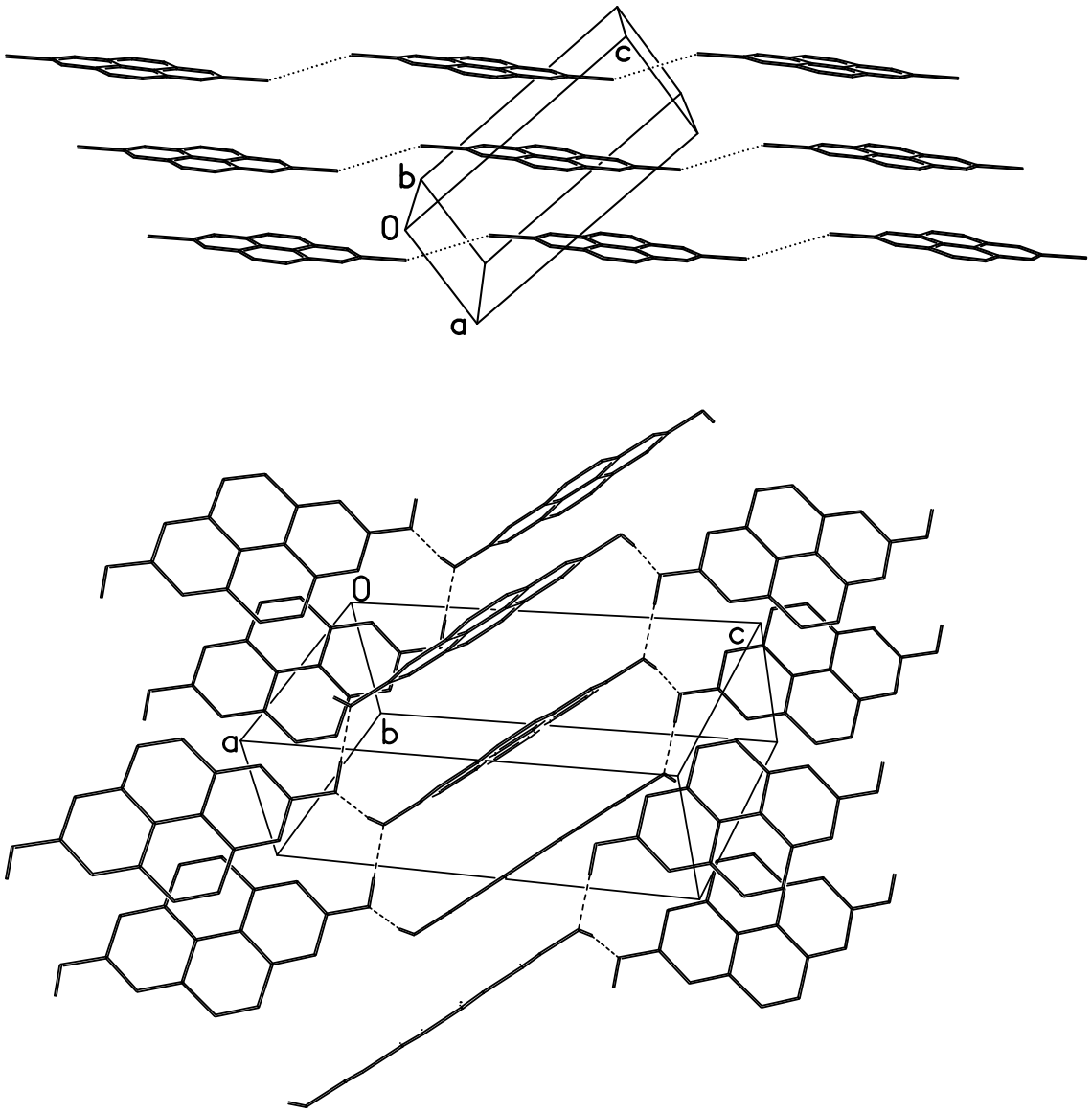

Figure 25 Crystal packing of **11** (top, dotted lines show shortest Br…Br contacts) and **15** (bottom, dashed lines show hydrogen bonds).

Due to the presence of strong π-π and absent C-H…π interactions, this structure can be assigned to type d (β). However, due to offset packing the shortest cell axes (also the stacking directions) are a = 4.71 Å in **11** and b = 4.61 Å in **15**, longer than usual for β structures (3.8-4.1 Å) and are similar to the type c (γ-structure: 4.6-5.4 Å). In **11**, the molecular planes are parallel with θ = 0°, while in **15**, the molecules in adjacent stacks are nearly perpendicular with θ = 85.2°. Molecule **11** is located on a special position (Figure 26). Molecule **15** has crystallographic C_i symmetry, with its hydroxyl hydrogen atom deviating 0.42 Å from the pyrene plane; this corresponds to a 25.5° twist around

the C-O bond (Figure 27). Similarly in 2-hydroxypyrene **16** there is a twist around the C-O bond of 26.0° (Figure 27). The crystal packing is also similar to that of **15**, with parallel pyrene moieties forming slanted stacks with an interplanar separation of 3.40 Å and θ = 85.9°. Adjacent stacks are chained into double-ribbons by interstack hydrogen bonds (Figure 28).

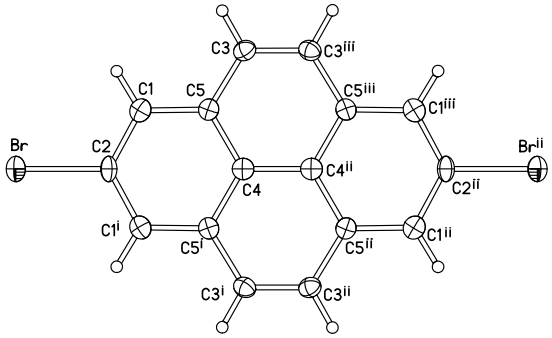

Figure 26 Molecular structure of **11**.

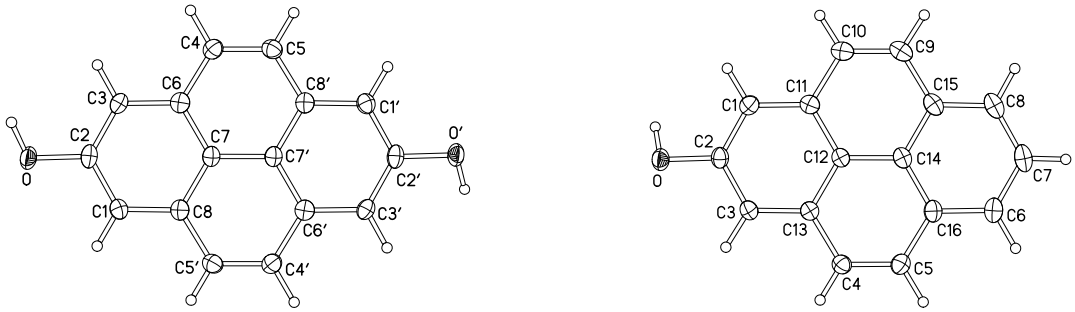

Figure 27 Molecular structures of **15** (left) and **16** (right).

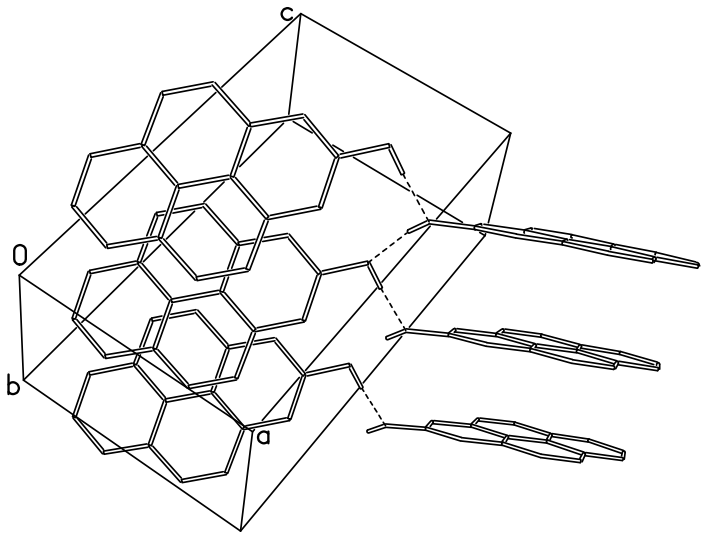

Figure 28 Crystal packing of **16**, showing hydrogen bonds as dashed lines. Non-hydroxyl H atoms are omitted.

Analysis of a crystal of molecule **17** (2,7-bis(OTf)-pyrene) at both 293 and 150 K revealed a centrosymmetric molecule with little disorder in the triflate groups (Figure 29). Packing is analogous to **7** and **9**, with segregated layers of polar triflate and non-polar pyrene moieties (Figure 30). The pyrene moities are packed in a herringbone motif similar to that found in naphthalene.[27] Upon cooling from 293 to 150 K, the *a* axis (perpendicular to the layers) and the *c* axis undergo contractions of 0.7% and 2.9% respectively, while the *b* axis expands by 0.4% and θ widens from 50.8 to 52.6°. Overall, there is a distortion in the herringbone pattern. Further cooling leads to a phase transition between 140 and 130 K, producing twinned crystals that are unsuitable for structure determination.

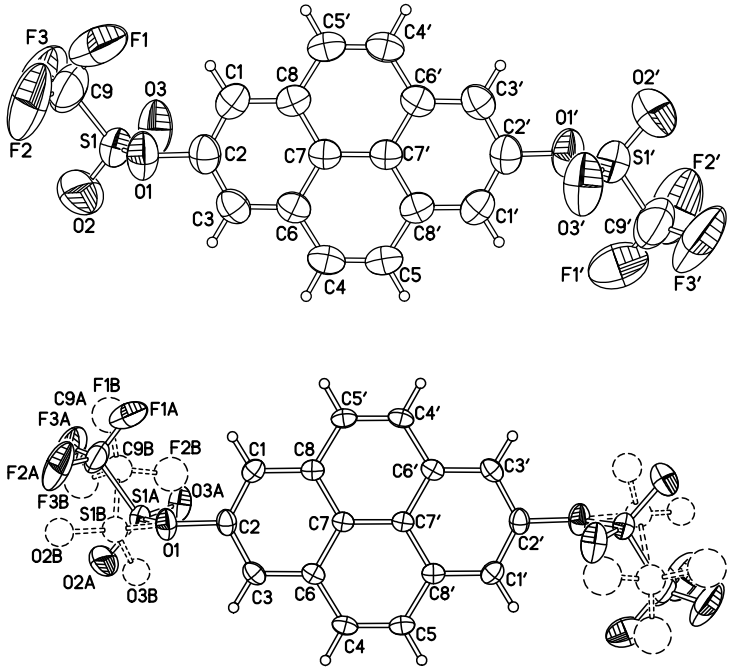

Figure 29 Molecular structure of **17** at 293 K (top, disorder omitted) and 150 K (bottom, disorder shown). Primed atoms are generated by the inversion centre.

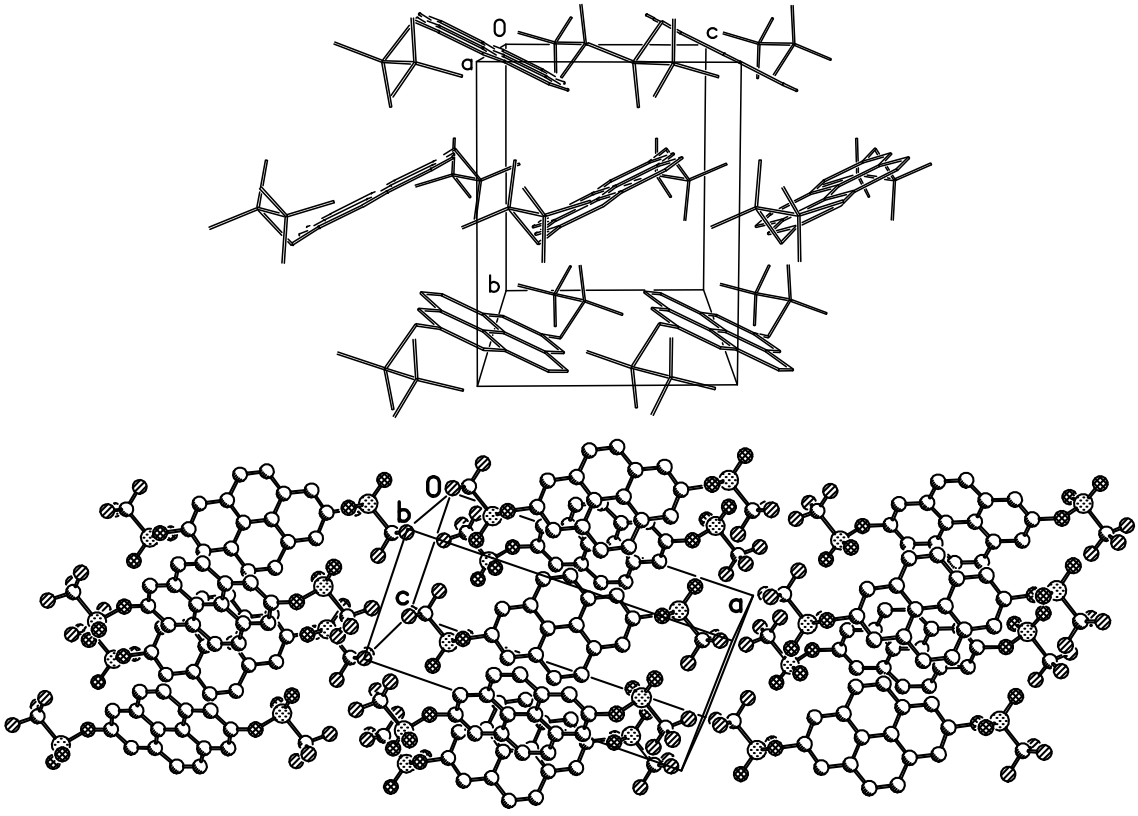

Figure 30 Crystal packing of **17** at 150 K, omitting hydrogen atoms and disorder.

Molecule **22** (2,7-bis(TMSA)-pyrene) was obtained from cross-coupling of TMSA with **17**. The molecule which has crystallographic C_i symmetry packs in stacks of severely slanted parallel pyrene moieties with uniform interplanar separations of 3.38 Å (Figure 31). The offset between adjacent molecules is so large that only the fringe carbon atoms actually overlap in almost eclipsed positions (C…C distances of 3.46-3.47 Å). As well as the π-π interactions, there are significant C-H…π interactions between adjacent stacks. Between stacks (θ = 77.4°), the pyrene moieties form herringbone type contacts, the shortest of which is C(1)H(1)…C(5) of 2.58 Å.

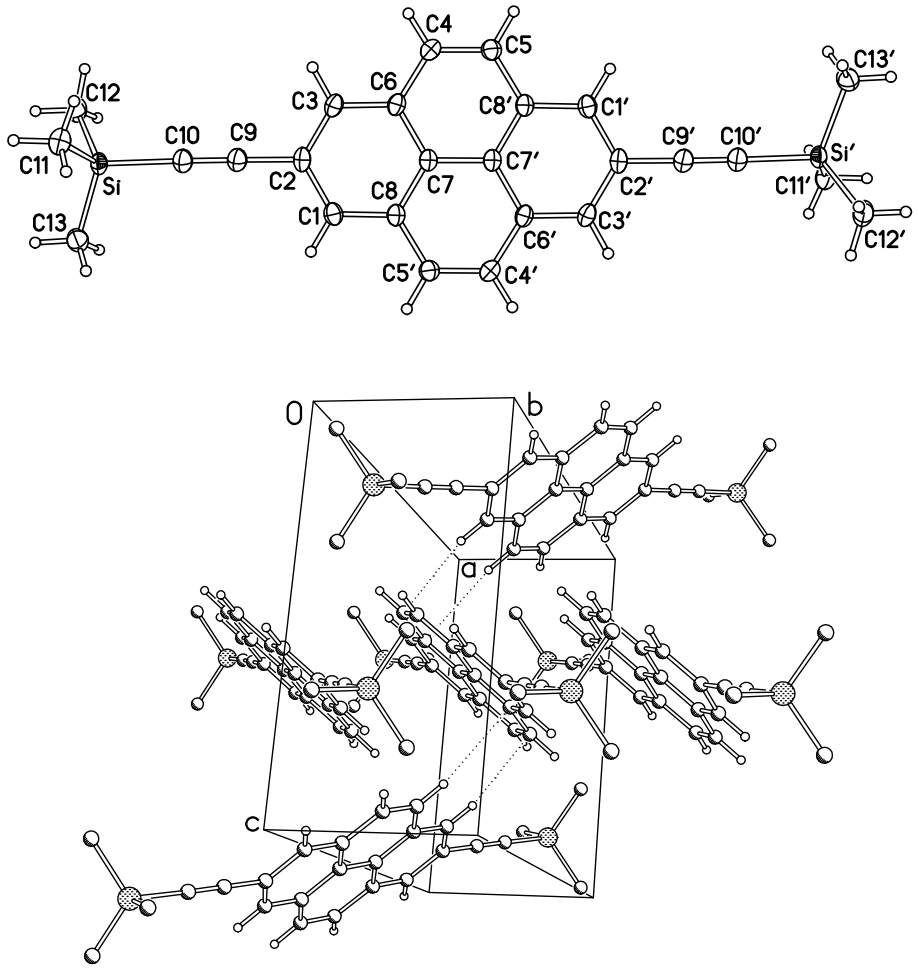

Figure 31 Molecular structure (top, primed atoms generated by the inversion centre) and crystal packing (bottom, dotted lines show short H…C contacts) of **22**.

The related ethynyl compound, **24** (2-phenylethynyl-pyrene), has an asymmetric unit consisting of two molecules, *A* and *B* (Figure 32). The intramolecular angles between

the pyrene and phenyl planes are of 26.9 and 20.8°, respectively. The molecules stack head-to-tail in slanted arrays (Figure 33). Within each array all molecules are symmetrically related via inversion or translation and hence their molecular planes are parallel. Stacks of molecule A have alternating interplanar separations of 3.53 and 3.79 Å, while those for molecule B are 3.55 and 3.68 Å. Between the pyrene planes of adjacent stacks, there is a dihedral angle of θ = 83.2° and some C-H…π interactions, suggesting a γ-type (*c*) structure, although the shortest cell length (*a* = 7.99 Å) is much longer than expected for this type.

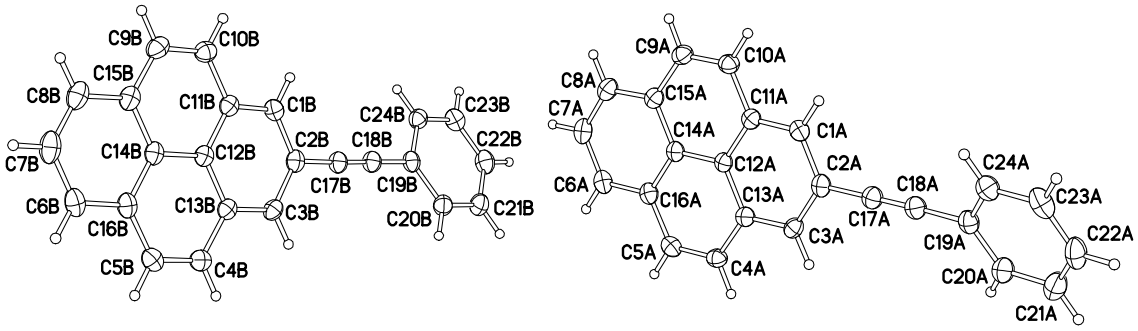

Figure 32 The asymmetric unit of **24**.

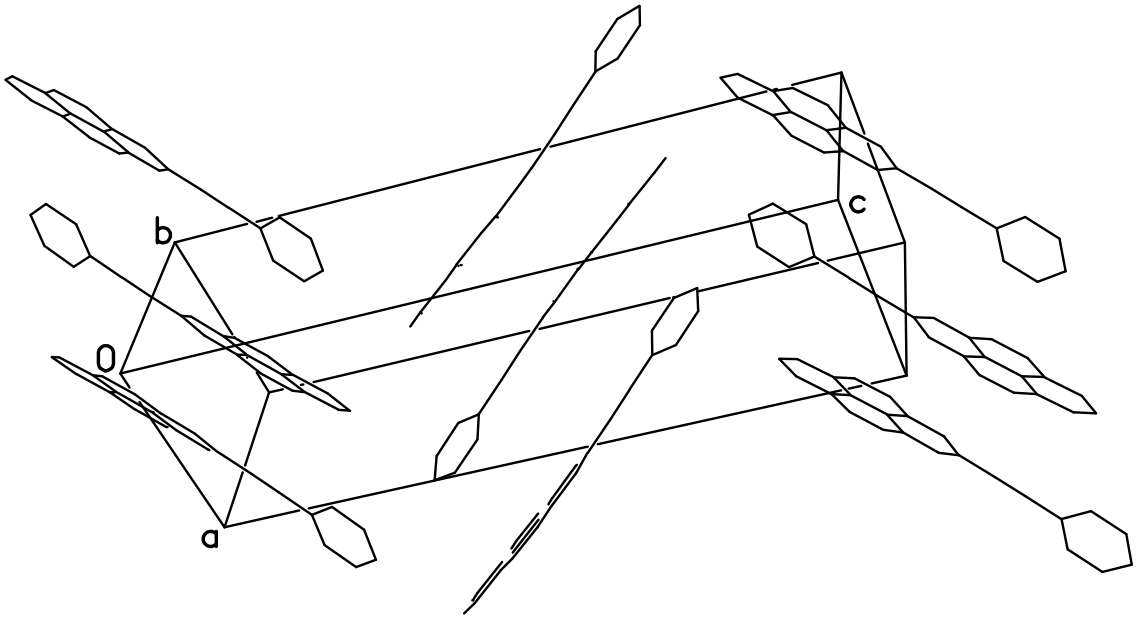

Figure 33 Crystal packing of **24** (H atoms are omitted).

3.0 Conclusions

A straightforward and high-yielding synthetic route to 2- and 2,7-substituted pyrene derivatives has been demonstrated.

The synthetic value of 2,7-bis(Bpin)pyrene **1** and 2-(Bpin)pyrene **2** is highlighted by converting them into nominally nucleophilic (e.g., $B(OH)_2$, BF_3K) and electrophilic (eg., Br, OTf) pyrene derivatives, which were further utilized in Suzuki-Miyaura, Sonogashira, Buchwald-Hartwig and Negishi cross-coupling reactions. Using this methodology, a library of 2- and 2,7-substituted pyrenes bearing donor and acceptor groups, including aryl, ethynyl, arylethynyl, alkyl, hydroxy, alkoxy, diarylamino, carboxylic acid and diarylboryl derivatives was prepared.

The solid-state structures of several derivatives obtained by single crystal X-ray diffraction revealed a diverse range of structures and packing modes. In particular, three polymorphs, two 1:1 co-crystals with toluene, and a rare 1:2 co-crystal with hexafluorobenzene were structurally characterized for 2,7-bis(Bpin)pyrene **1**. Likewise, pure mono-Bpin derivative **2** also crystallized in two polymorphs. However, in contrast to **1**, a 1:1 co-crystal with hexafluorobenzene was formed which exhibited the usual alternating π-stacked structure. 2,7-Dibromo pyrene **11**, 2,7-dihydroxypyrene **15** and 2-hydroxypyrene **16** all exhibit β-type π-stacked structures whereas pyrene-2,7-bis(trifluoromethanesulfonate) **17**, pyrene-2-trifluoroborate potassium salt **9** and pyrenyl-2-[4-(methylbenzoate)] **7** form layered herringbone structures in which the polar and non-polar (pyrene) moieties alternate. The propeller-like arrangement of the bulky triaryl boron moiety in 2-[(4-dimesitylboryl)phenyl]pyrene **10** precludes a π-stacked structure.

The unique photophysical properties of the 2- and 2,7-substituted pyrenes, in comparison to typical 1-substituted derivatives, are discussed in detail in the following chapter.

The high-yielding methodology described above, provides rapid access to derivatives which maintain the long two-fold rotational axis of pyrene and as such are expected to be particularly useful in the synthesis of conjugated rigid-rod systems, molecular rotors and organic and metal-organic frameworks. The new derivatives would also be useful in applications where the photophysical properties of a compound are of importance, as discussed in the next chapter.

Through collaborations with other groups, several of the above 2- and 2,7-derivatives have already found use in different applications:

Compound	Group	Application
2,7-$(B(OH)_2)_2$-pyrene **4**	Prof. Jim Wuest *University of Montréal, Canada*	Surface adsorption and crystallization of boronic acids
2,7-$(B(OH)_2)_2$-pyrene **4**	Prof. Zhengtao Xu *City University of Hong Kong, China*	Design and synthesis of MOFs. (See chapter 4)
2,7-$(Br)_2$-pyrene **11**	Prof. Anthony Davis *University of Bristol, UK*	Supramolecular chemistry applications
2-(Br)-pyrene **12**	Dr Andrew Beeby *Durham University, UK*	Pyridine ligands for iridium complexes.
2-(Br)-pyrene **12**	Dr Steven Cobb and Prof. Jon Steed *Durham University, UK*	Fluorescence labels for polypeptides.
2,7-$(OH)_2$-pyrene **15**	Prof. Howard Colquhoun *University of Reading, UK*	Binding studies in host-guest systems (*vide supra*).[14]

4.0 Experimental

General

Reagents purchased from commercial suppliers were tested for purity before use. Pyrene (Aldrich, 98%) was purified before use by passage through a 5 cm silica pad, eluting with hexane. The compounds (4-methoxy-phenyl)-phenyl-amine,[38] 4-bromo-butyric acid methyl ester[39], 1-bromopyrene[20] **36**, 1-phenylethynylpyrene[21,42] **37**, 1-dimesitylboryl-pyrene[22] **38**, 1-((4-dimesitylboryl)phenyl)pyrene[42] **39** and 1-Bpin-pyrene[23] **40** were synthesized as reported. Dimesitylboron fluoride was obtained by reaction of mesitylmagnesium bromide with $BF_3{\cdot}OEt_2$,[40] and was used to synthesize 1-iodo-4-(dimesitylboryl)benzene[8h] which in turn was used to synthesize 4-(dimesitylboryl)phenylethyne.[41] Reactions were monitored in situ by GC-MS, TLC or by ^{1}H NMR spectroscopy to assure consumption of starting materials prior to work up. GC-MS analyses were performed on an Agilent Technologies 6890 N gas chromatograph equipped with a 5973 Inert Mass Selective Detector and a 10 m fused silica capillary column (5% cross-linked phenylmethylsilicone) using the following operating conditions: injector temperature 250 ºC, detector temperature 300 ºC, the oven temperature was ramped from 50 ºC to 300 ºC at 20 ºC min^{-1}. UHP helium was used as the carrier gas. NMR spectra were recorded on Varian Mercury-200, Bruker Avance-400, Inova-500 and Varian VNMR 700 spectrometers at the following frequencies: ^{1}H: 200, 400, 500 and 700 MHz, ^{13}C{^{1}H}: 100 and 126 MHz, ^{19}F{^{1}H}: 376 MHz, ^{11}B{^{1}H}: 128 MHz. Mass spectra were obtained using a Waters Xevo QTOF equipped with Atmospheric Solids Analysis Probe (ASAP), a Thermo-Finnigan LTQ FT mass spectrometer for high resolution ESI spectra and an Applied Biosystems Voyager-DE STR spectrometer for MALDI-TOF analyses. High resolution EI mass spectra were recorded by the National Mass Spectrometry Service at Swansea, using a Finnigan MAT 95 XP spectrometer. Elemental analyses were performed using an Exeter Analytical E440 machine. Melting point values were measured on a Sanyo Gallenkamp apparatus and are uncorrected.

1: Pyrene-2,7-bis(4,4,5,5-tetramethyl-[1,3,2]dioxaborolane) *(2,7-bis(Bpin)pyrene))*

Using a variation of the procedure described by Coventry et al.[1a] In a nitrogen filled glove box, $[Ir(\mu\text{-OMe})COD]_2$ (0.06 g, 0.09 mmol), 4,4'-di-^{t}Bu-2,2'-bipyridine (dtbpy, 0.048 g, 0.18 mmol) and B_2pin_2 (0.10 g, 0.39 mmol) were dissolved in THF (5 mL). The

mixture was added to a tube, fitted with a Young's teflon tap, containing pyrene (1.80 g, 8.9 mmol) and B_2pin_2 (4.86 g, 19.13 mmol). After addition of THF (10 mL), the tube was sealed and the reaction mixture was stirred at 80 ºC for 16 h. Then, the reaction mixture was passed through a 5 cm silica pad eluting with CH_2Cl_2 and the solvent was removed under reduced pressure. The pale yellow residue was purified by sublimation (150 ºC @ 6 x 10^{-4} Torr) and then washed with refluxing hexane (100 mL) to afford **1** (3.8 g, 94%) as a white solid. mp 331-333 ºC; ^{1}H NMR (400 MHz, $CDCl_3$, δ): 8.62 (s, 4H), 8.08 (s, 4H), 1.46 (s, 24H). Characterization data for this compound was in agreement with that reported elsewhere.[1a]

2: 4,4,5,5-tetramethyl-2-pyren-2-yl-[1,3,2]dioxaborolane *(2-Bpin-pyrene)*

Using a variation of the procedure described by Coventry et al.[1a] In a nitrogen filled glove box, [Ir(μ-OMe)COD]$_2$ (0.06 g, 0.09 mmol), dtbpy (0.048 g, 0.18 mmol) and B_2pin_2 (0.10 g, 0.39 mmol) were dissolved in hexane (5 mL). The mixture was added to a Young's tap tube containing pyrene (2.0 g, 9.9 mmol) and B_2pin_2 (2.79 g, 11 mmol). Hexane (10 mL) was added, the tube sealed and the reaction mixture was stirred at 80 ºC for 16 h, at which time no B_2pin_2 was observed by GCMS. The reaction mixture was passed through a silica pad eluting with CH_2Cl_2, and the solvent was removed under reduced pressure. Purification of the residue by column chromatography (silica gel, hexane:CH_2Cl_2 1:1) and subsequent recrystallization from hexane afforded **2** (2.10 g, 65%) as a white solid. mp 127-128 ºC; ^{1}H NMR ($CDCl_3$, 400 MHz, δ): 8.67 (s, 2 H), 8.17 (d, J = 8 Hz, 2H), 8.13 (d, J = 9 Hz, 2H), 8.07 (d, J = 9 Hz, 2H), 8.02 (t, J = 8 Hz, 1H), 1.49 (s, 12H). Characterization data for this compound was in agreement with that reported elsewhere.[1a]

3: 2-(7-*tert*-butyl-pyren-2-yl)-4,4,5,5-tetramethyl-[1,3,2]dioxaborolane (*2-Bpin-7-^{t}Bu-pyrene*)

Using a modification of the procedure first described by Dr Zhiqiang Liu.[42] In a nitrogen filled Schlenk flask, [Ir(μ-OMe)COD]$_2$ (0.034 g, 0.05 mmol), dtbpy (0.027 g, 0.10 mmol) and B_2pin_2 (0.05 g, 0.20 mmol) were dissolved in hexane (2 mL). To this flask, 2-^{t}Bu-pyrene[2b] (1.01 g, 3.9 mmol) and B_2pin_2 (1.27 g, 5.0 mmol) in hexane (10 mL) were added and the mixture was stirred at 80 ºC for 16 h. The reaction mixture was passed through a silica pad eluting with CH_2Cl_2 and the solvent was removed under

reduced pressure. Purification of the residue by column chromatography (silica gel, hexane:CH_2Cl_2 5:1) and subsequent recrystallization from hexane gave **3** (1.27 g, 85%) as colourless crystals. mp 240-241 °C; ^{1}H NMR ($CDCl_3$, 700 MHz, δ): 8.63 (s, 2H), 8.22 (s, 2H), 8.09 (d, J = 8 Hz, 2H), 8.05 (d, J = 8 Hz, 2H), 1.59 (s, 9H), 1.46 (s, 12H); ^{13}C{^{1}H} NMR ($CDCl_3$, 175 MHz, δ): 149.8, 131.7, 131.4, 130.5, 127.9, 127.8, 127.7, 126.6, 123.1, 122.30, 84.3, 35.5, 32.2, 25.2; ^{11}B{^{1}H} NMR ($CDCl_3$, 224.5 MHz, δ): 31.4; EI-MS *m/z*: 384 (M^+); HRMS-EI: (M^+) Calcd for $C_{26}H_{29}{}^{10}BO_2$ 383.2177; Found 383.2285; Anal. Calcd for $C_{26}H_{29}BO_2$: C, 81.26; H, 7.61. Found: C, 81.02; H, 7.58.

4: Pyrene-2,7-bis(boronic acid)

Method 1: Using a modification of the procedure first described by Dr Nicolle Schwarz.[43] Compound **1** (1.0 g, 2.2 mmol) was dissolved in THF/H_2O (4:1, 20 mL) and $NaIO_4$ (3.83 g, 17.9 mmol) was added. The suspension was stirred for 40 min and then HCl (3 mL, 1 M) was added. The mixture was stirred for 48 h. The suspension was diluted with water (20 mL) and extracted with ethyl acetate (3 × 50 mL). The combined organic phases were washed with brine (50 mL) and H_2O (50 mL), dried over $MgSO_4$ and the solvent was removed under reduced pressure. The residue was washed with hexane (5 × 50 mL) and dried *in vacuo* to give **4** (0.50 g, 78%) as a light brown solid.

Method 2: Compound **8a** (1.23 g, 2.97 mmol) was suspended in THF (100 mL). To this suspension LiOH·H_2O (2.24 g, 53.40 mmol) in H_2O (20 mL) was added and the mixture was stirred for 16 h. The solvent was removed under reduced pressure and aqueous ammonium chloride (80 mL) and HCl (20 mL, 1 M) were added and the precipitate was collected by filtration. The residue was washed with H_2O (2 × 50 mL) and Et_2O (50 mL) to give **4** (0.77 g, 89%) as a cream solid. Characterization data was in agreement with that reported elsewhere.[6]

5: Pyrene-2-boronic acid

Method 1: Using a modification of the procedure first described by Dr Marie-Hélène Thibault.[44] Compound **2** (0.2 g, 0.61 mmol) was dissolved in THF/H_2O (20 mL 4:1) and $NaIO_4$ (0.39 g, 1.82 mmol) was added. The suspension was stirred for 40 min, then HCl (0.61 mL, 1 M) was added and the mixture was stirred for 48 h. The suspension was diluted with water (20 mL) and extracted with ethyl acetate (3 × 50 mL). The collected organic phases were washed with brine (50 mL) and H_2O (50 mL), dried over $MgSO_4$

and the solvent was removed under reduced pressure. The residue was washed with hexane (5 × 50 mL) and dried *in vacuo* to give **5** (0.12 g, 80%) as a light brown solid.
Method 2: Compound **9** (0.62 g, 2.0 mmol) was dissolved in THF/H_2O (4:1, 20 mL) and $LiOH{\cdot}H_2O$ (0.17 g, 4.1 mmol) was added. The solution was stirred at room temperature for 20 h and then acidified to pH 1-2 with saturated aqueous NH_4Cl (8 mL) and HCl (2 mL, 1M). The mixture was extracted with ethyl acetate (3 × 10 mL), the organic fractions were dried over $MgSO_4$ and the solvent was removed under reduced pressure to give **5** (0.42 g, 86%) as a light brown solid. Characterization data was reported by Dr Marie-Hélène Thibault.[44]

6: Pyrene-2,7-bis[4-(octylbenzoate)]
Using a modification of the procedure first described by Dr Nicolle Schwarz.[43] In a nitrogen-filled glove box, DMF (7 mL) and octyl-4-bromobenzoate (0.17 g, 0.55 mmol) were added to a tube fitted with a Young's tap containing compound **4** (0.08 g, 0.28 mmol) [$PdCl_2$(dppf)] (0.014 g, 0.02 mmol) and K_3PO_4 (0.30 g, 1.4 mmol, anhydrous). The tube was sealed and the reaction mixture was stirred at 80 ºC for 72 h then HCl (10 mL, 1M) was added to quench the reaction. The mixture was extracted into CH_2Cl_2 (3 × 30 mL) and the combined organic fractions were washed with brine (2 × 50 mL) and H_2O (50 mL) and then dried over $MgSO_4$. The solution was passed through a 5 cm silica pad eluting with CH_2Cl_2 and the solvent was removed under reduced pressure. The residue was purified by Kugelrohr distillation (140 ºC @ 1.4 x 10^{-2} mbar) to give **6** (0.14 g, 75%) as a yellow solid. mp 139-140 ºC; NMR and MALDI-TOF MS data were reported by Dr Nicolle Schwarz.[43] HRMS-CI: (M^+) Calcd for $C_{46}H_{50}O_4{\cdot}NH_4$ 684.4047; Found: 684.4047.

7: Pyrenyl-2-[4-(methylbenzoate)]
Using a modification of the procedure first described by Dr Zhiqiang Liu.[42] Under a nitrogen atmosphere, compound **5** (0.10 g, 0.41 mmol), methyl 4-iodobenzoate (0.11 g, 0.42 mmol), [$PdCl_2$(dppf)] (0.007 g, 0.01 mmol) and K_3PO_4 (0.26 g, 1.2 mmol) were dissolved in DMF (5 mL) and heated at 80 ºC for 16 h. The reaction was quenched with HCl (10 mL, 1 M) and extracted with CH_2Cl_2 (3 × 20 mL). The combined organic layers were washed with brine (2 × 80 mL) and H_2O (80 mL), dried over $MgSO_4$ and the solvent was removed under reduced pressure. Purification of the residue by column

chromatography (silica gel, hexane:CH_2Cl_2, 4:1) afforded **7** (0.083 g, 60%) as a pale yellow solid. Characterization data was reported by Dr Zhiqiang Liu.[42]

8a: Pyrene-2,7-bis(trifluoroborate) dipotassium salt

Compound **1** (1.5 g, 3.30 mmol) was dissolved in THF (30 mL). To this solution, KHF_2 (3.1 g, 39.7 mmol) in H_2O (10 mL) was added and the mixture was stirred at room temperature for 16 h. The mixture was concentrated under reduced pressure. The precipitate was collected by filtration and washed with H_2O (10 mL) and hexane (50 mL) to give **8a** (1.08 g, 79%) as a white solid. NMR (500 MHz, DMSO-d_6, δ): 8.13 (s, 4H), 7.90 (s, 4H); $^{13}C\{^1H\}$ NMR (125 MHz, DMSO-d_6, δ): 129.0, 128.1, 126.3, 123.3; C attached to B not observed; $^{11}B\{^1H\}$ NMR (128 MHz, DMSO-d_6, δ): 3.6; $^{19}F\{^1H\}$ NMR (376 MHz, DMSO-d_6, δ): -138.2.

8b: $[K_2(18\text{-crown-}6)_{1.5}]$ [pyrene-2,7-bis(trifluoroborate)]

Compound **1** (0.10 g, 0.22 mmol) and 18-crown-6 (0.35 g, 1.32 mmol) were dissolved in THF (20 mL). To this solution, KHF_2 (0.10 g, 1.28 mmol) in H_2O (20 mL) was added and the mixture was stirred at room temperature for 16 h. The precipitate was collected by filtration and was washed with acetone (3 × 10 mL) affording **8b** (0.13 g, 70%) as a white solid. mp 286-288 ºC; ^1H NMR (500 MHz, DMSO-d_6, δ): 8.13 (s, 4H), 7.90 (s, 4H), 3.52 (s, 36H); $^{13}C\{^1H\}$ NMR (125 MHz, DMSO-d_6, δ): 129.0, 128.1, 126.3, 123.3, 69.4; C attached to B not observed; $^{11}B\{^1H\}$ NMR (128 MHz, DMSO-d_6, δ): 4.0; $^{19}F\{^1H\}$ NMR (376 MHz, DMSO-d_6, δ): -137.9; MALDI-TOF MS (positive ion mode) *m/z*: 303 ((18-crown-6) K^+); (negative ion mode) *m/z*: 789 ($C_{16}H_8B_2F_6K_2 + C_{16}H_8B_2F_6K^-$), 375 ($C_{16}H_8B_2F_6K^-$), 317 ($C_{16}H_8B_2F_5^-$); Anal. Calcd for $C_{40}H_{56}B_2F_6K_2O_{12}$: C, 50.38; H, 5.47. Found: C, 50.63; H, 5.92.

9: Pyrene-2-trifluoroborate potassium salt

Using a modification of the procedure first described by Dr Zhiqiang Liu.[42] Compound **2** (0.33 g, 1.0 mmol) was dissolved in MeOH (10 mL). To this solution, KHF_2 (0.30 g, 3.8 mmol) in H_2O (5 mL) was added and the resulting white slurry was refluxed for 1 h. After cooling to ambient temperature, the white precipitate was collected by filtration and was washed with hexane (30 mL) and water (30 mL). Recrystallization from EtOH gave **9** (0.29 g, 94%) as colourless crystals. mp 313-314 ºC; ^1H NMR (DMSO-d_6, 500

MHz, δ): 8.32 (s, 2H), 8.17 (d, J = 8 Hz, 2H), 8.11 (d, J = 8 Hz, 2H), 8.04 (d, J = 8 Hz, 2H), 7.96 (t, J = 8 Hz, 1H); $^{13}C\{^{1}H\}$ NMR (DMSO-d_6, 125 MHz, δ): 130.5, 129.2, 129.1, 128.0, 125.7, 125.1, 124.4, 123.9, 122.8, C attached to B not observed; $^{19}F\{^{1}H\}$ NMR (acetone-d_6, 376 MHz, δ): 142.0; EI-MS m/z: 269 ($M\text{-}K^+$).

10: 2-((4-Dimesitylboryl)phenyl)pyrene

Using a modification of the procedure first described by Dr Zhiqiang Liu.[42] Under a nitrogen atmosphere, compound **9** (0.31 g, 1.0 mmol), 1-iodo-4-dimesitylboryl-benzene (0.45 g, 1.0 mmol), [$PdCl_2$(dppf)] (0.007 g, 0.01 mmol), K_2CO_3 (0.28 g, 2.0 mmol) were dissolved in EtOH (5 mL). The mixture was heated at 90 ºC for 16 h. The reaction was quenched with HCl (10 mL, 1 M) and extracted with CH_2Cl_2 (3 × 20 mL). The combined organic fractions were dried over $MgSO_4$ and the solvent was removed under reduced pressure. Recrystallization of the residue from hexane gave **10** (0.34 g, 65%) as a white solid. Characterization data was reported by Dr Zhiqiang Liu.[42] Anal. Calcd for $C_{40}H_{35}B$: C, 91.25; H, 6.70. Found: C, 90.45; H, 6.70.

11: 2,7-Dibromopyrene

Method 1: Using a similar method to that first described by Hartwig et al.[9] Compound **1** (0.7 g, 1.54 mmol) was dissolved in THF (5 mL) and MeOH (15 mL), and $CuBr_2$ (2.07 g, 9.3 mmol) in H_2O (15 mL) was added. The mixture was heated at 90 ºC for 16 h, and then concentrated under reduced pressure. H_2O (50 mL) was added and the white precipitate was collected by filtration and washed with H_2O (2 × 50 mL), Et_2O (30 mL) and hexane (3 × 50 mL). The product was extracted into hot toluene (3 × 30 mL) and the solvent was removed under reduced pressure to give **11** (0.39 g, 70%) as a cream-coloured solid. Pure samples were obtained after recrystallization from acetone.

Method 2: Using a similar method to that first described by Hartwig et al.[9] One-pot C-H borylation/bromination: In a nitrogen-filled glove box, [Ir((μ-OMe)COD]$_2$ (0.02 g, 0.030 mmol), dtbpy (0.02 g, 0.07 mmol) and B_2pin_2 (0.10 g, 0.39 mmol) were dissolved in THF (5 mL). The mixture was added to a tube, fitted with a Young's tap, containing pyrene (0.71 g, 3.50 mmol) and B_2pin_2 (1.95 g, 7.68 mmol). After addition of THF (10 mL), the tube was sealed and the reaction mixture was stirred at 80 ºC for 16 h. The mixture was transferred to a round bottomed flask and THF:MeOH (1:1, 60 mL) was added followed by $CuBr_2$ (4.42 g, 19.80 mmol) in H_2O (30 mL). The mixture was

heated at 90 ºC for 16 h, and then concentrated under reduced pressure. H_2O (50 mL) was added and the white precipitate was collected by filtration and washed with H_2O (2 × 50 mL), Et_2O (30 mL) and hexane (3 × 50 mL). The product was extracted into hot toluene (3 × 30 mL) and the solvent was removed under reduced pressure to give **11** (0.89 g, 71%) as a cream-coloured solid. mp 320-321 ºC; ^{1}H NMR (500 MHz, DMSO-d_6, δ): 8.53 (s, 4H), 8.23 (s, 4H); ^{13}C{^{1}H} NMR (125 MHz, DMSO-d_6, δ): 131.7, 127.3, 127.1, 121.6, 119.3; EI-MS *m/z*: 360 (M^+); HRMS-EI: (M^+) Calcd for $C_{16}H_8{}^{79}Br_2$ 357.8987; found 357.8993; Anal. Calcd for $C_{16}H_8Br_2$: C, 53.37; H, 2.24. Found: C, 53.06; H, 2.24. Characterization data was in agreement with that reported elsewhere.[10-11]

12: 2-Bromopyrene

Using a modification of the procedure first described by Dr Zhiqiang Liu.[42] To a round-bottomed flask fitted with a condenser, was added compound **2** (0.24 g, 0.73 mmol) and $CuBr_2$ (0.49 g, 2.19 mmol) were dissolved in MeOH:H_2O (15 mL, 1:1). The mixture was heated at 90 °C for 16 h until consumption of starting materials was observed by GC-MS, and cooled to RT. H_2O (25 mL) was added and a white precipitate was collected by filtration and washed with H_2O (2 × 30 mL). Recrystallization from hexane gave **12** (0.17 g, 88%) as a white solid. Characterization data was reported by Dr Zhiqiang Liu.[42]

One-Pot process: Using a similar method to that first described by Hartwig et al.[9] In a nitrogen filled glove box, [Ir(μ-OMe)COD]$_2$ (0.02 g, 0.03 mmol), dtbpy (0.02 g, 0.07 mmol) and B_2pin_2 (0.10 g, 0.39 mmol) were added to hexane (5 mL). The mixture was added to a vessel, fitted with a Young's tap, containing pyrene (0.62 g, 3.07 mmol) and B_2pin_2 (0.67 g, 2.64 mmol). After addition of hexane (10 mL), the tube was sealed and the reaction mixture was stirred at 80 ºC for 16 h. The mixture was transferred to a round bottomed flask and the solvent was removed under reduced pressure. MeOH (30 mL) was added followed by $CuBr_2$ (2.04 g, 9.13 mmol) in H_2O (30 mL). The mixture was heated at 90 ºC for 16 h, and then concentrated under reduced pressure. H_2O (30 mL) was added and the white precipitate was collected by filtration and washed with H_2O (3 × 30 mL). The product was then extracted into hot hexane (50 mL) and the solvent was removed under reduced pressure to give a mixture of **12** and pyrene (0.53 g, ~1:1 by GC-MS).

13: Pyrene-2,7-dicarboxylic acid

Compound **13** was synthesized from **11** as previously reported.[12] ^{1}H NMR (DMSO-d_6, 700 MHz, δ): 13.34 (s, 2H, COOH), 8.88 (s, 4 H), 8.36 (s, 4 H); ^{13}C{^{1}H} NMR (DMSO-d_6, 175 MHz, δ): 167.6, 131.1, 129.2, 128.5, 125.9, 125.4.

14: 2-(Dimesitylboryl)pyrene

Using a modification of the procedure first described by Dr Zhiqiang Liu.[42] Under a nitrogen atmosphere, compound **12** (0.28 g, 1.0 mmol) was dissolved in Et_2O (5 mL). The solution was cooled to -78 °C and a solution of ^{n}BuLi (1.6 M in hexane, 0.8 mL, 1.2 mmol) was added dropwise via syringe. The reaction was warmed to room temperature and stirred for 1 h. The system was cooled to -78 °C and a solution of dimesitylboron fluoride (0.27 g, 1.0 mmol) in Et_2O (5 mL) was added. The mixture was warmed to room temperature and was stirred overnight. The reaction was quenched with HCl (10 mL, 1 M) and extracted with CH_2Cl_2 (3 × 20 mL). The organic fractions were dried over $MgSO_4$ and the solvent was removed under reduced pressure. Purification of the residue by column chromatography (silica gel, hexane:CH_2Cl_2, 4:1) gave **14** (0.14 g, 30%) as a pale yellow solid. Characterization data was reported by Dr Zhiqiang Liu.[42]Anal. Calcd for $C_{34}H_{31}B$: C, 90.66; H, 6.94. Found: C, 90.90; H, 6.96.

15: 2,7-Dihydroxypyrene

Using a modification of the procedure first described by Drs Gilles Alcaraz[45] and Ibraheem A. I. Mkhalid.[46] Compound **1** (0.50 g, 1.10 mmol) and NaOH (0.26 g, 6.50 mmol) were dissolved in THF (50 mL) and to this mixture H_2O_2 (0.22 g, 6.50 mmol) was added. After stirring at room temperature for 4 h, the solution was acidified to pH 1-2 using HCl (1 M). The product was extracted into Et_2O (3 × 100 mL) and the organic fractions were dried over $MgSO_4$. Caution: care must be taken to destroy all peroxides in the aqueous phase by stirring with aqueous H_2SO_4 and CuI. The solvent was reduced to ca. 10 mL under reduced pressure and the product was precipitated by addition of hexane (200 mL). The light brown solid product **15** (0.23 g, 89%) was collected by filtration. mp 320-322 °C; ^{1}H NMR (400 MHz, DMSO-d_6, δ): 9.88 (s, 2H), 7.93 (s, 4H),

7.59 (s, 4H); $^{13}C\{^{1}H\}$ NMR reported by Dr Ibraheem A. I. Mkhalid.[46] ESI-MS *m/z*: 233 ($M\text{-}H^-$); HRMS-ESI: ($M\text{-}H^-$) Calcd for $C_{16}H_9O_2$ 233.0608; Found 233.0606.

16: 2-Hydroxypyrene

Using a modification of the procedure first described by Dr Marie-Hélène Thibault.[44] Compound **2** (1.0 g, 3.0 mmol) and NaOH (0.36 g, 9.0 mmol) were dissolved in THF/H_2O (10:1, 110 mL) and to this mixture H_2O_2 (0.31 g, 9.1 mmol) was added. After stirring for 4 h, the solution was acidified to pH 1-2 using HCl (1 M). The reaction mixture was extracted with Et_2O (3 × 50 mL). The organic fractions were dried over $MgSO_4$ and the solvent was removed by slow evaporation. Caution: care must be taken to destroy all peroxides in the aqueous phase by stirring with aqueous H_2SO_4 and CuI. The residue was washed with hexane (3 × 20 mL) to yield **16** (0.56 g 86%) as a light brown solid. Characterization data was reported by Dr Zhiqiang Liu.[42]

17: Pyrene-2,7-bis(trifluoromethanesulfonate)

Using a modification of the procedure first described by Drs Gilles Alcaraz[45] and Ibraheem A. I. Mkhalid.[46] Under a nitrogen atmosphere, compound **15** (0.33 g, 1.41 mmol) was dissolved in dry pyridine (30 mL). After cooling to -10 ºC, triflic anhydride (2.39 g, 8.47 mmol) in dry hexane (10 mL) was added dropwise over 30 min. The mixture was stirred at -10 ºC for 1 h and allowed to warm to room temperature overnight. The solvent was removed *in vacuo* and to the residue, H_2O (10 mL) was added. The reaction mixture was extracted with Et_2O (3 × 100 mL) and the organic fractions were dried over $MgSO_4$. After removal of the volatiles under reduced pressure, the residue was purified by column chromatography (silica gel, hexane:diethyl ether 8:2) to give **17** (0.42 g, 60%) as a light yellow solid. mp 192-194 ºC; NMR characterization data was reported by Dr Ibraheem A. I. Mkhalid[46]; EI-MS *m/z*: 498 (M^+), 365 ($M\text{-}SO_2CF_3^+$); HRMS-EI: (M^+) Calcd for $C_{18}H_8F_6O_6S_2$ 497.9661; Found 497.9668.

18: Pyrene-2-trifluoromethanesulfonate

Using a modification of the procedure first described by Dr Marie-Hélène Thibault.[44] Under a nitrogen atmosphere, compound **16** (0.66 g, 3.0 mmol) was dissolved in dry pyridine (30 mL). After cooling to 0 ºC, triflic anhydride (2.54 g, 9.0 mmol) was added.

The mixture was stirred at 0 ºC for 1 h and then allowed to warm to room temperature overnight. The reaction was quenched with H_2O (20 mL) and the mixture was extracted with CH_2Cl_2 (3 × 30 mL). The organic fractions were dried over $MgSO_4$ and the solvent was removed under reduced pressure. Purification of the residue by column chromatography (silica gel, hexane:CH_2Cl_2, 4:1) gave **18** (0.72 g, 69%) as a pale yellow solid. mp 143-145 ºC; Characterization data was reported by Dr Zhiqiang Liu.[42]

19: 2,7-Diphenylpyrene

Using a modification of the procedure first described by Dr Ibraheem A. I. Mkhalid.[46] Under a nitrogen atmosphere, compound **17** (0.08 g, 0.16 mmol), $PhB(OH)_2$ (0.04 g, 0.34 mmol), [$PdCl_2$(dppf)] (0.0034 g, 0.005 mmol) and K_3PO_4 (0.1 g, 0.47 mmol) were dissolved in DMF (10 mL) and H_2O (0.5 mL, degassed). The mixture was stirred at 80 ºC for 16 h. The reaction mixture was then extracted with Et_2O (3 × 50 mL). The combined organic fractions were dried over $MgSO_4$, and the solvent was removed under reduced pressure. The residue was purified by elution through a 5 cm silica pad with hot toluene. Recrystallization from benzene gave **19** (0.045 g, 79%) as a white solid. mp 290 ºC dec; Characterization data was reported by Dr Ibraheem A. I. Mkhalid;[46]

20: 2,7-Bis(phenylethynyl)pyrene

Using a modification of the procedure first described by Dr Ibraheem A. I. Mkhalid.[46] Under a nitrogen atmosphere, compound **17** (0.15 g, 0.30 mmol), [$PdCl_2(PPh_3)_2$] (0.0063 g, 0.009 mmol) and CuI (0.0011 g, 0.006 mmol) were dissolved in dry DMF (10 mL). Phenylethyne (0.061 g, 0.6 mmol) in Et_3N (5 mL) was then added. The mixture was stirred vigorously and then refluxed at 80 °C for 16 h. The reaction was quenched with HCl (10 mL, 1 M) and then extracted with Et_2O (3 × 50 mL). The ether fractions were dried over $MgSO_4$ and the solvent was removed on a rotary evaporator. Purification of the residue by column chromatography (silica gel, hexane : Et_2O 8:2) gave **20** (0.06 g, 50%) as a light yellow solid. mp 206-208 ºC; Characterization data was reported by Dr Ibraheem A. I. Mkhalid;[46] HRMS-EI: (M^+) Calcd for $C_{32}H_{18}$ 402.1403; Found: 402.1406.

21: 2,7-Bis[4-(dimesitylboryl)phenylethynyl)pyrene

Using a modification of the procedure first described by Dr Ibraheem A. I. Mkhalid. Under a nitrogen atmosphere, compound **17** (0.20 g, 0.40 mmol), $[PdCl_2(PPh_3)_2]$ (0.009 g, 0.013 mmol) and CuI (0.002 g, 0.011 mmol) were dissolved in dry DMF (10 mL) and 4-(dimesitylboryl)phenylethyne (0.28 g, 0.8 mmol) in Et_3N (5 mL) was then added. The mixture was stirred vigorously and then refluxed at 80 °C for 16 h. The reaction was quenched with HCl (10 mL, 1 M) and extracted with Et_2O (3 × 50 mL). After drying of the organic fractions over $MgSO_4$, the volatiles were removed and under reduced pressure. The residue was then purified by column chromatography (silica gel, hexane : diethyl ether 8 : 2) to give **21** (0.11 g, 31%) as a yellow solid. mp 310 ºC dec; Characterization data was reported by Dr Ibraheem A. I. Mkhalid;[46] HRMS-EI: (M^+) Calcd for $C_{68}H_{60}{}^{11}B_2$ 898.4876; Found: 898.4879.

22: 2,7-Bis(trimethylsilylethynyl)pyrene and **23**: 2-(trifluoromethanesulfonyl)-7-(trimethylsilylethynyl)pyrene

Method 1: Under a nitrogen atmosphere, compound **11** (0.07 g, 0.19 mmol), $[PdCl_2(dppf)]$ (0.003 g, 0.004 mmol) and CuI (0.001 g, 0.005 mmol) were added to dry THF (2 mL). To this mixture, Et_3N (5 mL) followed by trimethylsilylethyne (0.04 g, 0.41 mmol) were added and the reaction was refluxed for 16 h. The solvent was removed *in vacuo*, and the reaction mixture was passed through a silica pad eluting with hexane:Et_2O (3:2). The solvent was removed under reduced pressure. Recrystallization of the residue from hexane gave **22** (0.06 g, 80%) as a pale yellow solid.

Method 2: Using a modification of the procedure first described by Dr Ibraheem A. I. Mkhalid.[46] Under a nitrogen atmosphere, compound **17** (0.10 g, 0.20 mmol), $[PdCl_2(PPh_3)_2]$ (0.004 g, 0.006 mmol) and CuI (0.001 g, 0.005 mmol) were dissolved in dry THF (5 mL). Trimethylsilylethyne (0.04 g, 0.41 mmol) in Et_3N (15 mL) was then added. The mixture was stirred vigorously and then refluxed for 16 h. The reaction was quenched with HCl (10 mL, 1 M) and extracted with Et_2O (3 × 50 mL). The combined organic fractions were dried over $MgSO_4$. The solvent was removed under reduced pressure and the residue was purified by column chromatography (silica gel, hexane:Et_2O 4:1). Recrystallization of the separated fractions from hexane gave **22** (0.04 g, 51%) and **23** (0.02 g, 22%) as white solids.

22: mp 158-160 ºC; Characterization data was reported by Dr Ibraheem A. I. Mkhalid;[46] EI-MS *m/z*: 394 (M^+), 379 ($M\text{-}Me^+$); HRMS-EI: (M^+) Calcd for $C_{26}H_{26}Si_2$ 394.1568; Found 394.1561;

23: mp 136-138 ºC; Characterization data was reported by Dr Ibraheem A. I. Mkhalid;[46] EI-MS *m/z*: 446 (M^+), 431 ($M\text{-}Me^+$); HRMS-EI: (M^+) Calcd for $C_{22}H_{17}F_3O_3SSi$ 446.0614; Found: 446.0619.

24: 2-Phenylethynyl-pyrene

Using a modification of the procedure first described by Dr Zhiqiang Liu.[42] Under a nitrogen atmosphere in a Young's tap tube, compound **18** (0.10 g, 0.29 mmol), phenylethyne (0.045 g, 0.4 mmol), $[PdCl_2(PPh_3)_2]$ (0.007 g, 0.01 mmol) and CuI (0.002 g, 0.01 mmol) were dissolved in Et_3N (2 mL) and DMF (5 mL). The tube was sealed and heated at 90 ºC for 16 h. The reaction was quenched with HCl (10 mL, 1 M), extracted with CH_2Cl_2 (3 × 20 mL), and the CH_2Cl_2 fractions were dried over $MgSO_4$. The solvent was removed under reduced pressure and the residue was purified by column chromatography (silica gel, hexane:CH_2Cl_2, 4:1) to give **24** (0.068 g, 78%) as a pale yellow solid. Characterization data was reported by Dr Zhiqiang Liu.[42]

25: 2-Trimethylsilylethynylpyrene

Using a modification of the procedure first described by Dr Zhiqiang Liu.[42] Under a nitrogen atmosphere in a Young's tube, compound **18** (0.10 g, 0.29 mmol), trimethylsilylethyne (0.1 g, 1.0 mmol), $[PdCl_2(PPh_3)_2]$ (0.007 g, 0.01 mmol) and CuI (0.002 g, 0.01 mmol) were dissolved in Et_3N (2 mL) and DMF (5 mL). The tube was sealed and heated at 80 ºC for 16 h. The reaction was quenched with HCl (10 mL, 1 M) and extracted with CH_2Cl_2 (3 × 20 mL). The organic fractions were dried over $MgSO_4$ and the solvent was removed under reduced pressure. Purification of the residue by column chromatography (silica gel, hexane:CH_2Cl_2, 4:1) gave **25** (0.065 g, 75%) as a pale yellow solid. Characterization data was reported by Dr Zhiqiang Liu.[42]

26: 2,7-Bis((4-*N*,*N*-dimethylamino)phenylethynyl)pyrene

Under a nitrogen atmosphere, compound **11** (0.10 g, 0.28 mmol), 4-ethynyl-*N*,*N*-dimethylaniline (0.085 g, 0.59 mmol), $[PdCl_2(dppf)]$ (0.005 g, 0.007 mmol) and CuI (0.001 g, 0.005 mmol) were added to dry THF (2 mL). To this mixture, Et_3N (5 mL)

was added and the mixture stirred at RT for 16 h. The solvent was removed *in vacuo* and the residual solid was added to the top of a 5 cm alumina pad, which was first eluted with hexane (200 mL) to remove any unreacted starting materials. The column was then eluted with hexane:CH_2Cl_2 (1:3) and the solvents were removed under reduced pressure to give **26** (0.10 g, 73%) as a bright yellow solid. Pure samples were obtained after recrystallization from CH_2Cl_2. mp 140-143 ºC (dec); ^{1}H NMR (400 MHz, $CDCl_3$, δ): 8.27 (s, 4H), 7.99 (s, 4H), 7.51 (d, *J* = 8 Hz, 4H), 6.71 (d, *J* = 8 Hz, 4H), 3.01 (s, 12H); the ^{13}C NMR spectrum of this compound was not obtained due to its low solubility; MALDI-TOF MS (positive ion mode) *m/z*: 488 (M^+); HRMS-MALDI: (M^+) Calcd for $C_{36}H_{28}N_2$ 488.2252; Found: 488.2231.

27: 2,7-Diethynyl-pyrene

To a suspension of Na_2CO_3 (0.22 g, 2.08 mmol) in MeOH (30 mL) and H_2O (3 mL) compound **22** (0.11 g, 0.28 mmol) was added. After stirring for 16 h at RT, the mixture was diluted with H_2O (10 mL), concentrated under reduced pressure and extracted with Et_2O (3 × 50 mL). The ether fractions were dried over $MgSO_4$. The solvent was removed under reduced pressure and the residue was purified by elution with hexane: EtOAc (4:1) over a 5 cm silica pad. After removal of the solvents, the residue was recrystallized from acetone to give **27** (0.06 g, 86%) as a light brown solid. mp 154-155 ºC (dec); ^{1}H NMR (700 MHz, $CDCl_3$, δ): 8.30 (s, 4H), 8.03 (s, 4H), 3.26 (s, 2H); ^{13}C{^{1}H} NMR (175 MHz, $CDCl_3$, δ): 131.4, 128.8, 127.9, 124.3, 120.3, 84.2, 78.1; EI-MS *m/z*: 250 (M^+); HRMS-EI: (M^+) Calcd for $C_{20}H_{10}$ 250.0777; Found 250.0776.

28: 2-Ethynyl-pyrene

To a suspension of Na_2CO_3 (0.14 g, 1.32 mmol) in MeOH (30 mL) and H_2O (3 mL) was added compound **25** (0.11 g, 0.37 mmol). After stirring for 16 h at ambient temperature, the mixture was diluted with H_2O (10 mL), concentrated under reduced pressure and extracted with Et_2O (3 × 50 mL). The ether fractions were dried over $MgSO_4$. The solvent was removed under reduced pressure and the residue purified on a 5 cm silica pad, eluting with hexane:Et_2O (4:1) yielding **28** (0.068 g, 81%) as a pale-yellow solid. mp 107-109 ºC; ^{1}H NMR ($CDCl_3$, 500 MHz, δ): 8.28 (s, 2H), 8.18 (d, *J* = 8 Hz, 2H), 8.07 (d, *J* = 8 Hz, 2H), 8.01 (m, 3H), 3.23 (s, 1H); ^{13}C{^{1}H} NMR ($CDCl_3$, 125 MHz, δ):

131.5, 131.2, 128.4, 127.1, 126.7, 125.7, 125.2, 124.7, 124.5, 119.6, 84.6, 77.7; EIMS *m/z*: 226 (M^+); HRMS-EI: (M^+) Calcd for $C_{18}H_{10}$ 226.0777; Found: 226.0774.

29: 2,7-Bis(4-methoxy-phenyl)-phenyl-amine)-pyrene

Under a nitrogen atmosphere, a solution of $Pd_2(dba)_3$ (0.008 g, 0.008 mmol) in toluene (3 mL) followed by a solution of (4-methoxy-phenyl)-phenyl-amine (0.061 g, 0.31 mmol) in toluene (3 mL) were added to a tube fitted with a Young's tap containing **11** (0.05 g, 0.14 mmol) and Na^{t}OBu (0.09 g, 0.98 mmol). To this mixture was added P^{t}Bu$_3$ (0.003 g, 0.015 mmol, 12.2% w/w sol. in toluene). The tube was sealed and the reaction mixture was stirred at 110 ºC for 4 h. After cooling to room temperature, H_2O (30 mL) was added. The mixture was extracted into CH_2Cl_2 (3 × 30 mL) and the combined organic fractions were dried over $MgSO_4$ after which the solvent was removed under reduced pressure. The residue was placed on a 3 cm alumina pad and eluted with hexane : CH_2Cl_2 to give **29** (0.077 g, 93%) as a bright yellow solid. Analytically pure samples were obtained by recrystallization from hexane and $CHCl_3$. ^{1}H NMR (700 MHz, C_6D_6, δ): 7.90 (s, 4H), 7.42 (s, 4H), 7.24 (d, 4H, *J* = 8 Hz), 7.12 (m, 8H), 6.89 (t, 2H, *J* = 8 Hz), 6.73 (d, 4H, *J* = 8 Hz), 3.31 (s, 6H, Me); ^{13}C{^{1}H} NMR (176 MHz, C_6D_6, δ): 157.3, 149.6, 146.7, 142.1, 132.7, 130.0, 128.7, 128.6, 123.9, 122.8, 122.0, 120.8, 115.8, 55.4; ASAP-MS (positive ion mode) *m/z*: 597 (M + H^+); HRMS-ASAP: (M^+) Calcd for $C_{42}H_{32}N_2O_2$ 596.2464; Found 596.2453; Anal. Calcd for $C_{42}H_{32}N_2O_2 \cdot 0.67CHCl_3$: C, 75.77; H, 4.87; N, 4.14. Found: C, 75.96; H, 4.90; N, 4.13.

31: 4-(Pyren-2-yl)-butyric acid

To a solution of **33** (0.080 g, 0.26 mmol) in THF (10 mL) was added $LiOH \cdot H_2O$ (0.027 g, 0.64 mmol) in H_2O (2.5 mL). The mixture was stirred for 16 h at room temperature and then quenched with HCl (1 M, 50 mL), extracted into ethyl acetate (3 × 80 mL) and dried over $MgSO_4$. The solvent was removed under reduced pressure, the residue was dissolved in hot acetone (10 mL) and the product was precipitated by addition of hexane. Filtration and drying gave **31** (0.06 g, 80%) as a white solid. ^{1}H NMR (700 MHz, DMSO-d_6, δ): 12.08 (br s, 1H), 8.27 (d, 2H, *J* = 8 Hz), 8.16 (d, 2H, *J* = 8 Hz), 8.15 (d, 2H, *J* = 8 Hz), 8.14 (s, 2H), 8.04 (t, 1H, *J* = 8 Hz), 3.06 (t, 2H, *J* = 8 Hz), 2.33 (t, 2H, *J* = 8 Hz), 2.06 (m, 2H); ^{13}C{^{1}H} NMR (176 MHz, DMSO-d_6, δ): 174.3, 139.8, 130.7, 130.3, 127.3, 127.1, 125.8, 125.0, 124.9, 123.7, 122.4, 34.9, 33.3, 26.8; ES-MS

(negative ion mode) *m/z*: 575 ($2M\text{-}H^-$), 287 ($M\text{-}H^-$); HRMS-ES (negative ion mode): $(M\text{-}H)^-$ Calcd for $C_{20}H_{15}O_2$ 287.1072; Found 287.1091; Anal. Calcd for $C_{20}H_{16}O_2 \cdot 0.67H_2O$: C, 81.61; H, 5.71. Found: C, 81.31; H, 5.54.

32: 4-(Pyren-2-yloxy)-butyric acid

To a solution of **34** (0.08 g, 0.25 mmol) in THF (10 mL) was added $LiOH \cdot H_2O$ (0.026 g, 0.62 mmol) in H_2O (2.5 mL). The mixture was stirred for 16 h at room temperature. The reaction was quenched with HCl (1 M, 50 mL), extracted into ethyl acetate (3 × 80 mL) and dried over $MgSO_4$. The solvent was removed under reduced pressure, the residue was dissolved in hot acetone (10 mL) and the product was precipitated by addition of hexane. Filtration and drying gave **32** (0.05 g, 66%) as a cream-colored solid. ^1H NMR (700 MHz, DMSO-d_6, δ): 12.15 (br s, 1H), 8.24 (d, 2H, J = 8 Hz), 8.15 (d, 2H, J = 8 Hz), 8.10 (d, 2H, J = 8 Hz), 7.99 (t, 1H, J = 8 Hz), 7.89 (s, 2H), 4.30 (t, 2H, J = 6 Hz), 2.10 (m, 2H), the third CH_2 signal was obscured by the H_2O signal; $^{13}C\{^1H\}$ NMR (176 MHz, DMSO-d_6, δ): 174.3, 156.9, 132.2, 129.6, 127.9, 126.8, 125.3, 125.2, 123.8, 119.1, 111.0, 79.2, 67.2, 30.7; ES-MS (negative ion mode) *m/z*: 303 ($M\text{-}H^-$), 607 ($2M\text{-}H^-$); HRMS-ES (negative ion mode): ($M\text{-}H^-$) Calcd for $C_{20}H_{15}O_3$ 303.1021; Found 303.1023; Anal. Calcd for $C_{20}H_{16}O_3 \cdot 0.5H_2O$: C, 76.66; H, 5.47. Found: C, 76.48; H, 5.17.

33: 4-Pyren-2-yl-butyric acid methyl ester

Using a similar method to that first described by Huo.[19] Under a nitrogen atmosphere, Zn powder (0.27 g, 4.13 mmol) was added to a tube fitted with a Young's tap. After heating the tube at 70 ºC under vacuum for 45 min, I_2 (0.035 g, 0.14 mmol) in DMF (9 mL) was added and the mixture was stirred until the red color had faded (~ 5 min). Freshly distilled (80 ºC, 200 mTorr) 4-bromo-butyric acid methyl ester (0.50 g, 2.76 mmol) in DMF (1 mL) was added and the mixture was stirred at 70 ºC for 16 h. Inside a nitrogen filled glovebox, 1.56 mL of the stock solution containing the zinc reagent (0.11 g, 0.45 mmol) was added to a Young's tube containing **12** (0.1 g, 0.36 mmol) and $PdCl_2(PPh_3)_2$ (0.005 g, 0.007 mmol). The mixture was stirred for 16 h at room temperature, then H_2O (300 mL) was added. The mixture was extracted into Et_2O (3 × 100 mL) and the combined organic fractions were dried over $MgSO_4$ and the solvent was removed under reduced pressure. The residue was purified by column

chromatography (silica gel, hexane : CH_2Cl_2, 1 : 1) followed by recrystallisation from hexane to give **33** (0.08 g, 74%) as a white solid. ^{1}H NMR (400 MHz, $CDCl_3$, δ): 8.15 (d, 2H, *J* = 7 Hz), 8.03 (d, 2H, *J* = 9 Hz), 8.00 (d, 2H, *J* = 9 Hz), 7.98 (s, 2H), 7.96 (t, 1H, *J* = 7 Hz), 3.66 (s, 3H, Me), 3.09 (t, 2H, *J* = 8 Hz), 2.41 (t, 2H, *J* = 8 Hz), 2.18 (m, 2H); ^{13}C{^{1}H} NMR (125 MHz, $CDCl_3$, δ): 174.1, 139.4, 131.5, 131.1, 127.7, 127.4, 125.8, 125.3, 125.1, 124.8, 123.5, 51.8, 35.9, 33.7, 27.3; EIMS *m/z*: 302 (M^+); HRMS-ASAP (positive ion mode): (M^+) Calcd for $C_{21}H_{18}O_2$ 302.1307; Found 302.1317; Anal. Calcd for $C_{21}H_{18}O_2$: C, 83.42; H, 6.00. Found: C, 82.99; H, 5.99.

34: 4-(Pyren-2-yloxy)-butyric acid methyl ester

A mixture of **16** (0.10 g, 0.46 mmol) and Na^{t}OBu (0.05 g, 0.52 mmol) in DMF (6 mL) was stirred for 1 h and then was added dropwise over 30 min to a solution of 4-bromo-butyric acid methyl ester (0.37 g, 2.04 mmol) in DMF (6 mL). The mixture was stirred at room temperature for 1 h, then at 40 ºC for 1 h then at 80 ºC for 16 h. After cooling to room temperature, H_2O (300 mL) was added. The mixture was extracted into Et_2O (3 × 100 mL) and the combined organic fractions were dried over $MgSO_4$ and the solvent was removed under reduced pressure. The residue was purified by column chromatography (silica gel, CH_2Cl_2) followed by recrystallization from hexane to give **34** (0.11 g, 75%) as a cream-coloured solid. ^{1}H NMR (400 MHz, $CDCl_3$, δ): 8.15 (d, 2H, *J* = 8 Hz), 8.03 (d, 2H, *J* = 8 Hz), 7.96 (d, 2H, *J* = 8 Hz), 7.91 (t, 1H, *J* = 8 Hz), 7.68 (s, 2H), 4.30 (t, 2H, *J* = 7 Hz), 3.70 (s, 3H, Me), 2.64 (t, 2H, *J* = 7 Hz), 2.26 (m, 2H); ^{13}C{^{1}H} NMR (125 MHz, $CDCl_3$, δ): 174.0, 157.2, 132.8, 130.4, 128.3, 127.0, 125.5, 125.1, 124.8, 120.4, 111.1, 67.2, 51.9, 30.9, 25.0; ASAP-MS (positive ion mode) *m/z*: 318 (M^+); Anal. Calcd for $C_{21}H_{18}O_3$: C, 79.22; H, 5.70. Found: C, 78.59; H, 5.66.

35: 2-(12-Bromo-dodecyloxy)-pyrene

A mixture of **16** (0.15 g, 0.69 mmol) and Na^{t}OBu (0.068 g, 0.71 mmol) in DMF (6 mL) was stirred for 1 h, and then was added dropwise over 30 min to a solution of 1,12-dibromo-dodecane (1.13 g, 3.44 mmol) in DMF (5 mL). The mixture was stirred at room temperature for 2 h then at 80 ºC for 16 h, after cooling to room temperature, H_2O (400 mL) was added. The mixture was extracted into Et_2O (3 × 100 mL) and the combined organic fractions were dried over $MgSO_4$ and the solvent was removed under reduced pressure. The residue was purified by column chromatography (silica gel,

hexane : CH_2Cl_2) followed by recrystallization from hexane and $CHCl_3$ to give **35** (0.23 g, 72%) as a white solid. ^{1}H NMR (700 MHz, C_6D_6, δ): 7.94 (d, 2H, *J* = 8 Hz), 7.84 (d, 2H, *J* = 8 Hz), 7.80 (d, 2H, *J* = 8 Hz), 7.73 (t, 1H, *J* = 8 Hz), 7.72 (s, 2H), 3.96 (t, 2H, *J* = 7 Hz), 2.97 (t, 2H, *J* = 7 Hz), 1.82 (m, 2H), 1.51 (m, 4H), 1.34 (m, 8H), 1.18 (m, 4H), 1.09 (m, 2H); ^{13}C{^{1}H} NMR (125 MHz, $CDCl_3$, δ): 158.4, 133.6, 131.1, 128.8, 127.6, 126.0, 125.8, 125.5, 121.1, 111.8, 68.7, 34.1, 33.4, 30.4, 30.3, (2 peaks), 30.2, (2 peaks), 30.1, 29.4, 28.7, 27.0; ASAP-MS (positive ion mode) *m/z*: 466 ($M+H^+$); Anal. Calcd for $C_{28}H_{33}BrO$: C, 72.25; H, 7.15. Found: C, 72.33; H, 7.09.

5.0 References

[1] (a) Coventry, D. N.; Batsanov, A. S.; Goeta, A. E.; Howard, J. A. K.; Marder, T. B.; Perutz, R. N. *Chem. Commun.* **2005**, 2172-2174. (b) Crawford, A. G.; Liu, Z.; Mkhalid, I. A. I.; Thibault, M.-H.; Schwarz, N.; Alcaraz, G.; Steffen, A.; Batsanov, A. S.; Howard, J. A. K.; Dwyer, A. D.; Beeby, A.; Pålsson, L.-O.; Tozer, D. J.; Marder, T. B., 93rd Canadian Chemistry Conference and Exhibition, Toronto, Canada, May 29 - June 2, 2010, *Abstract* 0964.

[2] (a) Hazell, A. C.; Lomborg, J. G. *Acta Crystallogr.* **1972**, *B28*, 1059-1064. (b) Miura, Y.; Yamano, R.; Tanaka, A.; Yamauchi, J. *J. Org. Chem.* **1994**, *59*, 3294-3300.

[3] Hall, D. G., Ed. *Boronic Acids*, Wiley-VCH: Weinheim, 2005.

[4] Wanninger-Weiss, C.; Wagenknecht, H.-A. *Eur. J. Org. Chem.* **2008**, 64-71.

[5] (a) Yuen, A. K. L.; Hutton, C. A. *Tetrahedron Lett.* **2005**, *46*, 7899-7903. (b) Murphy, J. M.; Tzschucke, C. C.; Hartwig, J. F. *Org. Lett.* **2007**, *9*, 757-760.

[6] (a) Wan, S.; Guo, J.; Kim, J.; Ihee, H.; Jiang, D. *Angew. Chem. Int. Ed.* **2008**, *47*, 8826-8830. (b) Wan, S.; Guo, J.; Kim, J.; Ihee, H.; Jiang. D. *Angew. Chem. Int. Ed.* **2009**, *48*, 5439-5442.

[7] (a) Matsumi, N.; Naka, K.; Chujo, Y. *J. Am. Chem. Soc.* **1998**, *120*, 5112-5113. (b) Noda, T.; Ogawa, Y. S.; Shirota, Y. *Adv. Mater.* **1999**, *11*, 283-285. (c) Shirota, Y.; Kinoshita, T.; Noda, K.; Okumoto, T. O. *J. Am. Chem. Soc.* **2000**, *122*, 11021-11022. (d) Entwistle, C. D.; Marder, T. B. *Angew. Chem. Int. Ed.* **2002**, *41*, 2927-2931 and

references therein. (e) Entwistle, C. D.; Marder, T. B. *Chem. Mater.* **2004**, *16*, 4574-4585. (f) Qin, Y.; Cheng, G.; Achara, O.; Parab, K.; Jäkle, F. *Macromolecules* **2004**, *37*, 7123-7131. (g) Parab, K.; Quin, Y.; Jäkle, F. *Poly. Mater. Sci. Eng. Prepr.* **2005**, *93*, 422. (h) Jäkle, F. *Coord. Chem. Rev.* **2006**, *250*, 1107-1121. (i) Liu, X. Y.; Bai, D. R.; Wang, S. *Angew. Chem. Int. Ed.* **2006**, *45*, 5475-5478. (j) Haussler, M.; Tang, B. Z. *Adv. Polym. Sci.* **2007**, *209*, 1-58. (k) Wakamiya, A.; Mori, K.; Yamaguchi, S. *Angew. Chem. Int. Ed.* **2007**, *46*, 4273-4276. (l) Elbing, M.; Bazan, G. C. *Angew. Chem. Int. Ed.* **2008**, *47*, 834-838.

[8] (a) Yuan, Z.; Taylor, N. J.; Marder, T. B.; Williams, I. D.; Kurtz, S. K.; Cheng, L.-T. *J. Chem. Soc., Chem. Commun.* **1990**, 1489-1492. (b) Yuan, Z.; Taylor, N. J.; Marder, T. B.; Williams, I. D.; Kurtz, S. K.; Cheng, L.-T. in *Organic Materials for Non-linear Optics II*, ed. Hann R. A.; Bloor, D. RSC: Cambridge, 1991, 190-196. (c) Yuan, Z.; Taylor, N. J.; Sun, Y.; Marder, T. B.; Williams, I. D.; Cheng, L.-T. *J. Organomet. Chem.* **1993**, *449*, 27-37. (d) Yuan, Z.; Taylor, N. J.; Ramachandran, R.; Marder, T. B. *Appl. Organomet. Chem.* **1996**, *10*, 305-316. (e) Yuan, Z.; Collings, J. C.; Taylor, N. J.; Marder, T. B.; Jardin, C.; Halet, J.-F. *J. Solid State Chem.* **2000**, *154*, 5-12. (f) Charlot, M.; Porrès, L.; Entwistle, C. D.; Beeby, A.; Marder, T. B.; Blanchard-Desce, M. *Phys. Chem. Chem. Phys.* **2005**, *7*, 600-606; (g) Porrès, L.; Charlot, M.; Entwistle, C. D.; Beeby, A.; Marder, T. B.; Blanchard-Desce, M. *Proc. SPIE – Int. Soc. Opt. Eng.*, **2005**, 92, 5934-5936. (h) Yuan, Z.; Entwistle, C. D.; Collings, J. C.; Albesa-Jové, D.; Batsanov, A. S.; Howard, J. A. K.; Kaiser, H. M.; Kaufmann, D. E.; Poon, S.-Y.; Wong, W.-Y.; Jardin, C.; Fatallah, S.; Boucekkine, A.; Halet, J.-F.; Marder, T. B. *Chem. Eur. J.* **2006**, *12*, 2758-2771. (i) Zhou, G.; Ho, C.-L.; Wong, W.-Y.; Wang, Q.; Ma, D.; Wang, L.; Lin, Z.; Marder, T. B.; Beeby, A. *Adv. Funct. Mater.* **2008**, *18*, 499-511. (j) Weber, L.; Werner, V.; Fox, M. A.; Marder, T. B.; Schwedler, S.; Brockhinke, A.; Stammler, H.-G.; Neumann, B. *Dalton Trans.* **2009**, 1339-1351. (k) Weber, L.; Werner, V.; Fox, M. A.; Marder, T. B.; Schwedler, S.; Brockhinke, A.; Stammler, H.-G.; Neuman, B. *Dalton Trans.* **2009**, 2823-2831. (l) Braunschweig, H.; Herbst, T.; Rais, D.; Ghosh, S.; Kupfer, T.; Radacki, K.; Crawford, A. G.; Ward, R. M.; Marder, T. B.; Fernandez, I.; Frenking, G. *J. Am. Chem. Soc.* **2009**, *131*, 8989-8999. (m) Collings, J. C.; Poon, S.-Y.; Le Droumaguet, C.; Charlot, M.; Katan, C.; Pålsson, L.-O.; Beeby, A.; Mosely, J. A.; Kaiser, H. M.; Kaufmann, D.; Wong, W.-Y.; Blanchard-Desce, M.;

Marder, T. B.; *Chem. Eur. J.* **2009**, *15*, 198-208. (n) Entwistle, C. D.; Collings, J. C.; Steffen, A.; Pålsson, L.-O.; Beeby, A.; Albesa-Jové, D.; Burke, J. M.; Batsanov, A. S.; Howard, J. A. K.; Mosely, J. A.; Poon, S.-Y.; Wong, W.-Y.; Ibersiene, F.; Fathallah, S.; Boucekkine, A.; Halet, J.-F.; Marder, T. B. *J. Mater. Chem.* **2009**, *40*, 7532-7544.

[9] Murphy, J. M.; Liao, X.; Hartwig, J. F. *J. Am. Chem. Soc.* **2007**, *129*, 15434-15435.

[10] Irngartinger, H.; Kirrstetter, R. G. H.; Krieger, C.; Rodewald, H.; Staab, H. A. *Tetrahedron Lett.* **1977**, *18*, 1425-1428.

[11] Harvey, R. G.; Konieczny, M.; Pataki, J. *J. Org. Chem.* **1983**, *48*, 2930-2932.

[12] (a) Eddaoudi, M.; Kim, J.; Rosi, N.; Vodak, D.; Wachter, J.; O'Keeffe, M.; Yaghi, O. M. *Science* **2002**, *295*, 469-472. (b) Rowsell, J. L. C.; Yaghi, O. M. *J. Am. Chem. Soc.* **2006**, *128*, 1304-1315. (c) Dang, H.; Maris, T.; Yi, J.-H.; Rosei, F.; Nanci, A.; Wuest, J. D. *Langmuir* **2007**, *23*, 11980-11985.

[13] Echauarren, A. M.; Stille, J. K. *J. Am. Chem. Soc.* **1987**, *109*, 5478-5486.

[14] Colquhoun, H. M.; Zhu, Z.; Williams, D. J.; Drew, M. G. B.; Cardin, C. J.; Marder, T. B.; Crawford. A. G. *Chem. Eur. J.* **2010**, *16*, 907-918.

[15] (a) Stolka, M.; McGrane, K. M.; Facci, J. S. Photoconductive Imaging Members with Alkoxy Amine Charge Transport Molecules. U.S. Patent 4,588,666, May 13, 1986. (b) Bellmann, E.; Shaheen, S. E.; Thayumanavan, S.; Barlow, S.; Grubbs, R. H.; Marder, S. R.; Kippelen, B.; Peyghambarian, N. *Chem. Mater.* **1998**, *10*, 1668-1676. (c) Mitschke, U.; Bäuerle, P. *J. Mater. Chem.* **2000**, *10*, 1471–1507. (d) Low, P. J.; Paterson, M. A. J.; Puschmann, H.; Goeta, A. E.; Howard, J. A. K.; Lambert, C.; Cherryman, J. C.; Tackley, D. R.; Leeming, S.; Brown, B. *Chem. Eur. J.* **2004**, *10*, 83-91. (e) Bardecker, J. A.; Ma, H.; Kim, T.; Huang, F.; Liu, M. S.; Cheng, Y.-J.; Ting, G.; Jen, A. K.-Y. *Adv. Funct. Mater.* **2008**, *18*, 3964-3971.

[16] Wee, K.-R.; Ahn, H.-C.; Son, H.-J.; Han, W.-S.; Kim, J.-E.; Cho, D. W.; Kang, S. O. *J. Org. Chem.* **2009**, *74*, 8472-8475.

[17] (a) Vaughan, W. M.; Weber, G. *Biochemistry* **1970**, *3*, 464-473. (b) Ribou, A.-C.; Vigo, J.; Salmon, J.-M. *Photochem. Photobio.* **2004**, *80*, 274-280. (c) Berezin, M. Y.; Achilefu, S. *Chem. Rev.* **2010**, *110*, 2641-2684.

[18] (a) Takeuchi, T.; Kosuge, M.; Tadokoro, A.; Sugiura, Y.; Nishi, M.; Kawata, M.; Sakai, N.; Matile, S.; Futaki, S. *ACS Chem. Biol.* **2006**, *1*, 299-303. (b) Jablonski, A. E.; Kawakami, T.; Ting, A. Y.; Payne, C. K. *J. Phys. Chem. Lett.* **2010**, *1*, 1312-1315.

[19] Huo, S. *Org. Lett.* **2003**, *5*, 423-425.

[20] Vyas, P. V.; Bhatt, A. K.; Ramachandraiah, G.; Bedekar, A. V. *Tetrahedron Lett.* **2003**, *44*, 4085-4088.

[21] Yang, S.-W.; Elangovan, A.; Hwang, K.-C.; Ho, T.-I. *J. Phys. Chem. B* **2005**, *109*, 16628-16635.

[22] Zhao, S.-B.; Wucher, P.; Hudson, Z. M.; McCormick, T. M.; Liu, X.-Y.; Wang, S.; Feng, X.-D.; Lu, Z.-H. *Organometallics* **2008**, *27*, 6446-6456.

[23] Beinhoff, M.; Weigel, W.; Jurczok, M.; Rettig, W.; Modrakowski, C.; Brüdgam, I.; Hartl, H.; Schlüter, A. D. *Eur. J. Org. Chem.* **2001**, 3819-3829.

[24] (a) Robertson, J. M. *Proc. Roy. Soc. (London)* **1951**, *A207*, 101-110. (b) Desiraju, G. R.; Gavezzotti, A. *J. Chem. Soc., Chem. Commun.* **1989**, 621-623. (c) Desiraju, G. R.; Gavezzotti, A. *Acta Crystallogr.* **1989**, *B45*, 473–482.

[25] (a) Robertson, J. M.; White, J. G. *J. Chem. Soc.* **1947**, 358-368. (b) Allmann, R. *Z. Kristallogr.* **1970**, *132*, 416-416. (c) Hazell, A. C.; Larsen, F. K.; Lehmann, M. S. *Acta Crystallogr.* **1972,** *B28*, 2977-2984. (d) Kai, Y.; Hama, F.; Yasuoka, N.; Kasai, N. *Acta Crystallogr.* **1978**, *B34*, 1263-1270.

[26] (a) Knight, K. S.; Shankland, K.; David, W. I. F.; Shankland, N.; Love, S. W. *Chem. Phys. Lett.* **1996**, *258*, 490-494. (b) Frampton, C. S.; Knight, K. S.; Shankland, K.; Shankland, N. *J. Mol. Struct.* **2000**, *520*, 29-32.

[27] Fabbiani, F. P. A.; Allan, D. R.; Parsons, S.; Pulham, C. R. *Acta Crystallogr.* **2006**, *B62*, 826-842.

[28] Wallach, O. *Liebigs Ann. Chem.* **1895**, *94*, 90-143.

[29] Brock, C. P.; Schweizer, W. B.; Dunitz, J. D. *J. Am. Chem. Soc.* **1991**, *113*, 9811-9820.

[30] (a) Dahl, T. *Acta Crystallogr.* **1990**, *B46*, 283-288. (b) Williams, J. H. *Acc. Chem. Res.* **1993**, *26*, 593-598. (c) Dai, C.; Marder, T. B.; Scott, A. J.; Clegg, W.; Viney, C. *Chem. Commun.* **1999**, 2493-2494. (d) Collings, J. C.; Roscoe, K. P.; Thomas, R. L.; Batsanov, A. S.; Stimson, L. M.; Howard, J. A. K.; Marder, T. B. *New J. Chem.* **2001**, *25*, 1410-1417. (e) Collings, J. C.; Roscoe, K. P.; Robins, E. G.; Batsanov, A. S.; Stimson, L. M.; Howard, J. A. K.; Clark, S. J.; Marder, T. B. *New J. Chem.* **2002**, *26*, 1740-1746. (f) Watt, S. W.; Dai, C.; Scott, A. J.; Burke, J. M.; Thomas, R. Ll.; Collings, J. C.; Viney, C.; Clegg, W.; Marder, T. B. *Angew. Chem. Int. Ed.* **2004**, *43*, 3061-3063.

[31] Enright, G. D.; Udachin, K. A.; Ripmeester, J. A. *Chem. Commun.* **2004**, 1360-1361.

[32] Wang, Z.; Dötz, F.; Enkelmann, V.; Müllen, K. *Angew. Chem. Int. Ed.* **2005**, *44*, 1247-1250.

[33] Couderc, G.; Hulliger, J. *Chem. Soc. Rev.* **2010**, *39*, 1545-1554.

[34] Brese, N. E.; O'Keeffe, M. *Acta Crystallogr.* **1991**, *B47*, 192-197.

[35] Pauling, L. *J. Am. Chem. Soc.* **1929**, *51*, 1010-1026.

[36] Brunton, G. *Acta Crystallogr.* **1969**, *B25*, 2161-2162.

[37] Chase, P. A.; Henderson, L. D.; Piers, W. E.; Parvez, M.; Clegg, W.; Elsegood, M. R. J. *Organometallics* **2006**, *25*, 349-357.

[38] Driver, M. S.; Hartwig, J. F. *J. Am. Chem. Soc.* **1996**, *118*, 7217-7218.

[39] Olah, G. A.; Karpeles, R.; Narang, S. C. *Synthesis* **1982**, 963-965.

[40] (a) Brown, H. C.; Dodson, V. H. *J. Am. Chem. Soc.* **1957**, *79*, 2302-2306. (b) Pelter, A.; Smith, A.; Brown, H. C. *Borane Reagents*, Academic Press: London, **1988**, p. 428.

[41] (a) Zhou, G.; Wong, W.-Y.; Poon, S.-Y.; Ye, C.; Lin, Z. *Adv. Funct. Mater.* **2009**, *19*, 531-544. (b) An, Z.; Odom, S. A.; Kelley, R. F.; Huang, C.; Zhang, X.; Barlow, S.;

Padilha, L. A.; Fu, J.; Webster, S.; Hagan, D. J.; Van Stryland, E. W.; Wasielewski, M. R.; Marder, S. R. *J. Phys. Chem. A* **2009**, *113*, 5585-5593.

[42] Liu, Z. *Unpublished Results*.

[43] Schwarz, N. *Unpublished Results*.

[44] Thibault, M.-H. *Unpublished Results*.

[45] Alcaraz, G. *Unpublished Results*.

[46] Mkhalid, I. A. I. *Unpublished Results*.

Chapter 3: Experimental and Theoretical Studies of the Photophysical Properties of 2-, 2,7- and 1-Functionalized Pyrene Derivatives

1.0 Introduction

Pyrene is an important chromophore that displays long lived fluorescence and a propensity to form fluorescent excimers via π-π stacking interactions. These properties have led to its use in a number of applications (Chapter 1). However, nearly all these applications involve derivatives substituted at the 1-, 3-, 6- and 8-positions, the sites of maximum contributions of the HOMO and hence electrophilic aromatic substitution.

In the last chapter, the synthesis of a library of 2- and 2,7-substituted pyrene derivatives was described. These derivatives had previously been difficult to synthesize due to the presence of nodal planes in the HOMO and LUMO (Figure 1), which lie perpendicular to the molecule and pass through the 2- and 7-positions. As a result of the synthetic challenges associated with these derivatives, no detailed studies of their photophysical properties have been reported.

Figure 1 The HOMO (left) and LUMO (right) of pyrene.

Herein, the effects of the nature and position of substituents upon the photophysical properties of a series of 2-, 2,7- and 1-substituted pyrene derivatives are reported. To assist in the understanding of experimental observations, the results of time-dependent density functional theory (TD-DFT)[1] calculations using both the B3LYP[2] and CAM-B3LYP[3] functionals are discussed. The calculations were performed by Austin Dwyer (Durham University, UK).

2.0 Results and Discussion

2.1 Unsubstituted Pyrene

Before discussing the effects of substitution on pyrene, the photophysical properties of unsubstituted pyrene are considered. As a monomer in cyclohexane solution, the absorption spectrum of pyrene consists of four bands (Figure 2): a weak band ($S_1 \leftarrow S_0$) at 372 nm (ε = 510 mol^{-1} cm^{-1} L) with vibrational fine structure; two bands ($S_2 \leftarrow S_0$) at 334 nm and ($S_3 \leftarrow S_0$) at 272 nm with regular vibrational structure (ε = 55000 mol^{-1} cm^{-1} L and ε = 54000 mol^{-1} cm^{-1} L, respectively); and a strongly allowed band ($S_4 \leftarrow S_0$) at 243 nm (ε = 88000 mol^{-1} cm^{-1} L).[4] These transitions, summarized in Table 1, are referred to by a number of different nomenclatures including those introduced by Clar[5] and Platt[6] as well as those derived from the symmetry of the orbitals involved in the transitions.

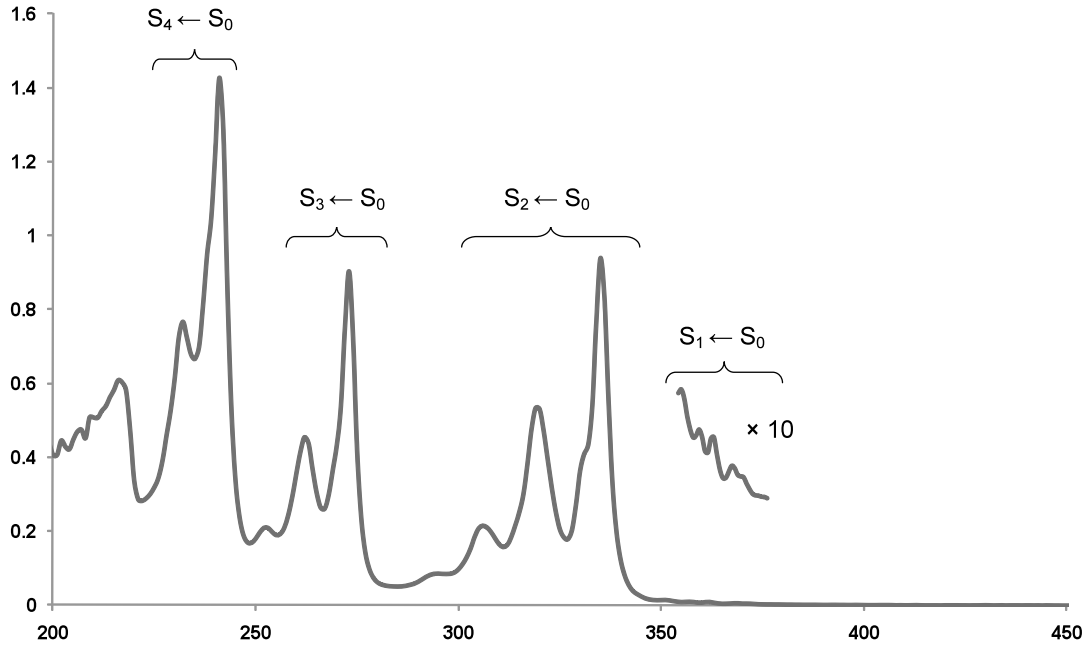

Figure 2 The absorption spectrum of pyrene (recorded in cyclohexane) with transitions labeled.

Transition	*Wavelength / nm, (ε (/mol^{-1}cm^{-1}L))*[a]	*Symmetry*	*Dominant configuration*	*Polarization*	*Clar*	*Platt*
$S_1 \leftarrow S_0$	372 (510)	B_{2u}	$b_{3u} \leftarrow b_{1g}$ - $a_u \leftarrow b_{2g}$	y	α	L_b
$S_2 \leftarrow S_0$	334 (55000)	B_{1u}	$a_u \leftarrow b_{1g}$	z	p	L_a
$S_3 \leftarrow S_0$	272 (54000)	B_{2u}	$b_{3u} \leftarrow b_{1g}$ + $a_u \leftarrow b_{2g}$	y	β	B_b
$S_4 \leftarrow S_0$	243 (88000)	B_{1u}	$b_{3u} \leftarrow b_{2g}$	z	β'	B_a

[a]Recorded in cyclohexane.

Table 1 Summary of terminology used to describe optical transitions in pyrene.[4a,c]

Theory and linear dichroism studies[7] show that the $S_1 \leftarrow S_0$ and $S_3 \leftarrow S_0$ transitions are polarized along the short, *y* axis of pyrene, while the $S_2 \leftarrow S_0$ and $S_4 \leftarrow S_0$ transitions are polarized along the long, *z* axis (for the coordinate system, see Figure 3).

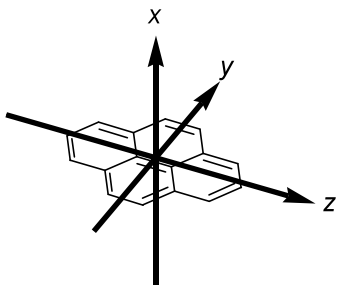

Figure 3 Principle Cartesian coordinate system used for pyrene.

After excitation to higher excited states, transient absorption spectroscopy (measurement of the absorbance at a particular wavelength as a function of time) has shown the build-up of the S_1 population to be complete within 2 ps, with a wavelength dependent time constant of 300-400 fs.[8] Fluorescence from the S_1 state is observed in the emission spectrum at 372 nm (in toluene) displaying fine structure consisting of a sequence of resolved vibronic transitions. The excited singlet state is exceptionally long lived, with a fluorescence lifetime of 354 ns in degassed solution.[4f] Rate constants of fluorescence, $k_F = 10^6$ s^{-1}, and intersystem crossing, $k_{ST} = 10^5$ s^{-1},[4e] along with an uncompetitive rate of internal conversion, typical of rigid aromatic molecules, give rise to a significant fluorescence quantum yield of 0.64, with the remainder of excited

singlet state undergoing intersystem crossing to a triplet state. Pyrene is widely known for its ability to form excimers in solution at concentrations above *ca*. 10^{-5} mol dm^{-3}, giving rise to a broad, structureless emission band centred at 480 nm, while the intensity of emission due to the monomer decreases with increasing concentration.[4]

The energies of the $S_n \leftarrow S_0$ excitations in pyrene have also been the subject of several theoretical studies.[9] Before going into detail, a brief comparison between theory and experiment is provided.

In theoretical studies (e.g., TD-DFT), the vertical excitation energy (ΔE_{vert}) is calculated. This is the energy difference between the ground state potential energy surface (PES), and the excited state PES (Figure 4) at the same geometry. In experimental absorption spectra, λ_{max} values are measured. The λ_{max} is the spectral band of highest intensity, resulting from an excitation from the ground vibrational state of the lower electronic state, to the most similar vibrational state in the excited electronic state (Figure 4), i.e. an excitation to a vibrational wavefunction that has the greatest overlap with the vibrational wavefunction of the ground electronic state (Franck-Condon principle). In the compounds described in this chapter, λ_{max} involves a transition between the lowest vibrational states (v' = 0, v = 0) of each electronic state and hence corresponds to a $S_n^{\,0} \leftarrow S_0^{\,0}$ transition.

For an effective comparison between λ_{max} and ΔE_{vert}, the region of greatest overlap between vibrational wavefunctions should correspond to the point on the PES directly above the ground state minimum. In simple systems, such as the diatomic in Figure 4, such a comparison is possible; however, a system like pyrene, which has many degrees of freedom, is much more complicated. Hence, comparison of experimental λ_{max} and theoretical ΔE_{vert} values in large molecules (such as the ones discussed in this chapter) is only an approximation.

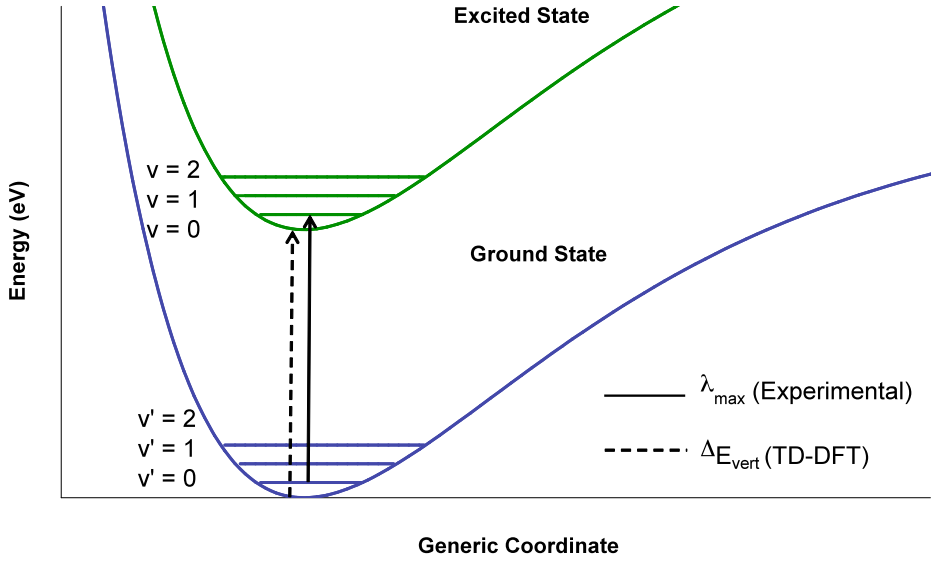

Figure 4 Theoretical and experimental excitations in a simple diatomic system. Vertical excitation energies (ΔE_{vert}) are calculated using TD-DFT, whereas λ_{max} values are measured experimentally.

Vertical excitation energies obtained from TD-DFT calculations using the commonplace B3LYP exchange-correlation functional were reported by Parac and Grimme.[9c] Comparison of these values with experimental band maxima (recorded in non-polar solvents) shows that B3LYP accurately reproduces the $S_2 \leftarrow S_0$ excitation energy, but overestimates the $S_1 \leftarrow S_0$ energy, such that the order of the two states is incorrect. This error is attributed to the aforementioned approximation in comparing λ_{max} and ΔE_{vert}. Studies[9e] to quantify this error use theoretical methods to examine the vibronic structure of the absorption spectrum and thus calculated both ΔE_{vert} and $\Delta E_{0\text{-}0}^{calc*}$ values. For the $S_2 \leftarrow S_0$ excitation, it was found that the B3LYP vertical excitation energy is 0.26 eV above the calculated $S_2^0 \leftarrow S_0^0$ ($\Delta E_{0\text{-}0}^{calc}$) transition energy. However, the value of the $\Delta E_{0\text{-}0}^{calc}$ transition energy was found to be 0.42 eV below the corresponding experimental $S_2^0 \leftarrow S_0^0$ value. Therefore, the reproduction[9c] of the $S_2 \leftarrow S_0$ excitation energy using B3LYP is largely a result of the cancellation of these two factors, i.e. the calculated excited state curve is too low in energy, but this is offset by

* $\Delta E_{0\text{-}0}^{calc}$ = the calculated energy for a $S_n^0 \leftarrow S_0^0$ transition.

calculating the vertical energy rather than the $\Delta E_{0\text{-}0}^{calc}$ transition energy. For the weakly allowed $S_1 \leftarrow S_0$ excitation, the vertical excitation energy was found to be 0.19 eV above the calculated $S_1^0 \leftarrow S_0^0$ ($\Delta E_{0\text{-}0}^{calc}$) transition energy. Unlike the $S_2 \leftarrow S_0$ excitation, the $\Delta E_{0\text{-}0}^{calc}$ transition energy for the $S_1 \leftarrow S_0$ excitation was found to be 0.20 eV above the corresponding experimental $S_1^0 \leftarrow S_0^0$ value. As a result, there is no cancellation of the errors in this calculation and the $S_1 \leftarrow S_0$ excitation with B3LYP lies well above the $S_1 \leftarrow S_0$ transition energy observed experimentally. From the above discussion, it is apparent that theoretical ΔE_{vert} values will often differ from experimental λ_{max} values due to the fact that ΔE_{vert} and λ_{max} correspond to fundamentally different transitions. Furthermore, it is worth noting that due to this difference between ΔE_{vert} and λ_{max} an accurate DFT functional will not necessarily be one that reproduces the experimental λ_{max} values but instead will be a functional that accurately reproduces the experimental excited state curve. Therefore, in the case of pyrene, an accurate functional will give values of ΔE_{vert} that are approximately 0.26 eV and 0.19 eV higher in energy than λ_{max} thus giving calculated wavelengths of 316 and 343 nm for the $S_2 \leftarrow S_0$ and $S_1 \leftarrow S_0$ excitations, respectively.[9e]

Calculations using the B3LYP functional (performed at Durham University) gave wavelengths of 340 and 333 nm for the $S_2 \leftarrow S_0$ and $S_1 \leftarrow S_0$ excitations respectively. These values were in good agreement with those reported elsewhere[9c] and highlight the incorrect ordering of states obtained using B3LYP. In order to reproduce the correct ordering of states in pyrene, the CAM-B3LYP Coulomb-attenuated functional[3] was used. Coulomb-attenuated exchange-correlation functionals,[10] such as CAM-B3LYP, have recently been shown to obtain the correct ordering of states in polyaromatic hydrocarbons, such as naphthalene.[11] Using this functional, the $S_2 \leftarrow S_0$ excitation is predicted to lie at 315 nm and the $S_1 \leftarrow S_0$ excitation at 316 nm. Thus when using CAM-B3LYP, the order of the first and second excited states is reversed from that found with B3LYP and correctly reproduced. Comparison of the CAM-B3LYP values with the aforementioned 'accurate wavelengths' of 316 and 343 nm, shows that the value (315 nm) for the $S_2 \leftarrow S_0$ excitation is accurately reproduced. However, CAM-B3LYP calculates the $S_1 \leftarrow S_0$ excitation (316 nm) to be much higher in energy than that of the 'accurate wavelength' (343 nm). The reason for this observation is beyond the scope of

this work, however, these observations are fully consistent with previous studies that use CAM-B3LYP.[12]

With both functionals, the $S_2 \leftarrow S_0$ excitation is primarily described by a HOMO→LUMO transition and the $S_1 \leftarrow S_0$ excitation has approximately equal contributions of HOMO-1→LUMO and HOMO→LUMO+1 transitions (Figure 5). Although this description of the orbitals involved in the $S_2 \leftarrow S_0$ and $S_1 \leftarrow S_0$ excitations appears counter-intuitive (the HOMO→LUMO transition is higher in energy than the HOMO-1→LUMO and HOMO→LUMO+1 transitions), it is correct, as in TD-DFT, the vertical excitation energy is not, in general equal, to the energy difference between two orbitals as orbitals are not "states".

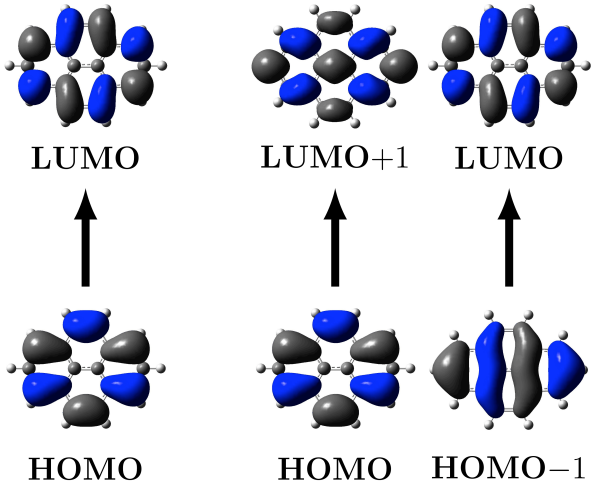

Figure 5 The dominant orbital contributions to the $S_2 \leftarrow S_0$ (left) and the $S_1 \leftarrow S_0$ excitations (right) in pyrene (B3LYP & CAM-B3LYP).

2.2 Substituted Pyrene

In order to compare the effects of substitution at the 1-, 2- and 2,7-positions of pyrene, absorption, excitation and emission spectra were recorded, and photoluminescence quantum yields and lifetimes were measured, for a series of derivatives. Spectroscopic data are given in Tables 2-4, selected spectra are presented in Figures 6-10, and absorption, emission and excitation spectra for all compounds can be found in the appendix. To avoid excimer formation, spectra were measured at low sample concentrations (10^{-5}-10^{-6} mol dm^{-3}); therefore, the discussion refers to the behaviour of

pyrene monomers in solution. Tables listing the first five calculated singlet excitations for the molecules described are presented in the appendix, and selected plots of key molecular orbitals contributing to the dominant transitions, along with a comparison of experimental and theoretical wavelengths are shown in Figures 11-15.

From the library of compounds synthesized in Chapter 2, a range of different derivatives was chosen for investigation of their photophysical properties. Most of the derivatives described in this chapter have potential for further application. The dimesitylboron ($B(Mes)_2$) moiety (**10**, **14**, **21**, **38**-**39**) behaves as an efficient π-acceptor[13] and is of interest in work involving π-conjugated organic compounds containing 3-coordinate boron centers which have found applications in OLEDs, sensors, solar cells and other materials.[13] Secondly, **29** (R = N(Ph)-C_6H_4-4-OMe) is related to *N*, *N*, *N'*, *N'*-tetraaryl-1,1'-biphenyl-4,4'diamines (TPDs), in which there is a biphenyl moiety instead of a pyrene. These compounds are an important class of hole transporters in OLED devices.[14] Investigation into the effects of extending the conjugation length of pyrene by substitution at the 2- and 2,7-positions with arylethnyl moities will be of interest, as it is known that conjugated systems involving substitution of various arylethynyl moities onto a central core molecule, such as benzene,[15] anthracene[16] and heterocyclopentadienes,[17] show interesting structural, electronic and luminescent properties. Borylated arene compounds synthesized by iridium-catalyzed C-H borylation are important precursors to a range of derivatives.[18] To help understand the electronic influence of the Bpin moiety on aromatic systems, the photophysical properties of **1**, **2** and **40** were investigated.

The fluorescence lifetimes of **31** (R = $C_3H_6CO_2H$) and **32** (R = $OC_3H_6CO_2H$) are compared to that of the known fluorescence probe, pyrene-1-butyric acid **30** (Chapter 1), which due to its long fluorescence lifetime (τ = 460 ns in MeOH) is used to determine oxygen concentrations in biological systems,[19] in biological labeling applications[20] and to investigate intracellular delivery of bioactive molecules.[21]

2.2.1 Optical Properties

Donor and Acceptor Systems

First, the effects of attaching a series of donor and acceptor substituents onto pyrene are discussed. The absorption spectra of 2-R-pyrenes {R = C_6H_4-4-CO_2Me **7**, C_6H_4-4-

$B(Mes)_2$ **10**, $B(Mes)_2$ **14**, $OC_3H_6CO_2H$ **32**, $O(CH_2)_{12}Br$ **35**} and 2,7-R_2 pyrenes {R = C_6H_4-4-$CO_2C_8H_{17}$ **6**, OH **15**, N(Ph)-C_6H_4-4-OMe **29**} are similar to that of unsubstituted pyrene, and the $S_2 \leftarrow S_0$ excitation in these derivatives can be described as 'pyrene-like'.[†] Despite the addition of strong acceptors (**10** and **14**), donors (**15** and **29**) and increasing the conjugation length through phenyl substituents (**6**, **7** and **10**), there are only negligible bathochromic shifts (0-7 nm) in the absorption maxima for the $S_2 \leftarrow S_0$ excitations (Figure 6). The vibrational progression is well resolved for compounds **15**, **32** and **35** with a spacing of 1400 cm^{-1}. In the remaining compounds, the same vibrational progression is often observed, highlighting the 'pyrene-like' nature of this excitation; however, the presence of overlapping higher energy electronic transitions often obscured some of the vibrational bands. Extinction coefficients for the $S_2 \leftarrow S_0$ excitation in 2- and 2,7-derivatives (ε = 54000-143000 mol^{-1} cm^{-1} L) are, in most cases, larger than that for pyrene (ε = 69000 mol^{-1} cm^{-1} L), with exceptionally high apparent values for R = C_6H_4-4-$B(Mes)_2$ **10**, OH **15** and N(Ph)-C_6H_4-4-OMe **29** (ε = 143000, 103000 and 112000 mol^{-1} cm^{-1} L, respectively). Closer examination of the spectra, especially for **10** and **29**, clearly shows that another absorption overlaps with the 'pyrene-like' one, contributing intensity and thus leading to anomalously large apparent ε values.

[†] 'Pyrene-like': This descriptor refers to transitions that occur between orbitals similar to the HOMO and LUMO in pyrene, i.e., the $S_2 \leftarrow S_0$ transition in pyrene (Figure 5).

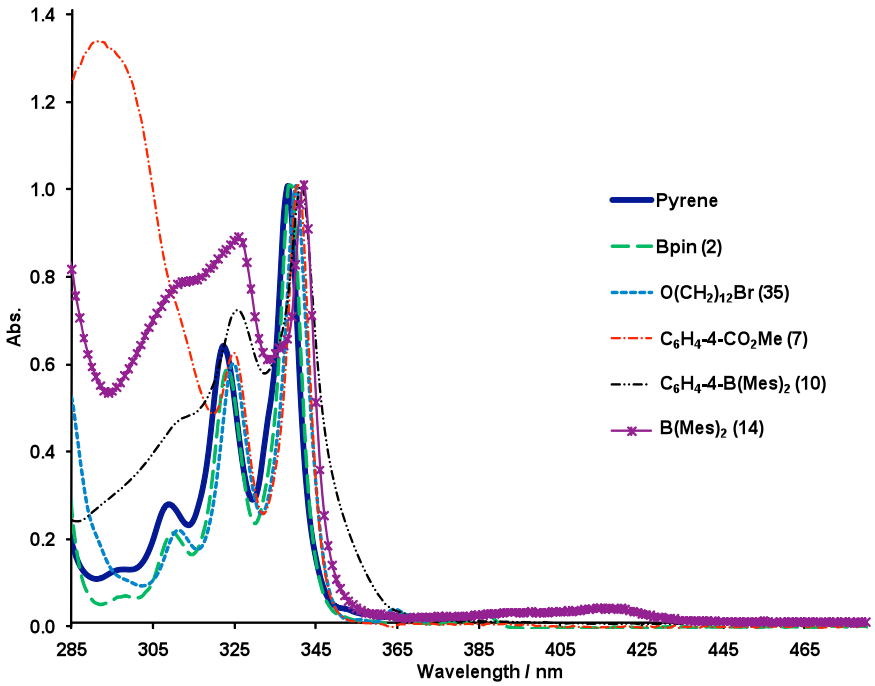

Figure 6 Absorption spectra of selected mono-2-substituted pyrene systems showing the negligible bathochromic shift in the $S_2 \leftarrow S_0$ transition compared to pyrene.

	R	$\lambda_{(S1\leftarrow S0)}$ / nm	ε /mol^{-1} cm^{-1}L	$\lambda_{(S2\leftarrow S0)}$ / nm	ε /mol^{-1} cm^{-1}L	λ_{em} / nm	ϕ^{a}	Stokes shift / cm^{-1}	τ_f / ns^{b}	τ_o / ns^{c}
Pyrene		362	600	338	69000	372	0.64	740	354	553
2	Bpin	385	1900	338	66000	386	0.72	70	82	114
7	C_6H_4-4-CO_2Me	364	1100	341	66000	406	0.43	2800	74	172
10	C_6H_4-4-$B(Mes)_2$	378	2700	339	143000[d]	414	0.47	2300	65	138
14	$B(Mes)_2$	413	2000	340	67000	434	0.68	1200	49	72
24	CCPh	390	1200	340	68000	399	0.44	600	71	161
31[e]	$C_3H_6CO_2H$	374	600	336	80000	374	0.52	0	622	1200
32[e]	$OC_3H_6CO_2H$	382	5000	336	73000	382	0.77	0	59	77
35	$O(CH_2)_{12}Br$	384	3800	340	54000	384	0.59	0	60	102

[a]Fluorescence quantum yield measured in degassed solvent. [b]Fluorescence lifetime measured in degassed solvent. [c]Calculated from τ/ϕ. [d]Value enhanced due to superposition with a broad low energy absorption band (see text). [e]Measured in MeOH.

Table 2 Spectroscopic data for 2-mono-substituted pyrene derivatives in toluene unless otherwise stated.

	R	$\lambda_{(S1\leftarrow S0)}$ / nm	ε /mol^{-1} cm^{-1}L	$\lambda_{(S2\leftarrow S0)}$ / nm	ε /mol^{-1} cm^{-1}L	λ_{em} / nm	ϕ^{a}	Stokes shift / cm^{-1}	τ_f / ns^{b}	τ_o / ns^{c}
Pyrene		362	600	338	69000	372	0.64	740	354	553
1	Bpin	398	5000	339	85000	400	0.88	250	36	41
6	C_6H_4-4-$CO_2C_8H_{17}$	404	1500	340	69000	421	0.33	1000	49	148
15[d]	OH	381	7000	338	103000[e]	405	0.93	430	29	31
20	CCPh	410	3900	332	117000[e]	418	0.29	460	16	55
21	CC-C_6H_4-4-$B(Mes)_2$	414	2800	344	120000[e]	426	0.46	680	58	126
22	CCTMS	407	1600	337	51000	407	0.19	0	99	521
26	CC-C_6H_4-4-NMe_2	421	3300	343	136000[e]	436	0.39	800	60	154
29	N(Ph)-C_6H_4-4-OMe	453	2600	345	112000[e]	482	0.30	1300	18	60

[a]Fluorescence quantum yield measured in degassed solvent. [b]Fluorescence lifetime measured in degassed solvent. [c]Calculated from τ/ϕ. [d]Measured in MeOH. [e]Value enhanced due to superposition with a broad low energy absorption band (see text).

Table 3 Spectroscopic data for 2,7-bis-substituted pyrene derivatives in toluene unless otherwise stated.

	R	$\lambda_{(S1\leftarrow S0)}$ / nm	ε /mol^{-1} cm^{-1}L	$\lambda_{(S2\leftarrow S0)}$ / nm	ε /mol^{-1} cm^{-1}L	λ_{em} / nm	ϕ^a	Stokes shift / cm^{-1}	τ_f / ns^b	τ_o / ns^c
Pyrene		362	600	338	69000	372	0.64	740	354	553
30[d]	$C_3H_6CO_2H$	375	1700	342	68000	375	0.68	0	460	680
37	CCPh	362[e]			59000	391	0.61	2000	3	5
38	$B(Mes)_2$	399[e]			54000	423	0.71	1400	3	4
39	C_6H_4-4-$B(Mes)_2$	355[e]			54000	431	0.61	5000	2	3
40	Bpin	378	7000	352	81000	379	0.81	70	35	43

[a]Fluorescence quantum yield measured in degassed solvent. [b]Fluorescence lifetime measured in degassed solvent. [c]Calculated from τ/ϕ. [d]Measured in MeOH. [e]Not possible to assign separate $S_2\leftarrow S_0$ and $S_1\leftarrow S_0$ excitations.

Table 4 Spectroscopic data for 1-mono-substituted pyrene derivatives in toluene unless otherwise stated.

In contrast, the $S_1 \leftarrow S_0$ excitation in pyrene is shown to be strongly affected by substitution at the 2- and 2,7-positions; hence this excitation is 'substituent-influenced'.* Bathochromic shifts of up to 90 nm in the $S_1 \leftarrow S_0$ excitation maxima are observed and the excitation becomes much more allowed: their extinction coefficients generally increase in magnitude. The most allowed $S_1 \leftarrow S_0$ excitations occur for the oxygen-substituted compounds, **15**, **32** and **35** (ε = 3800-7000 mol^{-1} cm^{-1} L, compared to pyrene for which ε = 600 mol^{-1} cm^{-1} L).

The absorption spectra of 1-R-pyrenes (R = $B(Mes)_2$ **38**, C_6H_4-4-$B(Mes)_2$ **39**) display large differences when compared to pyrene and the 2- and 2,7-derivatives. Instead of clearly defined excitations, a broad absorption band with no vibrational progression is observed (Figure 7). Straightforward assignment of the separate $S_2 \leftarrow S_0$ and $S_1 \leftarrow S_0$ excitations is no longer possible. There is only one discernible maximum in this band, which is bathochromically shifted from the $S_2 \leftarrow S_0$ excitation maximum in pyrene and is strongly allowed with ε = 54000 mol^{-1} cm^{-1} L. In the 1-substituted derivatives, substitution has a strong influence on both the $S_2 \leftarrow S_0$ and $S_1 \leftarrow S_0$ excitations.

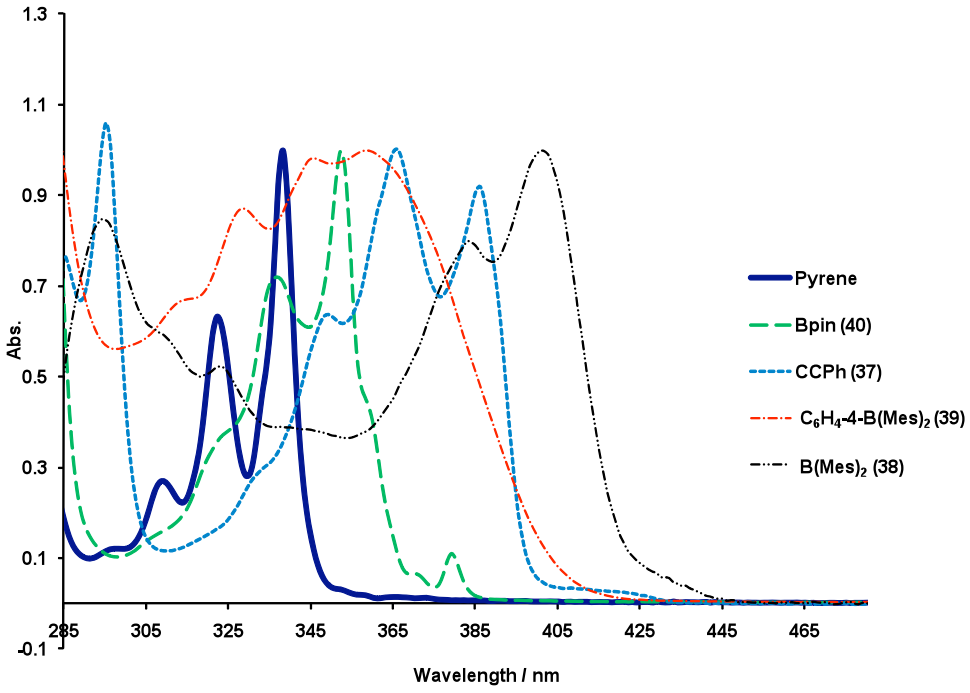

Figure 7 Absorption spectra of selected mono-1-substituted pyrene systems showing the large bathochromic shift in the absorption maxima compared to pyrene.

* 'Substituent-influenced': This descriptor refers to transitions that occur between orbitals similar to the HOMO-1/HOMO and LUMO/LUMO+1 in pyrene, i.e., the $S_1 \leftarrow S_0$ transition in pyrene (Figure 5).

Evidence for this 'substituent-influence' on the $S_1 \leftarrow S_0$ excitation is further observed in the emission spectra, which involve the reverse, i.e., $S_0 \leftarrow S_1$ transition (Figures 8 and 9). All compounds (regardless of substitution position) display a bathochromic shift from pyrene in their emission maxima, ranging from 10-110 nm.

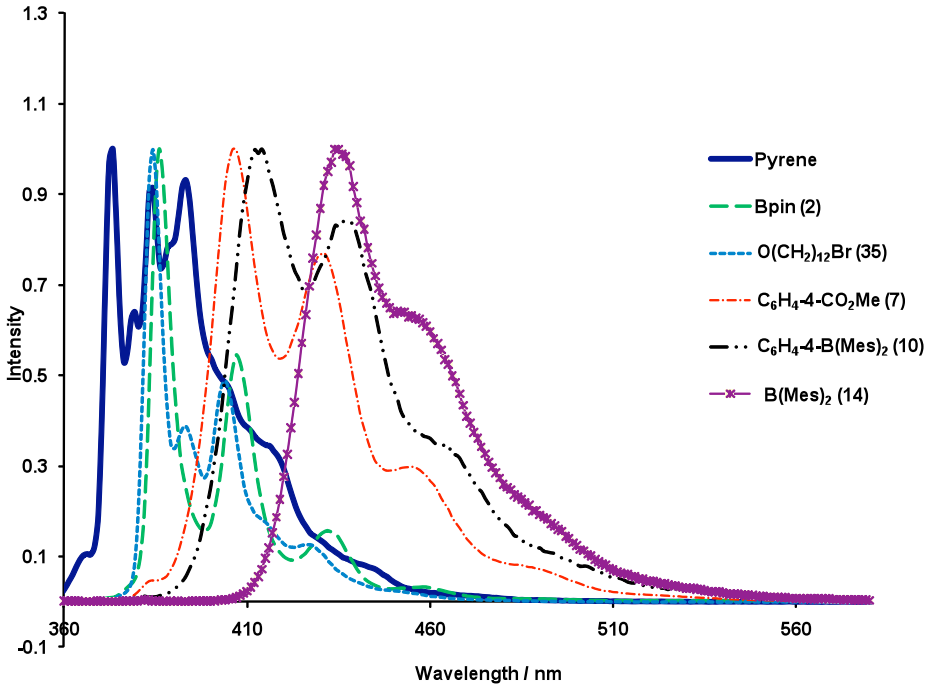

Figure 8 Emission spectra of selected mono-2-substituted pyrene systems.

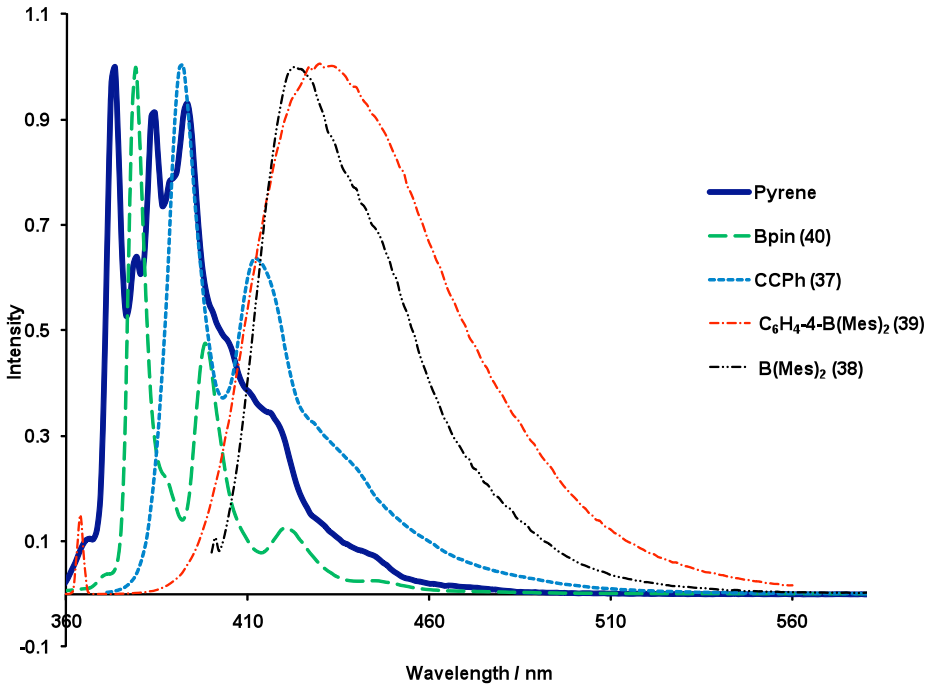

Figure 9 Emission spectra of selected mono-1-substituted pyrene systems, with loss of vibrational resolution for compounds **38** (R = $B(Mes)_2$) and **39** (R = C_6H_4-4-$B(Mes)_2$).

The structure of the emission band of **32** (R = $OC_3H_6CO_2H$) and **35** (R = $O(CH_2)_{12}Br$) is similar to that of pyrene, displaying fine vibrational structure, whereas on moving to strong donors (**15** and **29**) or acceptors (**14**, **38** and **39**) the band broadens and all fine structure is lost. Stokes shifts are sizeable for the esters (**6**, **7**), $B(Mes)_2$ derivatives (**10**, **14**, **38**, **39**) and the N(Ph)-C_6H_4-4-OMe derivative **29**, ranging from 1000-5000 cm^{-1}, suggesting that the excited state electronic structure and geometry is somewhat different from that of the ground state. Fluorescence lifetimes were found to be much shorter for all of the above compounds compared to that of pyrene (τ_f = 354 ns), consistent with the larger extinction coefficients observed for the $S_1 \leftarrow S_0$ excitation. Upon substitution at the 2- and 2,7-positions, the lifetimes are in the range of 18-74 ns, which are ca. 1-2 orders of magnitude longer than those for the 1-substituted derivatives, for which τ_f = 2-3 ns. It would appear that the effects on the allowedness of the S_1-S_0 transition are much more pronounced for 1-substituted derivatives than those substituted at the 2- and 2,7-positions, as evidenced by their shorter emission lifetimes. This observation is supported by comparing **29** with the known 1,6-isomer (1,6-bis[(4-methoxyphenyl)-*N*-

phenyl-amino]-pyrene);[22] the latter has a shorter fluorescence lifetime (τ_f = 9 ns) compared to **29** (τ_f = 18 ns).

Quantum yields for the above compounds are in the range of 0.30-0.93, and are generally smaller when the substituent is a phenyl derivative (**6**, **7**, **10** and **39**). The ϕ_f value for **38** in toluene (0.71) differs from that recorded previously[23] in CH_2Cl_2 (~1.0). However, the absorption and emission spectra recorded in toluene were in good agreement with those of Wang et al.[23]

Ethynyl Systems

Next, the effects of extending the conjugation length of pyrene with ethynyl substitutents are considered. Analogous to the donor and acceptor derivatives, a 'pyrene-like' $S_2 \leftarrow S_0$ excitation is observed in the absorption spectra. Despite the extended conjugation in compounds 2-(C≡C–Ph)pyrene **24** and 2,7-bis(C≡C–Ph)pyrene **20**, the $S_2 \leftarrow S_0$ absorption maxima undergo negligible shifts compared to unsubstituted pyrene. As well as these maxima, the absorption spectra also display a series of higher energy bands that are not well resolved. Similar behaviour is observed in the related 1,4-bis(phenylethynyl)benzene, where broadening at high energies due to the rotation of the phenyl rings with respect to one another is observed.[24]

The increase in conjugation length has an influence on the $S_1 \leftarrow S_0$ excitations, which undergo bathochromic shifts of 30-50 nm and become significantly more allowed [ε = 1200 (**24**), 3900 (**20**) mol^{-1} cm^{-1} L compared to pyrene (ε = 600 mol^{-1} cm^{-1} L)], again highlighting the 'substituent-influenced' nature of this transition. Consistent with the strong influence on both the $S_2 \leftarrow S_0$ and $S_1 \leftarrow S_0$ excitations observed for the aforementioned 1-substituted derivatives, the absorption spectrum of the related 1-(C≡C–Ph)pyrene **37**, shows a broad band with no clearly defined $S_2 \leftarrow S_0$ and $S_1 \leftarrow S_0$ excitations; however, unlike **20** and **24**, vibrational progression is observed with a spacing of 1400 cm^{-1}. This band has a maximum that is bathochromically shifted by 24 nm from the $S_2 \leftarrow S_0$ excitation in pyrene and is strongly allowed (ε = 59000 mol^{-1} cm^{-1} L). Emission spectra of the three phenylethynyl derivatives, **20**, **24** and **37** are almost identical. The Stokes shift for **37** (2000 cm^{-1}) is much larger than those for **20** and **24** (460 and 600 cm^{-1}, respectively). Quantum yields are somewhat lower for the 2- and 2,7-derivatives, with the lowest value of ϕ_f = 0.29 for **20** presumably due to the extra deactivation pathways from the excited state, caused by the additional phenyethynyl

moiety. Analogous to the above donor/acceptor compounds, which showed that the influence on the $S_1 \leftarrow S_0$ excitation is greatest when substitution is at the 1-position, the fluorescence lifetime of the 1-substituted derivative **37** (τ_f = 3 ns) is much shorter than those of **24** and **20** (τ_f = 71 and 16 ns, respectively).

The effects of altering the nature of the arylethynyl moiety on 2,7-bis(C≡C–Ph)pyrene **20** with a strong acceptor ($B(Mes)_2$ **21**) or a strong donor (NMe_2 **26**) in the *para*-position are now considered. Similar to other 2- and 2,7-pyrene derivatives, 'pyrene-like' $S_2 \leftarrow S_0$ excitation maxima are observed which are similar in energy to that of pyrene. Unlike **20**, the vibrational progression is better resolved and it is possible to measure a vibrational level spacing of 1500-1600 cm^{-1} (*cf.* 1500 cm^{-1} for pyrene). However, the absorption spectra of these compounds are dominated by a broad, featureless band at lower energy than the 'pyrene-like' transition (Figure 10).

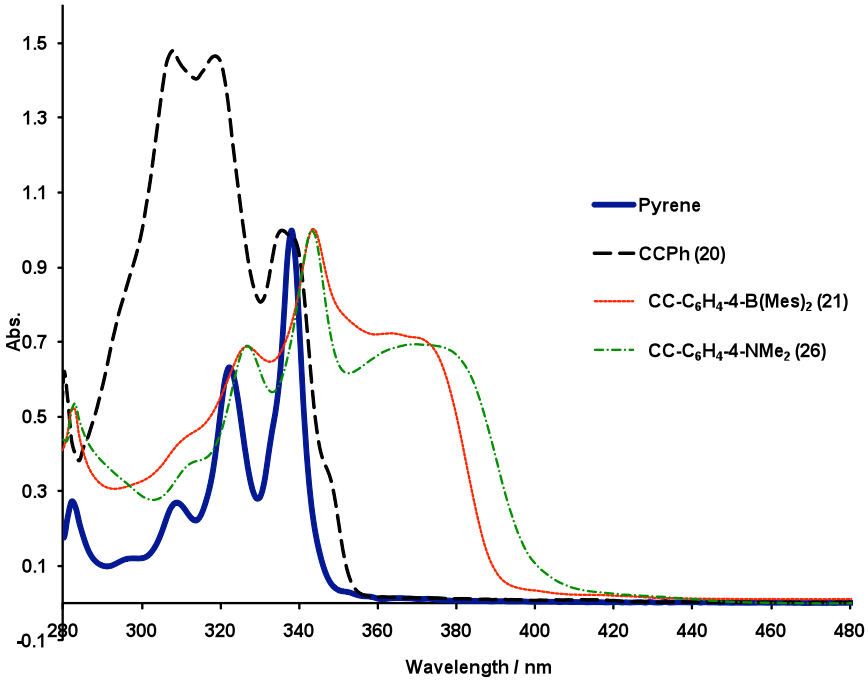

Figure 10 Absorption spectra of selected 2,7-bis-R-pyrene derivatives: R = C≡C-Ph (**20**), C≡C-C_6H_4-4-$(BMes)_2$ (**21**), C≡C-C_6H_4-4-NMe_2 (**26**).

In **20**, the band appears as a small shoulder, but in **21** and **26**, the band broadens significantly, presumably due to essentially free rotation of the acceptor- or donor-substituted aryl ethynyl moieties with respect to the pyrene core and indicative of extensive delocalization over the entire molecule.[24] The apparent extinction coefficients for the 'pyrene-like $S_2 \leftarrow S_0$' absorption for all three compounds are exceptionally large

(ε = 117000 (**20**), 120000 (**21**) and 136000 (**26**) mol^{-1} cm^{-1} L), highlighting a strongly allowed process. However, these values are likely to represent the superposition of the 'pyrene-like' absorption with that of the at least one other broad lower lying charge transfer type absorption (*vide infra*). In line with the other 2- and 2,7-substitued derivatives, the $S_1 \leftarrow S_0$ excitation is 'substituent-influenced' and, compared to pyrene, undergoes a bathochromic shift of 48-59 nm. All three compounds have similar $S_1 \leftarrow S_0$ extinction coefficients (2800-3900 mol^{-1} cm^{-1} L), which are much larger than that for pyrene. Despite the similarity of these extinction coefficients, the pure radiative lifetimes differ; the addition of a strong acceptor (**21**; τ_o = 126 ns) or donor (**26**; τ_o = 154 ns) increases the lifetime by a factor of three (**20**; τ_o = 55 ns). However, the fluorescence lifetime can be further increased when the aryl group is replaced with a trimethylsilyl (TMS) group. The compound, 2,7-bis(C≡C–TMS)pyrene **22** has a lifetime of 99 ns and a quantum yield of 0.19; hence, its pure radiative lifetime is 521 ns, almost equivalent to that of pyrene (τ_o = 553 ns). The effect of the TMS group is to reduce the conjugation length of the system and remove any rotational conformations associated with the phenyl group.[16f] This appears to have the effect of increasing the fluorescence lifetime, despite its, extinction coefficient for the $S_1 \leftarrow S_0$ transition (ε = 1600 mol^{-1} cm^{-1} L) being similar to those of the arylethynyl systems.

Bpin Derivatives

Substitution of pyrene with the Bpin moiety is now considered. The Bpin moiety is expected to be a modest π-acceptor and an inductive σ-donor. For 1-(Bpin)pyrene **40**, separate $S_2 \leftarrow S_0$ and $S_1 \leftarrow S_0$ absorptions can now be resolved (*cf*. **37-39**, for which it was not possible to assign separate $S_2 \leftarrow S_0$ and $S_1 \leftarrow S_0$ excitations). Absorption spectra of 2-(Bpin)pyrene **2**, 2,7-bis(Bpin)pyrene **1** and 1-(Bpin)pyrene **40** are very similar in overall appearance to that of pyrene; hence, the term 'pyrene-like' for the $S_2 \leftarrow S_0$ excitation is very applicable. However, in the 1-substituted derivative **40**, there is a bathochromic shift in the absorption maximum of 14 nm, compared to negligible shifts for **1** and **2**. Furthermore, despite all three compounds showing well-resolved vibrational progressions of 1400 cm^{-1}, there is a slight broadening in the structure of the $S_2 \leftarrow S_0$ bands for **40**. Clearly, substitution at the 1-position exerts a greater effect on the $S_2 \leftarrow S_0$ excitation than substitution at the 2- and 2,7-positions. Analogous to the above donor/acceptor/ethynyl compounds, the $S_1 \leftarrow S_0$ transition is 'substituent-influenced'.

The absorption has become more allowed, as reflected in the higher extinction coefficients (ε = 1900-7000 mol^{-1} cm^{-1} L, compared to ε = 600 mol^{-1} cm^{-1} L for pyrene). Interestingly, the bathochromic shifts for the $S_1 \leftarrow S_0$ absorption are significantly larger for **2** and especially **1** than for **40**. Further effects are seen in the emission maxima which undergo bathochromic shifts from pyrene (**1**: 28 nm; **2**: 14 nm; and **40**: 5 nm), again being much larger for **1** and **2** than for **40**. The Stokes shifts are small, being (70-250 cm^{-1}) suggesting little change in the geometry between the ground and excited states. Quantum yields range from 0.72-0.88, all being higher than that of pyrene (ϕ = 0.64), and their fluorescence lifetimes 4-10 times shorter than for pyrene, i.e., 35-82 ns compared to 354 ns. Interestingly, despite their different substitution positions, compounds **1** and **40** have almost identical lifetimes and quantum yields. Thus, these Bpin derivatives show similar behaviour to other pyrene derivatives (*vide supra*): substitution at the 2- and 2,7-positions has little influence on the $S_2 \leftarrow S_0$ absorption but a large influence on the $S_1 \leftarrow S_0$ absorption, whereas substitution at the 1-position influences both the $S_2 \leftarrow S_0$ and the $S_1 \leftarrow S_0$ absorptions. It is interesting to compare the mono-substituted derivatives 2-(Bpin)pyrene **2** and 2-($B(Mes)_2$)pyrene **14**. As expected from the fact that $B(Mes)_2$ is a stronger π-acceptor than Bpin,[25] the bathochromic shifts of the $S_1 \leftarrow S_0$ absorption and emission maxima are much greater for **14** than for **2**, whereas again, the $S_2 \leftarrow S_0$ absorption for both are essentially invariant from that of pyrene. For the analogous 1-substituted derivatives 1-(Bpin)pyrene **40** and 1-($B(Mes)_2$)pyrene **38**, whilst it was not possible to assign separate $S_2 \leftarrow S_0$ and the $S_1 \leftarrow S_0$ absorptions for **38**, its emission maximum (423 nm) is considerably red shifted from that of **40** (379 nm).

Butyric Acid Derivatives

Finally, 4-(pyren-2-yl)-butyric acid **31** is compared with the commercially available 4-(pyren-1-yl)-butyric acid **30**. For the purposes of this discussion, the butyric acid moiety is classified as a 'non-interacting' substituent, due to the absence of substantial conjugation, charge-transfer or inductive effects between the substituent and pyrene moiety. Absorption spectra of **30**, **31** and pyrene are almost identical, with extinction coefficients for the $S_2 \leftarrow S_0$ excitation in the range of ε = 68000-80000 mol^{-1} cm^{-1} L. Hence, unlike other substituents at the 1-position (*vide supra*), the butyric acid group

has a negligible influence on the $S_2 \leftarrow S_0$ excitation, which highlights the 'pyrene-like' nature of this transition.

The influence of substitution with butyric acid on the $S_1 \leftarrow S_0$ ('substituent-influenced') excitation is small, and both **30** and **31** have negligible bathochromic shifts in their emission maxima compared to pyrene. The Stokes shifts for **30** and **31** are 0 cm^{-1} compared to 740 cm^{-1} for pyrene, suggesting almost no differences between their excited and ground state geometries. Their quantum yields of 0.52-0.68 are again similar. However, the extinction coefficient for the $S_1 \leftarrow S_0$ excitation of **30**, almost triples to: ε = 1700 mol^{-1} cm^{-1} L for **30**, from ε = 600 mol^{-1} cm^{-1} L for **31** and pyrene. This observation is further reflected in the fluorescence lifetimes, where τ_f is even longer for the new compound **31** (622 ns in MeOH) than for **30** (460 ns in MeOH), both being longer than that of pyrene (354 ns in toluene). Thus, it is possible that **31** may be an even more efficient oxygen sensor in biological systems than **30** (see Chapter 1), and its unusually long fluorescence lifetime should make it amenable to use in time-resolved imaging applications. Analogous to the other compounds investigated in this study, it is apparent that even when a 'non-interacting' substituent is attached to pyrene, there is still an influence on the $S_1 \leftarrow S_0$ excitation, regardless of substitution position.

However, even in **30** and **31**, the influence on the $S_1 \leftarrow S_0$ absorption is much more pronounced when substitution occurs at the 1-position of pyrene, as seen by larger extinction coefficients and shorter fluorescence lifetimes, whereas when substituted at the 2-position, the influence on the $S_1 \leftarrow S_0$ excitation is much less and the molecule displays similar properties to those of unsubstituted pyrene.

2.2.1 TD-DFT Calculations*

The results obtained from TD-DFT calculations are now discussed. Initially, the discussion will focus on the data obtained using the B3LYP functional. As mentioned in Section 2.1, the comparison between experiment and theory is an approximation (λ_{max} vs. ΔE_{vert}); therefore, the following discussion will focus on trends in wavelengths, rather than absolute values. The theoretical data obtained for substituted derivatives will be compared to that calculated for unsubstituted pyrene. In particular, the influence on

* For TD-DFT calculations: The methyl groups on the Bpin substituent were replaced with hydrogens for compounds **1**, **2** and **40**; the C_8H_{17} group in compound **6** was replaced with a CH_3; calculations were not performed on compound **35**.

the orbital transitions associated with the $S_2 \leftarrow S_0$ 'pyrene-like' and $S_1 \leftarrow S_0$ 'substituent-influenced' excitations (shown in Figure 5) will be discussed. Assignment of these transitions in the substituted derivatives is undertaken by considering the nature of the orbitals involved in the transition. It is worth noting that, although the ordering of the orbitals might not be the same as that observed in pyrene, it is the nature of the orbitals involved in the relevant transition that are of interest.

Firstly, the calculations on 2- and 2,7-substituted pyrene derivatives are considered. The HOMO and LUMO orbitals of pyrene (Figure 1) show that there are nodal planes running through the 2- and 7-positions, which are perpendicular to the molecular plane. As a result, substitution at the 2- and 7-positions is unlikely to have any influence on the HOMO and LUMO. In contrast, the HOMO-1 and LUMO+1 orbitals have non-zero contributions at these positions (Figure 5); hence, substitution at the 2- and 7-positions is likely to influence these orbitals. The extent of this influence is dependent upon the nature of the substituent.

Nearly all of the 2- and 2,7-substituted pyrene derivatives investigated were found to have an electronic transition that involved orbitals similar to those of the $S_2 \leftarrow S_0$ (HOMO$\rightarrow$LUMO) transition in pyrene. Several examples are shown in Figure 11. In most compounds, it is the $S_2 \leftarrow S_0$ transition that involves similar orbitals to those involved in the $S_2 \leftarrow S_0$ transition in unsubstituted pyrene (HOMO$\rightarrow$LUMO). However, in the case of **10**, **20**, **21** and **31** the analogous transition, is the 4^{th}, 4^{th}, 14^{th} and 1^{st} excitation respectively (in the low-lying excitations considered here, compounds **6**, **26** and **29** have no identifiable transition, which is comparable to the $S_2 \leftarrow S_0$ transition in unsubstituted pyrene). As substitution at the 2- and 7-positions should have little influence on the orbitals involved in this transition, the energy of the transition should be similar to that calculated for the $S_2 \leftarrow S_0$ excitation in unsubstituted pyrene. Indeed, all of the transitions are within 10 nm of that calculated for pyrene; thus reproducing the small bathochromic shift in the $S_2 \leftarrow S_0$ 'pyrene-like' excitation maxima observed experimentally. In the case of **31**, the negligible influence of the butyric acid substituent on pyrene is also reproduced. In fact, the influence is small enough that the calculated results for **31** are almost identical to those for pyrene, including the incorrect ordering of the first two states.

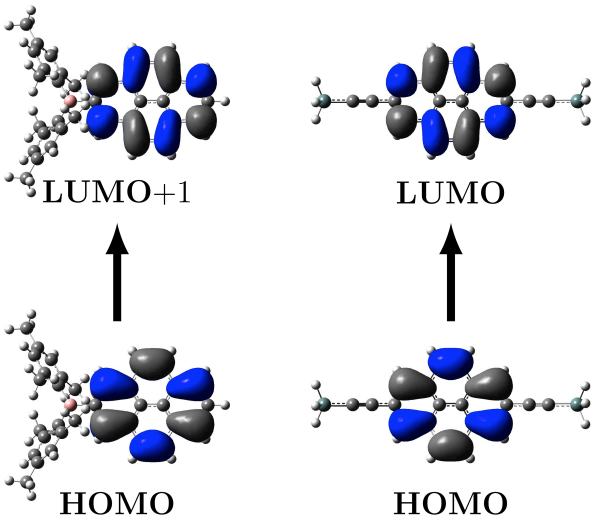

Figure 11 The pyrene-like transitions of compounds **14** and **22** (B3LYP).

Next, the influence on the $S_1 \leftarrow S_0$ excitation upon substitution at the 2- and 2,7-positions of pyrene is considered. The bathochromic shift in the $S_1 \leftarrow S_0$ excitation maxima that is observed experimentally is reproduced. This shift arises from the nature of the HOMO-1 and LUMO+1 orbitals involved in the $S_1 \leftarrow S_0$ transition, which have non-zero contributions at the 2- and 7-positions. It can be seen in Figure 12, that this leads to delocalization of these orbitals over both the pyrene moiety and the substituent. The effect of substitution can be seen when comparing the HOMO-1 and LUMO+1 orbitals in Figure 12 with those of unsubstituted pyrene shown in Figure 5. Hence, DFT calculations reproduce the experimental observation, that the $S_1 \leftarrow S_0$ excitation is 'substituent-influenced'. For some of the larger substituents, R = C≡C-C_6H_4-4-$(BMes)_2$ **21** and R = C≡C-C_6H_4-4-NMe_2 **26** the assignment of a transition that is similar to the $S_1 \leftarrow S_0$ transition in pyrene is problematic, as the orbitals are delocalized to a much larger extent and the contribution from each orbital transition is no longer equal. This may be the reason why the bathochromic shift in the $S_1 \leftarrow S_0$ transition is much larger in **21** and **26** than for the other compounds.

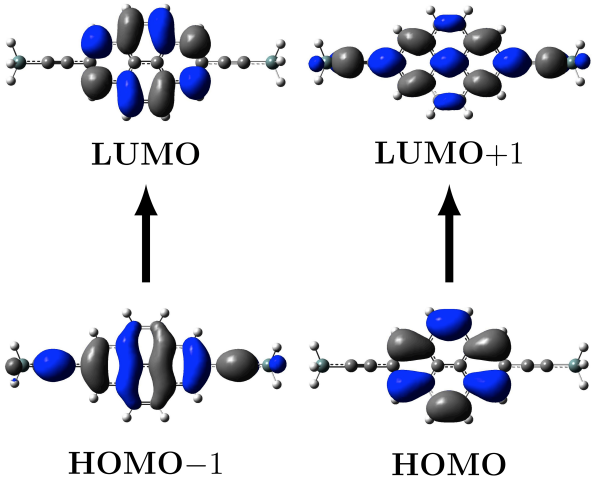

Figure 12 The substituent-influenced transitions of the $S_1 \leftarrow S_0$ excitation of compound **22** (B3LYP).

The DFT results for the 1-substituted pyrene derivatives are now discussed. There are non-zero contributions at the 1-position in all of the orbitals involved in the $S_2 \leftarrow S_0$ and $S_1 \leftarrow S_0$ excitations of pyrene. Hence, substitution at this position is expected to influence the wavelengths of both these excitations with respect to pyrene. The short fluorescence lifetimes of **37**-**39**, and the increased $S_1 \leftarrow S_0$ extinction coefficients for compounds **30** and **40** observed experimentally suggest that the $S_1 \leftarrow S_0$ transition becomes increasingly allowed when pyrene is substituted at the 1-position. The TD-DFT results show that the first excitation has a high oscillator strength, thereby confirming the experimental observations. However, the calculations also show that, for all five 1-substituted compounds, the lowest energy excitation arises from a transition that is similar to the $S_2 \leftarrow S_0$ (HOMO→LUMO) excitation in unsubstituted pyrene. As assignment of separate $S_2 \leftarrow S_0$ and $S_1 \leftarrow S_0$ excitations in the experimental absorption spectra was not possible for compounds **37**-**39**, it is also difficult to draw any firm conclusions about the agreement between experimental and theoretical data for these compounds.

The calculations performed using the CAM-B3LYP functional on the 2-, 2,7- and 1-derivatives show similar trends to those observed when using the B3LYP functional. When using CAM-B3LYP, the lowest energy transition for all of the 2- and 2,7-

substituted compounds, was found to be similar to the $S_1 \leftarrow S_0$ excitation in unsubstituted pyrene. Furthermore, states that were unidentifiable or difficult to assign with B3LYP were more easily assigned when using CAM-B3LYP. Analogous to B3LYP, the lowest energy transition for the 1-subsituted derivatives, was found to be similar to the $S_2 \leftarrow S_0$ transition in unsubstituted pyrene.

A comparison of the wavelengths obtained using B3LYP, CAM-B3LYP and those measured experimentally are plotted in Figures 13 and 14. The calculated wavelengths correspond to transitions that involve orbitals that are directly comparable to the orbitals involved in the $S_1 \leftarrow S_0$ and $S_2 \leftarrow S_0$ transitions in unsubstituted pyrene. It is clear that, for both transitions, theory is able to reproduce the general trend in the wavelengths that is observed experimentally. At first glance, it appears that B3LYP accurately reproduces the experimental wavelengths; however, this must be attributed to the cancellation of errors that was discussed in Section 2.1. With CAM-B3LYP the excitation wavelengths are overestimated. As also stated in Section 2.1, accurate DFT functionals should give vertical excitation energies that are higher in energy than the experimental $S_n^0 \leftarrow S_0^0$ values; hence, the data plotted in Figures 13 and 14 suggest that the results obtained using the CAM-B3LYP functional may be the more accurate.

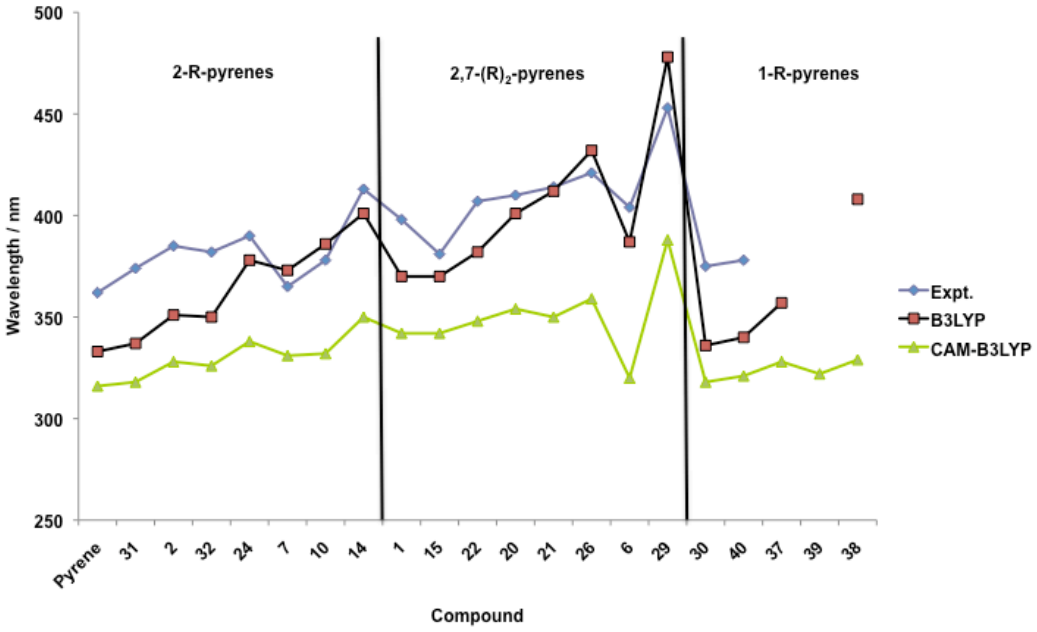

Figure 13 Comparison of theoretical and experimental wavelengths for the $S_1 \leftarrow S_0$ excitation in pyrene derivatives.

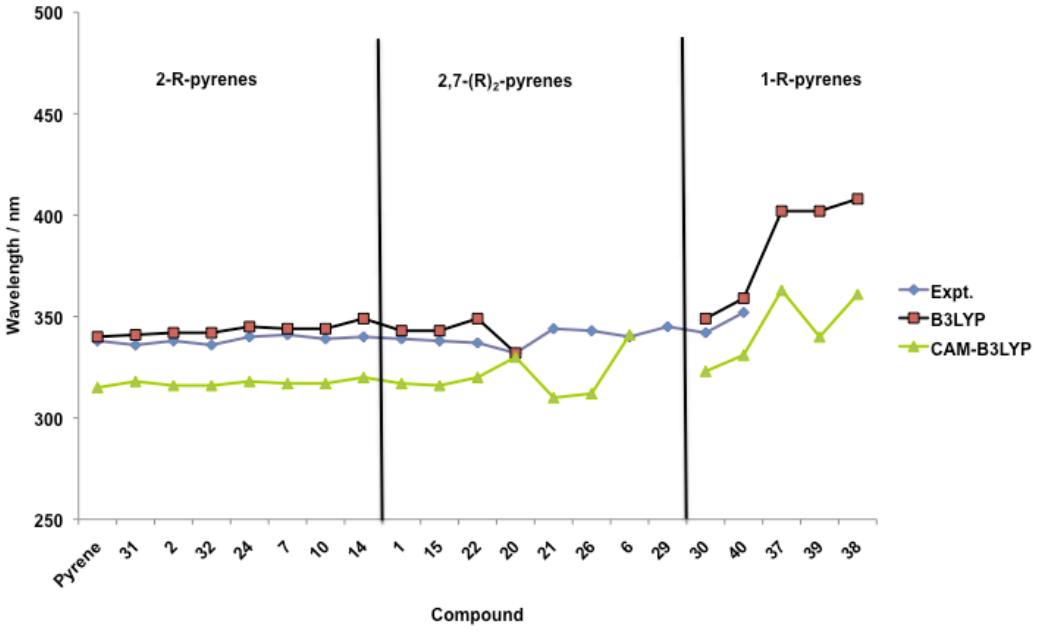

Figure 14 Comparison of theoretical and experimental wavelengths for the $S_2 \leftarrow S_0$ excitation in pyrene derivatives.

Like the experimental results, the theoretical calculations also show that certain substituents have a more significant influence than others. The Bpin substituted derivatives (**1**, **2** and **40**) show little variation in their excitation energies when compared to unsubstituted pyrene. The influence of $B(Mes)_2$ (**14** and **38**), C_6H_4-4-$B(Mes)_2$ (**10** and **39**) and $C{\equiv}C$-C_6H_4-4-$B(Mes)_2$ (**21**) is much more significant. As a result of this strong influence, identification of a 'substituent-influenced' $S_1 \leftarrow S_0$ transition was difficult for these compounds. It can be seen from the plots of the orbitals involved in the $S_1 \leftarrow S_0$ excitation, (Figure 15) that the role of boron in these two types of substituents (Bpin/$B(Mes)_2$) is significantly different. When bonded to the mesityl group, the empty *p*-orbital of boron facilitates extensive delocalization over the substituent. However, in the case of the Bpin group, hardly any delocalization is observed, which is a result of the empty *p*-orbital on boron been partially filled by electron density from π-bonding to the neighboring oxygen atoms.

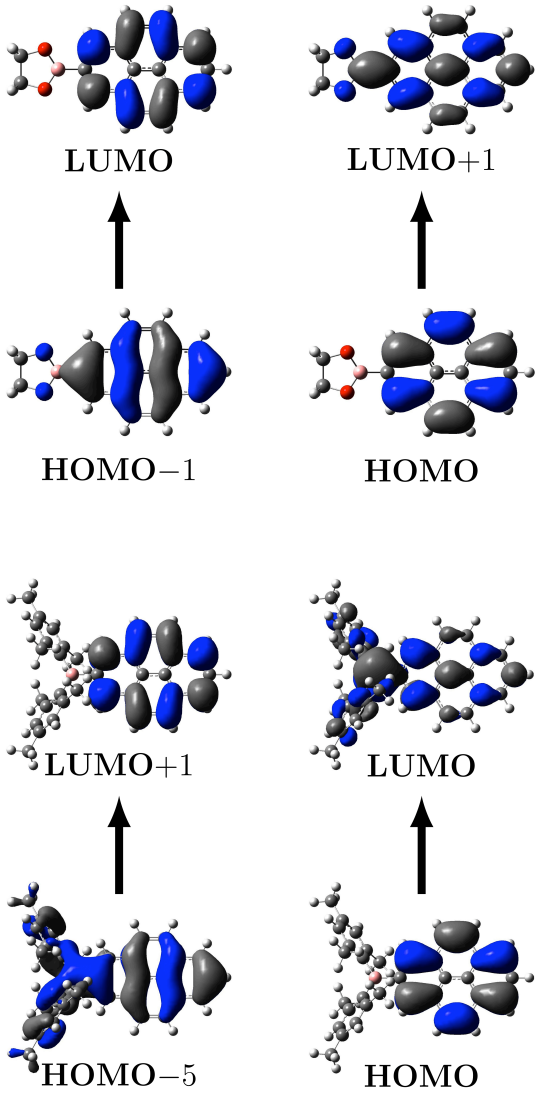

Figure 15 The $S_1 \leftarrow S_0$ excitation for 2-R-pyrene derivatives **2** (R = Bpin, top) and **14** (R = $B(Mes)_2$, bottom) highlighting the difference between the two boryl substituents (**2**: B3LYP; **14**: CAM-B3LYP).

Depending upon the nature of the substituent, pyrene is shown to behave as either an acceptor or a donor. Experimentally, donor substituents appear to have a greater influence on the $S_1 \leftarrow S_0$ transition. In **26** and **29**, the bathochromic shift in the absorption maxima and extinction coefficients for the $S_1 \leftarrow S_0$ transition are generally greater than for the acceptor substituted derivatives **6**, **14** and **21**. Hence, pyrene behaves more efficiently as an acceptor than as a donor in these compounds. The TD-DFT calculations also reproduce these observations. In both of the donor substituted derivatives, **26** and **29**, the HOMO has sizable contributions from the nitrogen atom

indicating that the low-lying transitions involve the redistribution of charge from the nitrogen lone-pair to the pyrene moiety. Whereas, in the acceptor substituted derivatives, **14** and **21**, the LUMO contains notable contributions from the boron atom; therefore, in the $S_1 \leftarrow S_0$ transition for these compounds, electron density moves from pyrene into the empty *p*-orbital on boron. As noted previously, for compounds **21** and **26** in particular, broad peaks observed in the absorption spectra overlap with the 'pyrene-like $S_2 \leftarrow S_0$' transition on the low energy side. For **21**, the TD-DFT calculations (CAM-B3LYP) show a strongly allowed transition (f = 3.39) involving HOMO→LUMO and HOMO-2→LUMO+1, only slightly higher in energy than the lowest energy transition for which f = 0.003 (see Table A3 in the Appendix). The intense absorption results from a delocalized state which generally involves charge transfer from the core towards the empty *p*-orbitals on the $B(Mes)_2$ groups. For compound **26**, a related situation arises. This time, a strongly allowed transition (f = 2.35) involving HOMO→LUMO+1 and HOMO-1→LUMO+2 results in charge transfer from the nitrogen lone pairs towards the core of the molecule. Thus, for both the extended π-acceptor and π-donor conjugated systems, these charge-transfer absorptions lie between the $S_1 \leftarrow S_0$ and 'pyrene-like $S_2 \leftarrow S_0$' ones.

3.0 Conclusions

The photophysical properties of a range of novel 2- and 2,7-substituted pyrene derivatives and known 1-substituted pyrenes were investigated using both experimental and TD-DFT studies. The TD-DFT calculations employed both the B3LYP and CAM-B3LYP functionals. Using CAM-B3LYP, the ordering of states in pyrene was correctly predicted for the first time. Furthermore, it was shown that both functionals were able to reproduce the general trends in wavelengths observed experimentally for the pyrene derivatives.

It was shown that, upon changing the substitution position and the nature of the substituent on pyrene, stark differences were observed in the photophysical properties of the compounds. Generally, for the 2- and 2,7-derivatives, the $S_2 \leftarrow S_0$ excitation can be considered to be 'pyrene-like', as indicated by a very small bathochromic shift in its energy and retention of the vibrational progression. However, the $S_1 \leftarrow S_0$ excitation in these derivatives is found to be 'substituent-influenced', as indicated by large bathochromic shifts in its energy; and an increase in its allowedness, reflected by higher

extinction coefficients and shorter lifetimes. The $S_2 \leftarrow S_0$ excitation generally involves the HOMO and LUMO orbitals which have nodes at the 2- and 7-positions. However, the $S_1 \leftarrow S_0$ excitation involves the HOMO-1 and LUMO+1 orbitals, which have non-zero contributions at the 2- and 7-positions; hence, the substituent influences this transition and the resulting emission considerably.

In contrast, substitution at the 1-position has a strong influence on both the $S_1 \leftarrow S_0$ and the $S_2 \leftarrow S_0$ excitations. In the case of highly conjugated 1-substituted systems, it is not possible to distinguish between the two excitations in the experimental spectra. However, from the very short fluorescence lifetimes, it is apparent that the influence on allowedness of the $S_1 \leftarrow S_0$ excitation is much stronger in the 1-substituted derivatives than in the 2- and 2,7-pyrenes. All of the orbitals involved in the $S_1 \leftarrow S_0$ and the $S_2 \leftarrow S_0$ excitations have non-zero contributions at the 1-position, hence the significant influence on both transitions in the 1-substituted pyrene derivatives.

For all derivatives, modest (0.19) to high (0.93) fluorescence quantum yields were observed. For the 2-, and 2,7-derivatives, fluorescence lifetimes exceeding 16 ns were measured with most being ca. 50-80 ns. The 4-(pyren-2-yl)-butyric acid derivative **31** has an exceptionally long fluorescence lifetime, 622 ns, significantly longer than that of the commercially available and widely employed 4-(pyren-1-yl)-butyric acid **30**, suggesting that it should be even more effective for measuring cellular oxygen concentrations, or as a probe for time-resolved imaging of biosystems.

Overall, the results reported above and in Chapter 2 show that 2- and 2,7-pyrene derivatives have a unique range of photophysical and structural properties that differ from the more 'traditional' 1-substituted pyrene derivatives. These new derivatives, now available via straightforward, high-yielding synthetic routes, will be of interest in a wide range of both existing and new applications, such as fluorescence probes and labels, OLED devices and molecular sensors.

4.0 Experimental

The syntheses of all compounds are reported in Chapter 2, except for **30**, which was purchased from Alfa Aesar. All photophysical measurements were carried out in HPLC-grade solvents. UV-Vis absorption spectra and extinction coefficients were obtained on a Hewlett-Packard 8453 diode array spectrophotometer using standard 1 cm width quartz cells. Fluorescence spectra were recorded on a Horiba Jobin-Yvon Fluorolog FL

3-22 Tau spectrophotometer. Photoluminescence quantum yields were measured using an integrating sphere (Horiba Jobin-Yvon) following reported methods.[26] Luminescence lifetimes of less than 50 ns were recorded on a home-built time correlated single-photon counting (TCSPC) spectrometer. Samples were excited using either a pulsed laser diode (IBH NanoLED, 373 nm, 1 MHz pulse train, FWHM 100 ps), or the third harmonic of a cavity-dumped, mode-locked Ti-sapphire laser (Coherent MIRA-D, 300 nm, 4.5 MHz pulse train, FWHM < 150 fs). Fluorescence from the sample was collected at 90° to the incident beam, and the emission wavelength was selected by a monochromator (Horiba Jobin-Yvon Triax-190) before detection using a single-photon avalanche diode (idQuanttque id100-50). The signal derived from the detector was used as the start pulse for a time-to-amplitude converter, TAC, (Ortec 567) operating in reverse-TAC mode. The stop pulse was derived from the cavity–dumper synchronization pulse or diode driver. The output of the TAC was measured using a pulse-height analyzer (Ortec Trump-8K) held in a PC. Instrument response functions for the two excitation sources, obtained using a Ludox® scatterer, were 180 and 110 ps FWHM respectively. Decays were analyzed by iterative reconvolution of the instrument response function with a sum of exponentials and non-linear least squares regression.[27] Goodness of fit was assessed by minimizing the reduced chi-squared function, χ^2, and a visual inspection of the weighted residuals. Each trace contained at least 10,000 counts in the peak channel. When the lifetimes exceeded 50 ns, they were recorded by the determination of the decay in fluorescence intensity as a function of time following excitation. The samples were excited by the output of either a nitrogen laser (337 nm, FWHM < 5 ns) or the third harmonic of a Q-switched Nd:YAG laser (355 nm, FWHM < 5 ns). Fluorescence was collected at 90° to the incident beam, the emission wavelength was selected by a monochromator (Horiba Jobin-Yvon Triax-320) and the emission intensity detected by a photomultiplier (Hamamatsu R928). Using 25 Ω termination, an instrument response function of < 15 ns FWHM was obtained. The output of the PMT was acquired using a digital storage oscilloscope (LeCroy WaveJet 324) and averaged over 265 laser shots before transfer to a PC and analysis (Excel).

5.0 References

[1] (a) Runge, E.; Gross, E. K. U. *Phys. Rev. Lett.* **1984**, *52*, 997-1000. (b) Casida, M. E. *Recent Advances in Density Functional Theory: Part 1*. World Scientific: Singapore, 1995, 155-192.

[2] (a) Vosko, S.; Wilk, L.; Nusair, M. *Can. J. Phys.* **1980**, *58*, 1200-1211. (b) Lee, C.; Yang. W.; Parr, R. G. *Phys. Rev. B*. **1988**, *37*, 785-789. (c) Becke, A. D. *J. Chem. Phys.* **1993**, *98*, 5648-5652. (d) Stephens, P. J.; Devlin, F. J.; Chabalowski, C. F.; Frisch, M. J. *J. Phys. Chem.* **1994**, *98*, 11623-11627.

[3] Yanai, T.; Tew, D. P.; Handy, N. C. *Chem. Phys. Lett.* **2004**, *393*, 51-57.

[4] (a) Birks, J. B. *Photophysics of Aromatic Molecules,* Wiley-Interscience: London, 1970. (b) Yoshinaga, T.; Hiratsuka, H.; Tanizaki, Y. *Bull. Chem. Soc. Jpn.* **1977**, *50*, 3096-3102. (c) Michl, J.; Thulstrup, E. W. *Spectroscopy with Polarized Light*, VCH Publishers Inc.: New York, 1986, 368. (d) Klessinger, M.; Michl, J. *Excited States and Photochemistry of Organic Molecules*, Wiley-VCH: New York, 1995. Ch. 1-2. (e) Turro, N. J.; Ramamurthy, V.; Scaiano, J. C. *Principles of Molecular Photochemistry, An Introduction,* University Science Books: Sausalito, 2009. (f) Values measured by author.

[5] Clar, E. J. *Polycyclic Hydrocarbons*, Academic Press: London, 1964.

[6] (a) Platt, J. R. *J. Chem. Phys.* **1949**, *17*, 484-495. (b) Platt, J. R. *J. Optical Soc. Am.* **1953**, *43*, 252-257. (c) Moffitt, W. *J. Chem. Phys.* **1954**, *22*, 320-333.

[7] (a) Nakajima, A. *Bull. Chem. Soc. Jpn.* **1971**, *44*, 3272-3277. (b) Kalyanasundaram, K.; Thomas, J. K. *J. Am. Chem. Soc.* **1977**, *99*, 2039-2044. (c) Perry, M.; Carra, C.; Chrétien, M. N.; Scaiano, J. C. *J. Phys. Chem. A* **2007**, *111*, 4884-4889.

[8] Foggi, P.; Pettini, L.; Sànta, I.; Righini, R.; Califano, S. *J. Phys. Chem.* **1995**, *99*, 7439-7445.

[9] (a) Goodpaster, J. V.; Harrison, J. F.; McGuffin, V. L. *J. Phys. Chem. A* **1998**, *102*, 3372-3381. (b) Bito, Y.; Shida, N.; Toru, T. *Chem. Phys. Lett.* **2000**, *328*, 310-315. (c) Parac, M.; Grimme, S. *Chem. Phys.* **2003**, *292*, 11-21. (d) Wang, B.-C.; Chang, J.-C.; Tso, H.-C.; Hsu, H.-F.; Cheng, C.-Y. *J. Mol. Struc.: THEOCHEM*. **2003**, *629*, 11-20.

(e) Dierksen, M.; Grimme, S. *J. Chem. Phys.* **2004**, *120*, 3544-3554. (f) Park, Y. H.; Cheong, B.-S. *Curr. Appl. Phys.* **2006**, *6*, 700-705. (g) Kerkines, I. S. K.; Petsalakis, I. D.; Theodorakopoulos, G.; Klopper, W. *J. Chem. Phys.* **2009**, *131*, 224315-224325.

[10] Iikura, H.; Tsuneda, T.; Yanai, T.; Hirao, K. *J. Chem. Phys.* **2001**, *115*, 3540-3544.

[11] Peach, M. J. G.; Benfield, P.; Helgaker, T.; Tozer, D. J. *J. Chem. Phys.* **2008**, *128*, 044118.

[12] Wiggins, P.; Williams, J. A. G.; Tozer, D. J. *J. Chem. Phys.* **2009**, *131*, 091101.

[13] See references 7-8 in Chapter 2.

[14] (a) Stolka, M.; McGrane, K. M.; Facci, J. S. Photoconductive Imaging Members with Alkoxy Amine Charge Transport Molecules. U.S. Patent 4,588,666, May 13, 1986. (b) Bellmann, E.; Shaheen, S. E.; Thayumanavan, S.; Barlow, S.; Grubbs, R. H.; Marder, S. R.; Kippelen, B.; Peyghambarian, N. *Chem. Mater.* **1998**, *10*, 1668-1676. (c) Mitschke, U.; Bäuerle, P. *J. Mater. Chem.* **2000**, *10*, 1471–1507. (d) Low, P. J.; Paterson, M. A. J.; Puschmann, H.; Goeta, A. E.; Howard, J. A. K.; Lambert, C.; Cherryman, J. C.; Tackley, D. R.; Leeming, S.; Brown, B. *Chem. Eur. J.* **2004**, *10*, 83-91. (e) Bardecker, J. A.; Ma, H.; Kim, T.; Huang, F.; Liu, M. S.; Cheng, Y.-J.; Ting, G.; Jen, A. K.-Y. *Adv. Funt. Mater.* **2008**, *18*, 3964-3971.

[15] (a) Nguyen, P.; Yuan, Z.; Agocs, L.; Lesley, G.; Marder, T. B. *Inorg. Chim. Acta* **1994**, *220*, 289-296. (b) Khan, M. S.; Kakkar, A. K.; Long, N. J.; Lewis, J.; Raithby, P.; Nguyen, P.; Marder, T. B.; Whittmann, F.; Friend, R. H. *J. Mater. Chem.* **1994**, *4*, 1227-1232. (c) Nguyen, P.; Lesley, G.; Marder, T. B.; Ledoux, I.; Zyss, J. *Chem. Mater.* **1997**, *9*, 406-408. (d) Biswas, M.; Nguyen, P.; Marder, T. B.; Khundkar, L. R. *J. Phys. Chem. A* **1997**, *101*, 1689-1695. (e) Li, H.; Powell, D. R.; Firman, T. K.; West, R. *Macromolecules* **1998**, *31*, 1093-1098. (f) Bunz, U. H. F. *Chem. Rev.* **2000**, *100*, 1605-1644. (g) Donhauser, Z. L.; Mantooth, B. A.; Kelly, K. F.; Bumm, L. A.; Monnell, J. D.; Stapleton, J. J.; Price, D. W.; Rawlett, A. M.; Allara, D. L.; Tour, J. M.; Weiss, P. S. *Science* **2001**, *292*, 2303-2307. (h) Dirk, S. M.; Price, D. W.; Chanteau, S.; Kosynkin, D. V.; Tour, J. M. *Tetrahedron* **2001**, *57*, 5109-5121. (i) Kim, J.; Swager, T. M. *Nature* **2001**, *411*, 1030-1034. (j) Schmitz, C.; Posch, P.; Thelakkat, M.; Schmidt, H. W.; Montak, A.; Feldman, K.; Smith, P.; Weder, C. *Adv. Funct. Mater.* **2001**, *11*, 41-46. (k)

Levitus, M.; Schmieder, K.; Ricks, H.; Shimizu, K. D.; Bunz, U. H. F.; Garcia-Garibay, M. A. *J. Am. Chem. Soc.* **2001**, *123*, 4259-4265. (l) Beeby, A.; Findlay, K. S.; Low, P. J.; Marder, T. B.; Matousek, P.; Parker, A. W.; Rutter, S. R.; Towrie, M. *Chem. Commun.* **2003**, 2406-2407. (m) Beeby, A.; Findlay, K. S.; Goeta, A. E.; Porrès, L.; Rutter, S. R.; Thompson, A. L. *Photochem. Photobiol. Sci.* **2007**, *6*, 982-986.

[16] (a) Nakatesuji, S.; Matsuda, K.; Uesugi, Y.; Nakashima, K.; Akiyama, S.; Fabian, W. *J. Chem. Soc., Perkin Trans. 1* **1992**, *7*, 755-758. (b) Nguyen, P.; Todd, S.; van den Biggelaar, D.; Taylor, N. J.; Marder, T. B.; Wittmann, F.; Friend, R. H. *Synlett* **1994**, 299-301. (c) Kawai, T.; Saski, T.; Irie, M. *Chem. Commun.* **2001**, 711-712. (d) Schmieder, K.; Levitus, M.; Dang, H.; Garcia-Garibay, M. A. *J. Phys. Chem. A* **2002**, *106*, 1551-1556. (e) Gimenez, R.; Pinol, M.; Serrano, J. L. *Chem. Mater.* **2004**, *16*, 1377-1383. (f) Beeby, A.; Findlay, K. S.; Goeta, A. E.; Porrès. L.; Rutter, S. R.; Thompson, A. L. *Photochem. Photobiol. Sci.* **2007**, *6*, 982-986.

[17] (a) Siddle, J. S.; Ward, R. M.; Collings, J. C.; Rutter, S. R.; Porrès, L.; Applegarth, L.; Beeby, A.; Batsanov, A. S.; Thompson, A.; Howard, J. A. K.; Boucekkine, A.; Costuas, K.; Halet, J.-F.; Marder, T. B. *New J. Chem.* **2007**, *31*, 841-851. (b) Matano, Y.; Nakashima, M.; Imahori, H. *Angew. Chem. Int. Ed.* **2009**, *48*, 4002-4005. (c) Steffen, A.; Tay, M.-G.; Batsanov, A. S.; Howard, J. A. K.; Beeby, A.; Vuong, K. Q.; Sun, X. Z.; George, M. W.; Marder, T. B. *Angew. Chem. Int. Ed.* **2010**, *49*, 2349-2353.

[18] Mkhalid, I. A. I.; Barnard, J. H.; Marder, T. B.; Murphy, J. M.; Hartwig, J. F. *Chem. Rev.* **2010**, *110*, 890-931.

[19] (a) Vaughan, W. M.; Weber, G. *Biochemistry* **1970**, *3*, 464-473. (b) Ribou, A.-C.; Vigo, J.; Salmon, J.-M. *Photochem. Photobio.* **2004**, *80*, 274-280. (c) Berezin, M. Y.; Achilefu, S. *Chem. Rev.* **2010**, *110*, 2641-2684.

[20] (a) Flamm, M.; Schachter, D. *Nature* **1982**, *298*, 290-292. (b) Fujimori, E.; Shambaugh, N. *Biochem. Biophys. Acta* **1983**, *742*, 155-161. (c) Lee, J. A.; Fortes, P. A. *Biochemistry* **1985**, *24*, 322-330. (d) Ebata, K.; Masuko, M.; Ohtani, H.; Kashiwasake-Jibu, M. *Photochem. Photobiol.* **1995**, *62*, 836-839. (e) Sugahara, D.; Amano, J.; Irimura, T. *Anal. Sci.* **2003**, *19*, 167-169.

[21] (a) Takeuchi, T.; Kosuge, M.; Tadokoro, A.; Sugiura, Y.; Nishi, M.; Kawata, M.; Sakai, N.; Matile, S.; Futaki, S. *ACS Chem. Biol.* **2006**, *1*, 299-303. (b) Jablonski, A. E.; Kawakami, T.; Ting, A. Y.; Payne, C. K. *J. Phys. Chem. Lett.* **2010**, *1*, 1312-1315.

[22] Wee, K.-R.; Ahn, H.-C.; Son, H.-J.; Han, W.-S.; Kim, J.-E.; Cho, D. W.; Kang, S. O. *J. Org. Chem.* **2009**, *74*, 8472-8475.

[23] Zhao, S.-B.; Wucher, P.; Hudson, Z. M.; McCormick, T. M.; Liu, X.-Y.; Wang, S.; Feng, X.-D.; Lu, Z.-H. *Organometallics* **2008**, *27*, 6446-6456.

[24] (a) Beeby, A.; Findlay, K. S.; Low, P. J.; Marder, T. B. *J. Am. Chem. Soc.* **2002**, *124*, 8280-8284. (b) Greaves, S. J.; Flynn, E. L.; Futcher, E. L.; Wrede, E.; Lydon, D. P.; Low, P. J.; Rutter, S. R.; Beeby, A. *J. Phys. Chem. A* **2006**, *110*, 2114-2121.

[25] Weber, L.; Werner, V.; Fox, M. A.; Marder, T. B.; Schwedler, S.; Brockhinke, A.; Stammler, H.-G.; Neumann, B. *Dalton Trans.* **2009**, 1339-1351.

[26] Porrès, L.; Holland, A.; Pålsson, L.-O.; Monkman, A. P.; Kemp, C.; Beeby, A. *J. Fluorescence* **2006**, *16*, 267-272.

[27] O'Connor, D. V.; Phillips, D. *Time Correlated Single Photon Counting*, Academic Press: New York, 1984.

Chapter 4: Further Iridium Catalyzed C-H Borylation and Metal-Catalyzed Cross-Coupling Reactions

1.0 Introduction

The substitution of pyrene at the 2- and 2,7-positions described in the preceding chapters was made possible by sterically controlled iridium-catalyzed C-H borylation. This approach gave the boronic esters 2,7-bis(Bpin)pyrene **1** and 2-(Bpin)pyrene **2** (pin = $OCMe_2CMe_2O$), which acted as starting materials for a wide range of new derivatives. In the synthesis of these new derivatives, a variety of metal-catalyzed cross-coupling reactions were used.

This chapter further explores the application of iridium-catalyzed C-H borylation and cross-coupling reactions on a range of substrates: 2,6-difluorobenzoic acid methyl ester, pyridine based ligands, 1,10-phenanthroline and ferrocene. These substrates were investigated because the functionalized products are of interest for further applications.

2.0 Iridium-Catalyzed C-H Borylation: An Overview

The direct and selective functionalization of C-H bonds on alkyl, alkenyl and aryl moieties gives access to a huge range of organic molecules that can be used in many applications.[1] The conversion of C-H bonds to C-B bonds is one type of C-H functionalization that has attracted interest over the last *ca*. 15 years. Several catalytic C-H borylation methodologies have been developed to provide access to a range of organic molecules containing a C-B bond.[2] One method is iridium-catalyzed C-H borylation of arenes, which was used earlier in this work to selectively borylate pyrene (Chapters 1-3). The following pages provide a more detailed overview of the mechanism and applicability of this catalytic method.

Iridium-based catalysts containing both phosphine- and nitrogen-based ligands are known to catalyze the borylation of arenes, and their development has been reported by several groups.[3-4] Early investigations found that, in arene solvents, reaction of [(η^5-indenyl)Ir(COD)] with excess HBcat (cat = 1,2-$O_2C_6H_4$) gave the trisboryl species [(η^6-arene)Ir(Bcat)$_3$] (arene = C_6H_6, C_6D_6, C_6H_5Me and 1,3,5-$C_6H_3Me_3$) and, for C_6H_6, C_6D_6 and C_6H_5Me, small amounts of borylated arene were detected by GC-MS.[5] Using these observations, Smith and Maleczka used combinations of [(η^5-indenyl)Ir(COD)] or [(η^6-

1,3,5-$Me_3C_6H_3$)Ir(Bpin)$_3$] with PMe_3 to generate a catalyst for the borylation of arenes with HBpin.[4] Further catalysts that used chelating phosphines such as dppe {1,2-bis(diphenylphosphino)ethane} and dmpe {1,2-bis(dimethylphosphino)ethane}, which led to increased activity and TONs, were also reported. In particular, [(η^5-indenyl)Ir(COD)] in conjunction with dmpe or dppe, was shown to borylate a range of mono-, and disubstituted arenes. In mono substituted arenes, a statistical mixture of *meta* and *para* isomers was observed; whereas, in 1,3-disubstituted arenes, borylation occurred exclusively at the *meta* position.[4]

Meanwhile, Ishiyama, Miyaura, Hartwig et al. focused on the borylation of arenes using iridium complexes with nitrogen-based ligands.[3] A combination of [Ir(Cl)COD]$_2$ and 2,2'-bipyridine (bpy) was shown to be effective for the borylation of arenes with B_2pin_2 at 80 ºC in neat arene solvent. Analogous to that observed with iridium-phosphine complexes (*vide supra*), borylation of mono substituted arenes gave statistical mixtures of *meta* and *para* products, 1,2-disubstituted arenes were borylated at the *para* position and 1,3-disubstituted arenes were borylated exclusively at the *meta* position (to both substituents), giving 1,3,5-trisubstituted arenes. The C-H functionalization, which is characterized by a lack of borylation *ortho* to substituents on the arene, suggests that it is the steric environment rather than the electronic one, which is responsible for the regioselectivity. In a later study, competition reactions were carried out.[3b] Equimolar mixtures of trifluoromethylbenzene and toluene, trifluoromethylbenzene and anisole, and toluene and anisole gave ratios of borylated products of 90:10, 85:15 and 40:60 respectively. Hence, electron-poor arenes are more reactive than electron-rich ones.

Optimization studies[6] were later carried out to investigate the influence of the iridium source and the bpy ligand on catalytic activity. Different [IrX(COD)]$_2$ complexes (X = Cl, BF_4, OH, OPh, OMe, and OAc) were combined with bpy to borylate benzene with B_2pin_2 at room temperature. It was found that the complexes containing strongly basic and nucleophilic anions, e.g. OMe, OH, were the most effective for borylating benzene. The enhanced catalytic activity of these (hydroxo)- or (alkoxo)iridium complexes is attributed to the more facile formation of (boryl)iridium complexes. A tris(boryl)iridium(III) complex is believed to be a key intermediate in the catalytic borylation of arenes (*vide infra*). These tris(boryl) complexes can form by oxidative addition of B_2pin_2 to mono(boryl)iridium(I) complexes, which in turn are formed by either oxidative addition of B_2pin_2 to (alkoxo)iridium(I) complexes followed by

reductive elimination of ROBpin, or via transmetallation between B_2pin_2 and the (alkoxo)iridium(I) species (Figure 1). In both cases, the ability of the alkoxo (or hydroxo) ligand to interact with the vacant boron *p*-orbital, and form a strong B-O bond, leads to enhanced reductive elimination of RO-Bpin and facile formation of (boryl)iridium complexes. The most effective iridium source was found to be $[Ir(OMe)(COD)]_2$ with 100% conversion of B_2pin_2 and a 80% yield of borylated benzene after 4 hours at room temperature.[6]

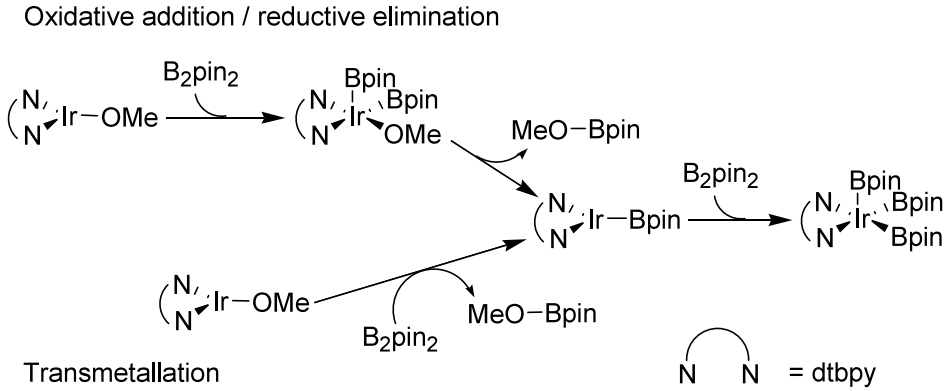

Figure 1 Formation of a tris(boryl)iridium(III) complex via a mono(boryl)iridium(I) complex.[6]

The influence of substituents on bpy was then considered. The highest catalytic activity was observed, when electron-donating substituents (NMe_2, OMe, ^{t}Bu) were placed at the 4,4'-positions of bpy. In particular, 4,4'-di-tert-butyl-2,2'-bipyridine (dtbpy) was show to be effective as the *tert*-butyl groups are believed to make the catalyst more soluble and protect the ligand against borylation. Using 1.5 mol % of $[Ir(OMe)(COD)]_2$ and 3 mol % of dtbpy, a range of arenes were borylated with one equivalent of B_2pin_2 in moderate to high yields (Table 1). The reactions were carried out in hexane as rates of borylation were found to be much faster in non-polar solvents than in polar ones.[6]

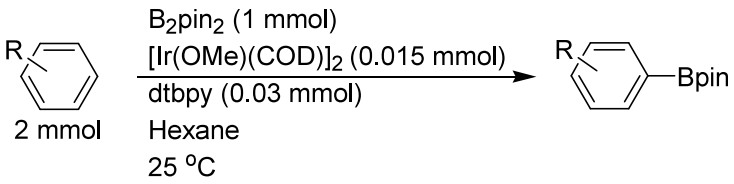

Product	Time (h)	Yield (%)[a]	Product	Time (h)	Yield (%)[a]
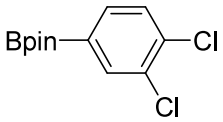	8	82	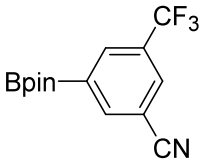	2	84
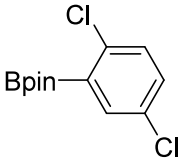	24	53	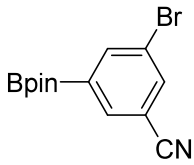	2	83
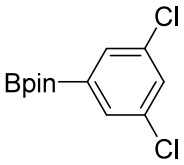	2	84	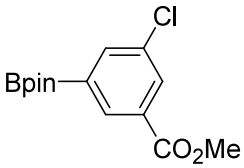	8	80
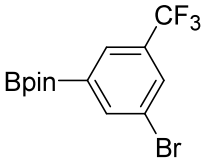	4	91	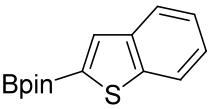	2	81
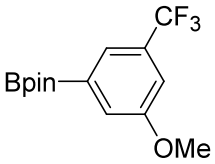	8	81	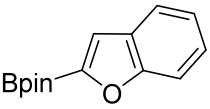	4	83
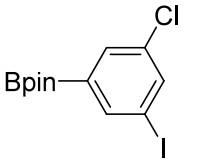	4	82	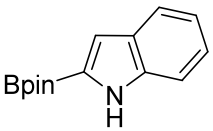	0.5	88

[a]GC yields based on B_2pin_2

Table 1 Iridium-Catalyzed C-H borylation of arenes.[6]

As well as giving straightforward access to borylated arenes, iridium-catalyzed C-H borylation is useful because of its steric control. Generally, borylation occurs at positions that are not *ortho* to any ring junction or substituent (*cf*. borylation of pyrene).

This steric control is believed to be the result of the crowded nature of an iridium trisboryl species, which is proposed to be a key intermediate in the catalytic cycle.

Extensive studies[3,7] using *in situ* NMR, isolation of kinetic intermediates and kinetic data, as well as theoretical calculations, have led to the following catalytic cycle been proposed (Figure 2).[8] Firstly, the [Ir(III)(dtbpy)(Bpin)$_3$] complex is formed from [Ir(OMe)(COD)]$_2$, dtbpy and B_2pin_2. During this formation, MeO-Bpin is eliminated and oxidative addition of B_2pin_2 to the mono(boryl)iridium complex occurs (*vide supra*). In addition, the COD ligand is reduced or hydroborated to give COE, which can then reversibly dissociate from the [Ir(III)(dtbpy)(Bpin)$_3$] species (COD = cyclooctadiene; COE = cyclooctene). It has been reported, that an induction period in which the COD is converted to COE can be observed experimentally.[3b,5] Furthermore, it was shown that when the complex [Ir(III)(dtbpy)(Bpin)$_3$(COE)] is directly added to the reaction mixture, no such induction period is observed, hence the conversion of COD to COE must occur before arene borylation.[3]

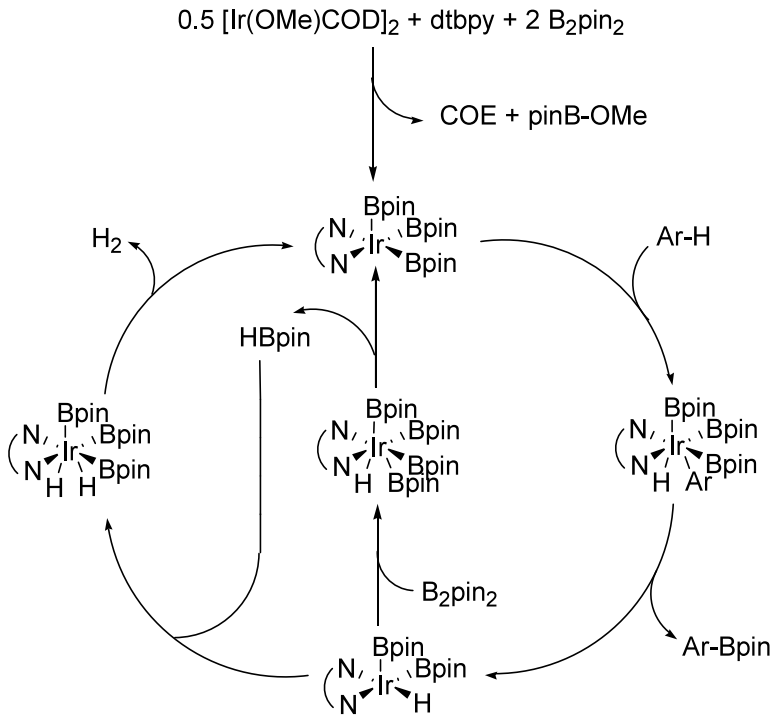

Figure 2 Proposed catalytic cycle for iridium-catalyzed C-H borylation.[8]

The resulting 16e$^-$ [Ir(III)(dtbpy)(Bpin)$_3$] species then reacts with the arene. This is believed to occur via coordination of the arene followed by oxidative addition of the

aryl C-H bond, leading to an Ir(V) intermediate. Recently, experimental and theoretical studies have shown that significant proton transfer character between the arene and an Ir-Bpin bond (as opposed to hydride transfer to an empty boron p orbital) exists in the transition state, suggesting that the Ir(V) intermediate is either [Ir(dtbpy)(Bpin)$_3$(Ar)(H)] or [Ir(dtbpy)(Bpin)$_2$(Ar)(η^2-H-Bpin)].[8b] Reductive elimination of the aryl-Bpin product then occurs and the resulting Ir(III) species undergoes oxidative addition of B_2pin_2 followed by reductive elimination of HBpin to regenerate the starting trisboryl species. Alternatively, HBpin can oxidatively add to the Ir(III) species and reductive elimination of H_2 gives the starting trisboryl complex.

Over 17 years have passed since the isolation of the first trisboryl species, during which iridium-catalyzed C-H borylation has become a widely used technique for the functionalization of C-H bonds in arenes. The methodology is found to be effective for a wide range of substrates, including heteroaromatics[9] such as thiophenes, furans and pyrroles. In these substrates, borylation occurs at the 2-position (adjacent to the heteroatom), except for *N*-substituted pyrroles, where other isomers are formed as a result of the steric hindrance from the *N*-substituent. In the case of indoles, borylation occurs adjacent to the nitrogen at the 2-position, unless a substituent is added to the nitrogen, which leads to borylation at the 3-position.[9c-d] Borylation of pyridine is found to occur in a statistical mixture at the 3- and 4-positions in a 42% yield, with no borylation observed at the 2-position, i.e. borylation does not occur *ortho* to the nitrogen.[8,9a] The low yield is believed to be the result of coordination of pyridine to the iridium, which inhibits borylation. It was later shown that addition of a single substituent *ortho* to the *N* centre is sufficient to inhibit *N*-coordination to the iridium centre, for example, 2-phenylpyridine is borylated at the 3- and 4-positions in a 67% yield.[9d] Elsewhere, borylation of metallocenes,[10] polycyclic arenes,[11] porphyrins and corroles[12] has been reported. The steric selectivity of the reaction has allowed access to arene derivatives with substitution patterns less accessible by conventional methodology. Furthermore, there are an ever increasing number of ways to convert the Bpin group into other useful functionalities (*cf.* Chapter 2). The scope of possible conversions is shown in Figure 3.[13] Most of these processes are one-pot procedures, thus highlighting a straightforward way of selectively substituting arenes with a wide variety of functionalities.

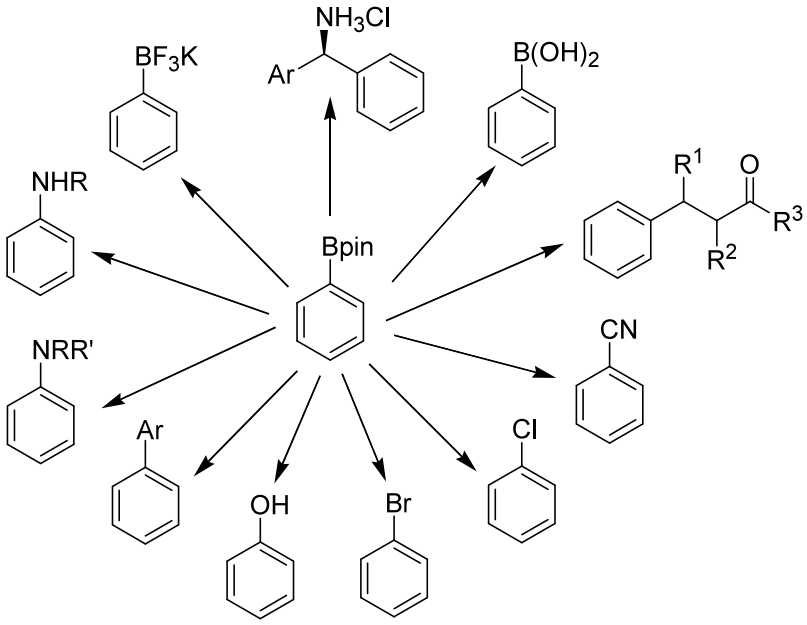

Figure 3 One-pot conversions of aryl boronic esters.

In terms of limitations, mixtures of products are obtained when there is more than one C-H bond not *ortho* to any ring junction or substituent. Several groups are investigating ways to improve the selectivity in such systems, either by the addition of directing groups[14] or changing the catalyst and ligands.[15] Alternative boron sources are also under investigation for this reaction such as HB(dan) (dan = 1,8-diaminonaphthalene)[16] and B_2eg_2 (eg = ethylene glycol).[17]

It is worth mentioning that aryl boronates can be synthesized by several other methods, such as the Miyaura borylation.[18] This involves a palladium-catalyzed coupling reaction between an aryl halide and B_2pin_2 in the presence of KOAc. The catalytic cycle for this reaction is analogous to that of metal-catalyzed cross-coupling reactions, which are discussed in the next section. Other methods to introduce the Bpin functionality involve the use of HBpin[19] and, more recently, the Cu-catalyzed borylation of C-X bonds.[20]

3.0 Metal-Catalyzed Cross-Coupling Reactions[21]

The formation of C-C bonds is one of the most useful processes in chemistry. Reactions that form such bonds are of great importance in the building of complex molecules from simple starting materials. Over the last 40 years, chemists have used metal catalysts as a direct route to form C-C bonds between vinyl, aryl, alkynyl and alkyl carbons via reactions known as cross-couplings. These reactions are now routinely used and are

important steps in the synthesis of drugs, fertilizers, optical materials and many other useful chemicals. The following pages give a brief overview of metal-catalyzed cross-coupling reactions, with the aim of introducing concepts that are related to chemistry discussed later on in this chapter.

Cross-coupling reactions take place between an aryl (or vinyl) halide or pseudo-halide e.g. (triflate) R-X, which provides the carbon electrophile, and an M-R' reagent, which consists of a carbon group bound to an electropositive metal, which is the source of the nucleophilic carbon. A coupling reaction between these two species occurs when a metal catalyst is added. The textbook catalytic cycle for cross-coupling reactions is shown in Figure 4. Key intermediates and fundamental catalytic steps are shown, although, in reality, ligand dissociation and even R group exchanges make this cycle more complicated.

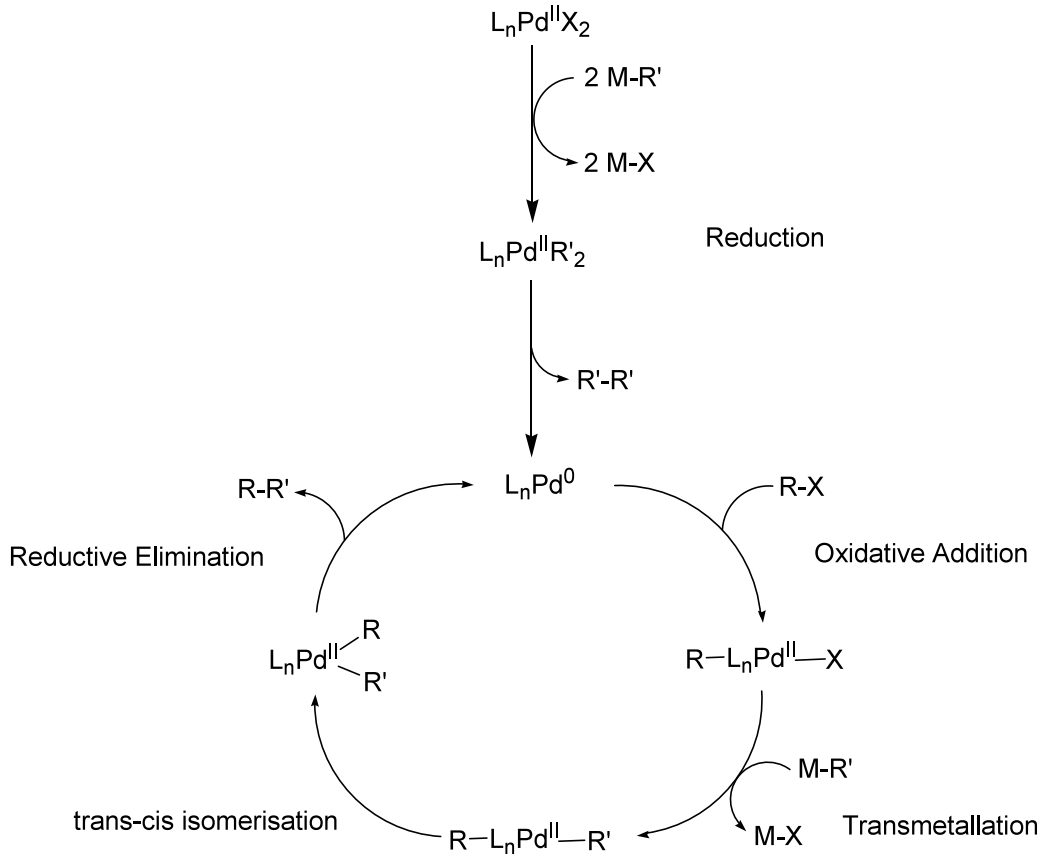

Figure 4 Generalised catalytic cycle for metal-catalyzed cross-coupling.[21b]

A Pd(0) source is used as the catalyst, which is either added directly or is formed by the *in situ* reduction of a Pd(II) source. As shown at the top of the cycle, the reduction of

Pd(II) leads to homocoupling of the nucleophilic reagent to form R'-R'; as a result, a small excess of M-R' is often added to ensure that yields are maximized.

The second step is oxidative addition of the aryl halide (R-X) to the Pd(0) metal centre. The oxidative addition pathway in a particular reaction, is dependent upon the metal ion and oxidation state, ligand, substrate and conditions. As a result, several different mechanisms for oxidative addition have been proposed. Furthermore, the nature of the active Pd(0) species is known to differ between individual reactions, with the Pd(0) active species bearing one (PdL) or two (PdL_2) ligands known (Figure 5).[22] In particular, the amount of steric bulk on a ligand can influence the nature of the active species involved in the oxidative addition reaction. Less bulky and bidentate ligands are more likely to promote oxidative addition via a PdL_2 species.[23] Whereas, evidence for monoligated PdL complexes is found, when bulky ligands such as P(*o*-tol)$_3$ and P^{t}Bu$_3$ are used.[24]

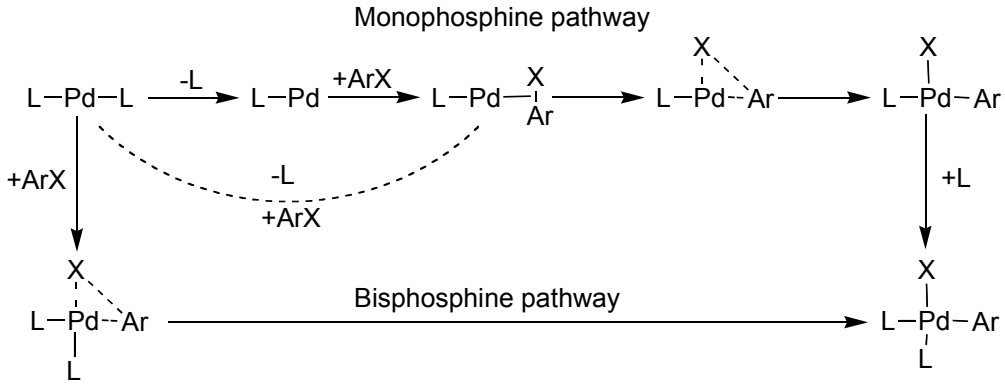

Figure 5 Pathways for oxidative addition of aryl halides to Pd(0) species.[22]

As well as ligand size, the nature of the aryl halide is also known to influence the oxidative addition step. The relative reactivity of the aryl halide towards oxidative addition has been shown to decrease in the order I>OTf>Br>>Cl.[25] Elsewhere, experimental[26] and DFT[22] studies on the oxidative addition of a range of aryl halides to various Pd catalysts, containing one or two phosphine ligands have been reported. For aryl chlorides, the monophosphine pathway (Figure 5) is favoured, with oxidative addition of ArCl to Pd(0) the rate determining step. Aryl bromides also favour the monophosphine route, with the initial ligand dissociation step found to be rate determining. In the case of aryl iodides, computations show that the monophosphine pathway is marginally favoured, however, with arenes that contain an electron

withdrawing group e.g. *p*-NC-C_6H_4-I, oxidative addition via the bisphosphine pathway (Figure 5) is favoured.[22]

To overcome the lower reactivity of aryl bromides and chlorides, the Pd(0) centre can be made more reactive by changing the ligands, as more electron-donating ligands will favour oxidative addition. This was highlighted in Chapter 2 when the more electron-donating dppf ligand (dppf = 1,1'-bis(diphenylphosphino)ferrocene) was used instead of PPh_3 to obtain higher conversions in the Sonogashira cross-coupling between 2,7-dibromopyrene **11** and TMSA.

After oxidative addition, transmetallation occurs from the M-R' reagent to the palladium metal centre. The different names of cross-coupling reactions relate to the different metals used (boron and silicon are considered as metals in this case): Suzuki-Miyaura (B), Negishi (Zn), Sonogashira (Cu), Kumada-Tamao (Mg), Stille (Sn) and Hiyama (Si).

After addition of both carbon groups to the Pd centre, reductive elimination of the C-C occurs. As reductive elimination occurs via a concerted mechanism, both carbon substituents must be *cis* to one another; therefore if monodendate ligands are used, trans-cis isomerization must first occurs to give the *cis* Pd(II) complex. In the cross-coupling of alkyl groups (*cf*. Negishi coupling to form **33** in Chapter 2), reductive elimination is an important catalytic step as it is in competition with β-hydride elimination. Upon reductive elimination to form the C-C bond, the Pd(0) species is regenerated and the catalytic cycle completed.

In this chapter, Suzuki-Miyaura cross-couplings are used due to the straightforward access to boron reagents provided by iridium-catalyzed C-H borylation (*vide supra*). For these couplings to proceed, a base is required, which is believed to facilitate the transmetallation step. However, the exact role of the base in these reactions is unclear, with proposals[27] (Figure 6) suggesting that either the three-coordinate boron is attacked by the base to give a four-coordinate anion, thus making the carbon centre more nucleophilic, or the base attacks the palladium and a subsequent σ-bond metathesis reaction takes place.

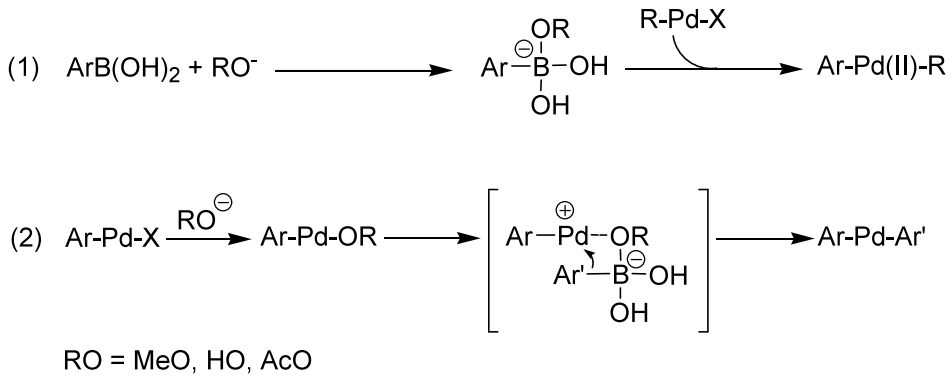

Figure 6 Proposed mechanisms of base activation in Suzuki-Miyaura cross-couplings.[27]

(1) Attack at three-coordinate boron by the base to give a four-coordinate anion.

(2) Attack at palladium by the base and subsequent σ-bond metathesis.

Many examples of the above cross-couplings exist with a huge variation in catalysts, ligands, substrates and conditions. Furthermore, the relative ease with which these reactions can be carried out has allowed them to become routine procedures in many laboratories around the world and in industry including 100+ ton/yr production. One limitation of these reactions is that they are not atom-efficient as both halide and metal generate waste. The next generation of cross-coupling reactions appears to involve the direct coupling of two nucleophiles,[28] thus removing the need to pre-functionalize the electrophilic substrates with halogens.

4.0 Results and Discussion

4.1 Synthesis of Organic Spacer Units based upon 2,6-difluorobenzoic acid methyl ester for Metal-Organic Framework Applications

Metal-organic frameworks (MOFs) consisting of metal ions linked together by organic bridging ligands are important systems for solid-state catalysts, electro-active materials, heavy-metal scavengers and gas storage.[29]

This section demonstrates the applicability of C-H borylation and metal-catalyzed cross-coupling chemistry to synthesize a range of organic bridging ligands, which then can be incorporated with metal ions to form MOFs. These ligands were based on the 2,6-difluorobenzoic acid methyl ester unit **41**, which was chosen for its electron-deficient nature. Furthermore, borylations and cross-couplings with **41** are unknown; hence this work establishes synthetic methodologies that lead to a range of previously

unknown derivatives. This work was carried out in collaboration with the group of Professor Zhengtao Xu (City University of Hong Kong, China) who have interests in the synthesis and properties of MOFs.[30] I synthesized and characterized the complete series of organic bridging ligands discussed below.

The initial compound to be synthesized was 4-Bpin-2,6-difluorobenzoic acid methyl ester **42**, which could then be used as a starting material in cross-coupling reactions to build more complex ligands. Iridium-catalyzed C-H borylation of **41** with B_2pin_2 (1 equiv.), $[Ir(COD)OMe]_2$ (1.5 mol %) and dtbpy (3 mol %) in MTBE under microwave conditions (80 °C, 30 min) gave a mixture of borylated products (Figure 7).

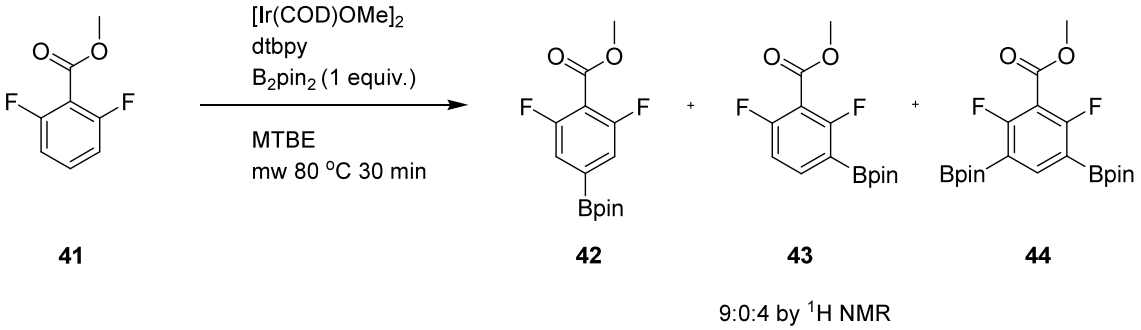

Figure 7 Iridium-catalyzed C-H borylation of **41** under microwave conditions. **43** was observed by *in-situ* GC-MS analysis of the reaction.

As well as the target *para*-borylated compound **42**, *meta*-borylation was also observed with evidence from *in-situ* GC-MS analysis for 3-Bpin-2,6-difluorobenzoic acid methyl ester **43**, and the bis-borylated 3,5-$(Bpin)_2$-2,6-difluorobenzoic acid methyl ester **44**. In the ^1H NMR spectrum, no signal for **43** was observed. The formation of *meta* products is perhaps surprising as borylation normally occurs at positions not *ortho* to any ring junction or substituent due to steric control (*vide supra*). However, because the fluorine atoms are so small, they are not sterically demanding enough to force borylation onto the *para* position exclusively, and a mixture of isomers is observed. Elsewhere, it has been shown that in iridium-catalyzed borylation reactions, fluorine has similar steric demands to that of a proton,[4,31] e.g. borylation of all three C-H bonds in 1,3,5-trifluorobenzene is reported in a 76% yield.[4]

The occurrence of bis-borylation and formation of H_2 (observed when the reaction vial is opened) shows that the HBpin is reacting, and hence **41** is very reactive towards

borylation (*cf.* pyrene, where at least 2.2 equivalents of B_2pin_2 are required for bis borylation). This finding is consistent with observations that electron-deficient arenes are more reactive towards Ir-catalyzed C-H borylation than electron-rich arenes.[3b]
Due to the potential difficulties in trying to separate *para* and *meta* isomers, a second set of borylation conditions were examined (Figure 8).

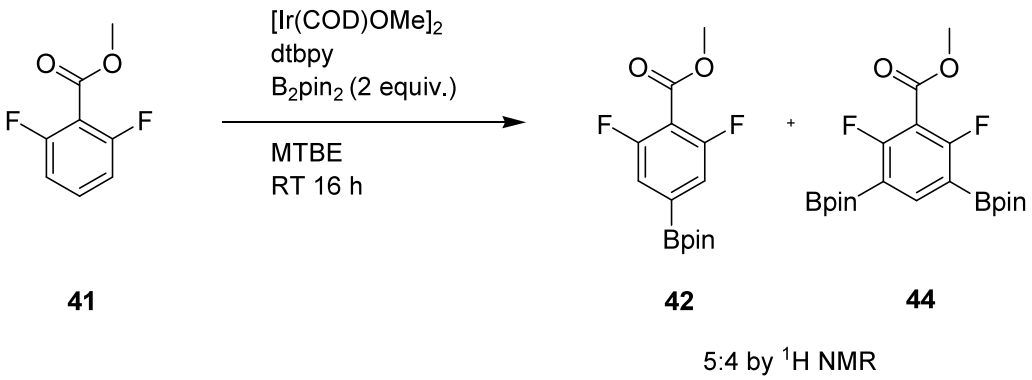

Figure 8 Iridium-catalyzed C-H borylation of **41** at room temperature.

Two equivalents of B_2pin_2 were used to ensure that any *meta* product formed would undergo a second borylation, giving an exclusive mixture of *para*- and bis-borylated derivatives, which would then be easier to separate. The reaction was also carried out at room temperature to see if changes in temperature had any effect on selectivity. After 16 hours, a 5:4 mixture (**42**:**44**) was observed by ^{1}H NMR and compares to the aforementioned mixture (9:4 {**42**:**44**}) obtained under microwave conditions. Having produced a mixture of borylated isomers of **41**, attempts to separate and purify the mixture were undertaken. When eluting the mixture through a silica column, it was found that only the starting material **41** was isolated; the Bpin moieties had been cleaved and replaced with a proton upon interaction with the silica. This phenomenon has also been observed with other electron-deficient arene-Bpin derivatives which appear to be susceptible to protio-deborylation on silica. Further purification attempts with alumina also failed as it was found that the borylated derivatives did not elute. Success was finally achieved by using a Kugelrohr distillation, which gave the *para*-product **42** in a 23% yield. Although enough of **42** was obtained to carry out full characterization, this method required long work-up times and a lot of product was lost, presumably due to decomposition at high temperatures (180 °C in the Kugelrohr oven).

Furthermore, it was not possible to isolate and thus characterize **43** and **44** using this method.

In order to overcome the problems of work-up and *meta* formation, an alternative strategy to form the *para*-isomer **42** was sought. This alternative route involved esterification of the commercially available 4-bromo-2,6-difluorobenzoic acid **45** followed by a Miyaura borylation to convert the bromine into a Bpin group (Figure 9).

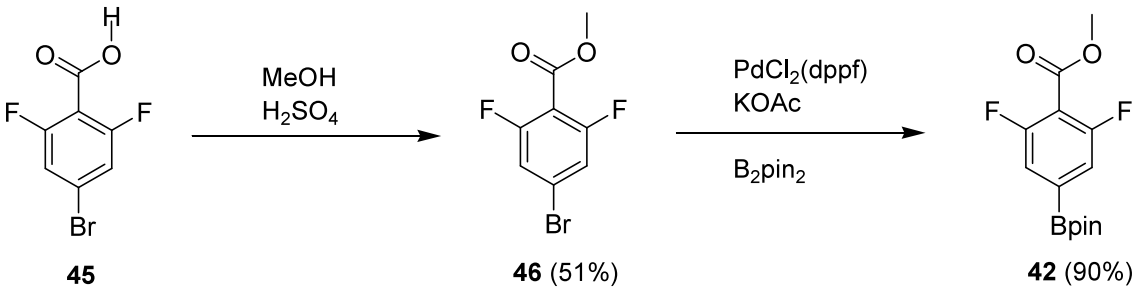

Figure 9 Esterification and Miyaura borylation reactions.

Esterification was carried out using concentrated H_2SO_4 in MeOH to give 4-bromo-2,6-difluorobenzoic acid methyl ester **46** in 51% yield. This moderate yield is perhaps due to the electron-withdrawing fluorines and bromine on the phenyl ring, which are classified as deactivating substituents. In the esterification process (Figure 10), a carbocation intermediate is formed by protonation of the carbonyl (ii in figure 10).[32] This intermediate is stabilized through resonance effects, which transfer the positive charge onto the phenyl ring. The resonance structures (Figure 10) show that the positive charges are most significant at the *ortho* and *para* positions. In the case of **45**, there are electron-withdrawing fluorines and a bromine at these positions, which remove electron density from the phenyl ring and therefore destabilize the carbocation (It is worth noting that fluorine also acts as a π-donor and also has a stabilizing influence). As a result of the lower stability of the intermediate, esterification becomes less favourable. Other reagents may be more effective for this esterification: for example, using $SOCl_2$ to make the acid chloride first and then adding MeOH to convert to the ester.

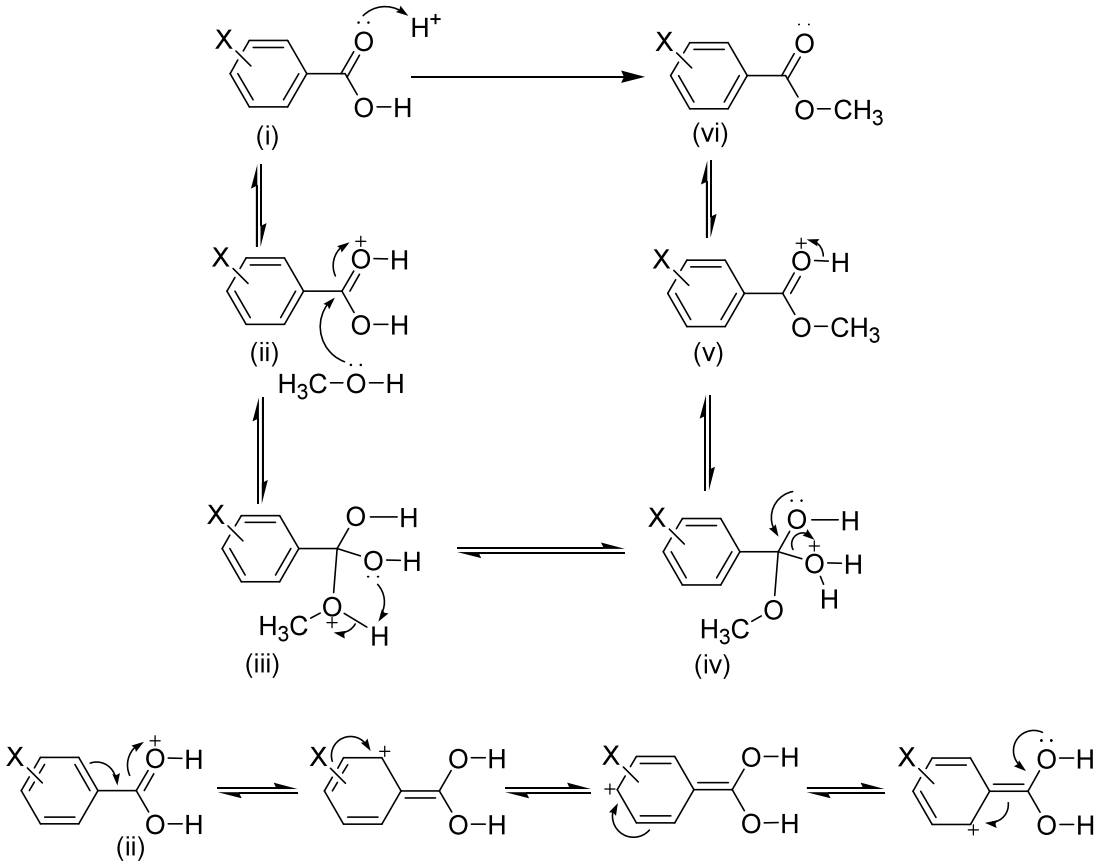

Figure 10 Mechanism of Fischer esterification (top) and the resonance structures of the carbocation intermediate (bottom).

Having formed **46**, a Miyaura borylation[18] using [$PdCl_2$(dppf)] (3 mol %), KOAc (3 equiv.) and B_2pin_2 (0.5 equiv.) was performed to give **42** in a 90% yield (Figure 9). To avoid protio-deborylation, column chromatography was not carried out and instead purification involved filtration, washing with water and removal of solvent. However, the straightforward work-up does not remove all impurities. Small amounts of homocoupled product, which are formed after the reduction of Pd(II) in the catalytic cycle (*vide supra*), are observed. If a pure sample is required, then Kugelrohr distillation could be used; however, **42** was synthesized as a building block for the construction of organic bridging ligands and these impurities can be removed by column chromatography at a later stage when protio-deborylation is no longer an issue. Using this Miyaura borylation method has the advantage that no bis- or *meta*-borylated derivatives are formed and the end-product is relatively homogenous.

With straightforward access to large quantities of **42**, a series of cross-couplings were performed to synthesize various organic bridging ligands for incorporation into MOFs

(Figure 11). The ligands based on benzene, anthracene and pyrene were chosen because they represent a range of different sizes and shapes as well as containing aromatic chromophores, which make them suitable for photophysical studies.

Using standard conditions for microwave-assisted cross-couplings,[33] the reaction of 3.3 equivalents of **42** with 1,3,5-tribromobenzene gave 1,3,5-tris(2,6-difluorobenzoic acid methyl ester)benzene **47** in a 27% isolated yield. Similarly, 2.2 equivalents of **42** reacted with 9,10-dibromoanthracene to give 9,10-di(2,6-difluorobenzoic acid methyl ester)anthracene **48** in a 26% yield. Both reactions successfully demonstrate the first cross-couplings of a 2,6-difluoro-benzoic acid methyl ester derivative. The low yield was reproducible. It was only when the coupling between **42** and **46** was performed in an attempt to form a dimeric ligand that insight into the low isolated yields was obtained. Instead of the ester dimer, the diacid 3,5,3',5'-tetrafluoro-biphenyl-4,4'-dicarboxylic acid **49** was isolated in a 24% yield. It appears that the use of a strong base (KOH) in the presence of water leads to ester hydrolysis and formation of the carboxylic acid. If this hydrolysis occurs on **42** or **46** before cross-coupling, then it is unlikely that the newly formed acids will undergo any further reaction due to their limited solubility and, as a result, yields are reduced. Furthermore, once the cross-coupled product has formed, further ester hydrolysis can occur as demonstrated in **49**, again reducing the yield of the ester. In-situ GC-MS analysis during reactions to form **47** and **48**, showed no signal for **42** suggesting that it has all been consumed and pointing to formation of carboxylic acids (it is not possible to observe these carboxylic acids in the GC-MS). To improve these reactions and obtain higher yields, a weaker base, such as K_2CO_3, could be used, along with less harsh conditions, such as thermal heating. An alternative route to **49** (and its ester counterpart), would be the homocoupling reaction of **46** using Ni and a PPh_3 ligand.[34]

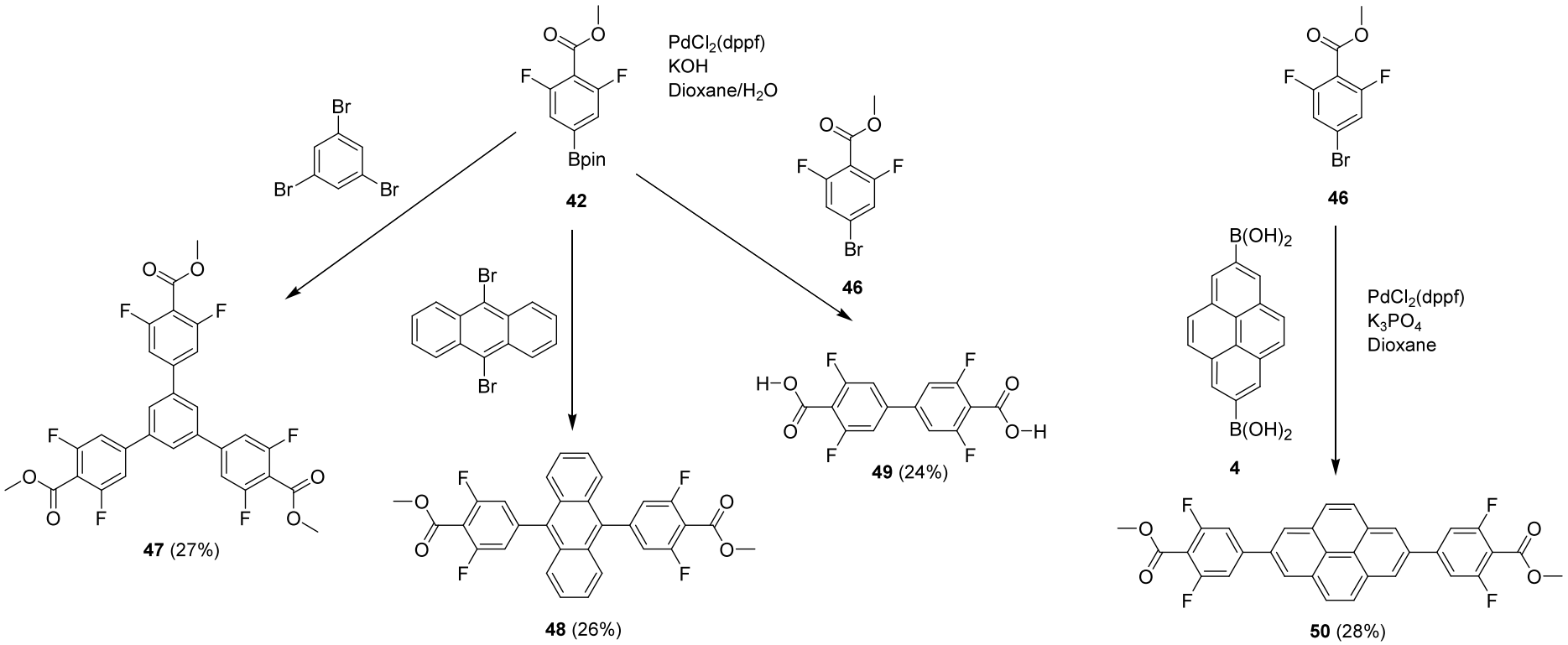

Figure 11 Suzuki-Miyaura cross-coupling reactions of **42** and **46**.

A further cross-coupling reaction between **46** and pyrene-2,7-bis(boronic acid) **4** was performed to yield 2,7-bis(2,6-difluorobenzoic acid methyl ester)pyrene **50** (Figure 11). In this case, a weaker base was used and no water was added (water was shown to reduce the yields of a cross-coupling between **4** and octyl-4-bromobenzoate in Chapter 2). Although the cross-coupling was successful, the yield was still low (28%). It is possible, that the boronic acid groups on **4** could produce OH^- anions which would act to hydrolyse the ester and thus reduce the yield. An alternative approach would be to use a different boron species (BF_3K), or even 2,7-dibromopyrene **11** to react with **42**. Perhaps, a more electron donating phosphine ligand is required to improve the yield of this reaction. As shown in Chapter 2, 2,7-bis-substituted pyrene derivatives often require more electron-donating ligands to obtain higher yields in cross-coupling reactions.

4.1.1 Conclusions

A series of previously unknown derivatives based on the 2,6-difluorobenzoic acid methyl ester moiety have been synthesized and characterized. Despite the simplicity of the starting material **41**, Ir-catalyzed borylation has proved problematic. This is due to the low steric control exhibited by the fluorines and subsequent tendency of **42** to protio-deborylate upon work-up. An alternative route using the Miyaura borylation is more effective. Successful cross-coupling reactions were carried out although yields were low due to ester hydrolysis and formation of carboxylic acids. Several modified approaches have been proposed to overcome these issues.

4.2 Borylation of Substituted Pyridine Ligands for Olefin Polymerization

Transition metal-catalyzed polymerization of olefins is an important process that converts 1-alkenes into long hydrocarbon chains. Several important polymers that find use in everyday items are synthesized using this method. Over several decades, a wide range of metal catalysts and ligands have been developed to improve the polymerization process; in particular, catalysts based upon metallocene complexes of group IV metals (Ti, Zr) have shown great promise. It has been shown that changing the ligands in these complexes has an effect on their catalytic reactivity and material properties in olefin polymerization reactions.[35]

In this section, I report the use of Ir-catalyzed borylation to functionalise selectively two ligands for use in olefin polymerization. It is hoped that the new borylated ligands can be further functionalized (using the methodology in Figure 3), so that their influence on the polymerization reaction can be tuned. The ligands were provided by the group of Professor Micheal C. W. Chan (City University of Hong Kong, China) who have developed many ligands and group IV metal catalysts for olefin polymerization.[36]

The ligands, 2,4-di-*tert*-butyl-6-[6-(trifluoromethyl-phenyl)-pyridin-2-yl]-phenol **51** and 2-(3,5-di-*tert*-butyl-2-methoxy-phenyl)-6-(3-trifluoromethyl-phenyl)-pyridine **52** have only two sites which are not *ortho* to any substituent or ring junction (Figure 12).

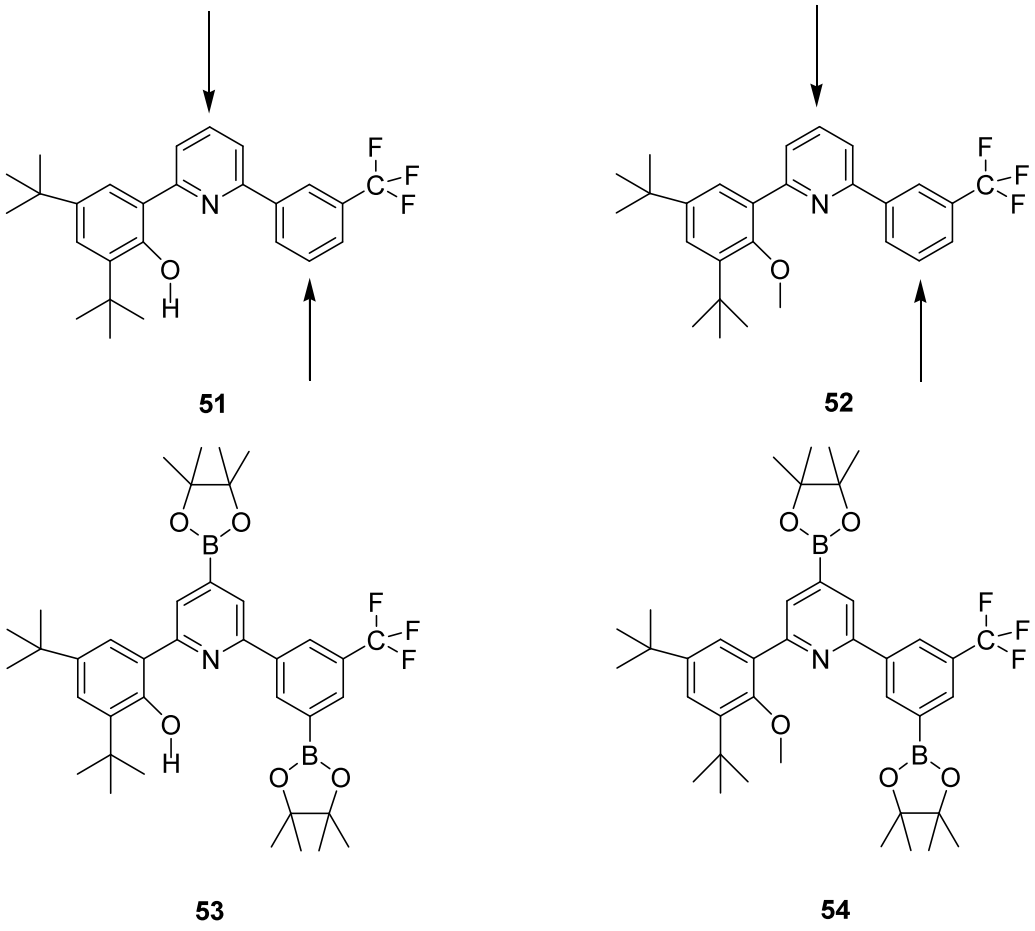

Figure 12 Sites of borylation on substituted pyridine ligands (top) and products isolated after borylation (bottom).

Iridium-catalyzed bis-borylation of the ligands with two equivalents of B_2pin_2 in MTBE under microwave heating at 80 °C for 30 min was carried out. The products **53** and **54**

(Figure 12) were isolated in 83 and 64% yields, respectively. Full assignment of the NMR spectra was undertaken using HMBC and HSQC 2D NMR techniques. An X-ray crystal structure of **54** (Figure 13), showed rotational disorder in the ^{t}Bu group, C(25), C(26) and C(27), with hydrogen positions A and B refined to 0.717(2) and 0.283(2) occupancies. The methoxy group is also disordered between positions A and B with occupancies refined to 0.947(2) and 0.053(2).

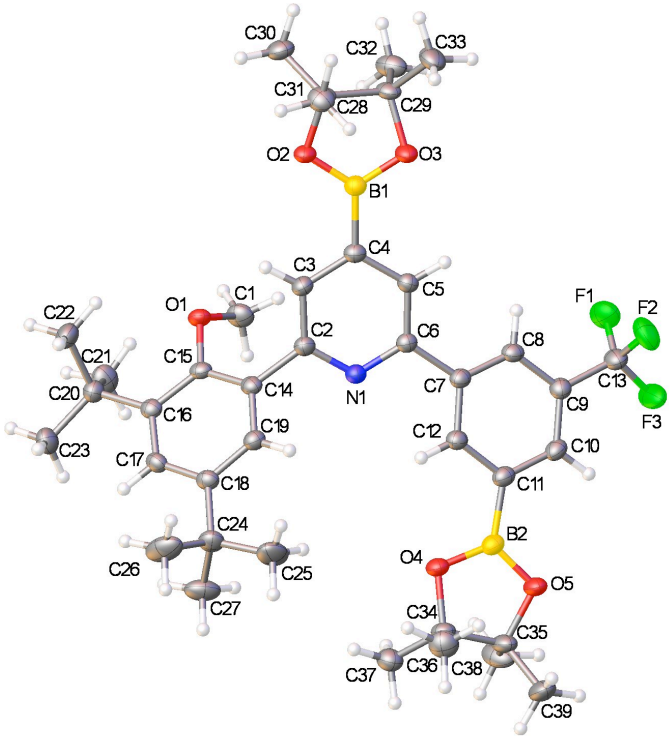

Figure 13 Molecular structure of 2-(3,5-di-tert-butyl-2-methoxy-phenyl)-4-(Bpin)-6-[3-(Bpin)-5-trifluoromethyl-phenyl]-pyridine **54**.

Coordination of the pyridine N of the substrate to the iridium catalyst, is avoided by 2,6-diaryl substitution (*cf*. Work by Marder et al,[9d] a single substituent *ortho* to a *N* centre is sufficient to inhibit *N*-coordination to the iridium centre). Thus, good to excellent yields of borylated products were obtained. Interestingly, the yield of the alcohol **53** (83%) is somewhat higher than that of the ester **54** (64%). It is possible that the alcohol proton in **51** is hydrogen bonded to the pyridine nitrogen, thus tying up the proton, inhibiting protonolysis of metal boryl intermediates and perhaps even activating the C-H bonds of the substrate. A crystal structure of either **51** or **53** would provide

useful information on the nature of any O—H···N bond; however, attempts to grow such a crystal were unsuccessful.

4.2.1 Conclusions

Iridium-catalyzed C-H borylation of two 2,6-diarylpyridine ligands has successfully been undertaken, highlighting the ease at which selective borylation can be carried out on novel substrates. The products **53** and **54** are now being used as starting materials by the group of Professor Chan to synthesize a range of ligands, designed to improve the performance of group IV olefin polymerization catalysts.

4.3 Borylation of 1,10-Phenanthroline

1,10-Phenanthroline (Phen) is a chelating bidentate ligand which is commonly used in coordination chemistry. Complexes of Phen with various metal ions have led to its use in a number of applications, including chemosensors for metal ions, ionophores and incalating agents for polynucleotides. [37] Functionalization of Phen allows its properties to be tuned. Direct C-H borylation would also allow easy access to polymers incorporating the Phen groups.

Due to the π-deficient nature of Phen caused by the electron-withdrawing imine nitrogen (C=N-), standard electrophilic substitution with X_2 requires harsh conditions. A number of methods have been developed including bromination with Br_2 in the presence of $SOCl_2$,[38] conversion of Phen to its more reactive HCl salt before bromination[39] and chlorination using PCl_5.[40] However, in all cases, yields are low (~35%) and selectivity is poor leading to a mixture of products. Later, it was found that bromination could be selectively achieved by refluxing Phen in a 1-chlorobutane solution in the presence of S_2Cl_2, pyridine and Br_2. This selectively led to 3,8-dibromophenanthroline in a 63% crude yield (Figure 14).[41] However, after further purification, the yield of the pure product was 34%.

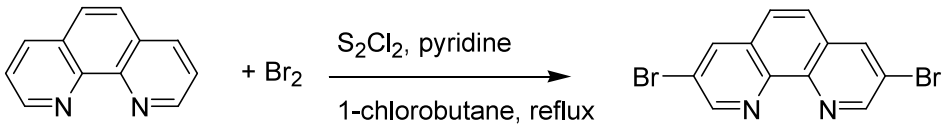

Figure 14 Bromination of 1,10-phenanthroline.[41]

Phen derivatives substituted at the 3- and 8-positions are considered to be important starting materials for liquid crystals, macrocycles and π-conjugated polymers; however, their use is hindered by low-yielding preparations.[41-42] When considering the selectivity of Ir-catalyzed C-H borylation, it can be seen that only the 3- and 8-positions are not *ortho* to any ring junction or to the nitrogen; hence borylation would give exclusive access to Phen derivatives substituted at these positions. In practice, borylation may be problematic as there is likely to be competition with dtbpy for coordination to the iridium metal.

To minimise the effects of any competition between ligand binding, the $[Ir(COD)OMe]_2$, dtbpy and a small amount of B_2pin_2 were mixed together in the reaction solvent to preform the catalytic trisboryl intermediate before the addition of any Phen. Furthermore, an excess of [Ir] (6 mol %) compared to dtbpy (1.5 mol %) was used to ensure enough of the catalytic species formed. Borylation of Phen with 2.2 equivalents of B_2pin_2 under microwave conditions was performed (Figure 15). In the GC-MS trace of the crude reaction mixture, a signal corresponding to a bis-borylated phenanthroline was observed. A crude ^1H NMR showed three singlets with a 1:1:1 intensity in the aromatic region, thus pointing to formation of 3,8-bis(Bpin)phenanthroline **55**. A second borylation which used the standard 1:1 ratio of [Ir] to dtbpy under the same heating conditions gave evidence for the formation of mono-borylated Phen **56** in the GC-MS (Figure 15). However, a suitable ^1H NMR of the crude mixture was not obtained, due to broadening of the signals in the spectrum. Therefore, it can only be speculated that borylation occurred at the 3-position.

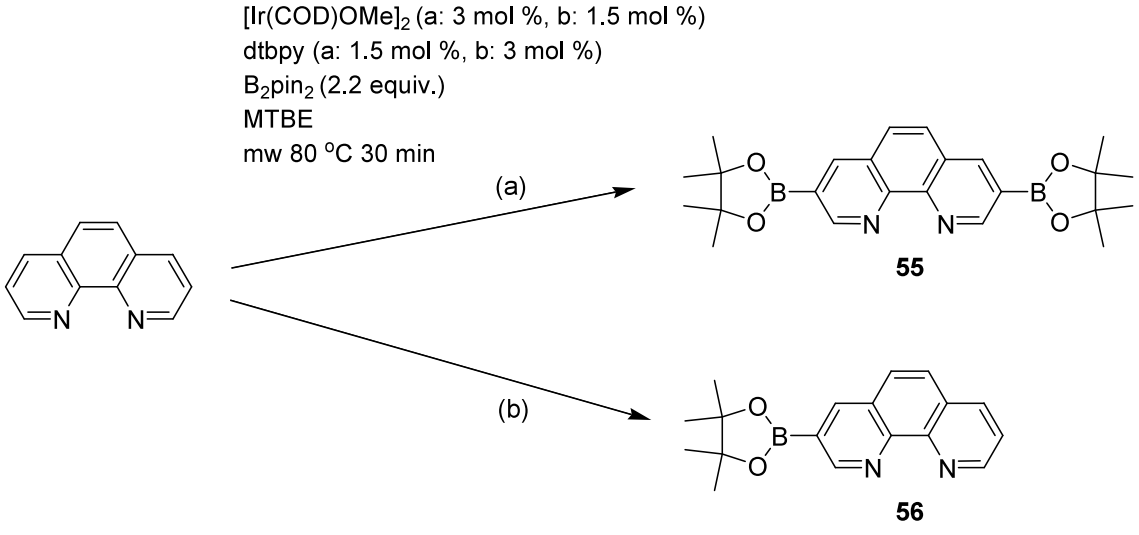

Figure 15 Iridium-catalyzed C-H borylation of 1,10-phenanthroline.

Attempts to isolate **55** and **56** proved ineffective. The mixture did not elute on silica, alumnia or Fluorosil® columns and attempts at sublimation also failed. Addition of hexane to the crude reaction mixture led to precipitation of a dark solid. Filtration and washing of this solid with various organic solvents, removed some the iridium metal and dark colour; however, I was unable to obtain good NMR spectra for the resulting solid. Presumably, these problems with work-up are due to the coordinating nature of the Phen nitrogens.

4.3.1 Conclusions

Having identified a need for a high-yielding straightforward route to 3,8-disubstituted phenanthrolines, Ir-catalyzed C-H borylation was used for the first time to selectively borylate Phen at the 3- and 8-positions. Despite evidence of successful borylation, isolation of the products has not been achieved. It is suggested that coordination of Phen to a metal such as zinc or copper before borylation, would not only reduce the effects of Phen binding to iridium, but may also improve the work-up.

4.4 The Synthesis and Reactivity of 1,1'-bis(Bpin)ferrocene **57**

This section reports interesting observations on the reactivity of ferrocene in cross-coupling and borylation reactions. Interest in this area began when I was asked by Professor Raymond Wong (Hong Kong Baptist University) to undertake the Suzuki-Miyaura cross-coupling reaction shown in Figure 16. The end-product 1,1'-bis(4-bromo phenyl)ferrocene **58** was to act as a starting material for the construction of molecular wires and polymers, which is an area of study for the Wong group.[43]

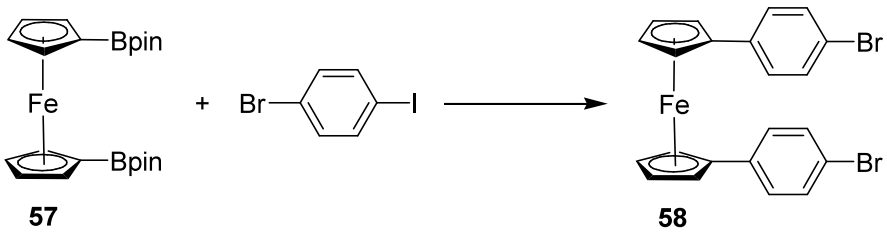

57 **58**

Figure 16 Proposed Suzuki-Miyaura cross-coupling of **57** with 1-bromo-4-iodobenzene.

However, several attempts using different reaction conditions (Table 2) all failed to give the desired product. Entries 1-4 involved use of a variety of bases, solvents and heating conditions, while in entry 5, CuCl was added to facilitate the transmetallation step in the cross-coupling cycle.[44] In most cases, the GC-MS of these cross-coupling reactions showed only the mono-coupled product 1-(Bpin)-1'-(4-bromophenyl)ferrocene **59** and often evidence for 1-(4-bromophenyl)ferrocene **60**, which presumably is formed by protio-deborylation of **59**. Using the conditions in entries 1 and 3, which involved hydroxide bases, it was found that all of the starting material **57** was consumed. Whereas large amounts of **57** were observed when using the conditions described in entries 2 and 5. Only the conditions for entry 3 yielded the desired product **58**, however, only in trace amounts. The sample in entry 3, was heated for another hour in the microwave and GC-MS analysis showed that no further reaction had occurred. The absence of any reaction in entry 4 is probably due the poor solubility of **57** in MTBE.

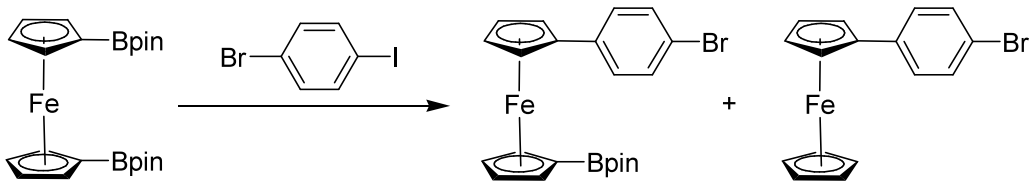

57 **59** **60**

	Catalyst	**Base**	**Solvents**	**Heating Conditions**	**GC-MS Ratios**
1	[$PdCl_2$(dppf)] (3 mol %)	KOH (3 equiv.)	DMF/H_2O (10:1)	80 °C 16 h	**57**:**59**:**60** (0:2:3)
2	[$PdCl_2$(dppf)] (3 mol %)	$K_3PO_4 \cdot H_2O$ (3 equiv.)	DMF	80 °C 16 h	**57**:**59**:**60** (10:2:1)
3	[$PdCl_2$(dppf)] (3 mol %)	NaOH (5 equiv.)	DME/H_2O (20:1)	100 °C 1 h μw	**57**:**59**:**60** (0:1:8) **58** (traces)

4	[$PdCl_2$(dppf)] (3 mol %)	NaOH (5 equiv.)	MTBE/H_2O (10:1)	100 °C 1 h μw	No rxn.
5	[$PdCl_2$(dppf)] (3 mol %) CuCl (1 equiv.)	$K_3PO_4 \cdot H_2O$ (3 equiv.)	DMF	100 °C 16 h	**57**:**59**:**60** (10:2:1)

Table 2 Suzuki-Miyaura cross-coupling reactions between 1,1'-bis(Bpin)ferrocene and 1-bromo-4-iodo-benzene.

In the literature, it was reported that the related 1,1'-bis(boronic acid)ferrocene, underwent Suzuki-Miyaura cross-coupling to form **58**; however, 6 days of heating were required to obtain a 60% yield.[45] This observation is consistent with fact that boronic acids are known to be more reactive than boronic esters (*cf*. reactivity of pyrene boronic esters and acids). More recently, the synthesis of **58** and related aryl-substituted ferrocene derivatives was reported in good yields using microwave assisted Negishi cross-coupling.[46] Before the cross-coupling, the authors lithiate 1,1'-dibromoferrocene and add $ZnCl_2$ to make the zinc reagent *in situ*. I repeated this reaction starting from ferrocene and first lithiating with nBuLi in the presence of TMEDA, before the addition of $ZnCl_2$ and subsequent cross-coupling (Figure 17). Although I was able to isolate **58** after column chromatography, I was unable to obtain the high yields reported in the literature. Even with the addition of $MgCl_2$ to the zinc reagent,[47] which has recently been shown to facilitate the transmetallation step and improve reactivity, yields were still very low (6%).

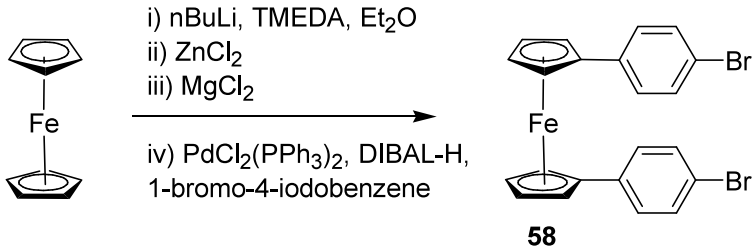

Figure 17 Negishi cross-coupling to synthesize **58**.

In order to try and rationalise the failure of **57** to undergo Suzuki-Miyaura cross-coupling at both Cp rings, the steric and electronic factors of the reaction are now considered. One possibility for the low reactivity of **57** in these reactions could be the presence of an iron-to-boron interaction which, during cross-coupling, might hinder transmetallation of the ferrocenyl moiety from the boron to the palladium. The nature of iron-to-boron interactions in borylferrocenes has been well studied,[48] where the interaction between the empty *p*-orbital on boron and filled iron *d*-orbitals is found to bend the boryl group towards the iron. The magnitude of this bending is found to be dependent upon the electronic nature of the boryl group. For example, the compound [$FcBC_4Ph_4$], which is highly Lewis acidic has a dip angle (angle between boryl group and Cp plane) of 29.4°,[48d] whereas the electronic saturated [$Fc(BH_2$-pyridine)] has a dip angle of only 0.1°.[48c] Elsewhere, it has been reported that a strongly Lewis acidic boron centre is required in order to induce even a relatively weak metal-to-boron interaction.[48a] To investigate the nature of the iron-to-boron interaction in the Bpin derivatives, crystals of **57** and the related 1-(Bpin)ferrocene **61** were grown and their structures analyzed (Figure 18).

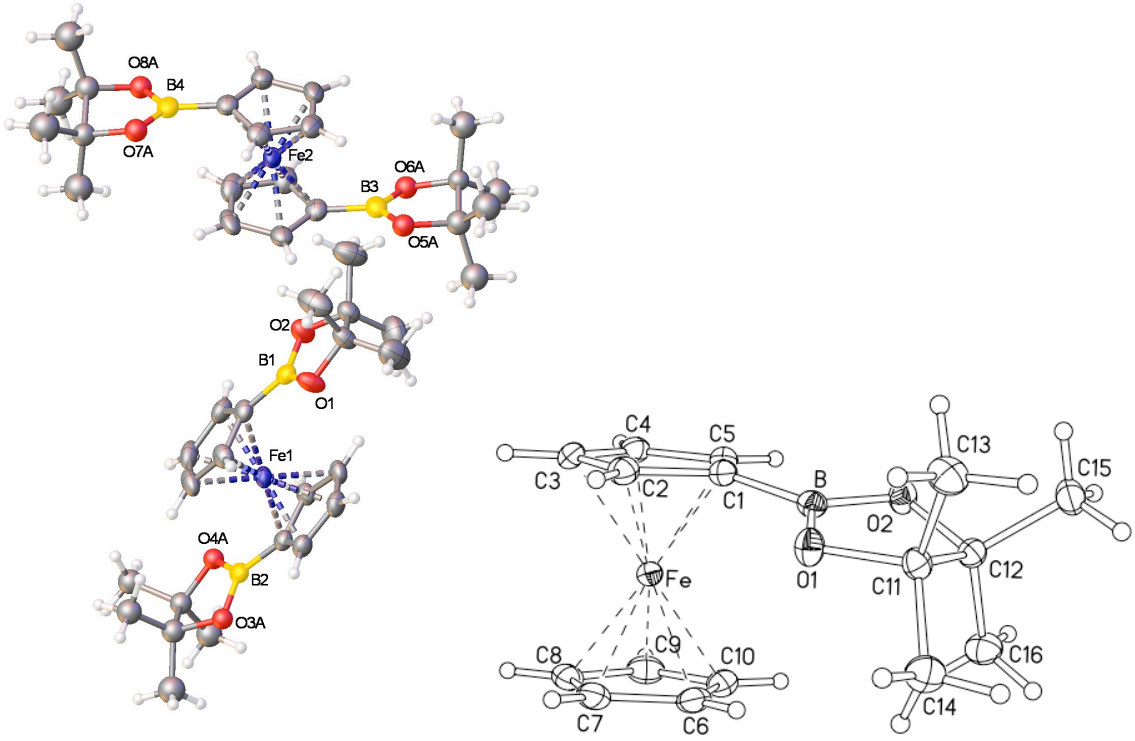

Figure 18 X-ray crystal structures of 1,1'-bis(Bpin)ferrocene **57** (left) and 1-(Bpin)ferrocene **61** (right).

Measurements at 200 K, showed **57** to crystallise in the triclinic space group $P\bar{1}$, which is a different polymorph from that previously reported (monoclinic, $P2_1/n$).[49] The asymmetric unit of the triclinic **57** was found to contain 2 molecules, A and B. Upon cooling to 120 K, an irreversible phase change occurred leading to the known monoclinic polymorph. In both polymorphs, the Bpin groups adopt a staggered conformation (Table 3, Tors. angle). **61** crystallises in a monoclinic space group, $P2_1/n$. Table 3 shows selected bond lengths, distances and angles for **57** and **61**. It can be seen that the dip angles are small, 3.14-7.94° (**57**) and 8.66° (**61**), suggesting a small iron-to-boron interaction. The $Cp_{centroid}$-Fe-$Cp_{centroid}$ angles are found to be around 180° and the Cp ring planes are almost parallel also suggesting very little iron-to-boron interaction. Furthermore, B-C and B-O bond distances are almost identical to those measured for other aryl-Bpin derivatives, e.g. 2,7-bis(Bpin)pyrene **1** (B-C: 1.558(4); B-O: 1.339(6), 1.342(6), 1.362(3), 1.366(3)),[11] suggesting no extra filling of the boron empty *p*-orbital and hence no changes in the bond orders of the Bpin moieties in **57** and **61**. These structures, show that there is a small iron-to-boron interaction present. Small dip angles have been found in electronically saturated borylferrocenes (*vide supra*). Therefore, the small dip angles measured for **57** and **61** are likely to be the result of partial filling of the empty boron *p*-orbital with electron density from neighbouring oxygens.

	57-A[a]	**57-B**[a]	**57**[49]	**61**		**57-A**[a]	**57-B**[a]	**57**[49]	**61**
B-O	1.364(4) 1.363(4) 1.380(5) 1.358(5)	1.358(5) 1.363(5) 1.370(6) 1.343(6)	1.358(2) 1.368(2) 1.368(2) 1.358(2)	1.3681(2) 1.3717(2)	α*	6.36 7.94	6.63 7.06	3.14 3.17	8.66
B-C	1.545(4) 1.544(4)	1.548(4) 1.542(5)	1.546(2) 1.549(2)	1.543(2)	α	0.82	0.83	2.14	3.49
B-Fe	3.092 3.119	3.114 3.114	3.176 3.169	3.084	β	179.43	179.68	179.32	177.70
					Tors.	174.27	179.60	113.02	

[a]Corresponds to the triclinic polymorph. α* = dip angle, α = tilt angle (angle between Cp ring planes). β = $Cp_{centroid}$-Fe-$Cp_{centroid}$ angle, Tors. = B-$Cp_{centroid}$-Fe-Cp'$_{centroid}$-B' angle.

Table 3 Selected bond lengths, distances [Å] and angles of **57** (including data from reference 49) and **61**.

From the solid-state structures it is not obvious that steric factors cause the low reactivity in the Suzuki-Miyaura cross-coupling of **57**. Before considering the electronic factors, it is worth noting that the Cp rings in ferrocene are considered to carry a partial negative charge, and hence the ferrocenyl group acts as an electron donor.[50] It has also been shown that electron-donating groups attached to aryl boronic esters and acids increase the rate of the protio-deborylation process.[51] During the cross-coupling of **57**, the formation of 1-(4-bromo phenyl)ferrocene **60** was observed by GC-MS. This suggests that a competing protio-deborylation process is occurring. After cross-coupling to the first Cp ring, it is possible that the addition of the aryl bromide moiety has a large enough electron-donating influence on 1-(Bpin)-1'-(4-bromo phenyl)ferrocene **59**, to favour protio-deborylation on the second Cp ring over transmetallation from the boron to palladium.

Hence, to achieve cross-coupling on both Cp rings of ferrocene, a coupling reaction that uses a transmetallation reagent that is not susceptible to protio-deborylation is required, such as zinc, as demonstrated in the aforementioned Negishi coupling.

As well as its low reactivity in Suzuki-Miyaura cross-coupling reactions, the formation of **57** by iridium-catalyzed C-H borylation is known to be problematic. Borylation of various metallocenes has been reported,[10] and it was found that although mono-borylation of ferrocene to give **61** occurred in good yields (60%), bis-borylation was only observed in 8% yield even when an excess of three equivalents of B_2pin_2 was used (Figure 18).

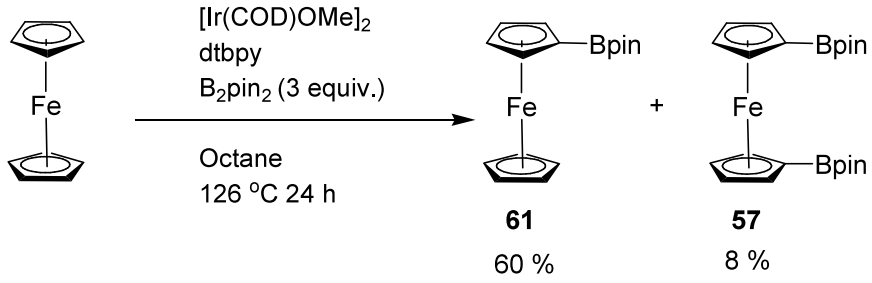

Figure 19 Iridium catalyzed borylation of ferrocene.[10]

The authors also isolated and attempted to further borylate **61**; however, no further reaction was observed. I was able to reproduce these observations, and also found that

using microwave-assisted borylation[33] the reactivity was the same. To obtain **57** in high yields, other synthetic methodologies are used such as condensation reactions between pinacol and halo-boryl ferrocenes[52] and, more recently, the reaction of B_2pin_2 with [2]boraferrocenophanes.[49]

The failure of ferrocene to undergo bis-borylation by iridium-catalyzed C-H borylation is now considered. It is unlikely that the ferrocene moiety is too sterically demanding to be borylated a second time by the iridium trisboryl intermediate. There are numerous examples of multiple borylations on molecules that are much bulkier than ferrocene, such as perylene,[11] porphyrins and corroles.[12] Furthermore, from the X-ray structure of **61** (*vide supra*), it was shown that there are C-H bonds on the unsubstituted Cp ring that are not in any way hindered by the borylated Cp ring. Electronically, it has already been stated that the ferrocenyl group acts as an electron donor and it is known that electron rich arenes are less reactive towards iridium-catalyzed C-H borylation than electron-deficient ones.[3b] Hence, iridium-catalyzed borylation could be hindered due to the electron-rich nature of the Cp ring. If this is the case, then this would mean the unsubstituted Cp ring in **61** is more electron-rich than the unsubsituted Cp rings in ferrocene (as borylation still occurs with ferrocene). This suggests that the Bpin group on the substituted Cp ring of **61** is having an influence on the unsubstituted Cp ring. In Chapter 3, it was shown that the Bpin moiety does have a very slight influence on the photophysical properties (and hence the electronic nature) of pyrene. It could be feasible that the small electronic influence of the Bpin moiety in **61** is enough to alter the electronic properties of ferrocene and to hinder further borylation. To ascertain if such an influence exists, further studies to probe the exact nature of the electronic structure in these systems are required.

4.4.1 Conclusions

A Suzuki-Miyaura cross-coupling between **57** and 1-bromo-4-iodo-benzene found that only cross-coupling to one Cp ring occurred with protio-deborylation of the second Cp ring instead of further cross-coupling. To obtain the target compound **58**, a Negishi cross-coupling was used.

When using iridium-catalyzed C-H borylation on ferrocene, it was found that only mono-borylation occurred.

An attempt to rationalise these surprising observations about the reactivity of ferrocene in Suzuki-Miyaura and iridium-catalyzed C-H borylation reactions was undertaken by considering both the steric effects (including an examination of the crystal structures of **57** and related **61**) and electronic effects. It is possible that the electron-rich nature of the Cp rings can cause protio-deborylation and hence restrict cross-coupling to one Cp ring. The electron-rich nature of the Cp rings could also be responsible for hindering iridium-catalyzed C-H borylation of a second Cp ring.

5.0 Experimental

General

Reagents purchased from commercial suppliers were tested for purity before use. B_2pin_2 was kindly provided by AllyChem Co. Ltd. (Dalian, China). 1,10-phenanthroline was purified by recrystallization from petroleum ether and drying under high vacuum. Ferrocene was purified by sublimation before use. Borylation reactions were prepared in an Innovative Technology Inc. glovebox under nitrogen (BOC). Microwave reactions were performed in septum-containing, crimp-capped, sealed vials in an EmrysTM Optimizer (Personal Chemistry) reactor. The wattage was automatically adjusted to maintain the desired temperature for the desired period of time. Reactions were monitored *in situ* by GC-MS, TLC or by ^{1}H NMR spectroscopy to ensure consumption of starting materials prior to work up. GC-MS analyses were performed on an Agilent Technologies 6890 N gas chromatograph equipped with a 5973 Inert Mass Selective Detector and a 10 m fused silica capillary column (5% cross-linked phenylmethylsilicone) using the following operating conditions: injector temperature 250 ºC, detector temperature 300 ºC, the oven temperature was ramped from 70 ºC to 250 ºC at 20 ºC min^{-1}. UHP helium was used as the carrier gas. NMR spectra were recorded on Bruker Avance-400, Inova-500 and Varian VNMR 700 spectrometers at the following frequencies: ^{1}H: 400, 500 and 700 MHz, ^{13}C{^{1}H}: 100, 125 and 175 MHz, ^{19}F{^{1}H}: 376, 470 and 658 MHz, ^{11}B{^{1}H}: 128 and 224 MHz. Mass spectra were obtained using a Waters Xevo QTOF equipped with Atmospheric Solids Analysis Probe (ASAP) and a Thermo-Finnigan LTQ FT mass spectrometer for high-resolution ESI spectra. High-resolution EI mass spectra were recorded by the National Mass Spectrometry Service at Swansea, using a Finnigan MAT 95 XP spectrometer. Elemental analyses were performed using an Exeter Analytical E440 machine.

42: 2,6-Difluoro-4-(4,4,5,5-tetramethyl-[1,3,2]dioxaborolan-2-yl)-benzoic acid methyl ester (4-Bpin-2,6-difluorobenzoic acid methyl ester)

Method 1: In a nitrogen-filled glove box, $[Ir(OMe)COD]_2$ (0.057 g, 0.086 mmol), 4,4'-di-^{t}Bu-2,2'-bipyridine (dtbpy, 0.046 g, 0.17 mmol) and B_2pin_2 (0.10 g, 0.39 mmol) were dissolved in MTBE (3 mL). The mixture was added to a microwave vial containing 2,6-difluoro-benzoic acid methyl ester **41** (1.00 g, 5.81 mmol) and B_2pin_2 (1.52 g, 5.99 mmol). The vial was capped and the reaction mixture was stirred at room temperature for 16 h. Outside the glove box, Et_2O (10 mL) was added and the mixture was washed with H_2O (3 × 25 mL), the organic layer was dried over $MgSO_4$ and the solvent removed under reduced pressure. Purification of the residue by Kugelrohr distillation (180 ºC, 2000 mTorr) gave **42** (0.39 g, 23%) as a colourless oil.

Method 2: In a nitrogen-filled glove box, 1,4-dioxane (4 mL) was added to a Young's tube containing $PdCl_2(dppf)$ (0.08 g, 0.11 mmol), KOAc (0.94 g, 9.6 mmol) and B_2pin_2 (0.89 g, 3.50 mmol). To this mixture was added 4-bromo-2,6-difluoro-benzoic acid methyl ester **46** (0.8 g, 3.19 mmol) in 1,4-dioxane (4 mL). The tube was sealed and the mixture was stirred at 80 ºC for 16 h. Outside the glovebox, hexane (60 mL) was added and the mixture was filtered through a Celite plug. The hexane solution was washed with H_2O (3 × 60 mL) and dried over $MgSO_4$. The solvent was removed under reduced pressure to give a crude sample of **42** (0.86 g, 90%) as a light yellow oil.

^{1}H NMR (700 MHz, C_6D_6, δ): 7.41 (d, 2H, $J_{H\text{-}F}$ = 8 Hz, Ar), 3.42 (s, 3H, OMe), 1.02 (s, 12H, CH_3); $^{13}C\{^1H\}$ NMR (175 MHz, C_6D_6, δ): 162.1, 160.9 (d, $J_{C\text{-}F}$ = 262 Hz), 118.2, 118.0, 114.6, 84.9, 52.6, 25.1; $^{11}B\{^1H\}$ NMR (224 MHz, C_6D_6, δ) 30.0; $^{19}F\{^1H\}$ NMR (658 MHz, C_6D_6, δ): -111.7; EIMS *m/z*: 298 (M^+); HRMS-EI: (M^+) Calcd for $C_{14}H_{17}{}^{10}BF_2O_4$ 298.1303; Found 298.1318; Anal. Calcd for $C_{14}H_{17}BF_2O_4$: C, 56.41; H, 5.75. Found: C, 56.47; H, 5.79.

43: 2,6-Difluoro-3-(4,4,5,5-tetramethyl-[1,3,2]dioxaborolan-2-yl)-benzoic acid methyl ester and **44** 2,6-Difluoro-3,5-bis(4,4,5,5-tetramethyl-[1,3,2]dioxaborolan-2-yl)-benzoic acid methyl ester

In a nitrogen-filled glove box, $[Ir(OMe)COD]_2$ (0.057 g, 0.086 mmol), 4,4'-di-^{t}Bu-2,2'-bipyridine (dtbpy, 0.046 g, 0.17 mmol) and B_2pin_2 (0.10 g, 0.39 mmol) were dissolved in MTBE (3 mL). The mixture was added to a microwave vial, containing 2,6-difluoro-benzoic acid methyl ester **41** (1 g, 5.81 mmol) and B_2pin_2 (1.52 g, 5.99 mmol). The vial was capped and the reaction mixture was heated for 30 min at 80 ºC in a microwave reactor. The crude reaction mixture was found to contain **42**, **43** and **44**.

43: EIMS *m/z*: 298 (M^+).

44: ^{1}H NMR (400 MHz, $CDCl_3$, δ): 8.19 (t, 1H, $J_{H\text{-}F}$ = 8 Hz, Ar), 3.90 (s, 3H, OMe), 1.34 (s, 24H, CH_3); $^{19}F\{^1H\}$ NMR (376 MHz, $CDCl_3$, δ): -95.8; EIMS *m/z*: 424 (M^+).

46: 4-Bromo-2,6-difluoro-benzoic acid methyl ester

To a round bottomed flask containing MeOH (20 mL), H_2SO_4 (0.25 g, conc. sol. 98%) was added. After stirring for 10 min, a solution of 4-bromo-2,6-difluorobenzoic acid **45** (1.00 g, 4.22 mmol) in MeOH (20 mL) was added and the mixture was heated at 70 ºC for 16 h. After cooling to room temperature, the solvent was removed under reduced pressure and Et_2O (100 mL) was added. The organic layer was washed with aqueous $NaHCO_3$ (1 M, 60 mL), aqueous NaCl (1 M, 60 mL) and H_2O (60 mL) and was dried over $MgSO_4$. The solvent was removed under reduced pressure and the residue placed on a 5 cm silica pad and eluted with hexane : CH_2Cl_2 (1 : 1). Removal of the solvent and drying under reduced pressure gave **46** (0.54 g, 51%) as a colourless solid. ^{1}H NMR (500 MHz, $CDCl_3$, δ): 7.15 (d, 2H, $J_{H\text{-}F}$ = 7 Hz, Ar), 3.92 (s, 3H, OMe); $^{13}C\{^1H\}$ NMR (125 MHz, $CDCl_3$, δ): 161.5, 160.9 (d, $J_{C\text{-}F}$ = 261 Hz), 125.8, 116.5, 116.3, 53.2; ^{19}F NMR (470 MHz, $CDCl_3$, δ): -108.60 (d, $J_{H\text{-}F}$ = 7 Hz); EIMS *m/z*: 250 (M^+); Anal. Calcd for $C_8H_5BrF_2O_2$: C, 38.28; H, 2.01. Found: C, 37.49; H, 1.95.

47: 1,3,5-tris(2,6-difluoro-4-carbomethoxylphenyl)benzene

In a nitrogen filled glove box, 1,4-dioxane (4 mL) was added to a microwave vial containing **42** (0.15 g, 0.50 mmol), 1,3,5-tribromobenzene (0.046 g, 0.15 mmol), $PdCl_2$(dppf) (0.007 g, 0.010 mmol). To this mixture was added KOH (0.042 g, 0.75 mmol) in H_2O (0.5 mL). The vial was capped and the mixture heated at 80 ºC for 1 h in the microwave reactor. After cooling to room temperature, the solvent was removed under reduced pressure. The residue was purified by column chromatography (hexane : ethyl acetate, 7 : 3) and the resulting product was dissolved in $CHCl_3$ (5 mL) and

precipitated with hexane (60 mL). Filtration and drying under vacuum gave **47** (0.024 g, 27%) as a white solid. ^{1}H NMR (700 MHz, $CDCl_3$, δ): 7.74 (s, 3H), 7.24 (d, 6H, $J_{H\text{-}F}$ = 10 Hz, Ar), 3.97 (s, 9H, OMe); ^{13}C{^{1}H} NMR (175 MHz, $CDCl_3$, δ): 161.9, 161.5 (d, $J_{C\text{-}F}$ = 258 Hz), 145.2, 140.3, 126.5, 111.2, 111.0, 53.1; ^{19}F{^{1}H} NMR (658 MHz, $CDCl_3$, δ): -108.5; ASAP-MS *m/z*: 588 (M^+); Anal. Calcd for $C_{30}H_{18}F_6O_6$: C, 61.23; H, 3.08. Found: C, 61.07; H, 3.02.

48: 9,10-bis(2,6-difluoro-4-carbomethoxylphenyl)anthracene

In a nitrogen-filled glove box, 1,4-dioxane (4 mL) was added to a microwave vial containing **42** (0.15 g, 0.50 mmol), 9,10-dibromoanthracene (0.073 g, 0.22 mmol), $PdCl_2$(dppf) (0.007 g, 0.010 mmol). To this mixture was added KOH (0.062 g, 1.10 mmol) in H_2O (0.5 mL). The vial was capped and the mixture heated at 80 ºC for 1 h in the microwave reactor. After cooling to room temperature, the solvent was removed under reduced pressure. The residue was purified by column chromatography (hexane : CH_2Cl_2, 7 : 3) and the resulting product was dissolved in CH_2Cl_2 (5 mL) and precipitated with hexane (60 mL). Filtration and drying under vacuum gave **48** (0.03 g, 26%) as a yellow solid. ^{1}H NMR (700 MHz, C_6D_6, δ): 7.40 (AA' part of AA'BB' system, 4H), 7.10 (BB' part of AA'BB' system, 4H), 6.68 (d, 4H, $J_{H\text{-}F}$ = 8 Hz, Ar), 3.56 (s, 6H, OMe); ^{13}C{^{1}H} NMR (175 MHz, C_6D_6, δ): 162.0, 161.4 (d, $J_{C\text{-}F}$ = 263 Hz), 145.1, 143.2, 135.1, 126.8, 126.7, 115.7, 115.5, 52.9; ^{19}F NMR (658 MHz, C_6D_6, δ): -109.9 ($J_{F\text{-}H}$ = 8 Hz); ASAP-MS *m/z*: 519 ($M+H^+$); Anal. Calcd for $C_{30}H_{18}F_4O_4$: C, 69.50; H, 3.50. Found: C, 68.78; H, 3.49.

49: 3,5,3',5'-Tetrafluoro-biphenyl-4,4'-dicarboxylic acid

In a nitrogen-filled glove box, 1,4-dioxane (4 mL) was added to a microwave vial containing **46** (0.07 g, 0.28 mmol), **42** (0.08 g, 0.27 mmol), $PdCl_2$(dppf) (0.004 g, 0.005 mmol). To this mixture was added KOH (0.076 g, 1.35 mmol) in H_2O (0.5 mL). The vial was capped and the mixture heated at 80 ºC for 1 h in the microwave. After cooling to room temperature, the solvent was removed under reduced pressure. HCl (1 M, 30 mL) was then added and the product extracted into Et_2O (3 × 30 mL) and dried over $MgSO_4$. The solvent was removed under reduced pressure and the residue washed with hexane (3 × 10 mL) to give **49** (0.02 g, 24%) as a light brown solid. ^{1}H NMR (700 MHz, DMSO-d_6, δ): 7.75 (d, 4H, $J_{H\text{-}F}$ = 9 Hz, Ar) acidic protons not observed; ^{13}C{^{1}H}

NMR (175 MHz, DMSO-d_6, δ): 161.8, 159.6 (d, $J_{C\text{-}F}$ = 249 Hz), 141.0, 111.0, 110.9; ^{19}F NMR (658 MHz, DMSO-d_6, δ): -111.2 (d, $J_{H\text{-}F}$ = 9 Hz); ES-MS *m/z*: 627 ($2M\text{-}H^-$), 313 ($M\text{-}H^-$), 269 ($M\text{-}CO_2H_2^-$).

50: 2,7-bis(2,6-difluoro-benzoic acid methyl ester)pyrene

In a nitrogen filled glove box, DMF (7 mL) was added to a Young's tube containing pyrne-2,7-bis(boronicacid) **4** (0.088 g, 0.30 mmol), **46** (0.15 g, 0.60 mmol), $PdCl_2$(dppf) (0.015 g, 0.02 mmol) and K_3PO_4 (0.32 g, 1.51 mmol). The tube was sealed and the mixture was stirred at 80 ºC for 64 h. HCl (1 M, 10 mL) was added and the product was extracted into CH_2Cl_2 (3 × 30 mL), the collected organic layers were washed with brine (2 × 50 mL), H_2O (50 mL) and dried over $MgSO_4$. The solvent was removed under reduced pressure and the residue was purified by column chromatography (hexane : CH_2Cl_2, 1 : 1, then CH_2Cl_2) and the resulting product was dissolved in $CHCl_3$ (5 mL) and precipitated with hexane (60 mL). Filtration and drying under vacuum gave **50** (0.045 g, 28%) as a cream solid. ^{1}H NMR (700 MHz, $CDCl_3$, δ): 8.36 (s, 4H), 8.17 (s, 4H), 7.49 (d, 4H, $J_{H\text{-}F}$ = 8 Hz, Ar), 4.00 (s, 6H, OMe); $^{13}C\{^1H\}$ NMR (175 MHz, $CDCl_3$, δ): 162.2, 161.5 (d, $J_{C\text{-}F}$ = 254 Hz), 136.1, 132.1, 131.5, 128.6, 126.0, 124.6, 123.9, 111.7, 111.5, 53.1; ^{19}F NMR (658 MHz, $CDCl_3$, δ): -109.1 ($J_{F\text{-}H}$ = 8 Hz); ASAP-MS *m/z*: 543 ($M+H^+$).

53: 2,4-Di-tert-butyl-6-{4-(4,4,5,5-tetramethyl-[1,3,2]dioxaborolan-2-yl)-6-[3-(4,4,5,5-tetramethyl-[1,3,2]dioxaborolan-2-yl)-5-trifluoromethyl-phenyl]-pyridin-2-yl}-phenol

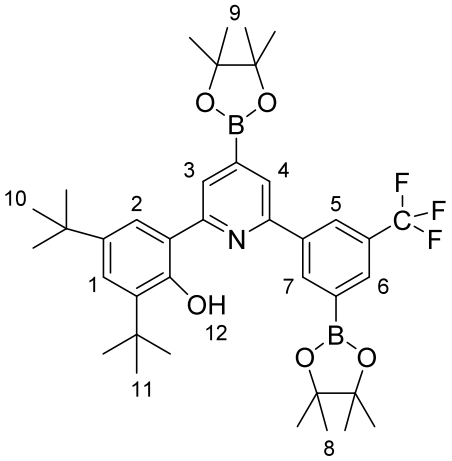

^{1}H NMR Labels

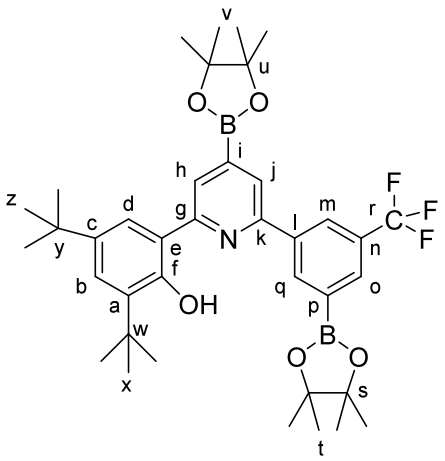

^{13}C NMR Labels

In a nitrogen-filled glove box, $[Ir(OMe)COD]_2$ (0.008 g, 0.012 mmol), dtbpy (0.006 g, 0.022 mmol) and B_2pin_2 (0.01 g, 0.04 mmol) were dissolved in MTBE (5 mL). The mixture was added to a microwave vial containing **51** (0.10 g, 0.23 mmol) and B_2pin_2 (0.11 g, 0.43 mmol). The tube was sealed and the mixture was stirred at 80 ºC for 30 min under microwave heating. Then, the reaction mixture was passed through a 5 cm silica pad eluting with hexane : CH_2Cl_2 (3:1) and the solvent was removed under reduced pressure to give **53** (0.13 g, 83%) as a yellow oil. Recrystallization from hexane gave a yellow powder. ^{1}H NMR (500 MHz, $CDCl_3$, δ): 8.61 (s, 1H, **7**), 8.32 (s, 1H, **6**), 8.21 (s, 1H, **3**), 8.14 (s, 1H, **5**), 8.01 (s, 1H, **4**), 7.42 (d, 1H, *J* = 3 Hz, **2**), 7.32 (d, 1H, *J* = 3 Hz, **1**), 1.50 (s, 9H, **11**), 1.42 (s, 12H, **9**), 1.40 (s, 9H, **10**), 1.38 (s, 12H, **8**), OH signal not observed; ^{13}C{^{1}H} NMR (125 MHz, $CDCl_3$, δ): 158.8 (**g**), 156.8 (**f**), 152.3 (**k**), 140.1 (**c**), 138.7 (**l**), 137.7 (**a**), 136.9 (**q**), 132.1 (**m**), 131.0 (q, $^2J_{C\text{-}F}$ = 42 Hz, **n**), 129.9 (**i/p**), 126.5 (2 peaks, **b** + **o**), 124.6 (**h**), 124.4 (q, $J_{C\text{-}F}$ = 273 Hz, **r**), 123.4 (**j**), 121.5 (**d**), 118.5 (**e**), 85.1 (**s/u**), 84.7 (**s/u**), 35.6 (**w**), 34.6 (**y**), 31.9 (**z**), 29.8 (**x**), 25.1 (**v+t**), second carbon attached to B not observed; ^{11}B{^{1}H} NMR (224 MHz, C_6D_6, δ): 30.1; MS-ASAP: *m/z* 680 $(M+H)^+$; HRMS-ASAP: $(M-H)^+$ Calcd for $C_{38}H_{51}{}^{10}B_2NO_5F_3$ 678.3978; Found 678.3953. ^{1}H, ^{13}C, HSQC and HMBC NMR spectra are shown in the appendix.

54: 2-(3,5-Di-tert-butyl-2-methoxy-phenyl)-4-(4,4,5,5-tetramethyl-[1,3,2]dioxaborolan-2-yl)-6-[3-(4,4,5,5-tetramethyl-[1,3,2]dioxaborolan-2-yl)-5-trifluoromethyl-phenyl]-pyridine

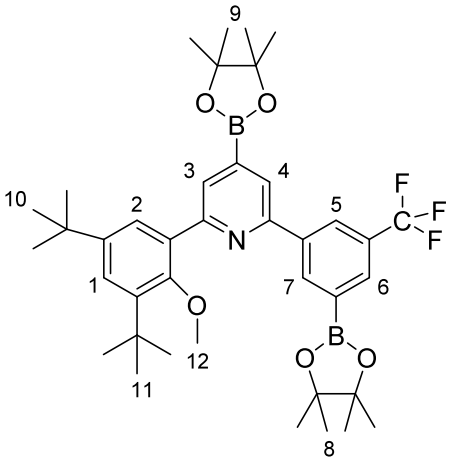

^{1}H NMR Labels

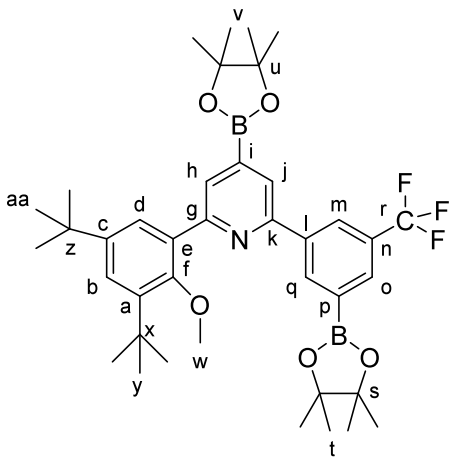

^{13}C NMR Labels

In a nitrogen-filled glove box, $[Ir(OMe)COD]_2$ (0.008 g, 0.012 mmol), dtbpy (0.006 g, 0.022 mmol) and B_2pin_2 (0.01 g, 0.04 mmol) were dissolved in MTBE (5 mL). The mixture was added to a microwave vial containing **52** (0.10 g, 0.23 mmol) and B_2pin_2 (0.11 g, 0.43 mmol). The tube was sealed and the mixture was stirred at 80 ºC for 30 min under microwave heating. Then, the reaction mixture was passed through a 5 cm silica pad eluting with hexane : CH_2Cl_2 (3:1) and the solvent was removed under reduced pressure to give **54** (0.10 g, 64%) as an orange oil. Recrystallization from hexane gave colourless crystals. ^{1}H NMR (500 MHz, $CDCl_3$, δ): 8.71 (s, 1H, **7**), 8.54 (s, 1H, **6**), 8.09 (br s, 2H, **3** + **5**), 8.07 (s, 1H, **4**) 7.62 (d, 1H, J = 3 Hz, **2**), 7.39 (d, 1H, J = 3 Hz, **1**), 3.38 (s, 3H, **12**), 1.45 (s, 9H, **11**), 1.38 (s, 12H, **8**), 1.37 (s, 12H, **9**), 1.36 (s, 9H, **10**); ^{13}C{^{1}H} NMR (125 MHz, $CDCl_3$, δ): 157.9 (**g**), 155.9 (**f**), 155.1 (**k**), 145.6 (**c**), 142.1 (**a**), 139.9 (**l**), 137.9 (**i/p**), 136.6 (**q**), 133.3 (**n**), 131.7 (**m**), 130.8 (**i/p**), 129.1 (**h**), 127.2 (**d**), 126.9 (**o**), 124.8 (**b**), 124.1 (q, $J_{C\text{-}F}$ = 272 Hz, **r**), 123.5 (**j**), 84.8 (**s/u**), 84.5 (**s/u**), 61.7 (**w**), 35.6 (**x**), 34.8 (**z**), 31.7 (**y**), 31.2 (**aa**), 25.1 (**v+t**), signal for **e** not observed; ^{11}B{^{1}H} NMR (224 MHz, C_6D_6, δ): 30.0; MS-ASAP: *m/z* 694 $(M+H)^+$; HRMS-ASAP: $(M-H)^+$ Calcd for $C_{39}H_{53}{}^{10}B_2NO_5F_3$ 692.4135; Found 692.4147. ^{1}H, ^{13}C, HSQC and HMBC NMR spectra are shown in the appendix.

55: 3,8-Bis-(4,4,5,5-tetramethyl-[1,3,2]dioxaborolan-2-yl)-[1,10]phenanthroline
In a nitrogen-filled glove box, $[Ir(OMe)COD]_2$ (0.050 g, 0.075 mmol), 4,4'-di-^{t}Bu-2,2'-bipyridine (dtbpy, 0.01 g, 0.037 mmol) and B_2pin_2 (1.35 g, 5.32 mmol) were dissolved in MTBE (10 mL). Using a syringe 2 mL of this stock solution was added to a microwave vial, containing 1,10-phenanthroline (0.10 g, 0.55 mmol). The vial was capped and the reaction mixture was heated for 30 min at 100 ºC in a microwave reactor. After cooling to room temperature, the solvent was removed under reduced pressure to give a black residue. ^{1}H NMR (400 MHz, $CDCl_3$, δ): 10.03 (s, 2H), 8.64 (s, 2H), 7.26 (s, 2H), 1.03 (s, 24H); EIMS *m/z*: 432 (M^+).

56: 3-(4,4,5,5-Tetramethyl-[1,3,2]dioxaborolan-2-yl)-[1,10]phenanthroline
In a nitrogen-filled glove box, $[Ir(OMe)COD]_2$ (0.010 g, 0.015 mmol), 4,4'-di-^{t}Bu-2,2'-bipyridine (dtbpy, 0.01 g, 0.037 mmol) and B_2pin_2 (0.29 g, 1.14 mmol) were dissolved in MTBE (4 mL). This solution was then added to a microwave vial, containing 1,10-phenanthroline (0.10 g, 0.55 mmol). The vial was capped and the reaction mixture was

heated for 30 min at 100 ºC in a microwave reactor. After cooling to room temperature, the solvent was removed under reduced pressure to give a black residue. EIMS *m/z*: 310 (M^+).

57: 1,1'-bis(4,4,5,5-Tetramethyl-[1,3,2]dioxaborolan-2-yl)ferrocene

Compound supplied by the group of Professor Raymond Wong (Hong Kong Baptist University). ^{1}H NMR (400 MHz, $CDCl_3$, δ): 4.39 (m, 4H), 4.35 (m, 4H), 1.33 (s, 24H); $^{13}C\{^1H\}$ NMR (100 MHz, $CDCl_3$, δ): 83.4, 74.7, 73.1, 25.1, C next to B not observed; EIMS *m/z*: 438 (M^+); Anal. Calcd for $C_{22}H_{32}B_2FeO_4$: C, 60.33; H, 7.36. Found: C, 60.49; H, 7.31.

58: 1,1'-bis(4-bromophenyl)ferrocene

Under a nitrogen atmosphere, to a mixture containing nBuLi (3.50 mL, 5.65 mmol, 1.6 M in hexane), TMEDA (0.66 g, 5.68 mmol) in Et_2O (20 mL) was slowly added a solution of ferrocene (0.50 g, 2.69 mmol) in Et_2O (10 mL). The mixture was stirred overnight then cooled to 0 ºC. $ZnCl_2$ (0.77g, 5.65 mmol) in THF (2 mL) was added via syringe and the mixture stirred for 2 h, $MgCl_2$ (0.54 g, 5.67 mmol) was then added and the mixture stirred for a further 2 h. In a separate flask, DIBAL-H (0.27 mL, 0.27 mmol, 1 M in hexane) was added to a solution of $PdCl_2(PPh_3)_2$ (0.09 g, 0.13 mmol) in Et_2O (5 mL), this mixture was then added to the ferrocene solution, followed by 1-bromo-4-iodo-benzene (1.60 g, 5.66 mmol) in Et_2O (5 mL). The reaction was stirred at 80 ºC for 5 h, and then quenched with aqueous NaOH (1 M, 50 mL), the crude mixture was extracted with CH_2Cl_2 (3 × 100 mL), dried over $MgSO_4$ and the solvent was removed under reduced pressure. Purification by column chromatography (silica gel, petroleum ether : CH_2Cl_2, 4 : 1) gave **58** (0.08 g, 6%) as a bright orange solid. ^{1}H NMR (700 MHz, $CDCl_3$, δ): 7.25 (d, J = 7 Hz, 2H), 7.04 (d, J = 7 Hz, 2H), 4.43 (br s, 2H), 4.22 (br s, 2H); $^{13}C\{^1H\}$ NMR (175 MHz, $CDCl_3$, δ): 136.8, 131.6, 127.5, 119.7, 85.2, 70.8, 67.9; EIMS *m/z*: 496 (M^+); Anal. Calcd for $C_{22}H_{16}Br_2Fe$: C, 53.27; H, 3.25. Found: C, 53.54; H, 3.28.

61: 1-(4,4,5,5-Tetramethyl-[1,3,2]dioxaborolane)ferrocene

Compound synthesized as previously reported.[10] Crystals were obtained from recrystallization with pentane. ^{1}H NMR (400 MHz, $CDCl_3$, δ): 4.50 (br s, 2H), 4.45 (br s, 2H), 4.22 (s, 5H), 1.31 (s, 12H); EIMS *m/z*: 312 (M^+).

6.0 References

[1] (a) Kakiuchi, F.; Murai, S. *Top. Organomet. Chem.* **1999**, *3*, 47-79. (b) Crabtree, R. H. *J. Chem. Soc., Dalton Trans.* **2001**, 2437-2450. (c) Kalyani, D.; Sanford, M. S. *Top. Organomet. Chem.* **2007**, *24*, 85-116. (d) Goldberg, K. I. and Goldman, A. S., Eds. *Activation and Functionalization of C-H Bonds*; ACS Symposium Series; American Chemical Society: Washington, DC, 2004; Vol. 885. (e) Selective Functionalization of C-H Bonds. *Chem. Rev.* **2010**, *110*, 575-1211. (f) Catalytic C-H and C-X Bond Activation. *Dalton Trans.* **2010**, *39*, 309-536.

[2] Mkhalid, I. A. I.; Barnard, J. H.; Marder, T. B.; Murphy, J. M.; Hartwig, J. F. *Chem. Rev.* **2010**, *110*, 890-931.

[3] (a) Ishiyama, T.; Takagi, J.; Ishida, K.; Miyaura, N.; Anastasi, N. R.; Hartwig, J. F. *J. Am. Chem. Soc.* **2002**, *124*, 390-391. (b) Boller, T. M.; Murphy, J. M.; Hapke, M.; Ishiyama, T.; Miyaura, N.; Hartwig, J. F. *J. Am. Chem. Soc.* **2005**, *127*, 14263-14278.

[4] (a) Tse, M. K.; Cho, J. Y.; Smith, M. R., III. *Org. Lett.* **2001**, *3*, 2831-2833. (b) Cho, J.-Y.; Tse, M. K.; Holmes, D.; Maleczka, R. E., Jr.; Smith, M. R., III. *Science* **2002**, *295*, 305-308.

[5] Nguyen, P.; Blom, H. P.; Westcott, S. A.; Taylor, N. J.; Marder, T. B. *J. Am. Chem. Soc.* **1993**, *115*, 9329-9330.

[6] Ishiyama, T.; Takagi, J.; Hartwig, J. F.; Miyaura, N. *Angew. Chem., Int. Ed.* **2002**, *41*, 3056-3058.

[7] Tamura, H.; Yamazaki, H.; Sato, H.; Sakaki, S. *J. Am. Chem. Soc.* **2003**, *125*, 16114-16126.

[8] (a) Ishiyama, T.; Miyaura, N. *J. Organomet. Chem.* **2003**, *680*, 3-11. (b) Vanchura, B. A., II; Preshlock, S. M.; Roosen, P. C.; Kallepalli, V. A.; Staples, R. J.; Maleczka, R. E., Jr.; Singleton, D. A.; Smith, M. R., III. *Chem. Commun.* **2010**, *46*, 7724-7726.

[9] (a) Takagi, J.; Sato, K.; Hartwig, J. F.; Ishiyama, T.; Miyaura, N. *Tetrahedron Lett.* **2002**, *43*, 5649-5651. (b) Ishiyama, T.; Takagi, J.; Yonekawa, Y.; Hartwig, J. F.; Miyaura, N. *Adv. Synth. Catal.* **2003**, *345*, 1103-1106. (c) Ishiyama, T.; Nobuta, Y.; Hartwig, J. F.; Miyaura, N. *Chem. Commun.* **2003**, 2924-2925. (d) Mkhalid, I. A. I.; Coventry, D. N.; Albesa-Jové, D.; Batsanov, A. S.; Howard, J. A. K.; Marder, T. B.; Perutz, R. N. *Angew. Chem. Int. Ed.* **2006**, *45*, 489-491.

[10] Datta, A.; Kollhofer, A.; Plenio, H. *Chem. Commun.* **2004**, 1508-1509.

[11] (a) Coventry, D. N.; Batsanov, A. S.; Goeta, A. E.; Howard, J. A. K.; Marder, T. B.; Perutz, R. N. *Chem. Commun.* **2005**, 2172-2174. (b) Crawford, A. G.; Liu, Z.; Mkhalid, I. A. I.; Thibault, M.-H.; Schwarz, N.; Alcaraz, G.; Steffen, A.; Batsanov, A. S.; Howard, J. A. K.; Dwyer, A. D.; Beeby, A.; Pålsson, L.-O.; Tozer, D. J.; Marder, T. B. , 93rd Canadian Chemistry Conference and Exhibition, Toronto, Canada, May 29 - June 2, 2010, *Abstract* 0964.

[12] (a) Hata, H.; Shinokubo, H.; Osuka, A. *J. Am. Chem. Soc.* **2005**, *127*, 8264-8265. (b) Hiroto, S.; Hisaki, I.; Shinokubo, H.; Osuka, A. *Angew. Chem. Int. Ed.* **2005**, *44*, 6763-6766. (c) Hata, H.; Yamaguchi, S.; Mori, G.; Nakazono, S.; Katoh, T.; Takatsu, K.; Hiroto, S.; Shinokubo, H.; Osuka, A. *Chem. Asian J.* **2007**, *2*, 849-859. (d) Mori, G.; Shinokubo, H.; Osuka, A. *Tetrahedron Lett.* **2008**, *49*, 2170-2172.

[13] (a) Maleczka, R. E., Jr.; Shi, F.; Holmes, D.; Smith, M. R., III. *J. Am. Chem. Soc.* **2003**, *125*, 7792-7793. (b) Holmes, D.; Chotana, G. A.; Maleczka, R. E., Jr.; Smith, M. R., III. *Org. Lett.* **2006**, *8*, 1407-1410. (c) Murphy, J. M.; Liao, X.; Hartwig, J. F. *J. Am. Chem. Soc.* **2007**, *129*, 15434-15435. (d) Tzschucke, C. C.; Murphy, J. M.; Hartwig, J. F. *Org. Lett.* **2007**, *9*, 761-764. (e) Murphy, J. M.; Tzschucke, C. C.; Hartwig, J. F. *Org. Lett.* **2007**, *9*, 757-760. (f) Kikuchi, T.; Nobuta, Y.; Umeda, J.; Yamamoto, Y.; Ishiyama, T.; Miyaura, N. *Tetrahedron* **2008**, *64*, 4967-4971. (g) Harrisson, P.; Morris, J.; Steel, P. G.; Marder, T. B. *Synlett* **2009**, 147-150. (h) Liskey, C. W.; Liao, X.;

Hartwig, J. F. *J. Am. Chem. Soc.* **2010**, *132*, 11389-11391. (i) Tajuddin, H.; Shukla, L.; Maxwell, A. C.; Marder, T. B.; Steel, P. G. *Org. Lett.* **2010**, *12*, 5700-5703.

[14] (a) Ishiyama, T.; Nobuta, Y.; Hartwig, J. F.; Miyaura, N. *Chem. Commun.* **2003**, 2924-2925. (b) Boebel, T. A.; Hartwig, J. F. *J. Am. Chem. Soc.* **2008**, *130*, 7534-7535. (c) Kawamorita, S.; Ohmiya, H.; Hara, K.; Fukuoka, A.; Sawamura, M. *J. Am. Chem. Soc.* **2009**, *131*, 5058-5059. (d) Hartung, C. G.; Snieckus, V. *The Directed ortho-Metalation Reaction. A Point of Departure for New Synthetic Aromatic Chemistry*, Wiley-VCH: New York, 2002 (e) Hurst, T. E.; Macklin, T. K.; Becker, M.; Hartmann, E.; Kügel, W.; Parisienne-La Salle, J.-C.; Batsanov, A. S.; Marder, T. B.; Snieckus, V. *Chem. Eur. J.* **2010**, *16*, 8155-8161.

[15] Bitterlich, B. *Unpublished results*.

[16] (a) Noguchi, H.; Hojo, K.; Suginome, M. *J. Am. Chem. Soc.* **2007**, *129*, 758-759. (b) Iwadate, N.; Suginome, M. *Org. Lett.* **2009**, *11*, 1899-1902.

[17] (a) Welch, C. N.; Shore, S. G. *Inorg. Chem.* **1968**, *7*, 225-230. (b) Kleeberg, C. H.; Bitterlich, B.; Sasaki. K.; Trenholme, W. *Unpublished results*.

[18] Ishiyama, T.; Murata, M.; Miyaura, N. *J. Org. Chem.* **1995**, *60*, 7508-7510.

[19] Murata, M.; Oyama, T.; Watanabe, S.; Masuda, Y. *J. Org. Chem.* **2000**, *65*, 164-168.

[20] Kleeberg, C.; Dang, L.; Lin, Z.; Marder, T. B. *Angew. Chem., Int. Ed.* **2009**, *48*, 5350-5354.

[21] (a) Diederich, F., Stang, P. J., Ed. *Metal-catalyzed Cross-coupling Reactions*, Wiley-VCH: Weinheim, 1998. (b) Marder, T. B. Organometallics in Synthesis Course Notes, Durham University, 2007.

[22] Lam, K. C.; Marder, T. B.; Lin, Z. *Organometallics* **2007**, *26*, 758-760.

[23] Galardon, E.; Ramdeehul, S.; Brown, J. M.; Cowley, A.; Hii, K. K.; Jutand, A. *Angew. Chem. Int. Ed.* **2002**, *41*, 1760-1763.

[24] (a) Hatanaka, Y.; Hiyama, T. *J. Org. Chem.* **1988**, *53*, 918-920. (b) Paul, F.; Patt, J.; Hartwig, J. F. *J. Am. Chem. Soc.* **1994**, *116*, 5969-5970. (c) Hartwig, J. F.; Paul, F. *J.*

Am. Chem. Soc. **1995**, *117*, 5373-5374. (d) Littke, A. F.; Dai, C.; Fu, G. C. *J. Am. Chem. Soc.* **2000**, *122*, 4020-4028. (e) Roy, A. H.; Hartwig, J. F. *J. Am. Chem. Soc.* **2001**, *123*, 1232-1233. (f) Stambuli, J. P.; Bühl, M.; Hartwig, J. F. *J. Am. Chem. Soc.* **2002**, *124*, 9346-9347. (g) Roy, A. H.; Hartwig, J. F. *J. Am. Chem. Soc.* **2003**, *125*, 13944-133945. (h) Roy, A. H.; Hartwig, J. F. *Organometallics* **2004**, *23*, 1533-1542.

[25] (a) Fauvarque, J.-F.; Pflüger, F.; Troupel, M. *J. Organomet. Chem.* **1981**, *208*, 419-427. (b) Amatore, C.; Pflüger, F. *Organometallics* **1990**, *9*, 2276-2282.

[26] Hartwig, J. F.; Barrios-Landeros, F. *J. Am. Chem. Soc.* **2005**, *127*, 6944-6945.

[27] Miyaura, N. *J. Organomet. Chem.* **2002**, *653*, 54-57.

[28] Lei, A.; Liu, W.; Liu, C.; Chen, M. *Dalton Trans.* **2010**, *39*, 10352-10362.

[29] (a) James, S. L. *Chem. Soc. Rev.* **2003**, *32*, 276-288. (b) Janiak, C.; Vieth, J. K. *New J. Chem.* **2010**, *34*, 2366-2388. (c) *Functional Metal-Organic Frameworks: Gas Storage, Separation and Catalysis*; Schröder, M., Ed.; Topics in Current Chemistry 293; Springer-Verlag: Berlin, 2010.

[30] (a) Sun, Y.–Q.; He, J.; Xu, Z.; Huang, G.; Zhou, X.–P.; Zeller, M.; Hunter, A. D. *Chem. Commun.* **2007**, 4779-4781 (b) Sun, Y.–Q.; Yang, C.; Xu, Z.; Zeller, M.; Hunter, A. D. *Crystal Growth & Design.* **2009**, *9*, 1663-1665. (c) Huang, G.; Yang, C.; Xu, Z.; Wu, H.; Li, J.; Zeller, M.; Hunter, A. D.; Chui, S. S.–Y.; Che, C.–M. *Chem. Mater.* **2009**, *21*, 541-546.

[31] Chotana, G. A.; Rak, M. A.; Smith, M. R., III. *J. Am. Chem. Soc.* **2005**, *127*, 10539-10544.

[32] (a) McMurry, J. *Organic Chemistry*, 3rd ed.; Brooks-Cole Publishing: Pacific Grove, California, 1992, p573-576. (b) Clayden, J.; Greeves, N.; Warren, S.; Wothers, P. *Organic Chemistry*, 1st ed.; Oxford University Press: Oxford, 2001.

[33] Harrisson, P.; Morris, J.; Marder, T. B.; Steel, P. G. *Org. Lett.* **2009**, *11*, 3586-3589.

[34] Iyoda, M.; Otsuka, H.; Sato, K.; Nisato, N.; Oda, M. *Bull. Chem. Soc. Jpn.* **1990**, *63*, 80-87.

[35] (a) Ittel, S. D.; Johnson, L. K.; Brookhart, M. *Chem. Rev.* **2000**, *100*, 1169-1204. (b) Gibson, V. C.; Spitzmesser, S. K. *Chem. Rev.* **2003**, *103*, 283-316. (c) Resconi, L.; Chadwick, J. C.; Cavallo, L. In *Comprehensive Organometallic Chemistry III*; Crabtree, R. H., Mingos, D. M. P., Bochmann, M., Eds.; Elsevier: Oxford, U.K., 2007; Vol. 4, pp 1005-1166. (d) Fujita, T.; Makio, H. In *Comprehensive Organometallic Chemistry III*; Crabtree, R. H., Mingos, D. M. P., Hiyama, T., Eds.; Elsevier: Oxford, U.K., 2007; Vol. 11, pp 691-734.

[36] Chan, M. C. W.; Tam, K.–H.; Pui, Y.–L.; Zhu, N. *J. Chem. Soc., Dalton. Trans.* **2002**, 3085-3087. (b) Chan, M. C. W.; Tam, K.–H.; Zhu, N.; Chiu, P.; Matsui, S. *Organometallics* **2006**, *25*, 785-792. (c) Tam, K.–H.; Lo, J. C. Y.; Guo, Z.; Chan, M. C. W. *J. Organomet. Chem.* **2007**, *692*, 4750-4759. (d) Tam, K.–H.; Chan, M. C. W.; Kaneyoshi, H.; Makio, H.; Zhu, N. *Organometallics* **2009**, *28*, 5877-5882.

[37] Bencini, A.; Lippolis, V. *Coord. Chem. Rev.* **2010**, *254*, 2096-2180.

[38] Dénes, V.; Chira, R. *J. Prakt. Chem.* **1978**, *320*, 172-175.

[39] Tzalis, D.; Tor, Y.; Failla, S.; Siegel, J. *Tetrahedron. Lett.* **1995**, *36*, 3489-3490.

[40] (a) Yamada, M.; Nakamura, Y.; Kuroda, S.; Shimao, I. *Bull. Chem. Soc. Jpn.* **1990**, *63*, 2710-2712. (b) Yamada, N.; Nakamura, Y.; Hasegawa, T.; Itoh, A.; Kuroda, S.; Shimao, I. *Bull. Chem. Soc. Jpn.* **1992**, *65*, 2007-2009.

[41] Saitoh, Y.; Koizumi, T.; Osakada, K.; Yamamoto, T. *Can. J. Chem.* **1997**, *75*, 1336-1339.

[42] Liu, S.–X.; Michel, C.; Schmittel, M. *Org. Lett.* **2000**, *2*, 3959-3962.

[43] (a) Wong, W.-Y.; Wang, X.-Z.; He, Z.; Djurisic, A. B.; Yip, C.-T.; Cheung, K.-Y.; Wang, H.; Mak, C. S. K.; Chan, W.-K. *Nat. Mater.* **2007**, *6*, 521-527. (b) Li, L.; Ho, C.-L.; Wong, W.-Y.; Cheung, K.-Y.; Fung, M.-K.; Lam, W.-T.; Djurisic, A. B.; Chan, W.-K. *Adv. Funct. Mater.* **2008**, *18*, 2824-2833. (c) Zhou, G.-J.; Wong, W.-Y.; Poon, S.-Y.; Ye, C.; Lin, Z.-Y. *Adv. Funct. Mater.* **2009**, *19*, 531-544. (d) Wong, W.-Y.; Ho, C.-L. *Acc. Chem. Res.* **2010**, *43*, 1246-1256.

[44] Deng, J. Z.; Paone, D. V.; Ginnetti, A. T.; Kurihara, H.; Dreher, S. D.; Weissman, A. A.; Stauffer, S. R.; Burgey, C. S. *Org. Lett.* **2009**, *11*, 345-347.

[45] Knapp, R.; Rehahn, M. *J. Organomet. Chem.* **1993**, *452*, 235-240.

[46] Baumgardt, I.; Butenschön, H. *Eur. J. Org. Chem.* **2010**, 1076-1087.

[47] Jin, L.; Liu, C.; Liu, J.; Hu, F.; Lan, Y.; Batsanov, A. S.; Howard, J. A. K.; Marder, T. B.; Lei, A. *J. Am. Chem. Soc.* **2009**, *131*, 16656-16657.

[48] (a) Wrackmeyer, B.; Dörfler, W.; Milius, W.; Herberhold, M. *Polyhedron* **1995**, *14*, 1425-1432. (b) Aldridge, S.; Bresner, C. *Coord. Chem. Rev.* **2003**, *244*, 71-92. (c) Scheibitz, M.; Bolte, M.; Bats, J. W.; Lerner, H. W.; Nowik, I.; Herber, R. H.; Krapp, A.; Lein, M.; Holthausen, M. C.; Wagner, M. *Chem. Eur. J.* **2005**, *11*, 584-603. (d) Braunschweig, H.; Fernandez, I.; Frenking, G.; Kupfer, T. *Angew. Chem. Int. Ed.* **2008**, *47*, 1951-1954.

[49] Braunschweig, H.; Grünewald, B.; Schwab, K.; Sigritz, R. *Eur. J. Inorg. Chem.* **2009**, 4860-4863.

[50] (a) Calabrese, J. C.; Cheng, L. T.; Green, J. C.; Marder, S. R.; Tam, W. *J. Am. Chem. Soc.* **1991**, *113*, 7227-7232. (b) Yuan, Z.; Taylor, N. J.; Sun, Y.; Marder, T. B.; Williams, I. D.; Cheng, L. T. *J. Organomet. Chem.* **1993**, *449*, 27-37. (c) Yuan, Z.; Stringer, G.; Jobe, I. R.; Kreller, D.; Scott, K.; Koch, L.; Taylor, N. J.; Marder, T. B. *J. Organomet. Chem.* **1993**, *452*, 115-120. (d) Elschenbroich, C.; Salzer, A. *Organometallics,* Wiley-VCH: Weinheim 2001, p 327. (e) Kinnibrugh, T. L.; Salman, S.; Getmanenko, Y. A.; Coropceanu, V.; Porter, W. W.; Timofeeva, T. V.; Matzger, A. J.; Bredas, J. L.; Marder, S. R.; Barlow, S. *Organometallics* **2009**, *28*, 1350-1357.

[51] (a) Kuivila, H. G.; Nahabedian, K. V. *J. Am. Chem. Soc.* **1961**, *83*, 2159-2168. (b) Florentin, D.; Fournié-Zaluski, M. C.; Callanquin, M.; Roques, B. P. *J. Heterocycl. Chem.* **1976**, *13*, 1265-1272. (c) Molander, G. A.; Biolatto, B. *J. Org. Chem.* **2003**, *68*, 4302-4314.

[52] Bresner, C.; Day, J. K.; Coombs, N. D.; Fallis, I. A.; Aldridge, S.; Coles, S. J.; Hursthouse, M. B. *Dalton Trans.* **2006**, 3660-3667.

Appendix

1.0 List of Publications

‘Synthetic and Crystallographic Studies of 2- and 2,7-Functionalized Pyrene Derivatives: An Application of Selective C-H Borylation’ Crawford, A. G.; Liu, Z.; Mkhalid, I. A. I.; Thibault, M.-H.; Schwarz, N.; Alcaraz, G.; Steffen, A.; Batsanov, A. S.; Howard, J. A. K.; Marder. T. B. *J. Am. Chem. Soc.,* Submitted for publication.

‘Experimental and Theoretical Studies of the Photophysical Properties of 2- and 2,7-Functionalized Pyrene Derivatives’ Crawford, A. G.; Dwyer, A. D.; Liu, Z.; Steffen, A.; Beeby, A.; Pålsson, L.-O.; Tozer, A. J.; Marder, T. B. *J. Am. Chem. Soc.,* Submitted for publication.

'Induced-Fit Binding of pi-Electron-Donor Substrates to Macrocyclic Aromatic Ether Imide Sulfones: A Versatile Approach to Molecular Assembly.'
Colquhoun, H. M.; Zhu, Z.; Williams, D. J.; Drew, M. G. B.; Cardin, C. J.; Gan, Y.; Crawford, A. G.; Marder, T. B. *Chem. Eur. J*. **2010**, *16*, 907-918.

'Borylene-Based Direct Functionalization of Organic Substrates: Synthesis, Characterization, and Photophyiscal Properties of Novel pi-conjugated Borirenes.'
Braunschweig, H.; Herbst, T.; Rais, D.; Ghosh, S.; Kupfer, T.; Radacki, K.; Crawford, A. G.; Ward, R. M.; Marder, T. B.; Fernández, I.; Frenking, G. *J. Am. Chem. Soc*. **2009**, *131*, 8989-8999.

2.0 List of Conferences Attended

‘Catalytic C-H and C-X Bond Activation’ Durham University, UK; 13-15th September 2010.

‘93rd Canadian Chemistry Conference and Exhibition’ Toronto, Canada; 29th May-2nd June 2010.

‘Catalysis: Fundamentals and Practice’ University of Liverpool, UK; 13-17th July 2009.

‘Mass Spectrometry Summer School’ Swansea University, UK; 1-3rd September 2008.

3.0 X-ray Experimental*

Single-crystal diffraction experiments (Section 4.0) were carried out on Bruker 3-circle diffractometers with CCD area detectors SMART 1000 (β-**1**, **2**·HFB, **7**, **10**, **16**, **17**-LT, **22**), SMART 6000 (**1**·2HFB, α and β-**1**·PhMe, α- and β-**2**, **3**, **9**, **11**, **15**, **17**-RT, **24**, **54**, **57**, **61**) or PLATINUM135 (γ-**1**) using graphite-monochromated K_a radiation from a sealed Mo-anode tube ($\bar{\lambda}$ = 0.71073 Å) or (for γ-**1**) a Microstar rotating Cu-anode source with cross-coupled Göbel mirrors ($\bar{\lambda}$ = 1.54184 Å). Crystals were cooled using Cobra (for γ-**1**) or Cryostream (Oxford Cryosystems) open-flow N_2 cryostats. The structures were solved by direct methods and refined by full-matrix least squares against F^2 of all data, using SHELXTL[1] and Olex2[2] software.

The crystal of β-**2** was non-merohedrally twinned by rotation around the reciprocal [0 1 1] axis (twin law −1 0 0 / −0.52 0.07 0.93 / −0.53 1.07 −0.07). Of the 23379 measured reflections, 5446 involved component 1 only, 5505 component 2 only and 12428 were overlapping; the component contributions were refined to 0.6685(4) and 0.3315(4). Reflection intensities from both components, corrected using the *TWINABS* program,[3] were used in the refinement, whereas the uncorrected data from component 1 gave an irreducible $R(F)$ = 0.14.

The triclinic lattice of **24** appears pseudo-monoclinic (with the unique axis *c*), but there is no corresponding pseudo-symmetry in the structure itself nor Laue pseudo-symmetry (R_{int} = 0.67). However, there is an approximate pseudo-monoclinic symmetry associated with the *C*-centred lattice derived from the reduced cell by the (−1 −1 0 / 1 −1 0 / 0 0 1) transformation, having the unit cell parameters a = 12.347, b = 10.234, c = 24.367 Å, α = 89.95, β = 90.38, γ = 89.69° and R_{int} = 0.26. The crystal was merohedrally twinned by rotation around the [1 1 0] real-space axis (twin law 0 −1 0 / −1 0 0 / 0 0 −1) with component contributions refined[4] to 0.915(1):0.085(1). Crystallographic data has been deposited with the Cambridge Crystallographic Data Centre as supplementary publication no. CCDC-779129-779147. These data can be obtained free of charge from the Cambridge Crystallographic Data Centre via www.ccdc.cam.ac.uk/data_request/cif.

* X-ray experimental compiled with the assistance of Dr Andrei Batsanov (Durham University).

[1] Sheldrick, G. M. *Acta Crystallogr*. **2008**, *A64*, 112-122.

[2] Dolomanov, O. V.; Bourhis, L. J.; Gildea, R. J.; Howard, J. A. K.; Puschmann, H. *J. Appl. Cryst*. **2009**, *42*, 339-341.

[3] Sheldrick, G. M. TWINABS, 2008, University of Göttingen.

[4] Herbst-Irmer, R.; Sheldrick, G. M. *Acta Crystallogr*. **1998**, *B54*, 443-449.

4.0 Crystal Data and Experimental Details

Table A1 (^{a} = non-standard setting)

Compound	β-**1**		γ-**1**		α-**1**·PhMe		β-**1**·PhMe	
Empirical formula	$C_{28}H_{32}B_2O_4$		$C_{28}H_{32}B_2O_4$		$C_{28}H_{32}B_2O_4 \cdot C_7H_8$		$C_{28}H_{32}B_2O_4 \cdot C_7H_8$	
Formula weight	454.16		454.16		546.29		546.29	
Temperature, K	120	290	120	290	120	230	120	230
Crystal system	monoclinic		monoclinic		triclinic		monoclinic	
Space group (no.)	$P2_1/n$ (#14^a)		$P2_1/n$ (#14^a)		$P\bar{1}$ (#2)		$P2_1/n$ (#14^a)	
a, Å	10.6980(4)	10.8827(7)	6.4525(1)	6.513(2)	7.2546(5)	7.287(2)	6.6050(4)	6.771(1)
b, Å	11.0555(6)	11.0789(6)	11.0823(2)	11.169(2)	9.8024(6)	9.924(3)	19.8267(12)	19.890(3)
c, Å	11.2465(6)	11.425(1)	16.9139(3)	17.126(4)	11.9441(8)	12.002(2)	11.7290(7)	11.848(2)
α, º	90	90	90	90	107.848(15)	108.13(2)	90	90
β, º	109.137(4)	109.625(5)	93.286(9)	93.38(2)	100.289(14)	100.46(2)	91.997(10)	92.92(2)
γ, º	90	90	90	90	101.533(15)	100.96(2)	90	90
V, Å^3	1256.6(1)	1297.5(2)	1207.50(4)	1243.6(6)	765.5(1)	782.4(4)	1535.04(16)	1593.5(5)
Z	2	2	2	2	1	1	2	2
ρ (calc.), g/cm^3	1.200	1.162	1.249	1.213	1.185	1.159	1.182	1.139
μ, mm^{-1}	0.08		0.64		0.08		0.07	
Refls collected	14824		6183		6951		22749	
Unique reflections	3547		2045		3503		4485	
Reflections I>2σ (I)	2881		1718		2316		2506	
R_{int}, %	3.1		2.1		7.8		8.4	
Refined parameters	218		158		193		234	
R(F) [I>2σ (I)], %	4.1		4.0		6.7		5.5	
wR(F^2) [all data], %	12.1		11.0		20.1		16.8	
CCDC dep. no.	779129		779130		779131		779132	

Compound	**1**·2HFB			α-**2**	β-**2**	**2**·HFB	**3**	**7**
Empirical formula	$C_{28}H_{32}B_2O_4 \cdot 2C_6F_6$			$C_{22}H_{21}BO_2$	$C_{22}H_{21}BO_2$	$C_{22}H_{21}BO_2 \cdot C_6F_6$	$C_{26}H_{29}BO_2$	$C_{24}H_{16}O_2$
Formula weight	826.28			328.20	328.20	514.26	384.30	336.37
Temperature, K	120	180	230	120	120	120	123	120
Crystal system	triclinic			monoclinic	triclinic	tetragonal	monoclinic	monoclinic
Space group (no.)	$P\bar{1}$ (#2)			$P2_1/n$ (#14[a])	$P\bar{1}$ (#2)	$P4_2/n$ (#86)	$P2_1$ (#4)	$P2_1/c$ (#14)
a, Å	6.9162(3)	6.9312(7)	6.9297(9)	25.4025(14)	6.9518(4)	26.578(2)	9.7268(5)	26.916(3)
b, Å	11.7567(5)	11.8046(11)	11.8666(14)	7.3852(4)	19.7285(12)	26.578(2)	12.3550(6)	6.7166(9)
c, Å	11.8539(5)	11.9300(13)	12.0462(17)	30.8651(15)	20.8481(12)	6.7405(10)	9.8841(5)	9.1495(11)
α, °	76.707(6)	76.822(8)	77.252(10)	90	70.17(2)	90	90	90
β, °	80.150(6)	80.464(8)	80.674(9)	113.39(1)	82.02(2)	90	115.812(7)	98.94(2)
γ, °	81.976(7)	81.938(9)	81.632(9)	90	87.41(2)	90	90	90
V, Å^3	919.14(7)	931.9(2)	947.2(3)	5314.7(5)	2663.6(4)	4761.5(9)	1069.3(1)	1634.0(3)
Z	1			12	6	8	2	4
ρ (calc.), g/cm^3	1.493			1.231	1.228	1.435	1.194	1.367
μ, mm^{-1}	0.14			0.08	0.08	0.07	0.07	0.09
Refls collected	16830			50216	20855	24260	14767	8120
Unique reflections	5361			9360	8937	4179	3245	3730
Reflections I>2σ (I)	4381			7345	5606	2451	2946	2923
R_{int}, %	2.8			3.4	3.8	11.1	2.7	9.6
Refined parameters	326			722	702	376	276	300
R(F) [I>2σ (I)], %	4.1			3.6	4.2	8.0	4.3	5.3
wR(F^2) [all data], %	12.1			9.6	9.4	12.2	12.2	14.1
CCDC dep. no.	779133			779140	779141	779142	779139	779147

Compound	**9**	**10**	**11**	**15**	**16**	**17**		**22**	**24**
Empirical formula	$C_{16}H_9BF_3^-K^+$	$C_{40}H_{35}B \cdot CDCl_3$	$C_{16}H_8Br_2$	$C_{16}H_{10}O_2$	$C_{16}H_{10}O$	$C_{18}H_8F_6O_6S_2$		$C_{26}H_{26}Si_2$	$C_{24}H_{14}$
Formula weight	308.14	646.86	360.04	234.24	218.24	498.36		394.65	302.35
Temperature, K	120	120	120	120	120	293	120	120	120
Crystal system	monoclinic	triclinic	monoclinic	monoclinic	monoclinic	monoclinic		monoclinic	triclinic
Space group (no.)	$P2_1/c$ (#14)	$P\bar{1}$ (#2)	$I2/m$ (#12[a])	$P2_1/c$ (#14)	$P2_1$ (#4)	$P2_1/c$ (#14)		$P2_1/c$ (#14)	$P\bar{1}$ (#2)
a, Å	20.707(1)	8.0386(5)	4.7115(3)	7.8951(4)	7.990(1)	16.1937(10)	16.083(2)	17.768(2)	7.9968(8)
b, Å	6.8278(4)	12.8471(8)	10.8788(8)	4.6096(3)	4.6472(6)	8.4509(5)	8.4858(10)	5.3992(5)	8.0398(7)
c, Å	9.0417(6)	16.5252(7)	11.5010(9)	14.3506(10)	13.899(2)	7.0509(4)	6.8530(9)	11.703(1)	24.367(2)
α, º	90	91.765(10)	90	90	90	90	90	90	89.74(1)
β, º	91.16(3)	98.809(9)	94.985(4)	91.51(1)	93.68(1)	93.617(3)	92.828(9)	98.76(1)	89.68(1)
γ, º	90	97.637(10)	90	90	90	90	90	90	79.31(1)
V, Å^3	1278.1(1)	1669.23(16)	587.26(7)	522.08(6)	515.0(1)	963.0(1)	934.1(2)	1109.7(2)	1539.4(2)
Z	4	2	2	2	2	2	2	2	4
ρ (calc.), g/cm^3	1.601	1.287	2.036	1.490	1.407	1.719	1.772	1.181	1.305
μ, mm^{-1}	0.44	0.30	6.88	0.10	0.09	0.36	0.38	0.17	0.07
Refls collected	18717	20512	3485	4401	7342	5808	10621	9704	15973
Unique reflections	2930	9241	710	1191	1640	1689	2475	2531	8845
Reflections I>2σ(I)	2593	7419	631	806	1524	1209	1981	2068	5960
R_{int}	2.9 (9.7)	2.2 (5.5)	5.5 (7.5)	5.0	1.9 (3.4)	8.5	2.8	5.5	3.1
Refined parameters	226	434	46	102	194	162	169	179	434
R(F) [I>2σ (I)]	3.4	4.7	3.1	4.8	3.7	6.4	4.3	4.4	4.9
wR(F^2) [all data]	9.6	13.4	7.8	13.5	11.1	21.0	12.6	10.3	14.0
CCDC dep. no.	779143	779145	779134	779135	779144	779136	779137	779138	779146

Compound	**54**	**57**	**61**
Empirical formula	$C_{39}H_{52}B_2F_3NO_5$	$C_{22}H_{32}B_2O_4Fe$	$C_{16}H_{21}BO_2Fe$
Formula weight	693.44	437.95	311.99
Temperature / K	120(2)	200	120
Crystal system	monoclinic	triclinic	monoclinic
Space group	$P2_1/n$	$P\bar{1}$	$P2_1/n$
a, Å	16.4127(6)	9.9717(5)	12.7042(4)
b, Å	13.1596(4)	12.4570(6)	7.5261(3)
c, Å	18.4331(6)	19.0043(11)	15.8313(5)
α /°	90.00	73.984(7)	90.00
β /°	103.971(7)	88.620(7)	104.497(5)
γ /°	90.00	87.385(8)	90.00
Volume / Å^3	3863.5(2)	2266.5(2)	1465.48(9)
Z	4	4	4
ρ_{calc} / mg mm^{-3}	1.192	1.283	1.414
μ / mm^{-1}	0.086	0.689	1.026
F(000)	1480	928	656
Crystal size /mm^3	0.50 × 0.45 × 0.33	0.12 × 0.2 × 0.4	0.3 × 0.12 × 0.11
Theta range for data collection	1.49 to 50°	1.70 to 50°	1.85 to 29.99°
Index ranges	$-19 \le h \le 19$, $-15 \le k \le 15$, $-21 \le l \le 21$	$-11 \le h \le 11$, $-14 \le k \le 14$, $-22 \le l \le 22$	$-17 \le h \le 17$, $-10 \le k \le 10$, $-22 \le l \le 22$
Reflections collected	31523	28395	19580
Independent reflections	6800[R(int) = 0.0792]	7977[R(int) = 0.0365]	4282[R(int) = 0.0533]
Data/restraints/ parameters	6800/0/503	7977/45/510	4282/0/265
Goodness-of-fit on F^2	1.053	1.048	1.045
Final R indexes [I>2σ (I)]	R_1 = 0.0402, wR_2 = 0.1071	R_1 = 0.0497, wR_2 = 0.1272	R_1 = 0.0322, wR_2 = 0.0842
Final R indexes [all data]	R_1 = 0.0542, wR_2 = 0.1161	R_1 = 0.0635, wR_2 = 0.1403	R_1 = 0.0379, wR_2 = 0.0871
Largest diff. peak/hole/e Å^{-3}	0.336/-0.289	0.592/-0.465	0.760/-0.350

5.0 Absorption, Emission and Excitation Spectra of Pyrene Derivatives

Absorption, emission and excitation spectra, fluorescence quantum yields and lifetimes were measured in toluene. The absorption spectrum of pyrene was measured in cyclohexane. Compounds **15**, **30**, **31** and **32** were measured in methanol.

The primary (left hand) y-axis is a logarithmic scale of the intensity of excitation. The secondary (right hand) y-axis is in arbitrary units, as the values of absorbance (for the $S_2 \leftarrow S_0$ transition) and intensity of emission are normalized.

Pyrene

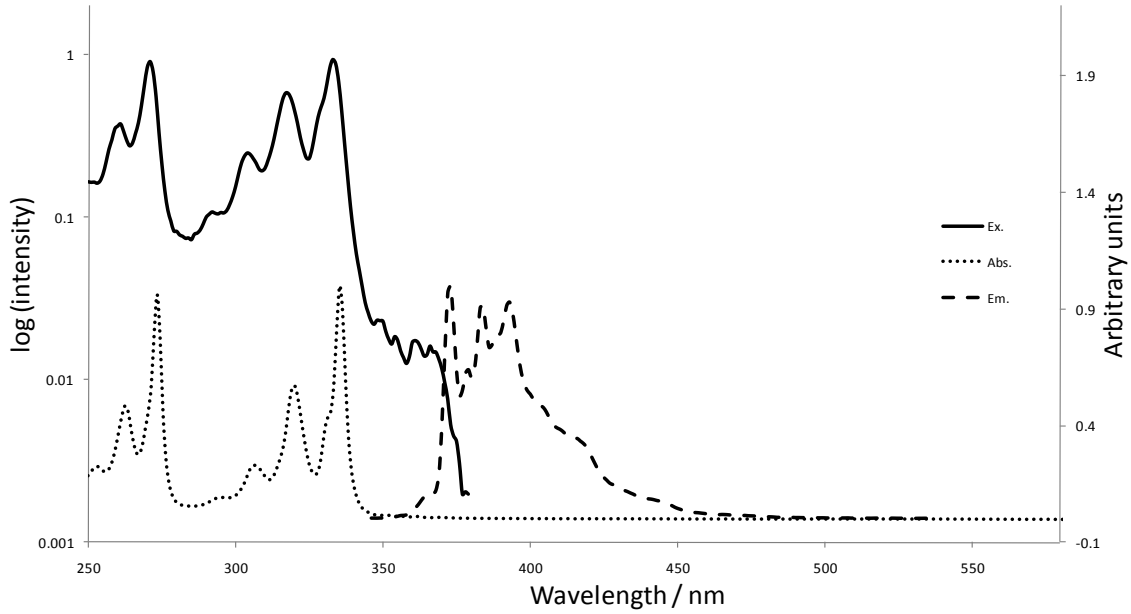

1: 2,7-Bis(Bpin)pyrene

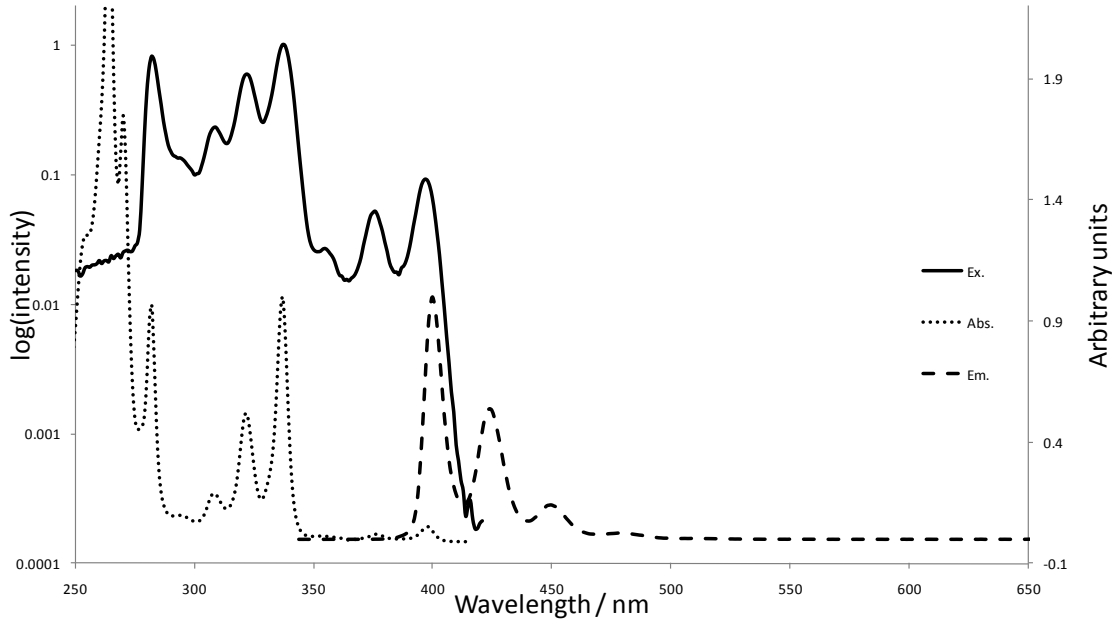

2: 2-(Bpin)pyrene

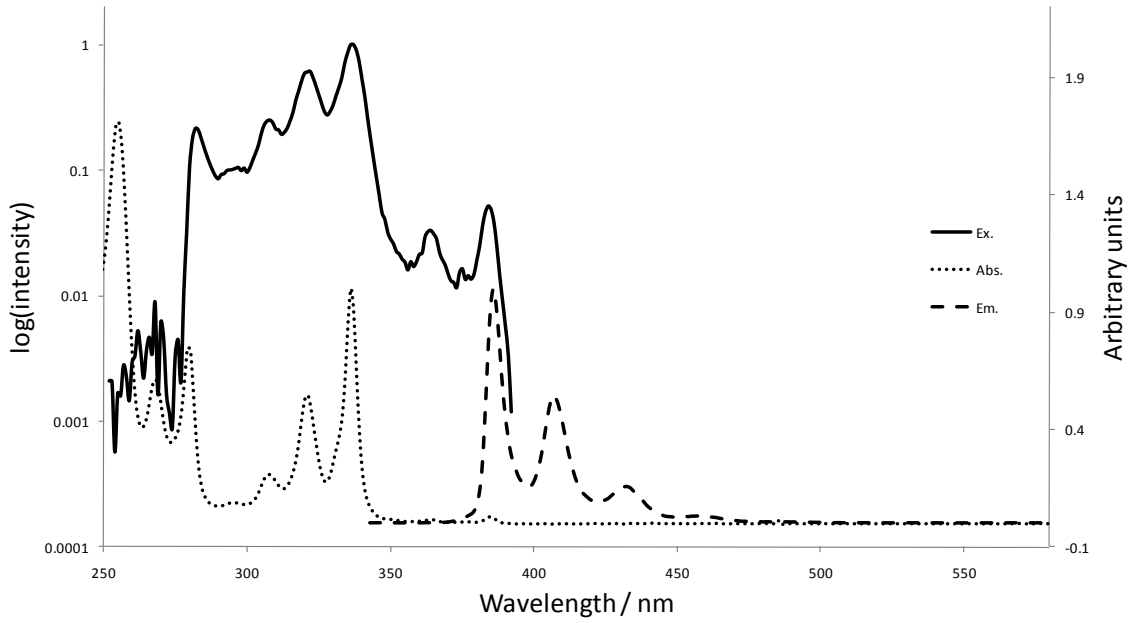

6: Pyrene-2,7-bis[4-(octylbenzoate)]

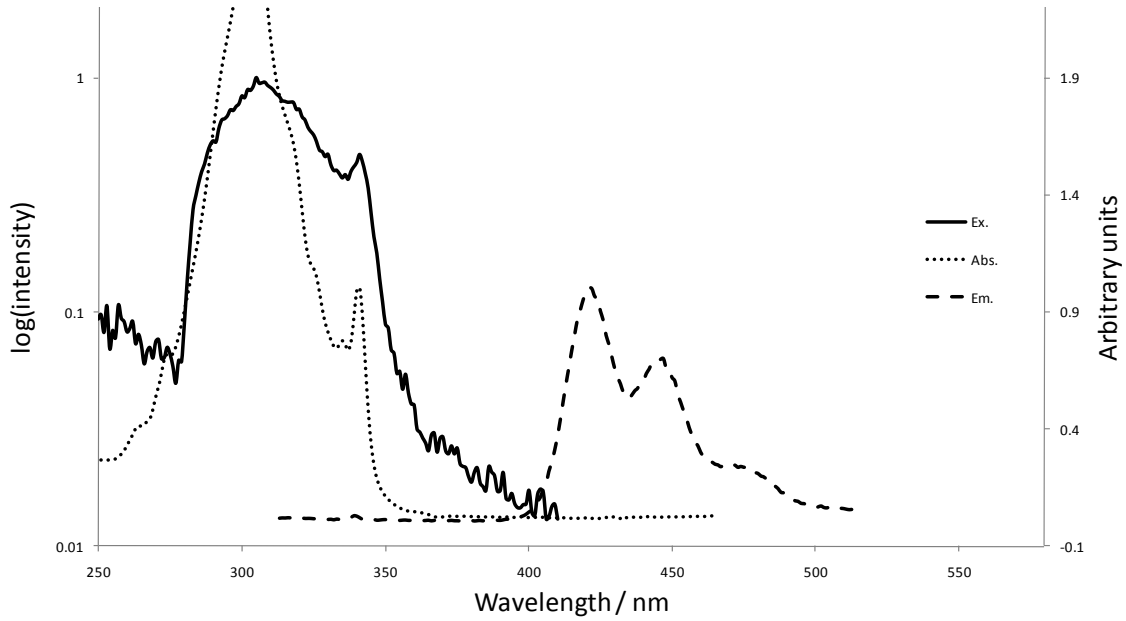

7: Pyrenyl-2-[4-(methylbenzoate)]

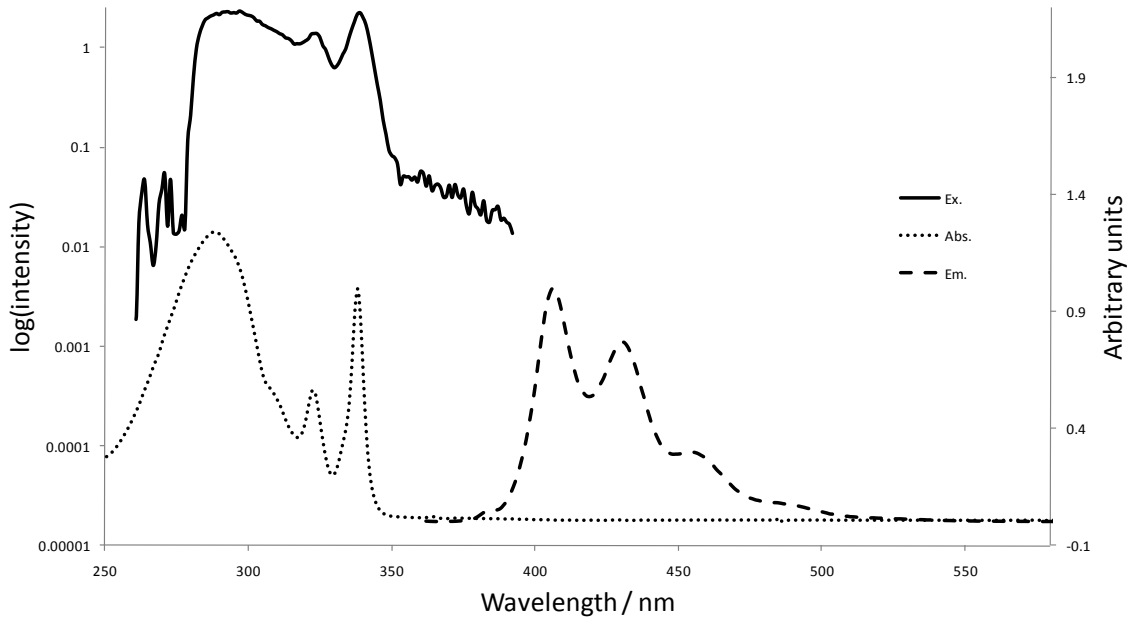

10: 2-[(4-Dimesitylboryl)phenyl]pyrene

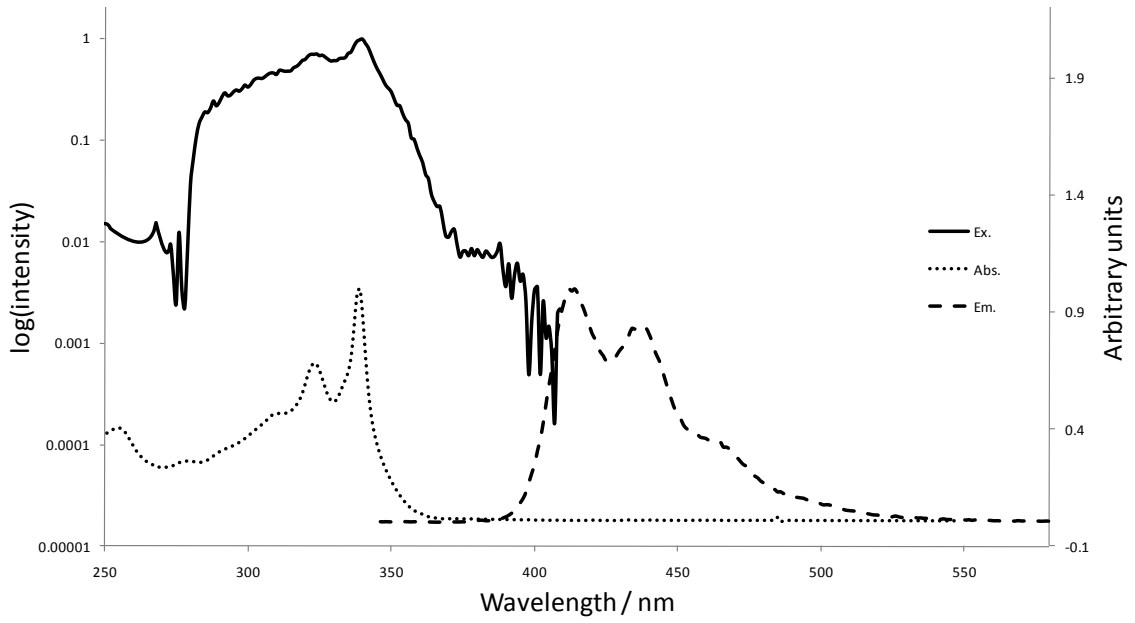

14: 2-(Dimesitylboryl)pyrene

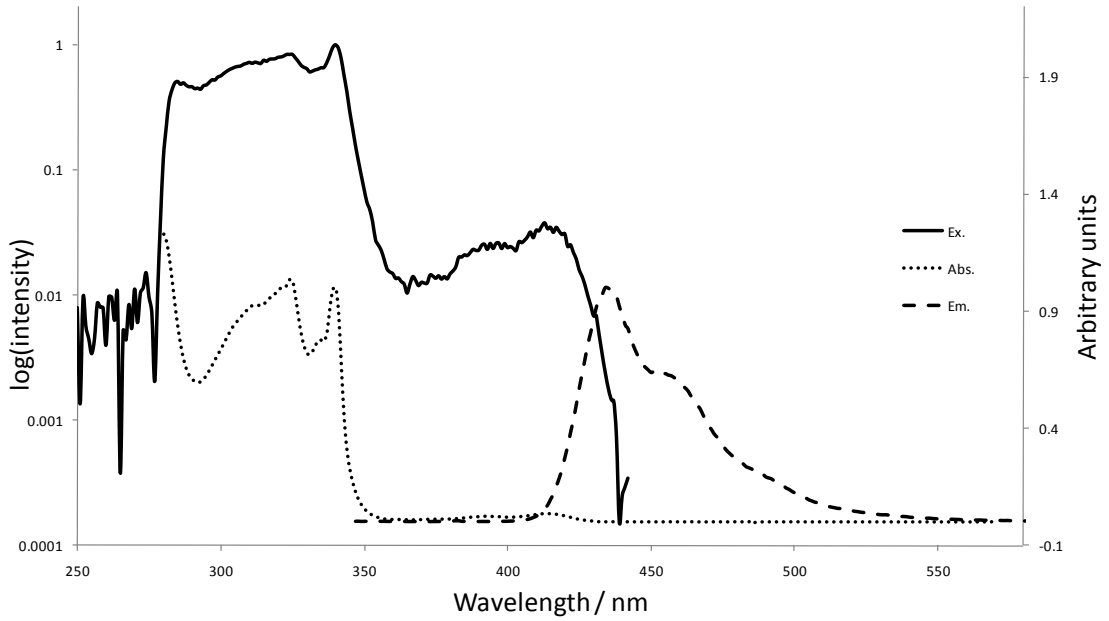

15: 2,7-Dihydroxypyrene

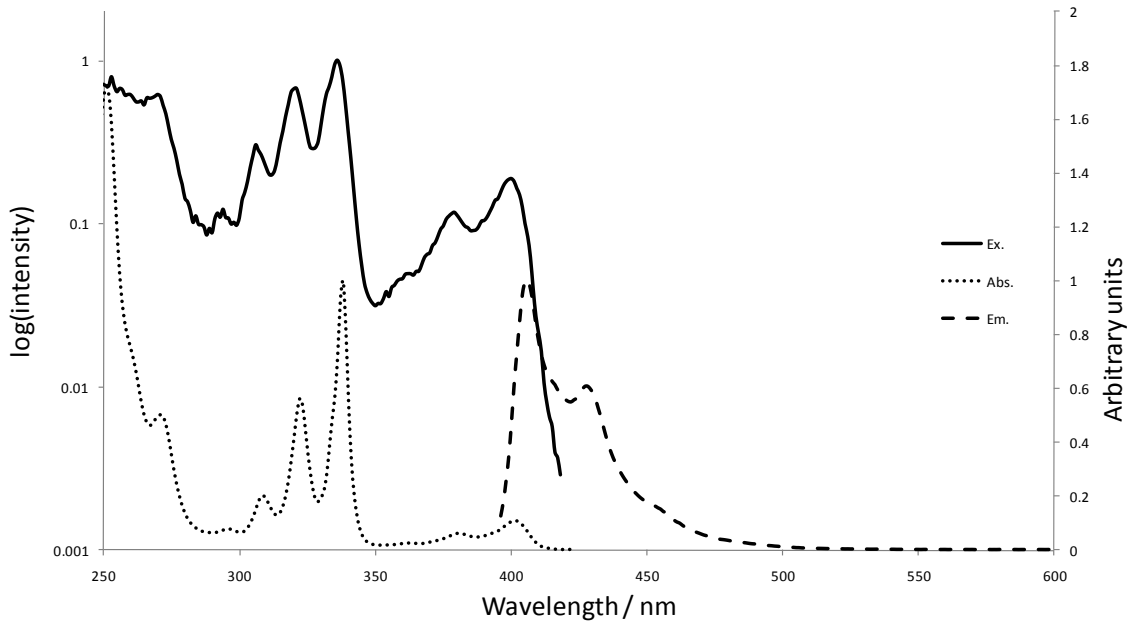

20: 2,7-Bis(phenylethynyl)pyrene

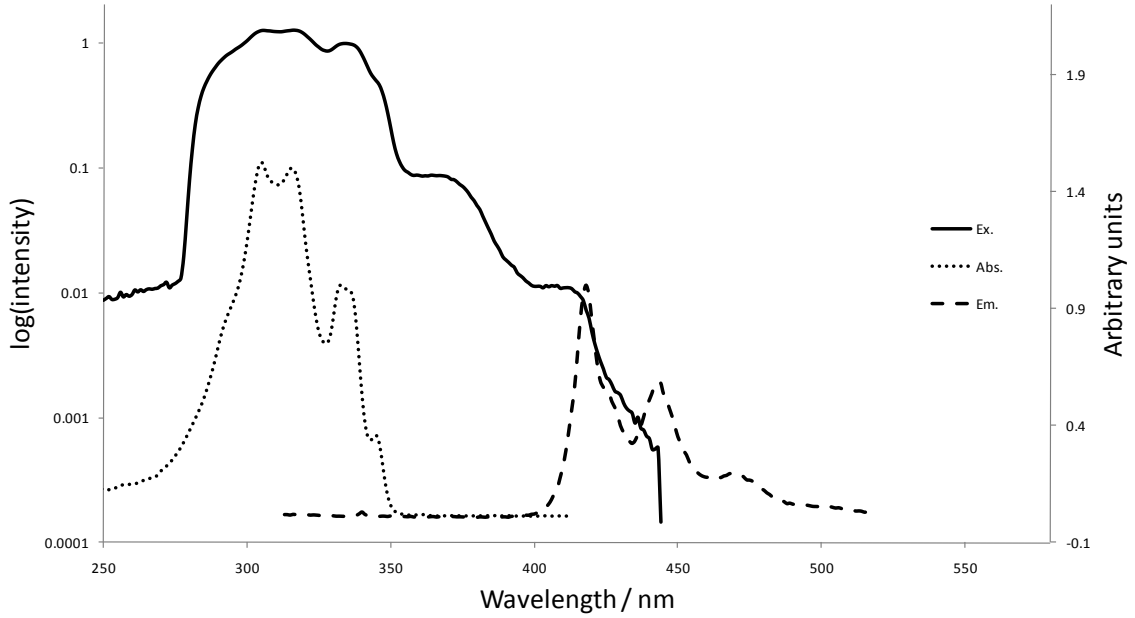

21: 2,7-Bis[4-(dimesitylboryl)phenylethynyl)]pyrene

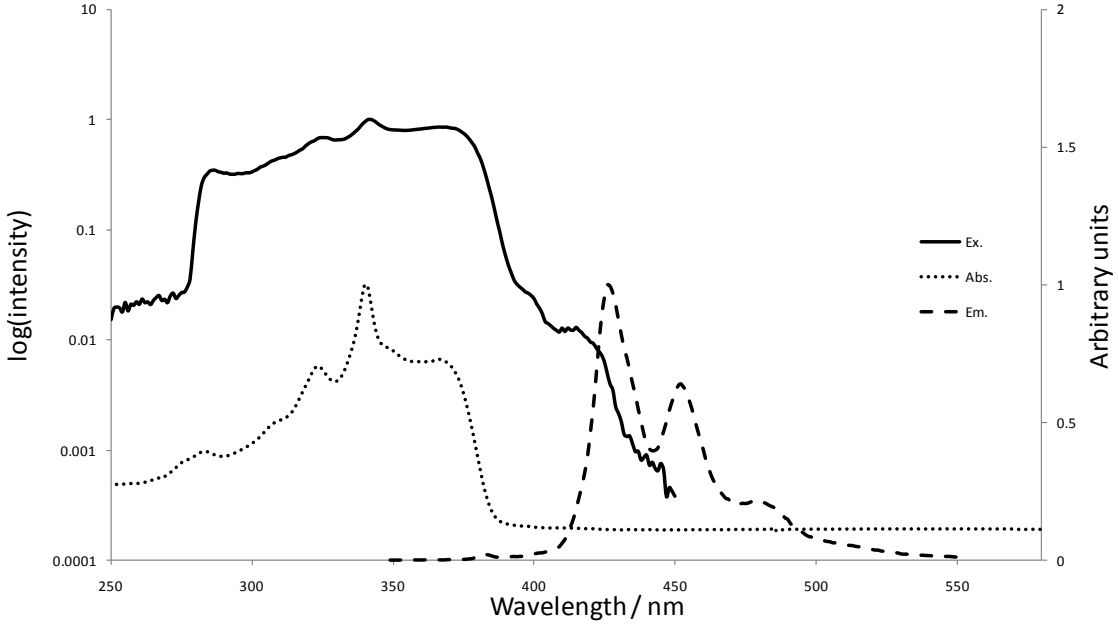

22: 2,7-Bis(trimethylsilylethynyl)pyrene

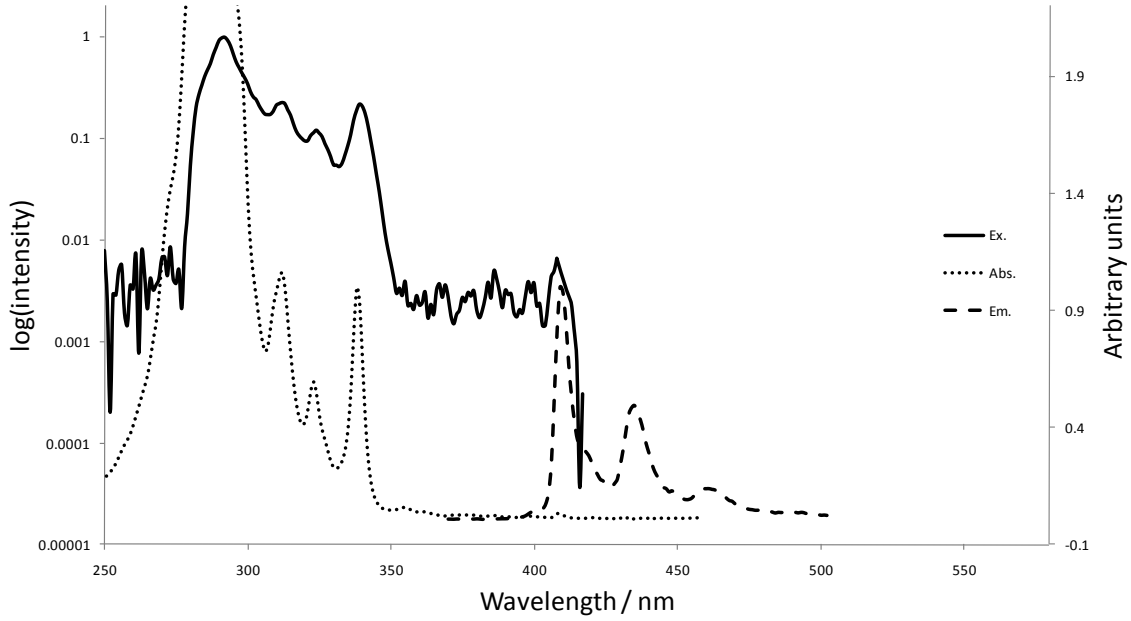

24: 2-Phenylethynylpyrene

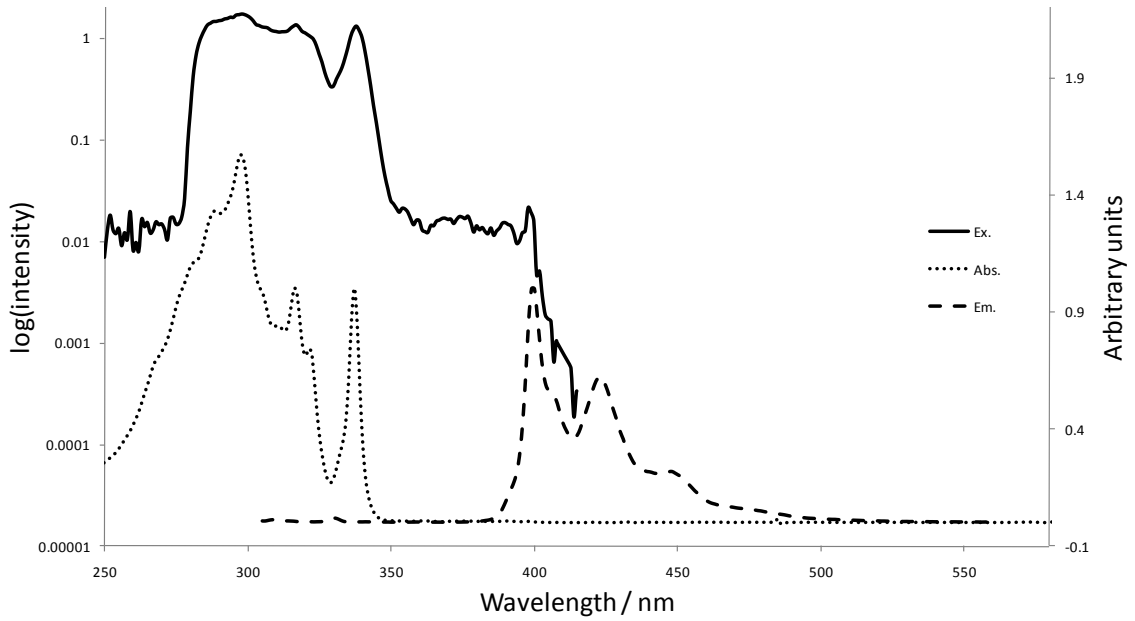

26: 2,7-Bis[(4-*N*,*N*-dimethylamino)phenylethynyl]pyrene

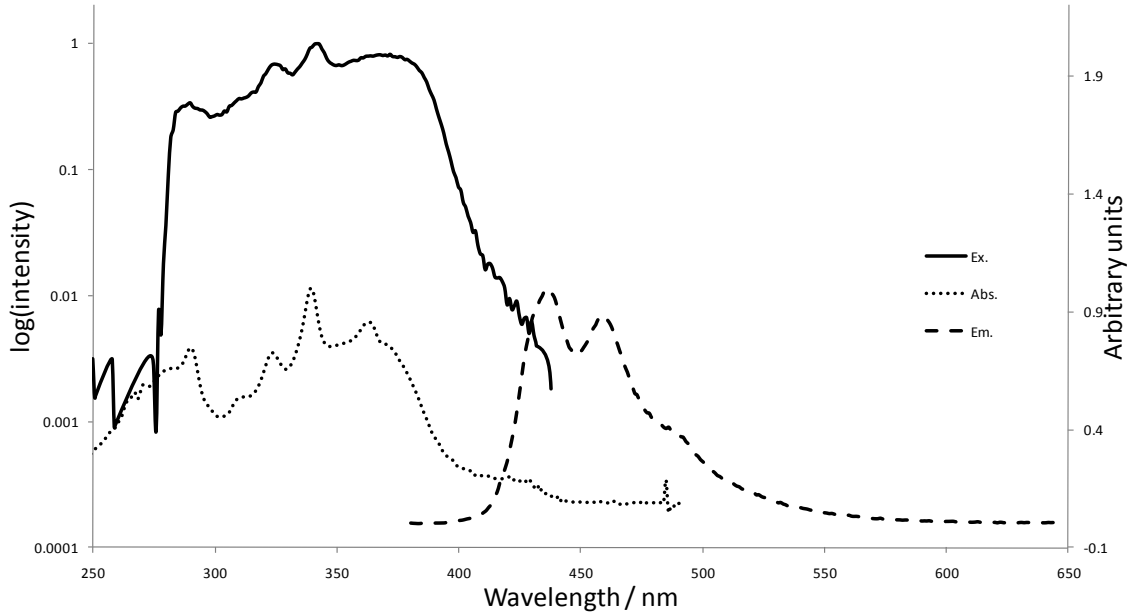

29: 2,7-Bis[(4-methoxy-phenyl)-phenyl-amino]pyrene

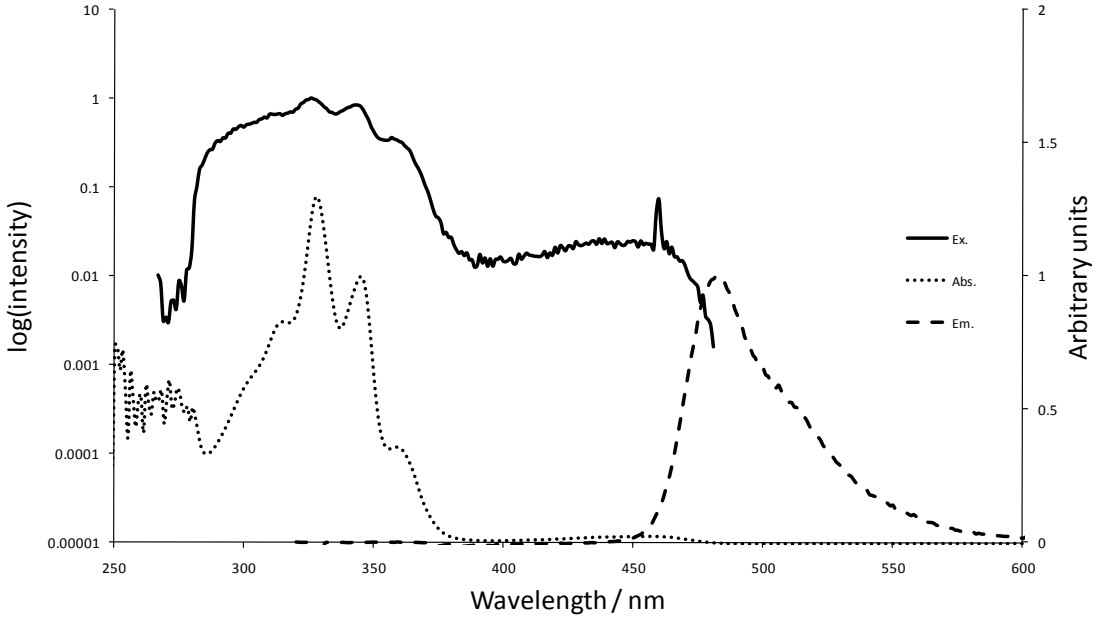

30: 4-(Pyren-1-yl)-butyric acid

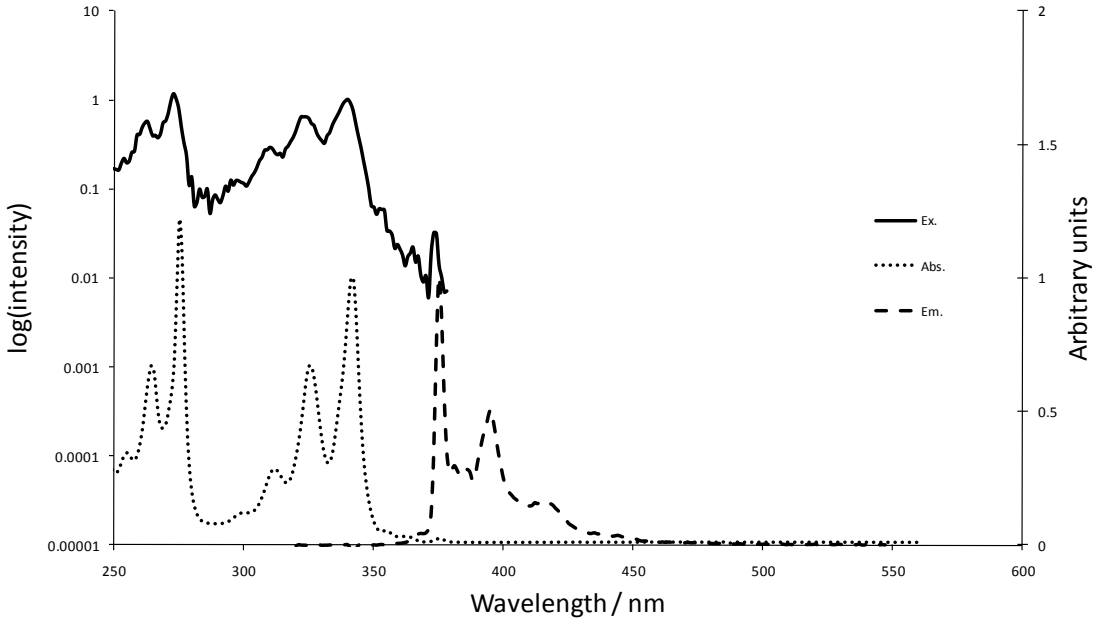

31: 4-(Pyren-2-yl)-butyric acid

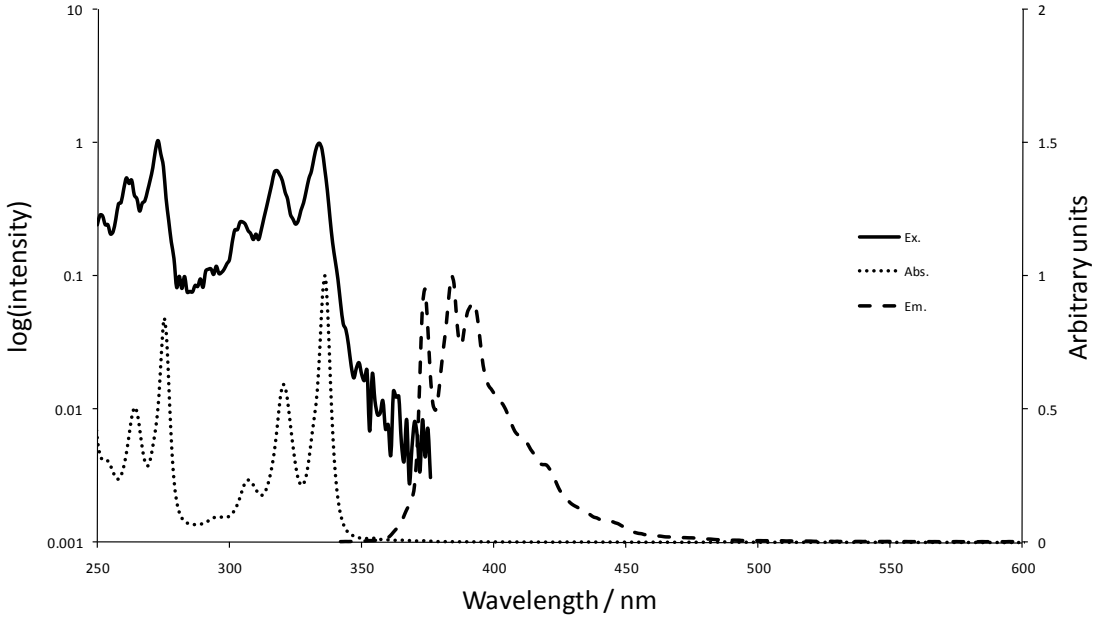

32: 4-(Pyren-2-yloxy)-butyric acid

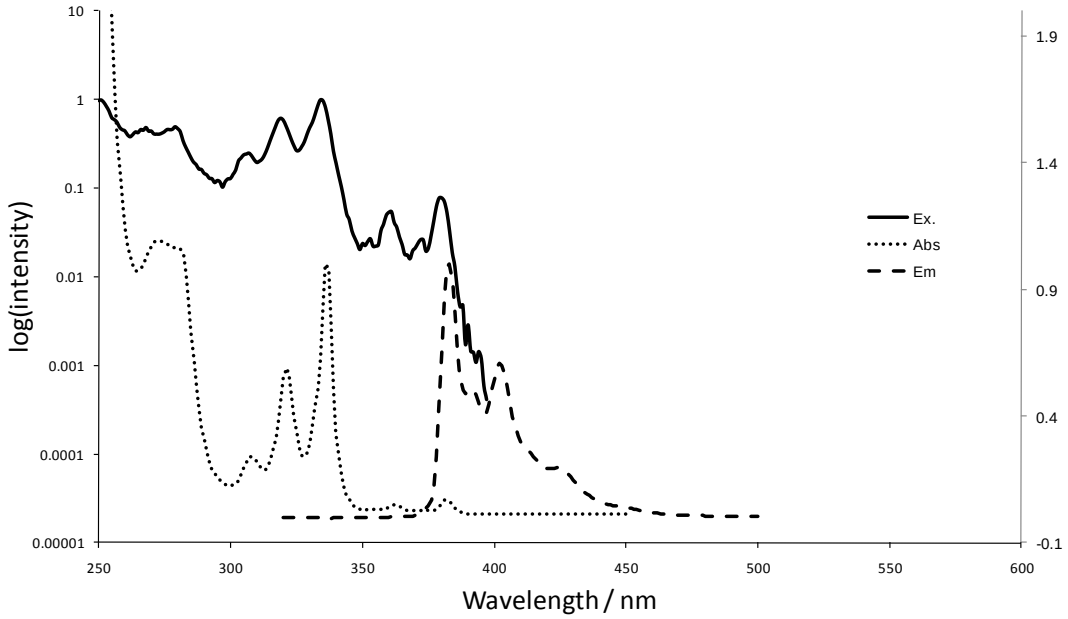

35: 2-(12-Bromo-dodecyloxy)-pyrene

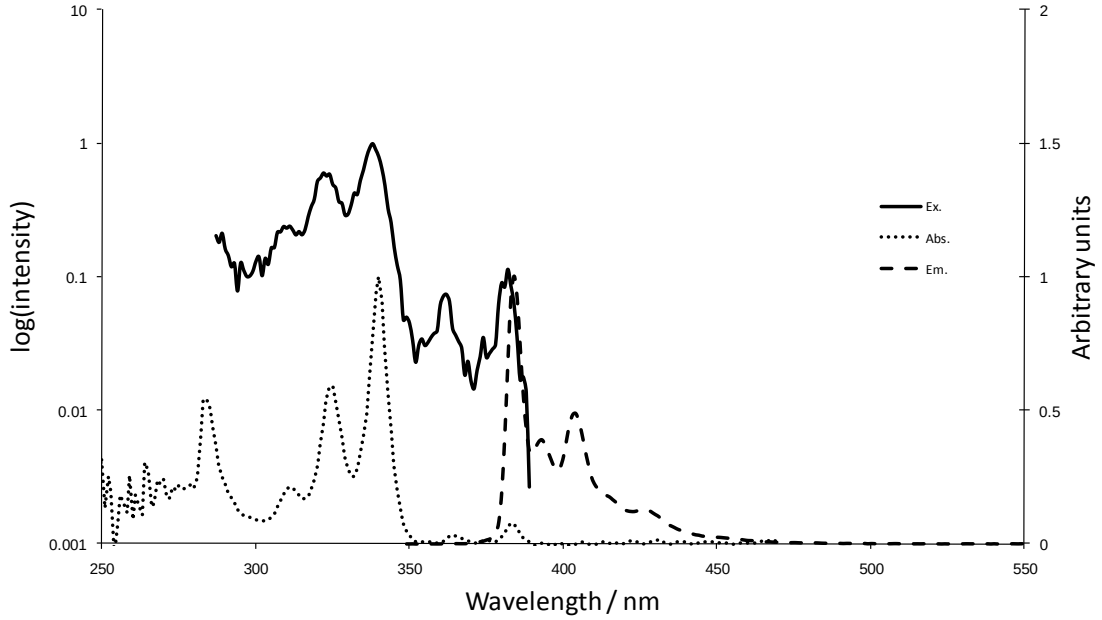

37: 1-Phenylethynylpyrene

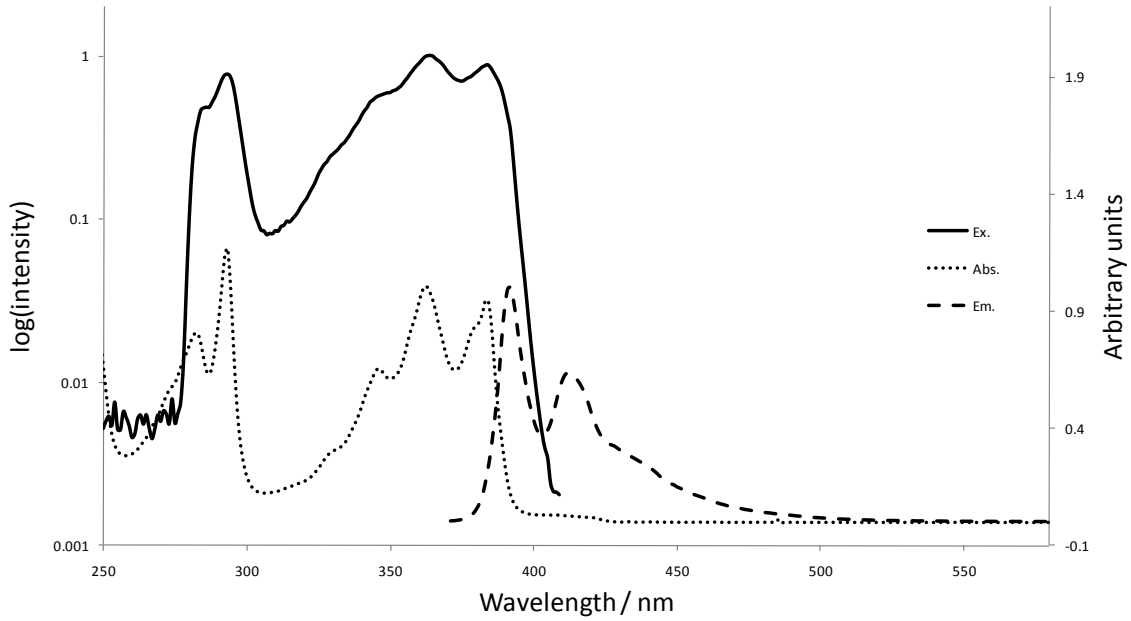

38: 1-(Dimesitylboryl)pyrene

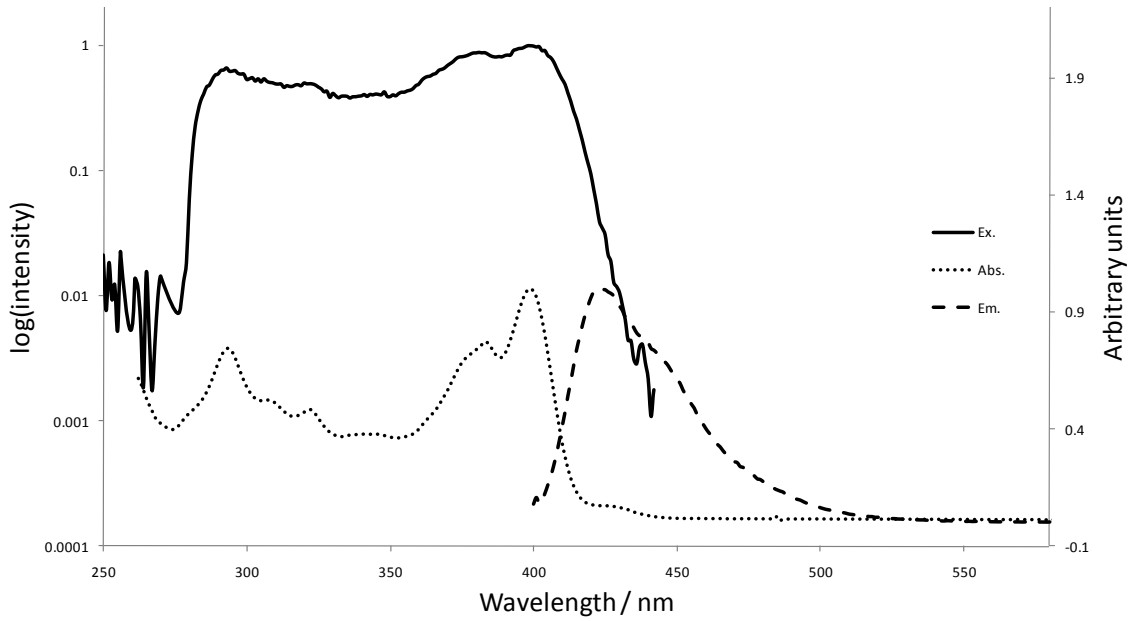

39: 1-[(4-Dimesitylboryl)phenyl]pyrene

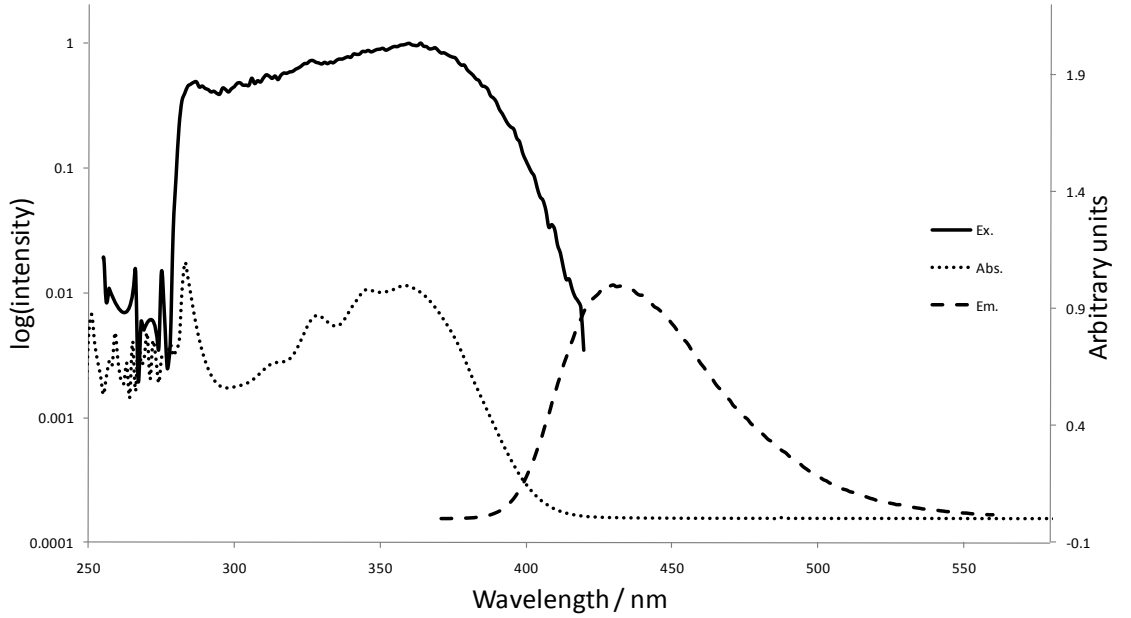

40: 1-(Bpin)pyrene

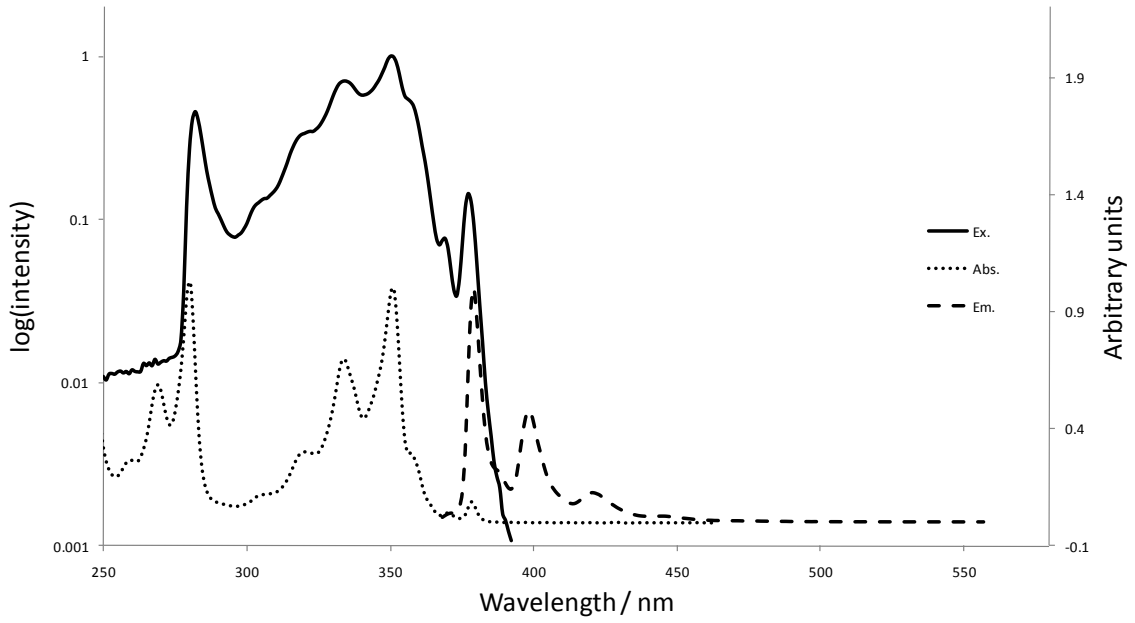

6.0 TD-DFT Experimental Details and Data for the Lowest Five Excitations of Pyrene Derivatives*

* TD-DFT experimental details and data for the lowest five excitations of pyrene derivatives compiled with the assistance of Austin Dwyer (Durham University).

TD-DFT Experimental

All calculations in this study were carried out at B3LYP/6-31G* optimized ground state geometries. All excitation energies are singlet vertical excitations for isolated molecules, determined using the cc-pVTZ basis set, except for excitations of the largest compound **21** which was performed using 6-31G*. Calculations were performed using both the B3LYP and CAM-B3LYP coulomb-attenuated approximations. To assess the influence of solvent, additional B3LYP/6-31G* calculations on pyrene and molecules **21** and **26** were performed using a toluene solvent-polarizable continuum model (PCM) with dielectric constant $\varepsilon = 2.379$. It is expected that these two molecules would experience the largest solvatochromic effects. The excitation energies decrease by no more than 0.1 eV. All calculations were carried out using the Gaussian 03[1] or Dalton[2] packages.

[1]Frisch, M. J.; Trucks, G. W.; Schlegel, H. B.; Scuseria, G. E.; Robb, M. A.; Cheeseman, J. R.; Montgomery, Jr., J. A.; Vreven, T.; Kudin, K. N.; Burant, J. C.; Millam, J. M.; Syengar, S. S.; Tomasi, J.; Barone, V.; Mennucci, B.; Cossi, M.; Scalmani, G.; Rega, N.; Petersson, G. A.; Nakatsuji, H.; Hada, M.; Ehara, M.; Toyota, K.; Fukuda, R.; Hasegawa, J.; Ishida, M.; Nakajima, T.; Honda, Y.; Kitao, O.; Nakai, H.; Klene, M.; Li, X.; Knox, J. E.; Hratchian, H. P.; Cross, J. B.; Bakken, V.; Adamo, C.; Jaramillo, J.; Gomperts, R.; Stratmann, R. E.; Yazyev, O.; Austin, A. J.; Cammi, R.; Pomelli, C.; Ochterski, J. W.; Ayala, P. Y.; Morokuma, K.; Voth, G. A.; Salvador, P.; Dannenberg, J. J.; Zakrzewski, V. G.; Dapprich, S.; Daniels, A. D.; Strain, M. C.; Farkas, O.; Malick, D. K.; Rabuck, A. D.; Raghavachari, K.; Foresman, J. B.; Ortiz, J. V.; Cui, Q.; Baboul, A. G.; Clifford, S.; Cioslowski, J.; Stefanov, B. B.; Liu, G.; Liashenko, A.; Piskorz, P.; Komaromi, I.; Martin, R. L.; Fox, D. J.; Keith, T.; Al-Laham, M. A.; Peng, C. Y.; Nanayakkara, A.; Challacombe, M.; Gill, P. M. W.; Johnson, B.; Chen, W.; Wong, M. W.; Gonzalez, C.; Pople, J. A. Gaussian 03, Revision C.02, Gaussian, Inc.,Wallingford, CT, 2004.

[2]DALTON, a molecular electronic structure program, Release 2.0, 2005, see http://www.kjemi.uio.no/software/dalton/dalton.html.

Data for the Lowest Five Excitations of Pyrene Derivatives

The following two tables show the lowest five excitations calculated using TD-DFT. The value k_{ia}, which measures the contribution of a particular orbital transition, is defined as:

$$\kappa_{ia} = X_{ia} + Y_{ia}$$

where i and a are the occupied and unoccupied orbitals and X_{ia} and Y_{ia} are the solutions of the generalized eigenvalue problem

$$\begin{pmatrix} \mathbf{A} & \mathbf{B} \\ \mathbf{B} & \mathbf{A} \end{pmatrix} \begin{pmatrix} \mathbf{X} \\ \mathbf{Y} \end{pmatrix} = \omega \begin{pmatrix} \mathbf{1} & \mathbf{0} \\ \mathbf{0} & -1 \end{pmatrix} \begin{pmatrix} \mathbf{X} \\ \mathbf{Y} \end{pmatrix}.$$

Table A2 TD-DFT B3LYP excitation energies calculated at B3LYP/6-31G* optimized geometries. All excitations were calculated using the cc-pVTZ basis set, except for compound **21**, which employed the 6-31G* basis set. Compound numbering in the order: 2-, 2,7-, then 1-substituted derivatives.

Compound	Excitation	E/eV	λ/nm	Pol.	Osc. Strength	$i \rightarrow a$	k_{ia}
Pyrene	1	3.65	340	Z	0.251	H→L	0.61
						H-1→L+1	0.25
	2	3.72	333	Y	0.000	H-1→L	0.49
						H→L+1	0.53
	3	4.30	288		0.000	H-2→L	0.15
						H→L+2	0.68
	4	4.55	273	Y	0.254	H-1→L	0.46
						H→L+1	0.41
	5	4.59	270		0.000	H-2→L	0.67
						H→L+2	0.13
31	1	3.63	341		0.275	H-1→L+1	0.25
						H→L	0.61
	2	3.68	337		0.000	H-1→L	0.52
						H→L+1	0.50
	3	4.30	288		0.000	H→L+2	0.68
	4	4.49	276		0.229	H-1→L	0.42
						H→L+1	0.44
	5	4.57	271		0.006	H-2→L	0.66
2	1	3.53	351	Y	0.011	H→L+1	0.61
						H-1→L	0.38
	2	3.63	342	Z	0.218	H→L	0.60
						H-1→L+1	0.27
	3	4.27	290	Y	0.004	H→L+2	0.67
						H-2→L	0.12
	4	4.42	280	Y	0.199	H-1→L	0.54
						H→L+1	0.29
	5	4.62	268		0.001	H-2→L	0.68
						H→L+2	0.11
32	1	3.54	350		0.048	H-1→L	0.56
						H→L	0.26
						H→L+1	0.32
	2	3.62	342		0.217	H-1→L	0.24
						H-1→L+1	0.23
						H→L	0.55
	3	4.31	288		0.017	H-2→L	0.25
						H→L+1	0.22
						H→L+2	0.60
	4	4.44	279		0.136	H→L+1	0.46
						H→L+2	0.33
	5	4.54	273		0.044	H-1→L	0.61
						H→L+1	0.24

24	1	3.28	378	Y	0.000	H→L+1	0.52
						H-1→L	0.48
	2	3.59	345	Z	0.008	H→L	0.55
						H-1→L+1	0.33
	3	3.79	327	Y	0.088	H-1→L	0.48
						H→L+1	0.44
	4	3.90	318	Z	2.044	H-1→L+1	0.56
						H→L	0.27
	5	4.29	289	Y	0.000	H→L+2	0.56
						H→L+3	0.30
7	1	3.32	373	Y	0.005	H→L+1	0.63
						H-1→L	0.31
	2	3.61	344	Z	0.158	H→L	0.59
						H-1→L+1	0.23
	3	3.89	318	Y	0.043	H-1→L	0.54
						H→L+1	0.28
						H→L+2	0.33
	4	4.13	300	Z	1.397	H-1→L+1	0.63
						H→L	0.17
	5	4.31	288	Y	0.010	H→L+4	0.61
						H→L+2	0.21
						H-2→L	0.22
10	1	3.21	386	Y	0.005	H→L	0.66
						H-1→L+1	0.20
	2	3.53	351	Y/X	0.074	H-2→L	0.69
						H-2→L+2	0.09
	3	3.55	350	Z	0.403	H-1→L	0.63
						H-4→L	0.24
	4	3.61	344	Z	0.404	H→L+2	0.58
						H-4→L	0.18
	5	3.70	335	Z	0.046	H-3→L	0.66
						H-4→L	0.19
14	1	3.09	401	Y	0.019	H→L	0.67
						H-5→L+1	0.17
	2	3.56	349	Z	0.062	H→L+1	0.54
						H-2→L	0.32
	3	3.58	346	Y	0.071	H-1→L	0.69
	4	3.68	337	Z	0.345	H-2→L	0.60
						H→L+1	0.23
	5	3.75	330	Z	0.065	H-3→L	0.68
						H-5→L	0.10

1	1	3.35	370	Y	0.023	H-1→L	0.32
						H→L+1	0.63
	2	3.61	343	Z	0.176	H-1→L+1	0.30
						H→L	0.60
	3	4.24	292		0.000	H-2→L	0.11
						H→L+2	0.69
	4	4.40	282	Y	0.179	H-1→L	0.59
						H→L+1	0.22
	5	4.77	260	Z	1.793	H-1→L+1	0.59
						H→L	0.20
15	1	3.35	370	Y(Z)	0.056	H-1→L	0.58
						H→L	0.27
	2	3.62	343	Z	0.214	H→L	0.55
						H-1→L	0.26
	3	4.31	288		0.000	H-2→L	0.54
						H→L+2	0.43
	4	4.45	278		0.000	H→L+2	0.53
						H-2→L	0.42
	5	4.64	267		0.000	H-1→L+2	0.66
						H-2→L+1	0.17
22	1	3.24	382	Y	0.006	H-1→L	0.58
						H→L+1	0.42
	2	3.55	349	Z	0.008	H→L	0.54
						H-1→L+1	0.39
	3	3.97	312	Y	0.165	H-1→L	0.53
						H→L+1	0.35
	4	4.19	296	Z	2.583	H-1→L+1	0.53
						H→L	0.31
	5	4.25	292		0.000	H→L+2	0.59
						H-2→L	0.33
20	1	3.09	401	Y	0.000	H-1→L	0.51
						H→L+1	0.50
	2	3.34	371	Z	1.034	H-1→L+1	0.62
						H→L	0.28
	3	3.63	342	Y	0.106	H→L+1	0.47
						H-1→L	0.45
	4	3.73	332	Z	2.355	H-1→L+1	0.55
						H→L	0.24
	5	3.98	311		0.000	H-2→L	0.63
						H→L+2	0.31

21	1	3.01	412	Y	0.004	H-1→L	0.60
						H→L+2	0.35
	2	3.03	409	Z	2.871	H→L	0.66
						H-2→L+1	0.15
	3	3.39	365	X	0.015	H-4→L	0.57
						H-3→L+1	0.38
	4	3.39	365	Y	0.099	H-3→L	0.57
						H-4→L+1	0.38
	5	3.40	365		0.000	H→L+1	0.52
						H-2→L	0.34
26	1	2.87	432	Y	0.007	H→L	0.65
						H-2→L+1	0.26
	2	3.07	404	Z	2.181	H→L+1	0.67
						H-2→L	0.10
	3	3.22	385		0.000	H-1→L	0.70
	4	3.44	360		0.000	H-1→L+1	0.68
						H→L+2	0.11
	5	3.50	354	Y	0.051	H-2→L+1	0.60
						H→L	0.23
6	1	3.21	387	Y	0.005	H→L	0.62
						H-1→L+1	0.34
	2	3.54	350	Z	0.004	H→L+1	0.53
						H-1→L	0.39
	3	3.75	331		0.000	H→L+2	0.69
	4	3.82	324	Y	0.074	H-1→L+1	0.57
						H→L	0.30
	5	3.90	318	Z	2.648	H-1→L	0.55
						H→L+1	0.32
29	1	2.60	478		0.020	H→L	0.68
	2	2.98	416		0.002	H-1→L	0.69
	3	3.31	375		0.205	H-2→L	0.34
						H→L+1	0.60
	4	3.62	343		0.366	H-2→L	0.26
						H→L+2	0.57
	5	3.66	339		1.417	H-2→L	0.45
						H→L+1	0.26
						H→L+2	0.33
30	1	3.55	349		0.314	H-1→L+1	0.23
						H→L	0.61
	2	3.69	336		0.001	H-1→L	0.49
						H→L+1	0.54
	3	4.25	292		0.004	H→L+2	0.67
	4	4.50	276		0.269	H-1→L	0.45
						H→L+1	0.40
	5	4.53	273		0.002	H-2→L	0.67

40	1	3.45	359	0.343	H→L	0.61
	2	3.65	340	0.017	H-1→L	0.54
					H→L+1	0.47
	3	4.28	290	0.014	H-2→L	0.49
					H→L+2	0.44
	4	4.39	283	0.008	H-2→L	0.40
					H→L+2	0.52
	5	4.44	279	0.239	H-2→L	0.26
					H-1→L	0.36
					H→L+1	0.43
37	1	3.08	402	0.853	H→L	0.63
	2	3.48	357	0.000	H-1→L	0.47
					H→L+1	0.50
	3	3.90	318	0.000	H-2→L	0.43
					H→L+2	0.50
	4	4.10	302	0.375	H-1→L	0.39
					H→L+1	0.33
					H→L+4	0.25
	5	4.19	296	0.125	H-2→L	0.28
					H→L+1	0.26
					H→L+4	0.46
39	1	3.08	402	0.508	H→L	0.65
	2	3.48	357	0.070	H-1→L	0.65
					H-1→L+1	0.25
	3	3.55	349	0.128	H-2→L	0.37
					H→L+1	0.39
					H→L+2	0.29
	4	3.62	342	0.014	H-2→L	0.53
	5	3.68	337	0.070	H→L+1	0.44
					H→L+2	0.38
38	1	3.04	408	0.385	H→L	0.63
					H-1→L+1	0.16
	2	3.36	369	0.060	H-1→L	0.68
	3	3.50	354	0.022	H-2→L	0.49
					H-5→L	0.27
					H-3→L	0.26
	4	3.56	348	0.009	H-3→L	0.56
					H-2→L	0.39
	5	3.63	341	0.005	H-4→L	0.50
					H-5→L	0.28

Table A3 TD-DFT CAM-B3LYP excitation energies calculated at B3LYP/6-31G* optimized geometries. All excitations were calculated using the cc-pVTZ basis set, except for compound **21**, which employed the 6-31G* basis set. Compound numbering in the order: 2-, 2,7-, then 1-substituted derivatives.

Compound	Excitation	E/eV	λ/nm	Pol.	Osc. Strength	$i \rightarrow a$	k_{ia}
Pyrene	1	3.92	316	Z	0.000	H→L+1	0.55
						H-1→L	0.51
	2	3.94	315	Y	0.310	H→L	0.63
						H-1→L+1	0.28
	3	4.71	263		0.000	H→L+2	0.67
						H-2→L	0.14
	4	4.99	248	Y	0.392	H-1→L	0.46
						H→L+1	0.41
	5	5.05	246		0.000	H-2→L	0.66
						H→L+2	0.12
31	1	3.89	318		0.000	H-1→L	0.54
						H→L+1	0.53
	2	3.93	316		0.336	H-1→L+1	0.27
						H→L	0.63
	3	4.72	263		0.000	H→L+2	0.67
	4	4.94	251		0.336	H-1→L	0.42
						H→L+1	0.43
	5	5.02	247		0.025	H-2→L	0.64
2	1	3.78	328	Y	0.010	H→L+1	0.60
						H-1→L	0.43
	2	3.93	316	Z	0.269	H→L	0.63
						H-1→L+1	0.29
	3	4.68	265	Y	0.006	H→L+2	0.67
						H-2→L	0.10
	4	4.88	254	Y	0.317	H-1→L	0.52
						H→L+1	0.32
	5	5.08	244	Y	0.006	H-2→L	0.65
						H-1→L+3	0.13
32	1	3.80	326		0.031	H-1→L	0.58
						H→L+1	0.40
	2	3.92	316		0.295	H-1→L+1	0.26
						H→L	0.61
	3	4.74	261		0.020	H→L+1	0.18
						H→L+2	0.64
	4	4.85	256		0.160	H-2→L	0.45
						H→L+1	0.39
	5	5.03	247		0.159	H-2→L	0.49
						H→L+1	0.33

24	1	3.67	338	Y	0.001	H→L+1	0.51
						H-1→L	0.45
	2	3.90	318	Z	0.029	H→L	0.58
						H-1→L+1	0.34
	3	4.25	292	Z	2.161	H-1→L+1	0.55
						H→L	0.27
	4	4.56	272	Y	0.230	H-1→L	0.48
						H→L+1	0.41
	5	4.72	262	Y	0.007	H→L+3	0.54
						H→L+2	0.40
7	1	3.75	331	Y	0.002	H→L+1	0.49
						H-1→L	0.46
	2	3.91	317	Z	0.250	H→L	0.62
						H-1→L+1	0.22
	3	4.61	269	Z	1.794	H-1→L+1	0.60
						H→L	0.15
	4	4.63	268	Y	0.156	H-1→L	0.42
						H→L+1	0.40
	5	4.74	261	Y	0.064	H→L+4	0.58
						H-1→L	0.22
10	1	3.74	332	Y/X	0.001	H-1→L+1	0.42
						H→L	0.42
						H→L+2	0.37
	2	3.91	317	Z	0.247	H→L+1	0.62
						H-2→L+2	0.19
	3	4.11	301	Z	1.121	H-1→L	0.55
						H-4→L	0.22
	4	4.13	300	Y/X	0.116	H-2→L	0.63
						H-2→L+2	0.24
	5	4.58	271	Y	0.136	H→L	0.45
						H-1→L+1	0.41
14	1	3.54	350	Y	0.020	H→L	0.62
						H-1→L+1	0.25
	2	3.88	320	Z	0.197	H→L+1	0.61
						H-1→L	0.26
	3	4.15	299	Y	0.106	H-2→L	0.65
						H-2→L+2	0.17
	4	4.25	292	Z	0.588	H-1→L	0.59
						H-5→L	0.22
	5	4.56	272	Y	0.083	H-1→L+1	0.36
						H-5→L+1	0.29

1	1	3.62	342	Y	0.023	H→L+1	0.63
						H-1→L	0.37
	2	3.91	317	Z	0.216	H→L	0.62
						H-1→L+1	0.32
	3	4.65	267		0.000	H→L+2	0.68
						H-3→L+1	0.12
	4	4.85	256	Y	0.290	H-1→L	0.58
						H→L+1	0.26
	5	5.10	243	Z	2.072	H-1→L+1	0.59
						H→L	0.22
15	1	3.62	342	Y(Z)	0.062	H-1→L	0.61
						H→L	0.24
						H→L+1	0.30
	2	3.92	316	Z	0.270	H→L	0.59
						H-1→L	0.23
						H-1→L+1	0.26
	3	4.78	259		0.000	H-2→L	0.61
						H→L+2	0.26
	4	4.82	257		0.000	H→L+2	0.60
						H-2→L	0.26
	5	5.08	244	Y(Z)	0.302	H→L+1	0.59
						H-1→L	0.20
22	1	3.57	348	Y	0.007	H→L+1	0.58
						H-1→L	0.44
	2	3.87	320	Z	0.025	H→L	0.57
						H-1→L+1	0.39
	3	4.55	272	Z	2.869	H-1→L+1	0.52
						H→L	0.31
	4	4.56	272	Y(Z)	0.280	H-1→L	0.52
						H→L+1	0.36
	5	4.70	264		0.000	H→L+2	0.61
						H→L+3	0.26
20	1	3.51	354	Y	0.001	H-1→L	0.53
						H→L+1	0.47
	2	3.75	330	Z	0.685	H→L	0.56
						H-1→L+1	0.37
	3	4.09	303	Z	3.127	H-1→L+1	0.52
						H→L	0.30
	4	4.37	284	Y	0.227	H-L+1	0.48
						H-1→L	0.42
	5	4.49	276		0.000	H-2→L	0.49
						H→L+2	0.40

21	1	3.54	350	Y	0.003	H-1→L	0.48
						H→L+2	0.44
	2	3.58	347	Z	3.391	H→L	0.59
						H-2→L+1	0.28
	3	3.96	313		0.000	H-2→L	0.43
						H→L+1	0.41
	4	4.00	310	Z	1.155	H-1→L+2	0.60
						H-2→L+1	0.18
	5	4.08	304	X	0.027	H-3→L+1	0.45
						H-4→L	0.41
26	1	3.46	359	Y	0.001	H→L	0.50
						H-2→L+1	0.45
	2	3.59	346	Z	2.347	H→L+1	0.61
						H-1→L+2	0.21
	3	3.97	312	Z	2.080	H-2→L	0.61
						H-1→L+2	0.18
	4	4.13	300		0.000	H-1→L+1	0.53
						H→L+2	0.34
	5	4.26	291	Y	0.184	H-2→L+1	0.49
						H→L	0.42
6	1	3.64	341	Y	0.002	H→L+1	0.52
						H-1→L	0.46
	2	3.88	320	Z	0.126	H→L	0.60
						H-1→L+1	0.30
	3	4.39	283	Z	3.289	H-1→L+1	0.56
						H→L	0.23
	4	4.52	274	Y	0.205	H-1→L	0.49
						H→L+1	0.41
	5	4.66	266		0.000	H→L+5	0.53
						H→L+2	0.40
29	1	3.20	388		0.030	H-2→L+1	0.24
						H→L	0.65
	2	3.75	331		0.009	H-2→L	0.48
						H→L+1	0.48
	3	3.83	324		0.018	H-1→L	0.59
						H→L+2	0.27
	4	4.11	302		2.449	H-2→L	0.42
						H→L+1	0.43
	5	4.25	292		0.021	H-2→L+1	0.28
						H-1→L+2	0.36
						H→L+3	0.44

30	1	3.84	323	0.379	H-1→L+1	0.25
					H→L	0.63
	2	3.89	318	0.008	H-1→L	0.50
					H→L+1	0.55
	3	4.66	266	0.001	H→L+2	0.67
	4	4.94	251	0.394	H-1→L	0.45
					H→L+1	0.40
	5	5.00	248	0.023	H-2→L	0.64
40	1	3.74	331	0.395	H→L	0.62
	2	3.87	321	0.045	H-1→L	0.54
					H→L+1	0.48
	3	4.72	263	0.002	H-2→L	0.38
					H→L+2	0.56
	4	4.83	257	0.029	H-2→L	0.54
					H→L+2	0.34
	5	4.89	254	0.378	H-1→L	0.38
					H→L+1	0.44
37	1	3.42	363	0.935	H→L	0.65
	2	3.78	328	0.000	H-1→L	0.45
					H→L+1	0.47
	3	4.47	278	0.415	H-1→L	0.31
					H→L+1	0.35
					H→L+2	0.29
	4	4.59	270	0.125	H-2→L	0.24
					H-1→L	0.29
					H→L+2	0.25
					H→L+4	0.43
	5	4.74	261	0.067	H-4→L	0.49
					H-2→L	0.34
					H→L+1	0.23
39	1	3.64	340	0.824	H→L	0.62
	2	3.85	322	0.001	H→L+2	0.53
	3	4.08	304	0.121	H-1→L	0.49
					H-1→L+1	0.43
	4	4.21	295	0.179	H-2→L	0.39
					H-2→L+1	0.27
					H→L+1	0.35
	5	4.46	278	0.046	H-3→L	0.29
					H→L+1	0.39

38	1	3.44	361	0.513	H→L	0.65
	2	3.77	329	0.018	H-1→L	0.40
					H→L+2	0.39
	3	4.04	307	0.119	H-1→L	0.45
					H-2→L	0.33
	4	4.29	289	0.044	H-2→L	0.40
					H-4→L	0.31
	5	4.46	278	0.016	H-3→L	0.49
					H-4→L	0.29

7.0 NMR Spectra of Compounds **53** and **54**

Compound 53

^{1}H NMR (500 MHz, $CDCl_3$)

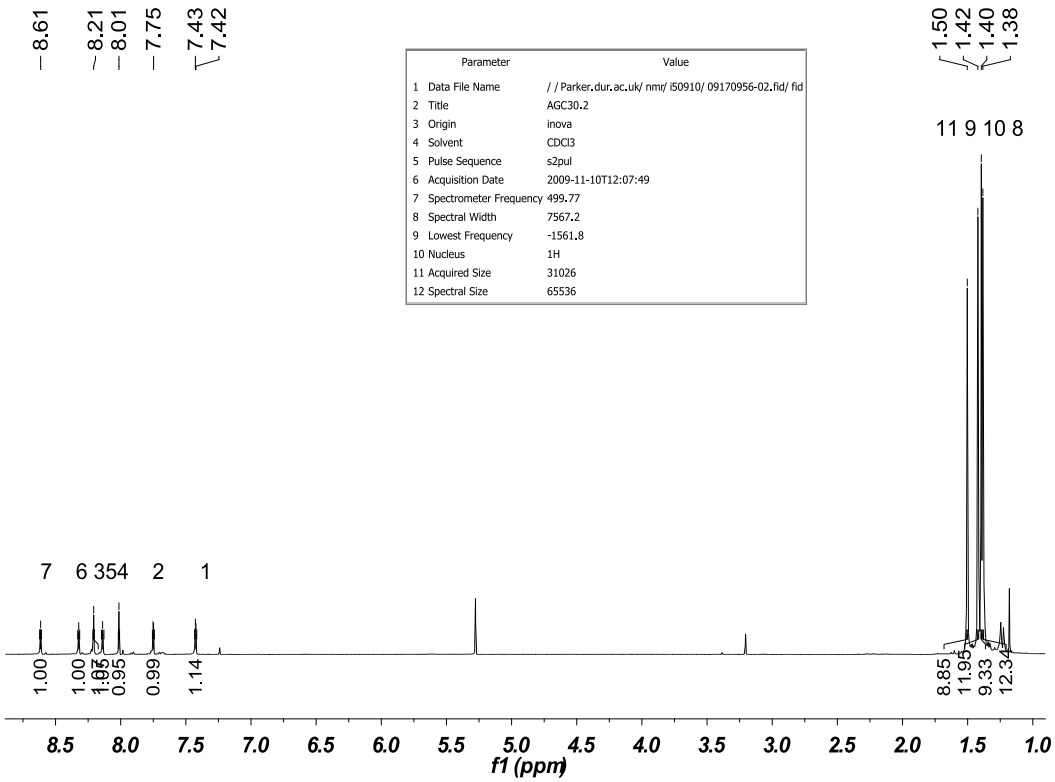

Parameter	Value
1 Data File Name	/ / Parker.dur.ac.uk/ nmr/ i50910/ 09170956-02.fid/ fid
2 Title	AGC30.2
3 Origin	inova
4 Solvent	CDCl3
5 Pulse Sequence	s2pul
6 Acquisition Date	2009-11-10T12:07:49
7 Spectrometer Frequency	499.77
8 Spectral Width	7567.2
9 Lowest Frequency	-1561.8
10 Nucleus	1H
11 Acquired Size	31026
12 Spectral Size	65536

^{13}C NMR (125 MHz, $CDCl_3$)

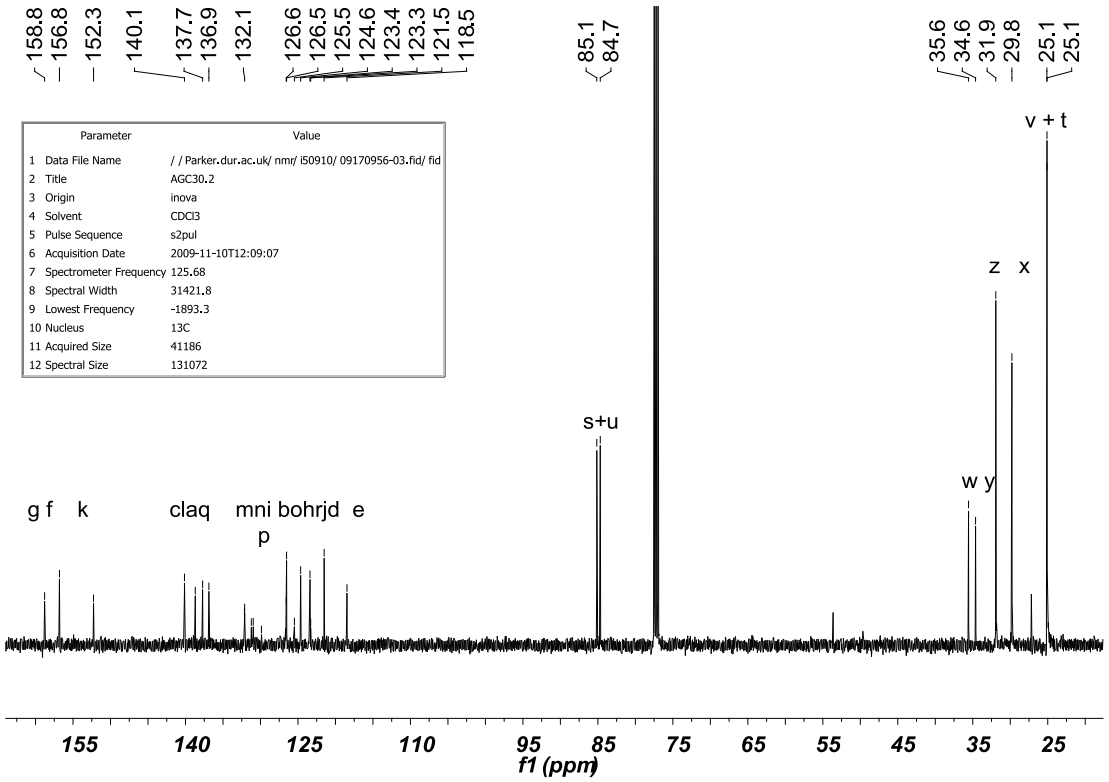

Parameter	Value
1 Data File Name	/ / Parker.dur.ac.uk/ nmr/ i50910/ 09170956-03.fid/ fid
2 Title	AGC30.2
3 Origin	inova
4 Solvent	CDCl3
5 Pulse Sequence	s2pul
6 Acquisition Date	2009-11-10T12:09:07
7 Spectrometer Frequency	125.68
8 Spectral Width	31421.8
9 Lowest Frequency	-1893.3
10 Nucleus	13C
11 Acquired Size	41186
12 Spectral Size	131072

HSQC 2D NMR (500/125 MHz, $CDCl_3$)

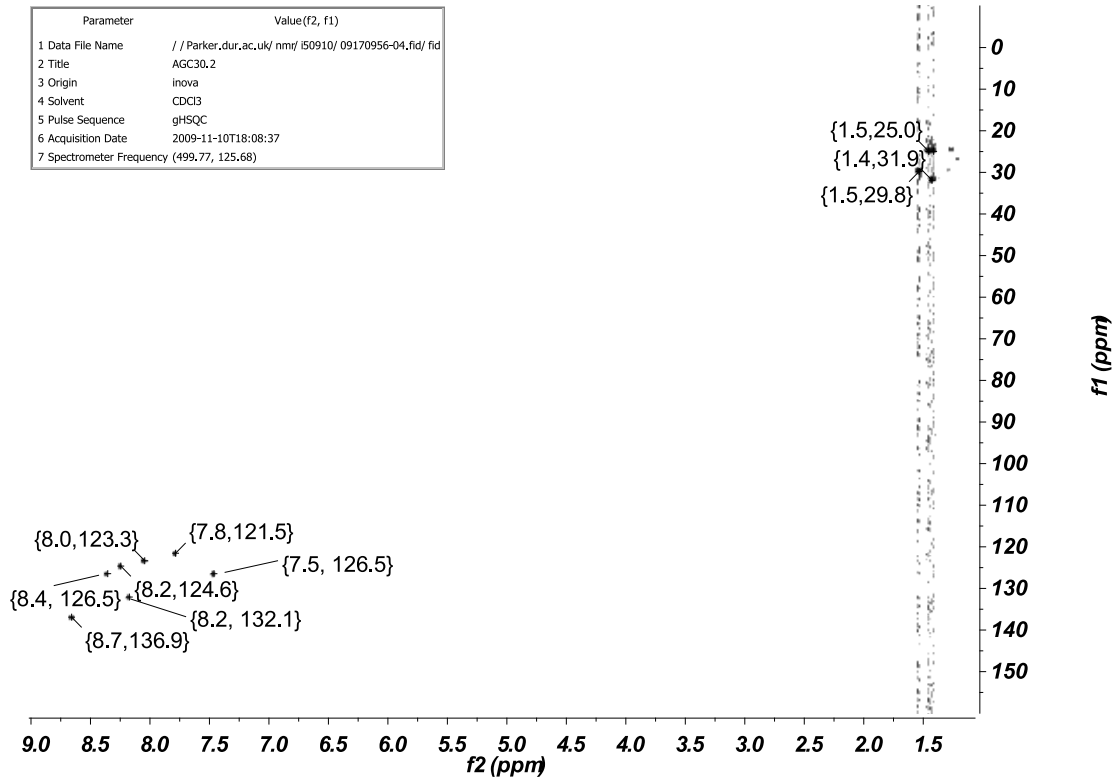

Parameter	Value(f2, f1)
1 Data File Name	/ / Parker.dur.ac.uk/ nmr/ i50910/ 09170956-04.fid/ fid
2 Title	AGC30.2
3 Origin	inova
4 Solvent	CDCl3
5 Pulse Sequence	gHSQC
6 Acquisition Date	2009-11-10T18:08:37
7 Spectrometer Frequency	(499.77, 125.68)

HMBC 2D NMR (500/125 MHz, $CDCl_3$)

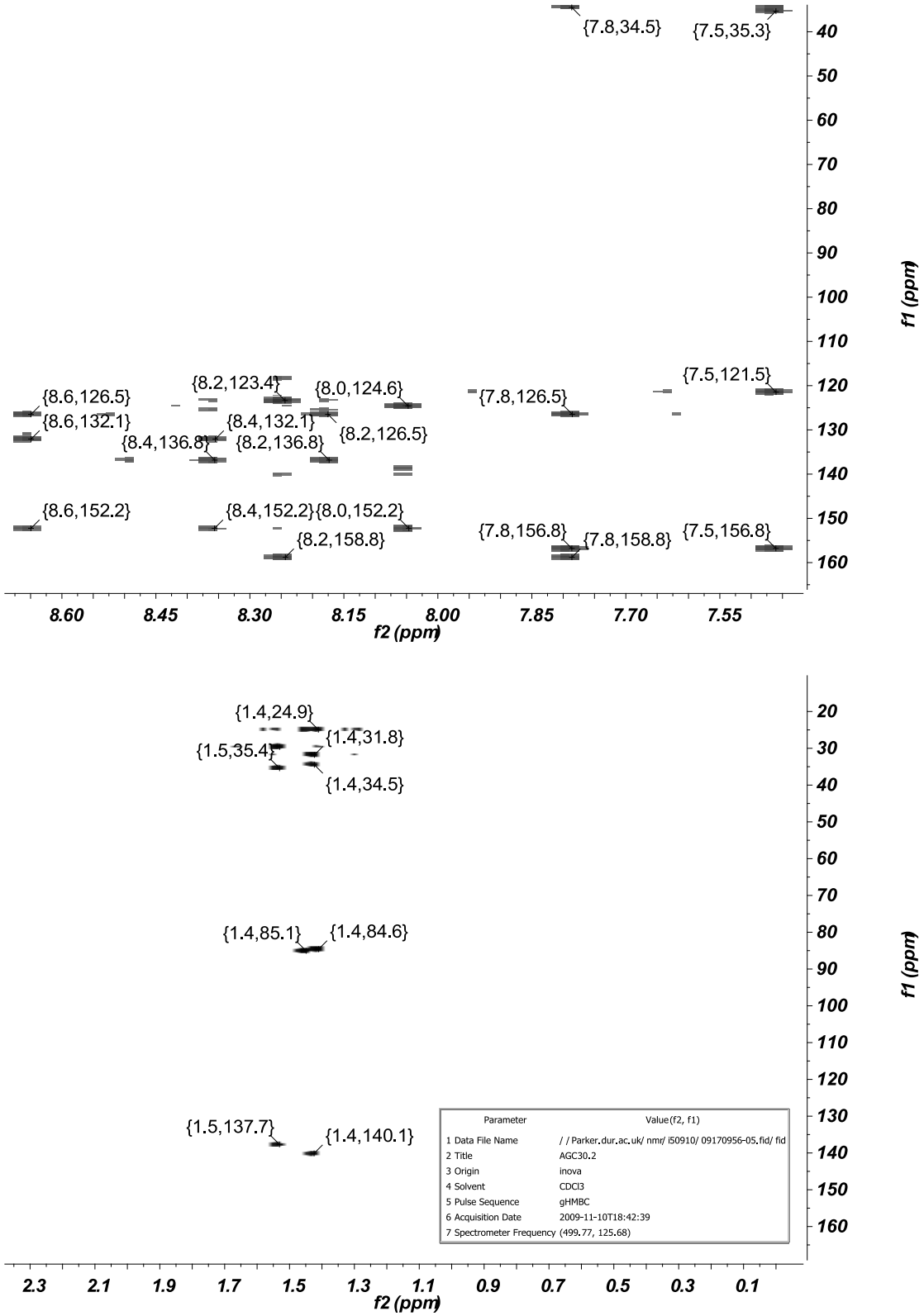

Compound 54

^{1}H NMR (500 MHz, $CDCl_3$)

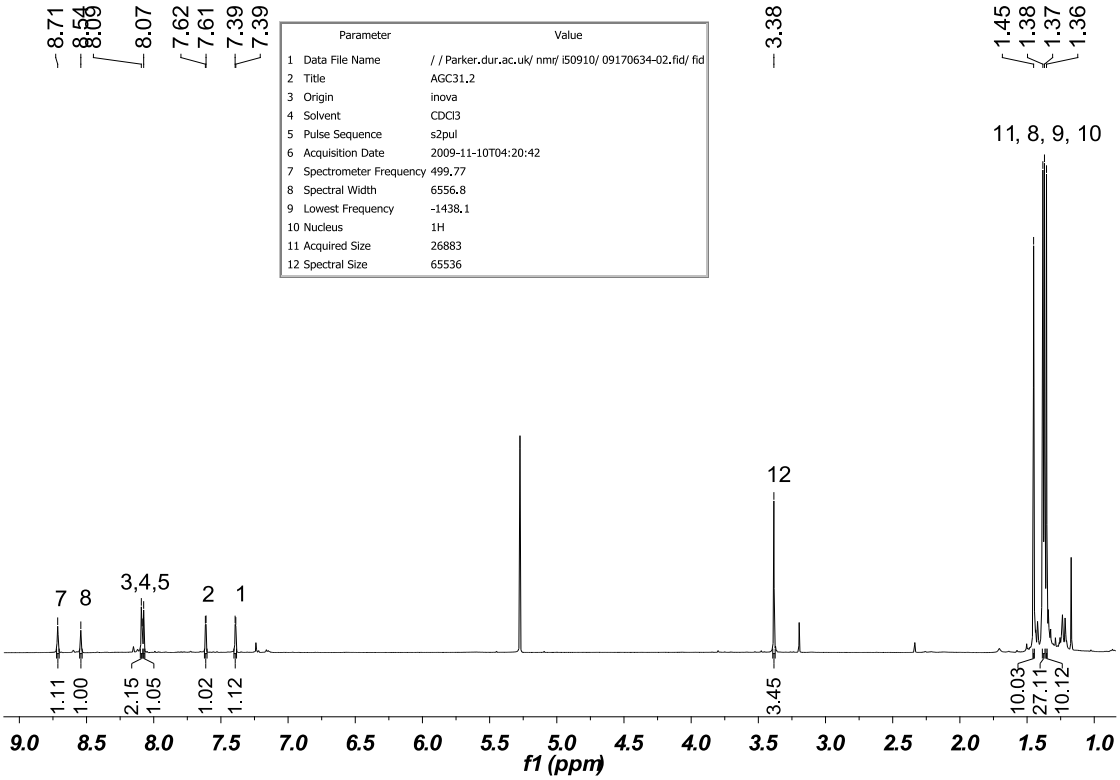

	Parameter	Value
1	Data File Name	/ / Parker.dur.ac.uk/ nmr/ i50910/ 09170634-02.fid/ fid
2	Title	AGC31.2
3	Origin	inova
4	Solvent	CDCl3
5	Pulse Sequence	s2pul
6	Acquisition Date	2009-11-10T04:20:42
7	Spectrometer Frequency	499.77
8	Spectral Width	6556.8
9	Lowest Frequency	-1438.1
10	Nucleus	1H
11	Acquired Size	26883
12	Spectral Size	65536

^{13}C NMR (125 MHz, $CDCl_3$)

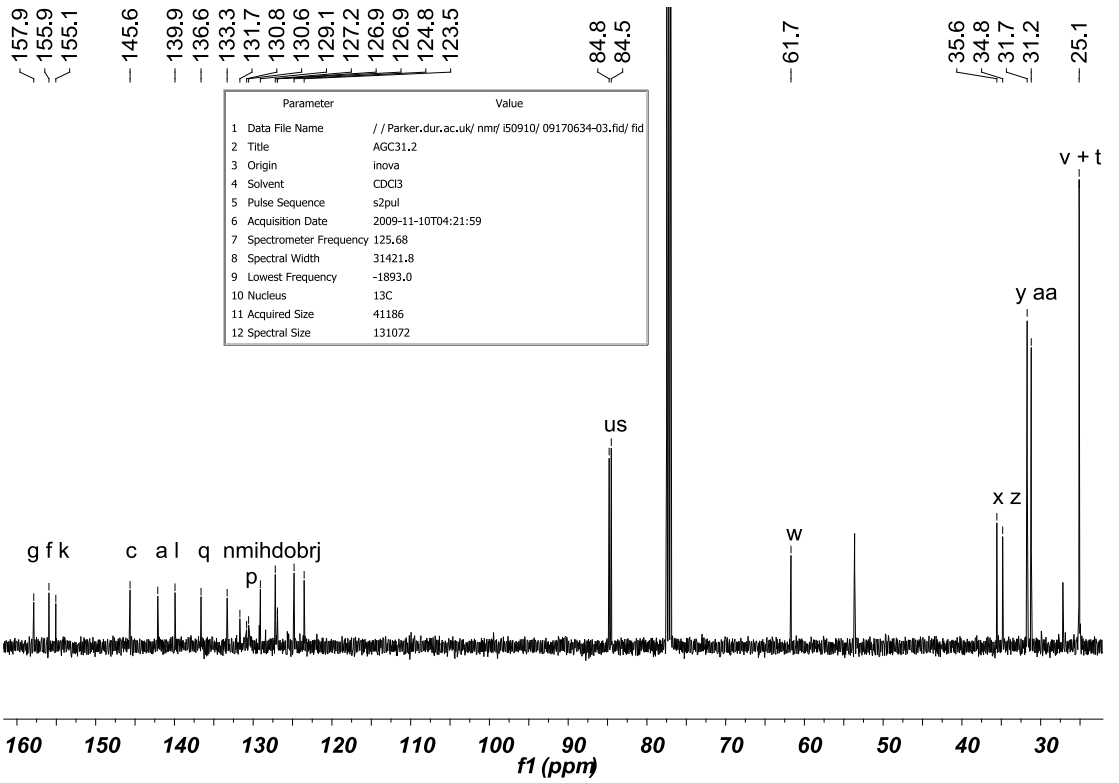

	Parameter	Value
1	Data File Name	/ / Parker.dur.ac.uk/ nmr/ i50910/ 09170634-03.fid/ fid
2	Title	AGC31.2
3	Origin	inova
4	Solvent	CDCl3
5	Pulse Sequence	s2pul
6	Acquisition Date	2009-11-10T04:21:59
7	Spectrometer Frequency	125.68
8	Spectral Width	31421.8
9	Lowest Frequency	-1893.0
10	Nucleus	13C
11	Acquired Size	41186
12	Spectral Size	131072

HSQC 2D NMR (500/125 MHz, $CDCl_3$)

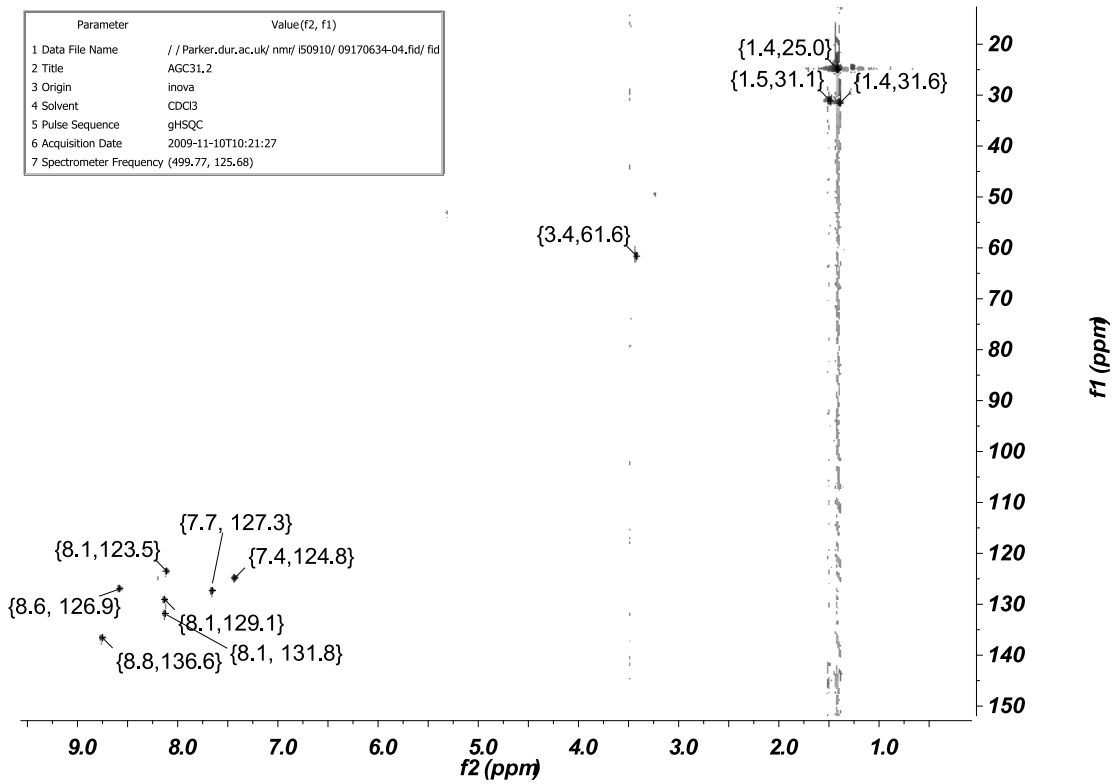

HMBC 2D NMR (500/125 MHz, $CDCl_3$)

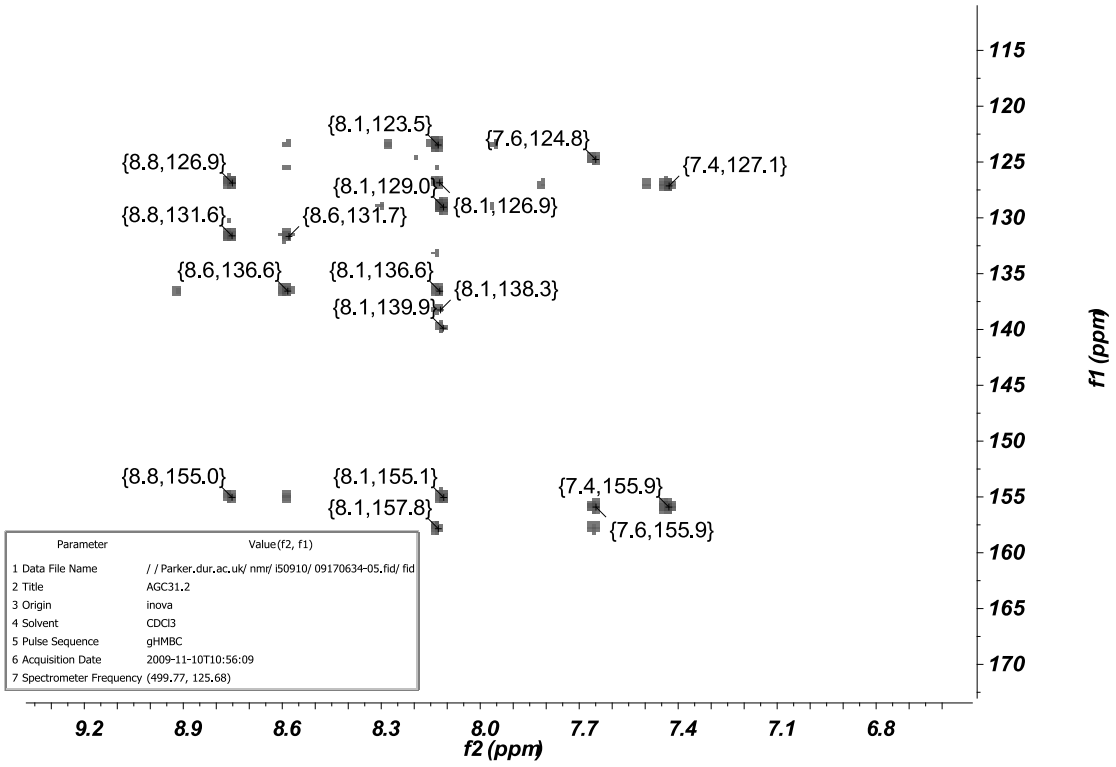

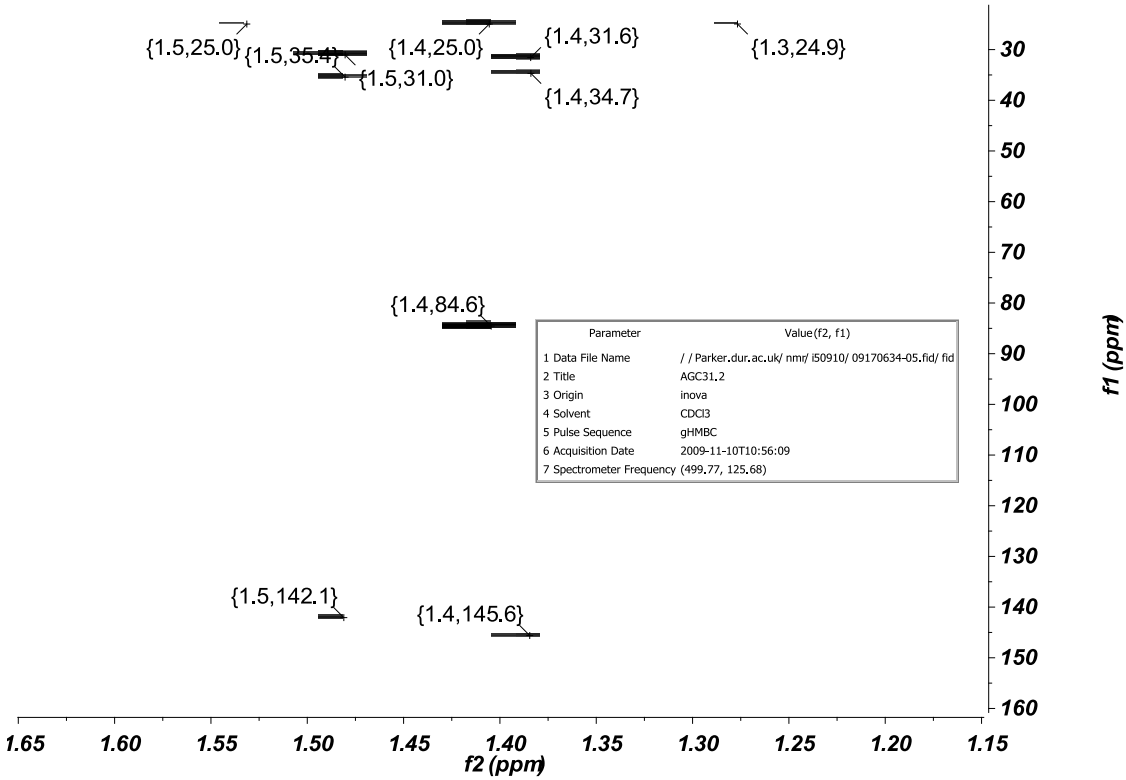
{1.5,25.0}
{1.5,35.4}
{1.5,31.0}
{1.4,25.0}
{1.4,31.6}
{1.4,34.7}
{1.3,24.9}
{1.4,84.6}
{1.5,142.1}
{1.4,145.6}
Parameter
Value(f2, f1)
1 Data File Name
/ / Parker.dur.ac.uk/ nmr/ i50910/ 09170634-05.fid/ fid
2 Title
AGC31.2
3 Origin
inova
4 Solvent
CDCl3
5 Pulse Sequence
gHMBC
6 Acquisition Date
2009-11-10T10:56:09
7 Spectrometer Frequency
(499.77, 125.68)
f1 (ppm)
f2 (ppm)